



HAL
open science

Development of an intensified process for the one-step production of isotropic and anisotropic polymeric nanoparticles

Javid Abdurahim

► **To cite this version:**

Javid Abdurahim. Development of an intensified process for the one-step production of isotropic and anisotropic polymeric nanoparticles. Chemical and Process Engineering. Université de Strasbourg, 2022. English. NNT: 2022STRAE023 . tel-04808271

HAL Id: tel-04808271

<https://theses.hal.science/tel-04808271v1>

Submitted on 28 Nov 2024

HAL is a multi-disciplinary open access archive for the deposit and dissemination of scientific research documents, whether they are published or not. The documents may come from teaching and research institutions in France or abroad, or from public or private research centers.

L'archive ouverte pluridisciplinaire **HAL**, est destinée au dépôt et à la diffusion de documents scientifiques de niveau recherche, publiés ou non, émanant des établissements d'enseignement et de recherche français ou étrangers, des laboratoires publics ou privés.



UNIVERSITÉ DE STRASBOURG

ÉCOLE DOCTORALE DE PHYSIQUE ET CHIMIE-PHYSIQUE

Institut Charles Sadron, CNRS UPR 22

THÈSE présentée par :

Javid ABDURAHIM

Soutenue publiquement le 20 Octobre 2022

Pour obtenir le grade de : **Docteur de l'Université de Strasbourg**

Discipline : *Génie des procédés*

Spécialité : *Chimie-Physique et Ingénierie des Microprocédés Polymères*

**Development of an Intensified Process for the One-step
Production of Isotropic and Anisotropic Polymeric Nanoparticles**

Pr. Cécile NOUVEL	Université de Lorraine	Rapporteuse externe
Dr. Christophe DROUET	Université de Toulouse	Rapporteur externe
Dr. Madeline VAUTHIER	Université de Strasbourg	Examinatrice interne
Pr. Christophe SERRA	Université de Strasbourg	Directeur de thèse

“In the middle of the difficulty lies the opportunity”

Albert Einstein

Remerciements

Quand je suis arrivé à l'aéroport de Strasbourg en hiver 2019, c'était une nuit froide et pluvieuse. Au début c'était très difficile, j'étais perdu. Christophe Serra est venu me chercher à l'aéroport de Strasbourg, et ses paroles dès le premier jour m'ont donné confiance dans ma décision. Cela a continué pareil avec Madeline Vauthier, et depuis ce temps-là, nous avons travaillé ensemble trois ans et j'ai ressenti leur soutien tout le temps. Je tiens à leur exprimer mes profonds remerciements pour leur soutien et disponibilité.

Merci aux permanents de l'ICS pour leur accueil chaleureux, leur gentillesse et leur bonne humeur. Merci particulièrement aux gérants des plateformes de caractérisation, Christian Blanck, Mark Schmutz pour les images MET, et Christophe Contal pour les images l'AFM, et ses conseils. Un grand merci à Wiebke Drenckhan, Delphine Chan-Seng, Leondro Jacomine, Olivier Felix, Laurence Oswald, Melanie Legros, Catherine Foussat pour ses aide et conseils pendant trois ans. Je remercie également Jerome Kelle, l'ambassadeur Zacharie Gross, Charlotte Payen, Dunya Babanly, Vice-président de l'Unistra Jean-Marc Planeix pour leur validation, et leur soutien à se faire accepter en doctorat.

Je me dois aussi de remercier ceux qui m'entourent et m'ont soutenu depuis plus longtemps; Jean Muller, Eulalie Lafarge, ils étaient les meilleurs amis et aussi les meilleurs supporters. Également, j'ai gagné beaucoup d'amis et beaucoup de soutien de leur part, je leur suis reconnaissant à tous, en particulier à Andrea, Felipe, Wasif, Haseb, Laurie, Martin, Stephane, Jonathan, Eirini, Imen, Charlli, Quentin, Lisa, Ricardo, Fedir, Florence, Soraya, Ismayil, Abbas, Alexis, Christian, Capucine, Anais, Teodor, Lorenzo, Thibault, Senem, Sevetlana, également doctorants de l'institut Le bel, Nizami, Irina, Shamkhal, Baylar, bien d'autres, nous avons eu des jeux amusants, des déjeuners savoureux et de longues pauses café, et j'étais toujours content de vous tous, et tous les autres avec qui on jouait au foot toutes les semaines, Sisouk, Michel, Antonio, Damien, Morvan, Friedrich, Nicolas et d'autres. Je remercie également tous mes stagiaires, Raphaël, Julie, Ahmed, et les autres. Ce fut une bonne expérience de travailler avec vous.

Des gens avec qui je m'amusais, merci à vous!

et même avant que je ne sois arrivée!

Mes remerciements les plus chaleureux vont à mes proches qui m'ont soutenu depuis que j'existe dans ce monde peu importe combien de milliers de kilomètres, les océans nous séparent, mes parents Samira, Karim et ma sœur Sabina sont toujours derrière moi ! Et ma famille, Minaya m'a toujours soutenu, aidé et encouragé, je vous remercie tous et je suis heureux que vous soyez dans ma vie.

Enfin, Sara et Davud, si vous lisez et comprenez ce qui est écrit ici, peut-être êtes-vous en 2040, et peut-être êtes-vous un professionnel dans ce que vous aimiez faire, peu importe, je vous aime tellement que cela ne peut être comparé à rien au monde, et je suis reconnaissant à Dieu de vous avoir. Soyez toujours heureux et brillez toujours d'une lumière pleine d'espoir que tout le monde trouve morceau et confiance avec vous!

Table of Content

Résumé de thèse: Des macromolécules aux nanoparticules

1	Introduction	13
2	Résultats et discussion	14
2.1	Production en une étape de nanoparticules de PLGA monodisperses et à taille contrôlée pour la libération d'un médicament modèle hydrophobe.	14
2.2	Synthèse en une étape de nanoparticules polymères complexes et anisotropes sous flux élongationnel	17
2.3	Le dispositif capillaire côte à côte pour produire des nanoparticules de polyélectrolytes (PEC).	18
3	Conclusion	19
4	Références	20

General introduction: Polymeric nanoparticle production

Abbreviations

Chapter 1: Production process design and development of polymeric nanoparticles; state of the art

1.1	INTRODUCTION	31
1.2	POLYMERIC NANOPARTICLES DESIGN, FABRICATION, AND APPLICATIONS	32
1.2.1	Definition	32
1.2.2	Fabrication	35
1.2.2.1	Multi-step process	37
1.2.2.2	One-step process	39
1.2.3	Production design	40
1.2.4	Applications of polymeric nanoparticles	43

1.3	MINIEMULSION-BASED PRODUCTION DESIGNS	45
1.3.1	Towards polymeric nanoparticles via miniemulsions	45
1.3.2	Production techniques	49
1.3.2.1	High-energy methods	50
1.3.2.2	Low energy methods	55
1.3.2.3	Process and pre-process parameters	62
1.3.3	Theoretical aspects	63
1.3.3.1	Interfacial free energy	63
1.3.3.2	Utility of surfactants	64
1.3.3.3	Energy density and critical capillary number	66
1.4	NON-EMULSION-BASED PRODUCTION DESIGNS	68
1.4.1	List of the non-emulsion methods	68
1.4.2	Process and pre-process parameters	74
1.4.3	Theory behind the non-emulsion-based PNP formation	74
1.4.3.1	Diffusion-advection relations by Peclet number	74
1.4.3.2	Mixing time	75
1.5	POST-PRODUCTION POSSIBILITIES WITH PNPs	77
1.5.1	Stability of polymeric nanoparticles	77
1.5.2	Drug release studies	77
1.5.3	Safety of polymeric nanoparticles	79
1.6	CONCLUSION	80
1.7	BIBLIOGRAPHY	81

Chapter 2: Materials and Methods

PREFACE	99	
2.1	MATERIALS	99
2.1.1	Solvents	99
2.1.1.1	Polar solvents	100
2.1.1.2	Non-polar solvents	100
2.1.2	Polymers	101
2.1.3	Emulsifiers	103

2.1.4	Rifampicin	104
2.1.5	Other materials	105
2.2	METHODS OF PREPARATION	105
2.2.1	Emulsion methods	105
2.2.1.1	Elongational-flow reactor and mixer	106
2.2.1.2	Shear-mixing	111
2.2.1.3	Sonication	113
2.2.2	Solvent removal	115
2.2.3	Non-emulsion method	118
2.2.4	Polymeric nanoparticle purification	119
2.3	METHODS OF CHARACTERIZATION	120
2.3.1	Analyses by spectroscopic methods	120
2.3.1.1	Dynamic Light Scattering & Zeta Potential	120
2.3.1.2	UV-visible Spectroscopy	122
2.3.1.3	Fourier Transform Infrared	123
2.3.1.4	Nuclear Magnetic Resonance	123
2.3.2	Methods of microscopic characterization	124
2.3.2.1	Transmission Electron Microscopy	124
2.3.2.2	Scanning Electron & Keyence Microscopies	124
2.3.2.3	Atomic Force Microscopy	124
2.3.3	Interfacial Tension Measurements	125
2.3.4	Other characterization methods	126
2.4	METHODS OF APPLICATION	126
2.4.1	Drug delivery studies	126
2.4.2	Stability	127
2.5	BIBLIOGRAPHY	128

Chapter 3: One-step Production of Highly Monodisperse size-controlled Poly(lactic-co-glycolic acid) nanoparticles for the release of a hydrophobic model drug

3.1	INTRODUCTION	133
3.2	PROCESS ELABORATION RESULTS	134
3.2.1	Influence of the operating parameters on the PLGA nanoparticles	134
3.2.2	Polydispersity index of the produced PNPs	137
3.2.3	Heat emission during the process of emulsification	138
3.2.4	Process volume influence on PNP fabrication	139
3.3	PLGA NANOPARTICLES AS DRUG CARRIERS	140
3.3.1	Rifampicin's calibration curve	141
3.3.2	PLGA size and size distribution influenced by the drug encapsulation	143
3.3.3	Understanding the size reduction at different material concentrations	145
3.3.4	Coherence of results from two different characterization techniques	147
3.4	DRUG RELEASE FROM PLGA NANOPARTICLES	148
3.4.1	Influence of the initial drug weight content on the drug release	148
3.5	CONCLUSION	152
3.6	BIBLIOGRAPHY	153

Chapter 4: One-step elongational-flow synthesis of anisotropic polymeric nanoparticles used as drug carriers

4.1	INTRODUCTION	159
4.2	ELABORATION OF ANISOTROPIC POLYMERIC NANOPARTICLES	160
4.2.1	Influence of the process parameters	161
4.2.2	Influence of the C/D volume ratio and the phase pre-saturation conditions	163
4.2.3	Influence on the polymers' ratio	164
4.3	SINGLE, BLEND AND JANUS STRUCTURES	167
4.3.1	Morphology analysis	167

4.3.2	Solid FTIR characterization of the produced particles	169
4.3.3	Comparison of the PNP's capacity to encapsulate a model drug	171
4.3.4	Drug release from single and anisotropic PNPs	173
4.4	ADDITIONNAL CHARACTERIZATIONS AND CONSIDERATIONS	175
4.4.1	Observations on size and size distribution	175
4.4.2	Some notes to be considered for the next studies	177
4.5	CONCLUSION	178
4.6	BIBLIOGRAPHY	179

Chapter 5: Process design and optimization of polyelectrolyte complex nanoparticles' production

5.1	INTRODUCTION	185
5.2	POLYELECTROLYTES FORMED VIA EMULSIONS	187
5.2.1	Characterization of pre-formed polyelectrolytes and their complexes	187
5.2.2	Characterization of polyelectrolyte nanoparticles and their complexes	189
5.2.3	Sign of improved electrostatic attraction	191
5.2.4	Side-by-side capillary device to improve electrostatic interactions	193
5.3	NON-EMULSION DESIGN WITH SIDE-BY-SIDE CAPILLARY DEVICE	195
5.3.1	Process optimization	195
5.3.2	PEC NPS formation mechanism	196
5.3.3	Other polyelectrolytes capable of forming PEC NPs	198
5.3.4	Side-by-side capillary collecting tubing	199
5.3.5	Polymer molecular weight effect on final product properties	201
5.3.6	Morphological characterizations	202
5.4	CONCLUSION	204
5.5	BIBLIOGRAPHY	205

General conclusion and perspectives

Production Scientific

Résumé de Thèse

1 Introduction

Le développement de nanoparticules polymères (PNPs) est un domaine de recherche largement étudié de nos jours en raison de leurs nombreuses potentielles applications. Par exemple, en médecine, ces matériaux peuvent être des vecteurs de médicaments prometteurs pour améliorer les traitements. Des études antérieures suggèrent que les médicaments présentant des problèmes d'administration pourraient être encapsulés dans des PNPs biodégradables d'un diamètre aussi petit que 200 nm pour améliorer leur stabilité et ajuster leurs profils de libération [1]. Il n'est pas toujours possible de contrôler avec précision les propriétés des PNPs telles que la taille, la distribution de taille, la composition et la morphologie avec les procédés utilisant des équipements conventionnels. Compte tenu des défis de production tels que l'opérabilité limitée, le blocage fréquent, la biodisponibilité ou des rendements massiques très faibles, les PNPs nécessitent l'emploi de procédés appropriés et de surcroît adaptés aux domaines d'application visés [2]. Par ailleurs, l'emploi des PNPs en essais cliniques reste difficile en raison de la disponibilité limitée de méthodes de production simples, cohérentes et permettant d'assurer des quantités suffisantes. En effet, la conception et les méthodes de production jouent un rôle important pour obtenir les propriétés requises [3], [4]. Ainsi, au cours de cette thèse, différents procédés de production de PNPs en fonction de leur application ont été développés et comparés.

Dans une première étude, nous proposons de mettre en œuvre la méthode d'émulsification-évaporation pour la production en une seule étape de nanoparticules biodégradables à base d'acide poly(lactique-co-glycolique) (PLGA) pour encapsuler un médicament modèle (Rifampicine). L'influence de trois dispositifs différents, de leurs paramètres à la fois procédés (temps d'émulsification, température et paramètres de mélange) et matériau (concentration de médicament) sur le diamètre moyen des nanoparticules et les profils de libération du médicament est étudiée en profondeur. Les principaux objectifs de ce travail sont de développer des PNPs ayant une gamme de taille spécifique (entre 50 nm et 200 nm) et une faible valeur de dispersité de taille grâce à l'optimisation du procédé et de ses paramètres. Ceux-ci rendent possible la production de PNPs capables d'encapsuler le médicament avec une efficacité suffisante dans un processus en une étape pour une administration ultérieure du médicament avec des effets secondaires réduits. Les trois dispositifs différents (sonicateur, mélangeur à cisaillement et émulsificateur microfluidique à flux élongationnel) sont étudiés pour élaborer une approche efficace afin de développer des nanoémulsions huile-dans-eau hautement stables qui, lors de la nanopréciptation induite par

l'évaporation du solvant organique, sont converties en systèmes d'administration de médicaments appropriés. Étant donné qu'une augmentation de l'encapsulation du médicament peut entraîner certaines altérations, telles qu'une érosion massive du PLGA en milieu acide, des études de libération du médicament *in vitro* en maintenant des conditions spéciales à différents rapports d'encapsulation de médicament sont présentées.

Puis, suite à la publication récente de notre équipe sur le sujet précédent [5], nous proposons une nouvelle composition de PNPs à la fois complexes et anisotropes produits grâce à un nouveau procédé d'émulsification-évaporation en une seule étape, et leurs applications pour l'administration de médicaments. Dans cette partie, la pré-saturation en phase continue est appliquée à la méthode d'émulsification microfluidique et d'évaporation de solvant suite à notre premier article publié [5], afin de i) augmenter la quantité de médicament modèle hydrophobe encapsulé (rifampicine) et ii) améliorer le contrôle du diamètre et la distribution de taille des PNPs.

Dans le dernier chapitre expérimental de cette thèse, nous proposons un nouveau dispositif permettant la production à l'échelle commerciale de PNP complexes sans émulsification préalable ni tensioactif et l'optimisation de ses paramètres de procédé. Ici, des nanoparticules de polyélectrolyte ont été produites dans un dispositif capillaire côte à côte.

2 Résultats et discussion

2.1 Production en une étape de nanoparticules de PLGA monodisperses et à taille contrôlée pour la libération d'un médicament modèle hydrophobe.

Du PLGA commercial, un surfactant, et éventuellement le médicament ont ainsi été dissouts dans de l'acétate d'éthyle et émulsifiés avec une phase majoritaire aqueuse sous forme de nanogouttelettes. L'émulsion obtenue fut alors récupérée et placée sous une hotte afin d'évaporer le solvant organique pour d'obtenir les PNPs.

Premièrement, trois dispositifs différents ont été étudiés pour produire des PNPs de PLGA de taille et dispersité appropriées pour les systèmes d'administration de médicaments. Cependant, le sonicateur ainsi que le mélangeur à cisaillement engendrèrent des augmentations de température néfastes à la stabilité du médicament ($T \geq 60^\circ\text{C}$). Par contre, l'émulsificateur microfluidique à flux élongationnel ne conduisit à aucune augmentation de température et fut ainsi choisi comme dispositif de choix. L'optimisation menée sur la base de la taille des nanoparticules et leur dispersité permet de retenir les paramètres opératoires suivants : 150 cycles à 30 mL/min. Ensuite, l'influence de la concentration

en médicament a été étudiée. A cet effet, le médicament a été introduit dans la phase dispersée (PLAG + acétate d'éthyle) à différentes teneurs pondérales en PLGA, allant de 1%/PLGA w/w à 10%/PLGA w/w (les échantillons étaient respectivement appelés R1 à R10) et les nanoparticules chargées en médicament (DNPs) résultantes ont été analysées par spectroscopie UV-visible à 332 nm après établissement d'une courbe d'étalonnage. L'augmentation de la teneur en poids initial de rifampicine a réduit de manière inattendue la taille des DNPs de 94 ± 4 nm à $69 \text{ nm} \pm 2$ nm (Figure 1a). Ce résultat s'explique par une diminution de la tension interfaciale entre les phases continue et dispersée sans ($\sigma_0 = 3,2$ mN/m) et avec du médicament à 5% w/w par rapport au PLGA ($\sigma_5 = 2,8$ mN/m), en raison des interactions intermoléculaires qui se produisent entre le PLGA et la rifampicine et en raison de la présence de rifampicine à la surface des gouttelettes.

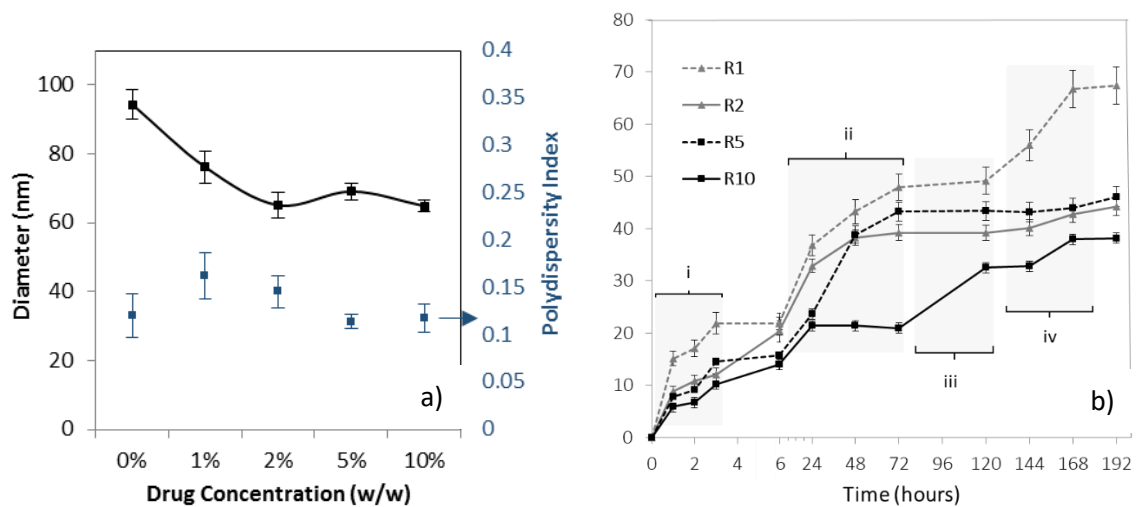


Figure 1. a) Évolution de la taille et de l'indice de polydispersité des DNPs pour différentes teneurs en poids de médicament par rapport au PLGA. b) Profils de libération du médicament *in vitro* en quatre étapes (i, ii, iii et iv) à 1 % p/p (R1), 2 % p/p (R2), 5 % p/p (R5) et 10 % p/p (R10) de teneur en poids de rifampicine/polymère.

Sur la Figure 1.b, la première observation était que la quantité de médicament libéré augmentait avec le temps, prouvant que le système développé obtenait une libération de médicament durable au fil du temps. De plus, quatre étapes ont été identifiées pour le processus de libération du médicament : (i) l'effet de libération imédiate a été remarqué dans les 3 premières heures; (ii) de 6 à 72 heures, une libération cumulative de médicament due à la diffusion constante des DNPs dans l'eau a été observée; (iii) une résilience partielle s'est produite entre 3 et 5 jours, ce qui peut s'expliquer par le piégeage du médicament près de la surface interne des DNPs; (iv) lors de la dernière étape, le médicament encapsulé au centre des DNPs a commencé à se diffuser dans l'eau après avoir atteint la surface des DNPs. De plus, la quantité de médicament libérée en 8 jours était de 129 ± 12 μg (67 %), 147 ± 10 μg (46 %), $175 \mu\text{g} \pm 9$ μg (45 %) et $242 \mu\text{g} \pm 9$ μg (38 %) pour R1, R2, R5 et R10 respectivement. Pour mieux comprendre le mécanisme de libération du médicament, les

images de microscopie électronique à transmission (MET) ont été discutées (Figure 2).

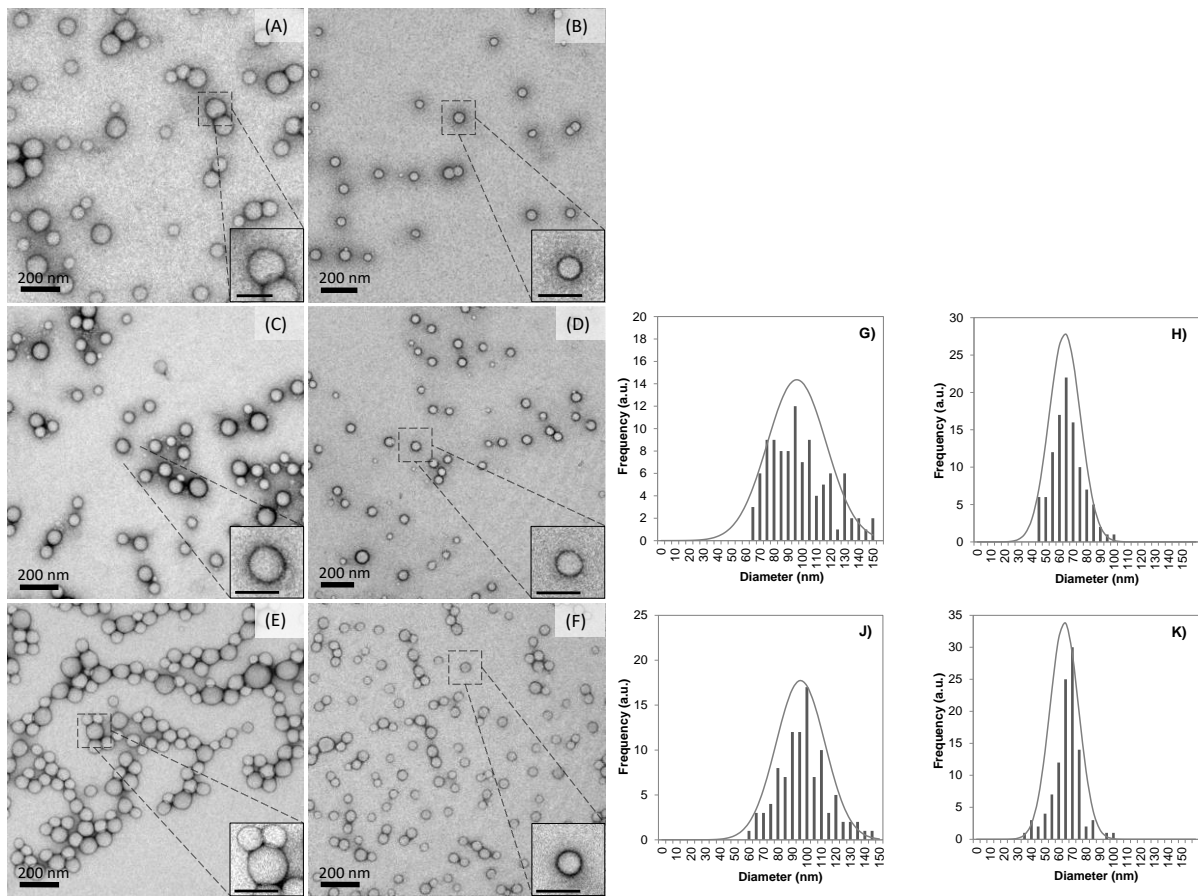


Figure 2. Images MET (A-F) et analyse statistique (G-K) des PNPs de PLGA sans encapsulation (A, C, E, G, J) et a 5 % w/w en médicament (B, D, F, H, K) après le 1er (A, B), 3e (C, D) et 8e jour (E, F). L'analyse statistique des diamètres des PNPs (G, J) et des DNP (H, K) est présentée pour le 1er jour (G, H) et après 8 jours d'incubation (J, K) à 37°C et pH = 7,4).

Dans la figure 2, les images MET ont montré que tous les PNPs and DNPs étaient de forme sphérique. Dès le stade initial, les PNPs (A) et les DNPs (B) produits avec les mêmes paramètres procédés et matériaux avaient une différence de taille de plus de 30 nm. Ainsi, la différence de taille entre les PNPs (G, 98 nm) et les DNPs (H, 64 nm) au premier jour a confirmé les résultats de taille obtenus par diffusion dynamique de la lumière (DLS) discutés précédemment. La courbe gaussienne plus large obtenue pour les PNPs a également prouvé un indice de polydispersité (PDI) plus élevé par rapport aux DNPs. Les PNPs au 3ème jour (C) et au 8ème jour (E) ont montré, par MET, une propriété de stabilité morphologique élevée similaire aux DNPs au 3ème jour (D) et au 8ème jour (F), et l'analyse statistique (G-K) a confirmé ces résultats.

2.2 Synthèse en une étape de nanoparticules polymères complexes et anisotropes sous flux élongationnel

Dans la deuxième partie de cette thèse, des PNPs à structure anisotrope, composées de deux polymères différents, ont été produites par la méthode d'émulsification-évaporation à flux élongationnel. Ainsi des nanoparticules de poly(méthacrylate de méthyle) (PMMA, neutre) et de polystyrène (PSS, chargé) ont été obtenues suite à l'optimisation d'une concentration en polymère au stade initial de la nanofabrication. À une concentration supérieure à 75 % en poids de PMMA (25 % en poids pour le PSS), il a été possible de produire des PNPs monomodales de tailles inférieures à 130 nm (Figure 3).

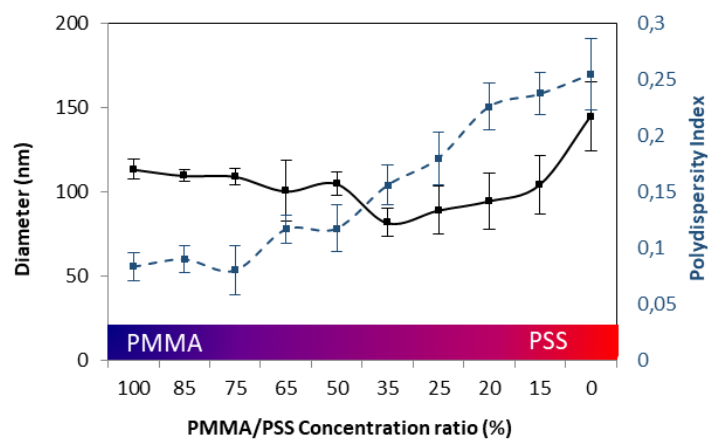


Figure 3. Effet du rapport de concentration entre le PMMA et le PSS sur les propriétés des nanoparticules obtenues avec la méthode d'émulsification-évaporation à flux élongationnel (150 cycles, 30 ml/min).

Suite à l'évaporation du solvant organique, les deux polymères se séparèrent sous l'effet de conditions thermodynamiques peu favorables au mélange pour former, pour la première fois en une étape, des nanoparticules présentant deux parties distinctes (particules Janus) (Figure 4a).

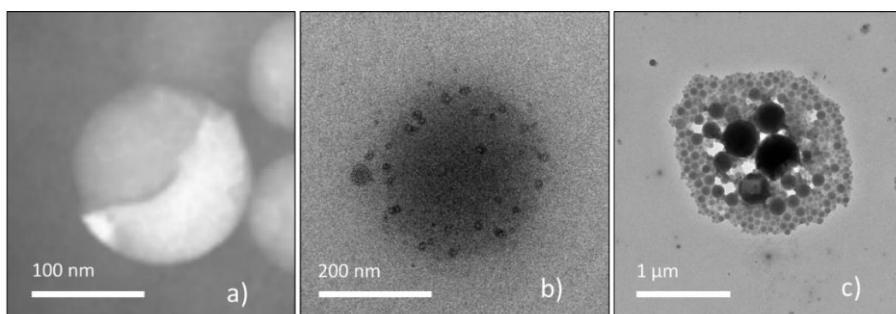


Figure 4. Images MET de nanoparticules polymères de morphologies différentes obtenues avec la méthode d'émulsification-évaporation à flux élongationnel (150 cycles, 30 ml/min); a) nanoparticule polymère Janus de PSS-PMMA (130 nm, PDI = 0,2), b) nanoparticules de complexes de polyélectrolytes de PAA-PDADMAC (200 nm, PDI = 0,17), c) agrégat de nanoparticules individuelles de PAA (50 nm, PDI = 0,1) et de PDADMAC (220 nm, PDI = 0,25).

L'emploi de deux polymères chargés comme l'acide polyacrylique (PAA, chargé négativement) et le chlorure de poly(diallyldiméthylammonium) (PDADMAC, chargé positivement) conduit par contre à l'obtention de nanoparticules de complexes de polyélectrolytes (Figure 4b). D'autres morphologies originales ont pu être obtenues comme celle de la Figure 4c. Elle présente un agrégat de taille micrométrique de nanoparticules de polyélectrolytes obtenus séparément et mélangés selon la méthode d'émulsification-évaporation à flux élongationnel.

2.3 Le dispositif capillaire côte à côte pour produire des nanoparticules de polyélectrolytes (PEC).

Afin de réaliser des NPs complexes, ce que n'a pas permis le précédent procédé, une nouvelle méthode sans tensioactif et non basée sur une émulsion a été développée. Cette méthode est basée sur l'emploi d'un système microfluidique à deux capillaires, placés côte-à-côte, par lesquels sont injectés les deux solutions de polyélectrolytes dans un flux d'une phase continue de propane-2-ol. Les résultats obtenus sont présentés en Figure 5.

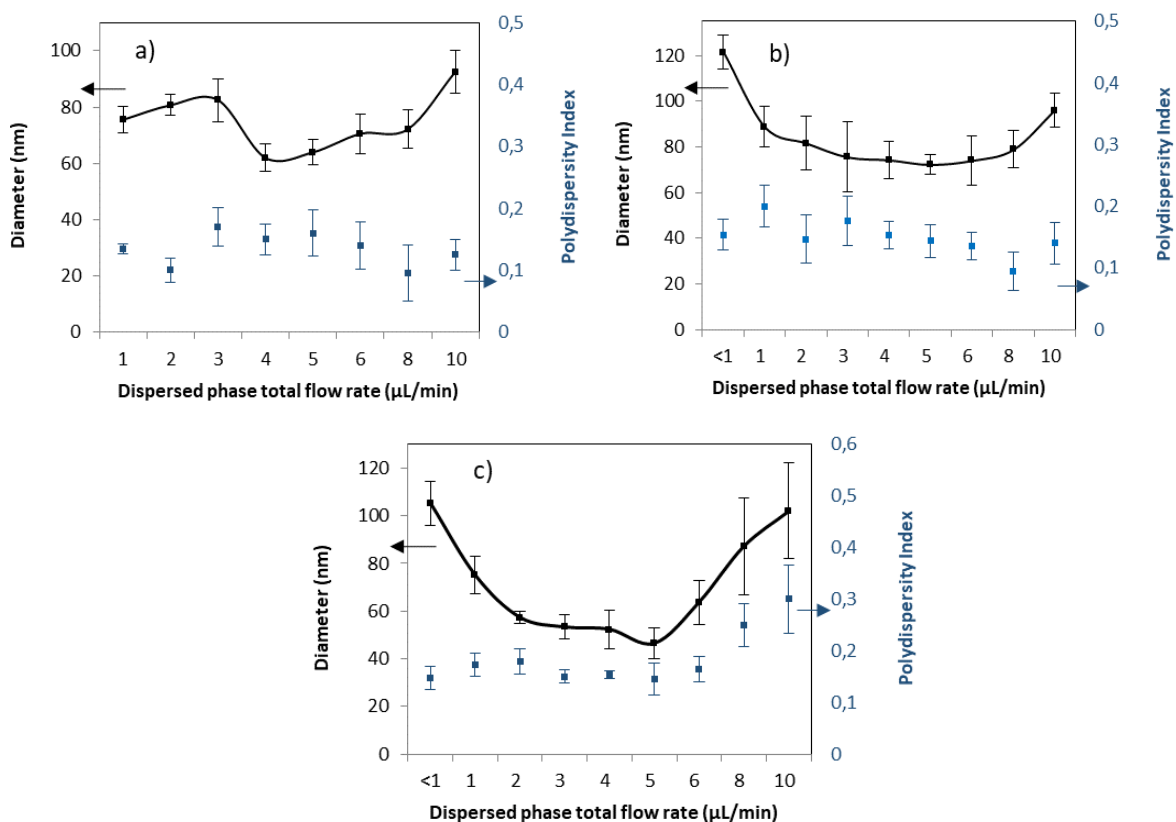


Figure 5. Résultats de la taille moyenne DLS et de la distribution de taille des NPs PAA/PDADMAC produites avec le dispositif capillaire côte à côte à des débits dispersés/continus de 6/200 μL/min (ID capillaire de 0,4

mm) et en faisant varier le diamètre du tube collecteur a) 1,6 mm, b) 1 mm, c) 0,5 mm.

Il a été possible d'observer la formation d'un seul jet résultant du mélange des deux phases polymère et donc la production des PEC NPs. Les débits ont été maintenus à 3 $\mu\text{L}/\text{min}$ avec le premier capillaire, 3 $\mu\text{L}/\text{min}$ avec le second capillaire et 200 $\mu\text{L}/\text{min}$ pour la phase continue. Les NP PEC produites ont été directement collectées dans l'alcool et analysées au MET (Figure 6).

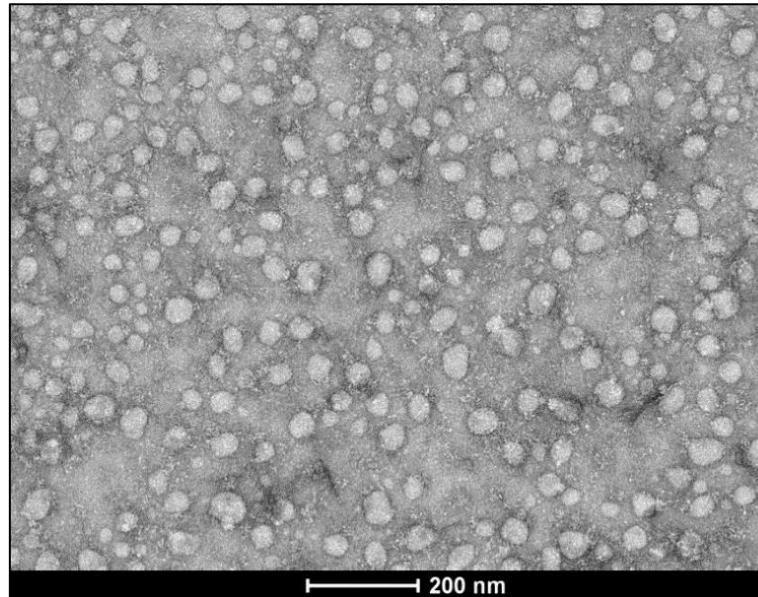


Figure 6. Image MET des NPs complexes PAA/PDADMAC produites avec le dispositif capillaire côte à côte.

Suite à l'imagerie MET effectuée sur 500 particules environ, il a été vérifié que les PEC NPs produites avaient une taille nanométrique de l'ordre de 60 nm en moyenne, étaient étroitement distribuées (PDI = 0.15) et de forme quasi sphérique. Une seule couleur observée par TEM était un signe de matériau PEC.

Dans l'ensemble, ce travail a proposé de mettre en œuvre un dispositif capillaire côte à côte pour fabriquer des PEC NPs dans un processus continu sans tensioactif en une seule étape. Il a permis de fabriquer des PEC NPs de différents matériaux plus rapidement que les méthodes d'émulsion conventionnelles. A l'avenir il semble possible que ces PEC NPs puissent encapsuler une molécule d'intérêt pour différentes application.

3 Conclusion

Au cours de cette thèse, des nanoparticules polymères pour l'administration de médicaments ont été produites en une seule étape par différents procédés d'émulsification. L'émulsification microfluidique à flux élongationnel s'est avérée être une méthode efficace et reproductible pour la

fabrication de PNPs avec une dispersion de taille faible et une taille contrôlée et ajustable. Des PNPs de morphologies originales à base de polyélectrolytes ont également été élaborées, telles que des PNPs PMMA-PSS de type Janus de taille inférieure à 200 nm. On peut conclure que les méthodes microfluidiques offrent des voies intéressantes pour comprendre et contrôler les propriétés des PNPs. Une nouvelle méthode plus efficace de fabrication de PNPs, où des PNPs complexes de taille comprise entre 50 à 100, fut également développée. L'influence de la structure du polymère, de son poids moléculaire mais également des débits microfluidiques a été étudiée et a révélé la possibilité de produire une large gamme de PNPs et DNPS aux propriétés et morphologies variables et ajustables. Ce travail ouvre ainsi des perspectives innovantes pour la conception de systèmes de libération contrôlée de médicaments.

4 Références

- [1] Ding, S., Serra, et al., 2019a. Production of dry-state ketoprofen-encapsulated PMMA NPs by coupling micromixer-assisted nanoprecipitation and spray drying. *Int. J. Pharm.* 558, 1–8. <https://doi.org/10.1016/j.ijpharm.2018.12.031>
- [2] C. A. Serra et al., “Coupling microreaction technologies, polymer chemistry, and processing to produce polymeric micro and nanoparticles with controlled size, morphology, and composition,” *Macromol. React. Eng.*, vol. 7, no. 9, pp. 414–439, 2013, doi: 10.1002/mren.201300101.
- [3] I. U. Khan, C. A. Serra, N. Anton, and T. F. Vandamme, “Production of nanoparticle drug delivery systems with microfluidics tools,” *Expert Opin. Drug Deliv.*, vol. 12, no. 4, pp. 547–562, 2015, doi: 10.1517/17425247.2015.974547.
- [4] W. Yu et al., “Development of an Elongational-Flow Microprocess for the Production of Size-Controlled Nanoemulsions” *Macromol. React. Eng.*, vol. 11, no. 1, pp. 1–10, 2017, doi: 10.1002/mren.201600025.
- [5] M. Vauthier and C. A. Serra, “One-step production of polyelectrolyte nanoparticles,” *Polym. Int.*, vol. 70, no. 6, pp. 860–865, 2021, doi: 10.1002/pi.6178.
- [6] J. Abdurahim, C. A. Serra, C. Blanck, and M. Vauthier, “One-step production of highly monodisperse size-controlled poly(lactic-co-glycolic acid) nanoparticles for the release of a hydrophobic model drug,” *J. Drug Deliv. Sci. Technol.*, vol. 71, no. May, p. 103358, 2022, doi: 10.1016/j.jddst.2022.103358.

General Introduction

Background overview and context

Polymeric nanoparticles (PNPs) are part of nanomaterials that is intensively studied since the last decade. These are 3D nanomaterials made of polymers with all three dimensions of below 500 nm scale. PNPs are particularly interesting because of their wide range of applications due to their well-controlled composition, reactive end groups, solubility, stability, and molecular weight for tuning desired properties. PNPs can be found in agriculture, cosmetics, food, drugs, implants, and even in motor oils in car industries, etc. This is emanated from the very broad properties that polymers provide, through being tailored according to the final application.

PNPs' production can be found in a variety of methods. However, some production challenges, like limited operability, frequent clogging, bioavailability, or remarkably insufficient process yields, can be frequently found, making it difficult to achieve the requested material properties. To fulfill the final products' requirements, these methods are generally classified into several groups according to their i) number of production steps, ii) chemical synthesis routes, iii) processes employed, iv) process conditions, v) application field and/or vi) biocompatibility. The majority of multi-step batch processes to fabricate PNPs are well-described, however, microfluidic mixing has recently attracted the major focus of researchers since it allows producing PNPs in one-step continuous production, and fulfills all the listed requirements. Also, there is an increased interest in developing environmentally friendly processes in last few years, which makes some methods eventually fade away.

In this context, the present PhD thesis is dedicated to studying and developing one-step strategies for PNPs production and is supported by the French Embassy in Azerbaijan (French Ministry for Europe and Foreign Affairs). The goal is to create a wide range of products and properties as well as to develop eco-friendly and more efficient processes to provide PNPs. To achieve this, firstly, the literature on PNPs, and their most recent fabrication methods are deeply studied. Following these studies, all the main fabrication methods that are widely used are classified into two design groups: i) emulsion-based fabrication design, and ii) non-emulsion-based fabrication design. Here, an emulsion is a dispersion of two immiscible liquids, such as water and oil. A good example of an emulsion can be mayonnaise, where oil is mixed with vinegar and egg yolk (as an emulsifier). The first design includes emulsions, which are mainly produced with help of emulsifiers, and emulsification methods. Then, it is followed by solidification, and purification to achieve the final product. In the second design, some of these requirements are avoided, since in this design no emulsification methods are

involved. This may sound very promising for non-emulsion-based design, however, other disadvantages like limited encapsulation, frequent clogging, and challenges to control size and size distribution can be found being reported in the literature. In this context, we started with an elaboration of different emulsification methods to achieve monomodal biodegradable PNPs of sizes (diameters) smaller than 200 nm, to later study in drug delivery applications. Then, we modified the composition of these PNPs with the goal of i) achieving anisotropic Janus structure, and ii) understanding drug delivery properties' dependency on PNPs composition and morphology. This allowed producing PNPs with two different material properties, including anionic surface charge with hydrophilic polymer on one side, and non-ionic hydrophobic polymer on another side. Following this, we tried to replace the non-ionic side of PNPs with a cationic polymer, to achieve a Janus structure with two oppositely charged surfaces. However, all the given efforts to achieve this structure allowed producing complex PNPs *via* initially conventional methods, then with a side-by-side capillary device. Since the latter has never been used to fabricate any kind of nanoparticles before, the novelty, and efficiency of this newly developed method have attracted interest for the development of large-scale industrial applications.

This doctoral manuscript comprises five different chapters, that describe production of different PNPs on the bases of eco-friendly pre-formed polymer materials. In the following part, the general overview of each chapter is briefly described. These include a literature review, materials & methods, and three experimental chapters. In the end, the conclusion and perspectives, also scientific dissemination are given as part of this manuscript.

In **Chapter 1**, the ***state of the art*** is presented in which a review of PNPs design, types of production, post-treatment, characterization, and applications are described. All the fabrication methods are classified into two major groups emulsion-based-design, and non-emulsion-based-design. First, emulsification devices to produce PNPs are listed and compared, then other methods of producing PNPs are listed, and evaluated. A variety of emulsification processes are used worldwide to achieve PNPs, the most dominant emulsion methods are high-shear mixing, sonication, and high-pressure homogenizers, regardless of their high-level energy consumption. Other methods like nanoprecipitation, spray-drying, electrohydrodynamic co-jetting, etc. use less energy, and don't involve emulsification, however, due to insufficient production rates, these methods have limited industrialization.

In **Chapter 2**, the ***materials and methods*** used in the experimental parts of this research are delineated. Firstly, the description for solvents, polymers and emulsifiers is given. Then, three different emulsification methods; i) shear-mixing, ii) sonication, and iii) elongational-flow

micromixing are described for achieving size-controlled PNPs with a single polymer. Then, a side-by-side capillary device to produce complex PNPs is given. To better understand the produced material properties, different characterization methods are listed, and classified into i) spectroscopic methods, and ii) microscopic methods. In the end, application methods are described.

In **Chapter 3**, Poly(lactic-co-glycolic-acid) (PLGA) NPs are elaborated using high shear mixing, sonication and elongational-flow micromixing homogenization devices. Process parameters, such as rotation speed, ultrasound amplitude, flow rates, mixing element geometries, and residence time along with pre-process parameters, such as the composition, and phase ratio of the produced **miniemulsions** are assessed. The influence on the PNPs size under the changes of the different parameters is thoroughly discussed. Then, the elaborated PLGA NPs are used to encapsulate and deliver rifampicin in a weekly release study.

Chapter 4 is devoted to the depiction of single, blend, anisotropic PNPs made of different polymers in a **one-step elongational flow micromixing** device that is previously discussed in chapter 3. Using this device, first, **miniemulsions** are prepared, and then PNPs are achieved. The aim is to obtain different PNPs in a continuous flow and compare them in their carrier properties.

In **Chapter 5**, Initially, emulsions are used to achieve the designed product. Then, instead of using emulsions, PNPs are produced using the microfluidic side-by-side capillary device in a two-step process. Then, this process is developed into a one-step production process, that doesn't require emulsions. This **non-emulsion-based design** uses nanoprecipitation and electrostatic attraction forces to yield polyelectrolyte complex NPs. The effect of the flow rate along with the polymer type, molecular weight, and collecting tubing diameter on the particle properties are investigated.

Abbreviations

AC	Acrylamide
AFM	Atomic force microscopy
API	Active pharmaceutical ingredient
aPNPs	Anisotropic polymeric nanoparticles
AMB	Amphotericin B
ATRP	Atom transfer radical polymerization
BBB	The blood-brain barrier
BCS	Biopharmaceutical classification system
BSA	Bovine serum albumin
BSE	Backscattered electrons
CDCl ₃	Chloroform
C/D	Continuous to dispersed phase ratio
CTAB	Cetyl-trimethylammoniumbromide
CS	Chitosan
C16E8	Octaethylene glycol monohexadecyl ether
DCM	Dichloromethane
D/C	Dispersed to continuous phase ratio
DD	Drug delivery
DDS	Drug delivery system
DL	Drug load
DOX	Doxorubicin
DLS	Dynamic light scattering
DNA	Deoxyribonucleic acid
DNPs	Drug loaded nanoparticles
EE	Encapsulation efficiency
ENPs	Engineered nanoparticles
EOs	Essential oils
FDA	Food and Drug Administration
FTIR	Fourier transform infrared spectroscopy
GRAS	Generally regarded as safe
HF	High-frequency
HLB	Hydrophilic-lipophilic balance
HPLC	High Performance Liquid Chromatography
HPH	High-pressure homogenizer
HPIMM	High-pressure interdigital multilamination micromixer
ID	Inner diameter
MAOTIB	2-methacryloyloxyethyl (2, 3, 5-triiodobenzoate) monomer
MMA	Methyl methacrylate
MS	Microspheres
NPs	Nanoparticles
NNPs	Natural nanoparticles
NMR	Nuclear magnetic resonance
OD	Outer diameter
O/W	Oil-in-water

O/W/O	Oil-in-water in oil
PAA	Poly(acrylamide)
PBS	Phosphate buffered saline
PCL	Poly(ϵ -caprolactone)
PDADMAC	Poly(diallyldimethylammonium chloride)
PE	Polyelectrolyte
PEC	Polyelectrolyte complex
PNPs	Polymeric nanoparticles
PLGA	Poly(lactic-co-glycolic acid)
PLA	Poly(lactic acid)
PVA	Poly(vinyl Alcohol)
PEG	Poly(ethylene glycol)
PEI	Poly(ethylenimine)
PEO	Poly(ethylene oxide)
PPO	Poly(propylene oxide)
PDI	Polydispersity index
PDMS	Poly(dimethylsiloxane)
PMMA	Poly(methyl methacrylate)
PIC	Phase inversion composition
PIT	Phase inversion temperature
PSS	Poly(styrene sulfonate)
PTFE	Polytetrafluoroethylene
RMX	Reactor and mixer
μ RMX	Reactor and micromixer
RNA	Ribonucleic Acid
Rpm	Rotation per minute
RSM	Rotor stator mixer
SAW	Surface atomic wave
Sd	Standard deviation
Span	Sorbitan oleate
SDS	Sodium dodecyl sulfate
SEM	Scanning electron microscopy
TEM	Transmission
TB	Tuberculosis
TC	Temperature control
TIPS	Thermally induced phase separation
THF	Tetrahydrofuran
TPP	Tripolyphosphate
UT	Ultra Turrax
UV	Ultraviolet
WHO	World Health Organization
W/O	Water-in-oil
W/O/W	Water-in-oil in water

Chapter 1: Production process design and development of polymeric nanoparticles; state of the art

1.1	INTRODUCTION	31
1.2	POLYMERIC NANOPARTICLES DESIGN, FABRICATION, AND APPLICATIONS	32
1.2.1	Definition	32
1.2.2	Fabrication	35
1.2.2.1	Multi-step process	37
1.2.2.2	One-step process	39
1.2.3	Production design	40
1.2.4	Applications of polymeric nanoparticles	43
1.3	MINIEMULSION-BASED PRODUCTION DESIGNS	45
1.3.1	Towards polymeric nanoparticles via miniemulsions	45
1.3.2	Production techniques	49
1.3.2.1	High-energy methods	50
1.3.2.2	Low energy methods	55
1.3.2.3	Process and pre-process parameters	62
1.3.3	Theoretical aspects	63
1.3.3.1	Interfacial free energy	63
1.3.3.2	Utility of surfactants	64
1.3.3.3	Energy density and critical capillary number	66
1.4	NON-EMULSION-BASED PRODUCTION DESIGNS	68
1.4.1	List of the non-emulsion methods	68
1.4.2	Process and pre-process parameters	74
1.4.3	Theory behind the non-emulsion-based PNP formation	74
1.4.3.1	Diffusion-advection relations by Peclet number	74
1.4.3.2	Mixing time	75
1.5	POST-PRODUCTION POSSIBILITIES WITH PNPs	77
1.5.1	Stability of polymeric nanoparticles	77
1.5.2	Drug release studies	77
1.5.3	Safety of polymeric nanoparticles	79
1.6	CONCLUSION	80
1.7	BIBLIOGRAPHY	81

Chapter 1

Production process design and development of polymeric nanoparticles; state of the art

1.1 INTRODUCTION

Nanoindustry is one of the fastest growing industries since many international nanotechnology programs started in 2000th years, which involved more than 60 nations worldwide [1]. Very significant contributions of nanotechnology can be found nowadays in multidisciplinary research fields for human flourishing [2], expected to reach a market capitalization of \$0,1 Trillion by 2025 [3]. In a variety of sectors, including adhesives [4], agriculture [5], medicine [6]–[8], cosmetics [9], electronics [10], food technology [11], textiles, and bioengineering [12], nanoparticles (NPs) are of great interest with a wide range of available properties [13]. For example, in medicine over 25 nanotechnologies were approved by Food and Drug Administration (FDA), and 45 were going through trials on the clinical landscape with the goal of increased biocompatibility, therapeutic action followed by reduced dosage, and side effects, especially for patients with reduced metabolism [14]. In food industries, nanotechnologies are essential to improve absorption for masking, maintain controlled release of vitamins, minerals to deliver these ingredients to the food matrix, and parallelly protect the encapsulated substances [3]. Until less than a decade ago, it was believed that NPs reduce drug toxicity and side effects but researchers then realized that, in some circumstances, these NPs can impose risks by themselves. For instance, only 5 years ago 10 nm silver nanoparticles were found to be one of the most toxic materials in the liver due to an ionic silver that occurred during the treatment, however, these NPs were one of the most widely used nanomaterials in consumers products like food, several decades before until this information was revealed [15]. In another study, one of the FDA approved medical nanotechnologies, superparamagnetic iron oxide NPs were recently found to undergo Haber–Weiss and Fenton reactions during the therapy in the human body where free Fe^{2+} ions interact with cell powerhouse by altering its DNA and causing genotoxicity or cellular inflammation. These NPs were recently eliminated from the list of approved medical nanotechnologies by FDA following the recent studies, after multiple years of use in medicine [16]. Also, many diseases that require a specific drug for effective treatment cannot be treated due to limited clinical use such as crossing a blood-brain barrier in the brain [17]. The major strategy to avoid these reverse NP functioning can be in the proper production design, methods, and materials

to achieve the needed properties like improved bioavailability, and reduced material quantity involved to achieve the goal [18], [19]. Above all NPs, polymeric NPs (PNPs) are particularly interesting because of their well-controlled composition, reactive end groups, solubility, stability, molecular weight for tuning desired properties, and most importantly their facile fabrication [20], [21]. For example, chitosan NPs were successfully used to safely pass the blood-brain barrier and rapidly deliver an active pharmaceutical ingredient directly to the brain [6], [22]. To produce these PNPs, the batch methods were well-described, however, microfluidic mixing was able to attract the major focus of researchers [18], [23] since the production challenges such as limited operability, frequent clogging, bioavailability, or remarkably insufficient process yields, can be avoided through a proper production design that provides an improved mixing [23], [24].

1.2 POLYMERIC NANOPARTICLES DESIGN, FABRICATION, AND APPLICATIONS

1.2.1 Definition

PNPs are solid-state nanomaterials in the range of 1–500 nm in size made of polymers [24]. These nanomaterials can appear in the form of natural nanoparticles (NNPs) or engineered nanoparticles (ENPs) [5], [25]. NNPs are generally formed during natural combustion, corrosion, or wear processes, while, ENPs don't appear naturally, and are human-made nanomaterials, thus, purposefully fabricated for targeted applications [4], [26]. Recently, many nanomaterials made of polymers such as PNPs [27], [28], polymer micelles [29] or dendrimers [30], and polymersomes [31] have been developed. The reason for the growing interest in PNPs evolves from their improved properties at the nanoscale, in their tiny size polymeric materials are refashioning their physicochemical characteristics, eventually inaugurating the advantages of nanotechnology [10]. Bulk counterparts of these polymeric materials completely differ in the means of physico-chemical, optical, mechanical, electrical, and magnetic properties [13], [23], [32] due to their small size and large surface area, and improved surface chemistry and reactivity. PNPs' physicochemical properties can be particularly dependent on structural morphology [33]. The properties of the produced PNPs are also designed according to specific requirements by selecting the type of materials, and fabrication methods that are suitable [27]. These aspects lead to a wide range of possible applications from foods [11], [34], cosmetics [9], [35] medicine [8], agriculture [5], vehicle components [36], electronics [10], etc. Thus, the very first PNPs with approximately 80 nm size were developed in a multi-stage micelle polymerization of acrylamide monomer in aqueous solution in the 1970s [37], as they started attracting the attention of many researchers [38]–[40]. Later, flower-like charged poly(methyl

methacrylate)-based NPs were produced [41]. Anisotropic polymeric NPs have been produced in a multi-step process by Rahiminezhad *et al.* [42].

The possible control over properties like morphology, functionality, size, size dispersity, surface charge, and in some cases anisotropy structure shows that PNPs are promising materials having possible bioavailability, biostability, and stability [27], [43]. For instance, it has been accepted that PNPs are promising for the treatment of major diseases through having a window for therapy, improved drug pharmacokinetics, biodistribution, and also imaging [23]. Simultaneously, translation of PNPs into the clinic is remaining challenging due to the limited availability of facile production methods that are consistent, and sufficient in quantities. Some technologies are promising to address these challenges by accelerating the clinical translation of PNPs [18], [19] such as microfluidic precipitation to produce ligand-terminated poly(lactic-co-glycolic acid-co-ethylene glycol) nanoparticles able to target the prostate-specific membrane antigen on prostate cancer cells [23].

In the literature, morphology of PNPs can be found analyzed by TEM and AFM techniques to confirm the particle's size distribution and shape. In some studies, produced PNPs were passed through dialysis to purify sample before the analysis [44]. For example, to maintain a sustained release of an antibiotic, Vancomycin-loaded N-trimethyl chitosan NPs showing an average diameter of 220 nm and an apparent Zeta Potential of +15 mV (DLS reports) were prepared by ionic complexation, and then analyzed with two different techniques (Figure 1.1) [45].

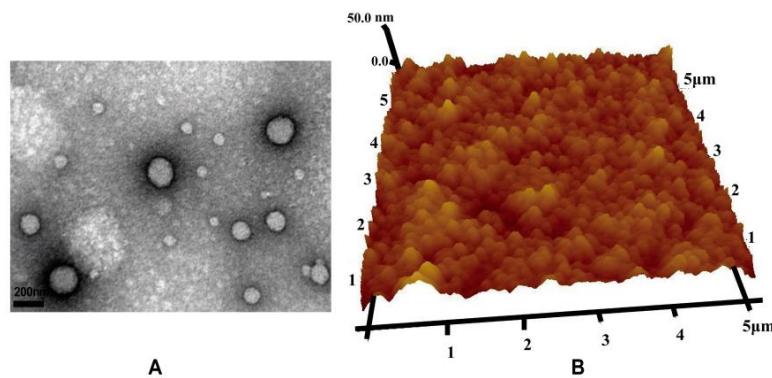


Figure 1.1. Morphology of Vancomycin loaded N-trimethyl chitosan NPs. (A) TEM image; and (B) AFM image in contact mode [45].

Methyl substituted ladder-type poly(*para*-phenylene) NPs at 150 nm diameter size together with different soluble derivatives of polyfluorene were produced by ultrasound emulsification and evaporation process in the presence of SDS at different (0,6%-1,8%) concentrations to stabilize the system (Figure 1.2).

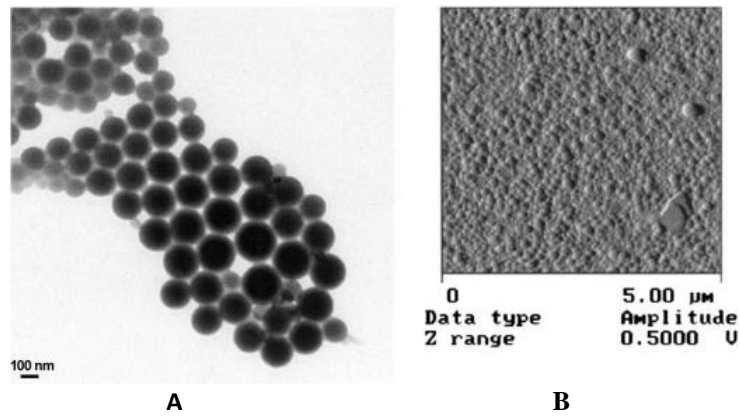


Figure 1.2. Morphology of Methyl substituted ladder-type poly(*para*-phenylene) NPs. (A) TEM image; and (B) AFM image in tapping mode [46].

Morphology of the produced semiconducting PNPs was observed by TEM and AFM techniques (Figure 1.2) [47], [48].

In another study, PNPs were produced via hydrodynamic flow focusing nanoprecipitation, and produced PLGA-PEG NPs were characterized with the electron microscopy by showing spherical corona structure [49].

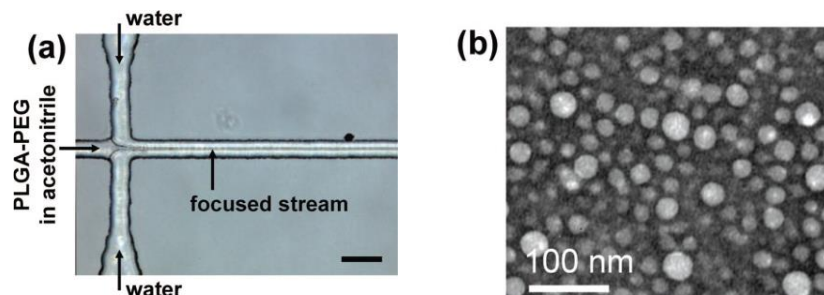


Figure 1.3. A microfluidic device for hydrodynamic flow focusing nanoprecipitation (a) of polymeric NPs in water (scale bar = 50 μm), view of produced PLGA-PEG nanoparticles captured by TEM of (b) [49].

This type of microfluidic device can be fabricated with poly-dimethyl siloxane (PDMS) for achieving a hydrodynamic flow-focusing nanoprecipitation with the organic solution of the polymer (Figure 1.3.a). To achieve the formation of the PLGA-PEG nanoparticles in this device, the total volume of the outlet acetonitrile and water stream solution was kept at around 5 $\mu\text{L}/\text{min}$, thus, the collected samples were imaged after dispersing in water. Following the staining of the hydrophobic PLGA core in uranyl acetate, while the hydrophilic PEG groups did not, spherical NPs of around 50 nm diameters were observed under electron microscopy (Figure 1.3.b) [24], [49].

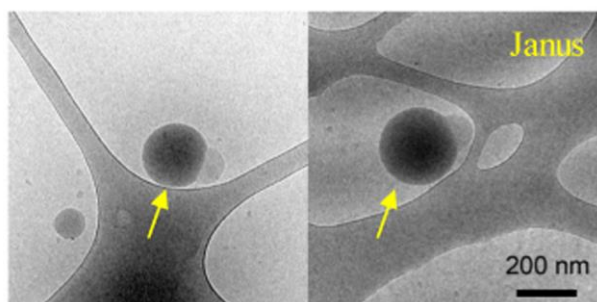


Figure 1.4. Cryo-TEM characterization of the Janus PNPs obtained with the elongational-flow micromixing method [27].

Janus-type biodegradable PNPs having a diameter of below 200 nm produced by the emulsification-evaporation method were characterized by TEM (Figure 1.4). Here, the ethyl-acetate solution of PLGA and PSS was emulsified with surfactant aqueous solution by using the elongational-flow micromixing technique. Following the evaporation of the solvent Janus-type PNPs were observed under microscopy [27].

In general, the polymer dispersions can be obtained either by the polymerization of monomer droplets or following solvent evaporation or solvent diffusion methods with pre-formed polymers, where latex starts forming inside a droplet of the preformed polymer [24], [27], [46]. Moreover, the size, shape, and crystallinity of a material can vary according to the method used and process conditions such as residence time, feed volume ratio, concentration, and process parameters like temperature, pressure, flow rate [33], [50]. In this context, important fabrication methods allowing to control material parameters, also methods that allow PNP fabrication with polymerization or with pre-formed polymers are described in the next part.

1.2.2 Fabrication

Considering the daily emerging, wide range of PNP applications, there is a huge demand for cost-effective, environmentally friendly, fast, and reproducible fabrication approaches [33]. Most of the conventional methods, such as shear-mixing or ultrasonic homogenization, are applicable today [51], [52], however, they mainly lead to limited control within multistage non-continuous fabrication involving high heat emissions, energy and material loss, long cleaning procedures, poor compatibility accompanied by organic solvents, and lack of reproducibility [53]. Fabricate materials having geometries at nano-range can be achieved through different approaches like bottom-up [54]–[56], where the complex structure formation on molecular or atomic scale is maintained, or top-down [10], [33], [57], where bulk materials are processed by breaking down into small pieces. This can be achieved also by using lithographic techniques such as X-ray, etching, and techniques where particles

can get cut, milled, and shaped, such as mechanical, thermal, and electrochemical treatment to produce NPs [41].

However, PNPs are generally produced on small scale and it is difficult to shift to scale up the processes [24], [33]. This is why, in industries, PNPs are usually fabricated through the chemical growth of molecules and clusters, which is also referred to as the bottom-up method. [24], [33]. This method can be divided into two steps of (i) nucleation and (ii) growth [24], [33], [41]. The starting materials precipitate in solution during the first nucleation phase, then, the chemical reaction occurs when nucleation stops by reaching its supersaturation state. Finally, in the growth stage, the solute particles aggregate to form NPs with desired properties controlled by the temperature, the pressure, the polymer molecular weight, and the solubility, for instance. To maintain well-controlled nucleation and growth of PNPs, it's extremely important to have a uniform fabrication environment and conditions [41]. In this context, to achieve rapid and uniform mixing while maintaining control over heat, temperature, mass, and pressure, Kolishetti's [23], Serra's [24], and Amreen's [33] teams recently proved the power of microfluidic devices to design PNPs. More recently, It has also been suggested that assembling different materials can generate a new physicochemical property, such as an anisotropy driven by two different polymers showing different material natures like hydrophilicity or a surface charge for instance [27], [41].

As we mentioned in the introduction part, several methods are available for PNPs fabrication on both laboratory and industrial scales: considering the materials' future applications, requested properties, and logistics. In general, we divided these techniques as (i) heterogeneous polymerization-based methods, which can be either in emulsion or in suspension, such as a reversible addition-fragmentation chain-transfer polymerization [58], and (ii) non-synthetic methods, requiring a bulk of preformed linear polymers, such as solvent-evaporation emulsification, diffusion and displacement or nanoprecipitation [53]. Nanoprecipitation is well-known as one of the non-synthetic methods, used for instance by Wallyn *et al.* to elaborate poly (ethylene glycol) PEGylated PNPs [43]. Materials such as PEGylated polymers and surfactants, enable the formulation to target tumor cells by incorporating these materials into the PNP surface to protect an encapsulated ligand against antibodies. This conjugation can be employed for a specific tumor cell targeting application with an active targeting ligand like Dexamethasone [20]. They first prepared the iodinated homopolymer through the radical polymerization of the 2-methacryloyloxyethyl (2,3,5-triiodobenzoate) monomer (MAOTIB) with 62 wt% iodine content in DCM solution with, then DCM was removed before dissolving a powder of prepared polymer into THF as a good solvent and forming hydrophilic poly(MAOTIB) NPs by dropping method in PEGylated stabilizer ethanol solution under 500 rpm stirring. Some PNPs' production techniques without emulsification were reported as spray-drying, extrusion/spherization, or prilling, however, the majority of PNPs pass through the emulsification

step [19], [53]. As a definition, an emulsion can be defined as a biphasic system consisting of two immiscible liquids, with one of them being dispersed as small spherical droplets distributed in the other liquid [59]–[61].

Because emulsions are thermodynamically unstable systems and are quite open to destabilization, it was suggested that the incorporation of essential oils (EOs) can potentially yield a much more stable system, especially for encapsulation in medical and food industries, where a long-term miniemulsion stability is requested [11], [62].

Overall, there are numerous ways to fabricate PNPs, and it's possible to classify these fabrication methods according to the number of production process steps required for achieving needed material properties. These production processes can be divided into two classes as multi-step processes [63], and a single-step process [64].

1.2.2.1 Multi-step process

Two-step or multi-step is the number of production steps that are involved in the fabrication of any product and they are mainly considered while shifting to large-scale material production, and estimating the production costs. In previous studies, the majority of PNPs' fabrications contain at least two steps [44], [63], [65], [66]. For example, it's almost a century since the very first multi-step emulsification process design for double emulsions (also referred as emulsions of emulsions) was introduced, however, it was highly unstable, and rapidly phase separated [67]. Regardless of the instability challenges of the final product, following thirty-five years of intensive research, it was finally possible to encapsulate insulin by this multi-step process [24], [31], [68]. In a recent study, high-molecular weight chitosan dissolved in a sodium acetate-acetic acid buffer (pH 4.0) and paraffin oil containing sorbitan oleate (Span80) were emulsified by stirring to produce a polydisperse emulsion of around 1 μm size, then this emulsion was sonicated in the second step to reduce the droplet size and polydispersity index (PDI) value before the solvent removal step to achieve CS PNPs [69]. Sonication was mainly used in order to produce miniemulsion, and reduce the PNPs size. For instance, a two-step ultrasonication process was used to prepare water-in-DCM-in-water double-emulsions resulting in poly(lactic acid) (PLA) NPs of 200 nm diameter size dispersed in water [31]. These PLA NPs were developed to encapsulate and release hydrophilic ingredients like protein and peptides, where these molecules were first entrapped in water droplets surrounded by the hydrophobic polymer matrix and dispersed again in water. Fabrication of double-emulsions using PNP inside the middle phase (colloidosomes) can also be referred to as multi-step production [47], [70]. We can also cite poly(ϵ -caprolactone) (PCL) NPs fabrication through emulsification in the presence of 0,5 % w/v polyvinylalcohol (PVA) in water [71]. Here, two-step ultrasound emulsification

was used to fabricate PCL NPs in the water. This was achieved by first emulsifying water phase with PCL solution in dichloromethane (DCM), then in the second step, emulsifying the produced emulsion with PVA aqueous solution to finally yield PNPs following the solvent evaporation for potential drug delivery (DD) applications [71]. To improve the chemical stability of drugs, a natural polysaccharide, arabinogalactan was modified by folic acid and methotrexate by reaction under stirring in a multi-step process including extensive dialysis, then, in an additional step, this product was used to fabricate PNPs for cancer cells targeting [53], [72].

PNPs can also be produced in a microfluidic continuous-flow process consisting of several production steps including polymerization [53]. An example of multi-step microfluidic fabrication of 100nm PNPs can be given where methacrylic (co)monomers, catalyst, and initiator in a solvent were pumped into a thermoregulated tubular microreactor and polymerized by atom transfer radical polymerization (ATRP) following microfluidic emulsification process [50].

In some scenarios, multi-step processes can provide a specific structure that is challenging, or nearly impossible to achieve in a single step [42]. A good example of this is the three-step PNPs (230 nm poly(tri(propylene glycol) diacrylate-co-methyl methacrylate) NPs) encapsulated inside 300 μm poly(acrylamide) Janus microparticles by microfluidic approach (Figure 1.5) in 2017 by Yu *et al.* [19]. In this preparation, UV polymerization was used first in nanodroplet polymerization, and the second time in microparticle polymerization to achieve spherical polymeric microparticles with two different material properties on their surface [19]. In another similar study, nanoemulsions were first prepared by elongational-flow micromixing method followed by the UV or thermal polymerization of acrylamide (AC) in water containing a water-soluble photoinitiator, crosslinker to yield nanosuspension in polydimethylsiloxane (PDMS). Then this nanosuspension was purified and dispersed into water with again a monomer, photoinitiator, and crosslinker to be the inner phase of microfluidic capillaries-based droplets. The droplets in capillary device were formed due to a shear force induced by highly viscous PDMS as the continuous phase. After one more polymerization step, polymeric microparticles containing thousands of PNPs were characterized [19].

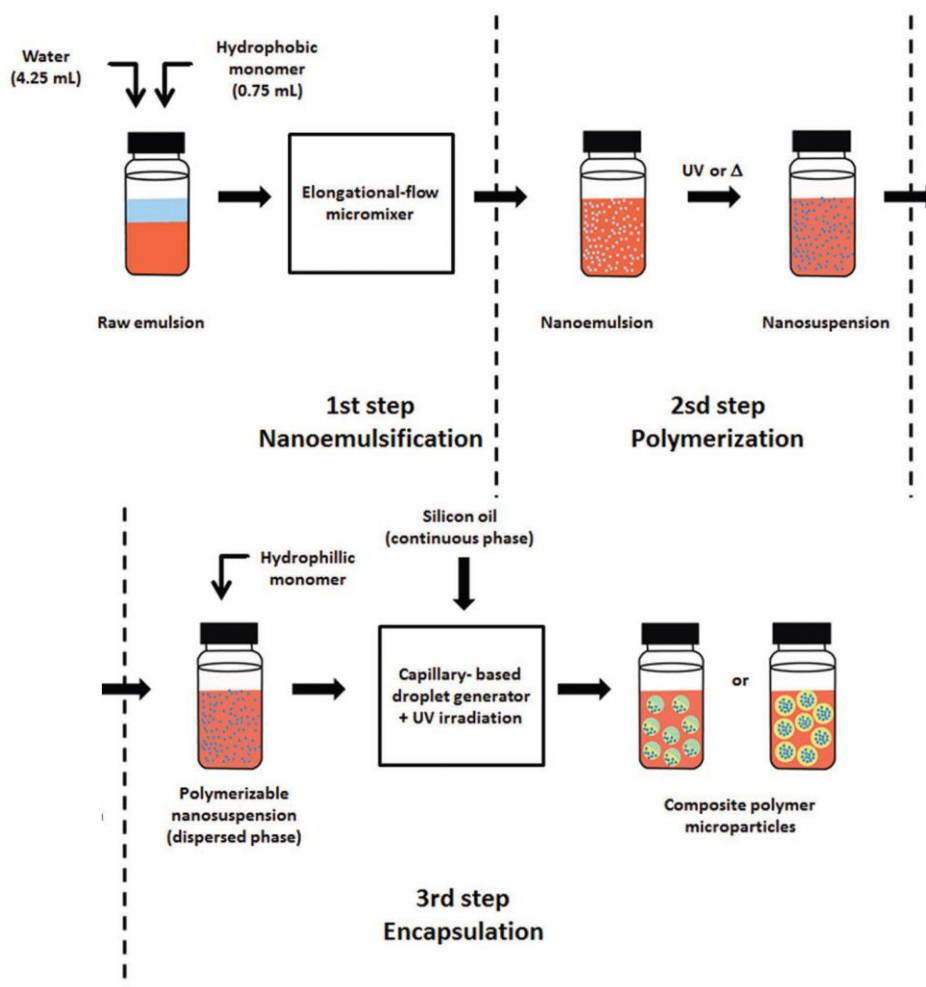


Figure 1.5. The three-step microfluidic fabrication of PMMA NPs encapsulated inside microparticles [19].

The described methods in this part consisted of more than one process steps. However, in order to limit the possible material loss or contamination during each step, it could be interesting to develop one-step methods.

1.2.2.2 One-step process

Even though the one-step PNPs productions are highly demanded due to their efficiencies, it has been reported in the literature that PNPs' diameter and size distribution control is a challenging task, especially in bottom-up approaches, which was popularized by Eric K. Drexler in the 1980s by positioning reactive molecules with atomic precision for chemical reactions [57]. To maintain well-distributed NPs' size, the process parameters like residence time, flow rate, energy dissipation, material concentrations, solubilities, viscosities, and ratios have to be precisely monitored. In this context, one-step processes are faster and more efficient to produce a certain material, however, these processes require a precise control over all the chemical and physical forces occurring at the

nanoscale to build large structures based on single atoms or molecules of materials that co-exist in a single system [24], [33]. For instance, to prepare water-in-oil emulsion for encapsulating hydrophilic molecules inside Chitosan NPs, the paraffin oil was emulsified with polymer solution in the presence of a more lyophilic surfactant (sorbitan oleate). Emulsification of two immiscible phases was realized by using the stirring method at 500 rpm with a mechanical stirrer. The product of this single-step process was larger than 1.5 μm and highly polydisperse (PDI = 1), and required an additional step to reach a nano range [69]. By using microfluidic devices the particles' size and PDI appears to be much easier to control in a single step [18]. The *in-situ* nanoassembling can be also an example, which was used to produce flower-shaped PNPs around 300 nm [41], also Janus polymeric microparticles [24] in a single-step. In 2021, Vauthier *et al.* demonstrated the possible way to fabricate Janus and core-shell PNPs having a chemical anisotropy property in single-step process, thanks to the elongational-flow micro-mixing method [27].

1.2.3 Production design

PNPs are nanomaterials made of polymers that are widely used in different fields. These NPs demonstrate all three dimensions below 500 nm scale [13], [18], [73]. Considering these tiny geometries, PNPs require a specific production method. In previous reviews, PNPs are classified according to the number of steps required to produce them [24] and/or their physical, physicochemical, and chemical preparation methods [10]. Here, considering the production methods, we classify them into two different classes: miniemulsion-based design and non-emulsion-based design. These designs include a variety of production equipments, like specific devices, power density, geometries, employed in different methods to fabricate PNPs. Some devices can be employed to fabricate PNPs with both designs. For example, microfluidic tools can be used to operate in both mini-emulsion-based and non-emulsion-based designs [19], [53]. The advantages of microfluidic techniques are numerous and include a continuous production process, small and controlled reagent consumption at 1 – 10⁵ μL range, laminar flow based on a small Reynolds number [74], rapid mixing time, high operability, etc. [18]. For example, it is possible to use monomers and polymerize them to yield PNPs in continuous microfluidic production with emulsification [50], and non-emulsion methods [75]. While designing the production, it can be necessary to consider the process yield to compare different approaches. The process yield is simply a ratio between the particle's weight and the weight of the total components. It is the percentage value of a produced material fulfilling the designed material properties. The process yield is more frequently referred to while studying the methods for shifting to the industrial production scale, however, can be helpful to compare different fabrication methods.

Miniemulsion-based design

All the methods requiring an emulsification step in PNP fabrication are classified as the methods of the miniemulsion-based fabrication design. In this design, the particles are generated through homogeneous, micellar, and coagulative nucleation. Here, the particle's size and the number of particles that are formed during the process, are affected by the physicochemical nature of the initial materials used to develop the system [41], [53], [76]. For example, miniemulsion-based design can require specific emulsifier to insure stability [11], [77], and polymers can be found in both the aqueous and oil phases of miniemulsions [8], [19], [26]. Double emulsions (emulsion of emulsions) require more attention where flocculation and coalescence can easily disturb the system [31], [47]. When using miniemulsions, one of the key advantages can be shown as the number of particles (N_p) being controlled [76], such as in the elongational-flow emulsification method [19], [27].

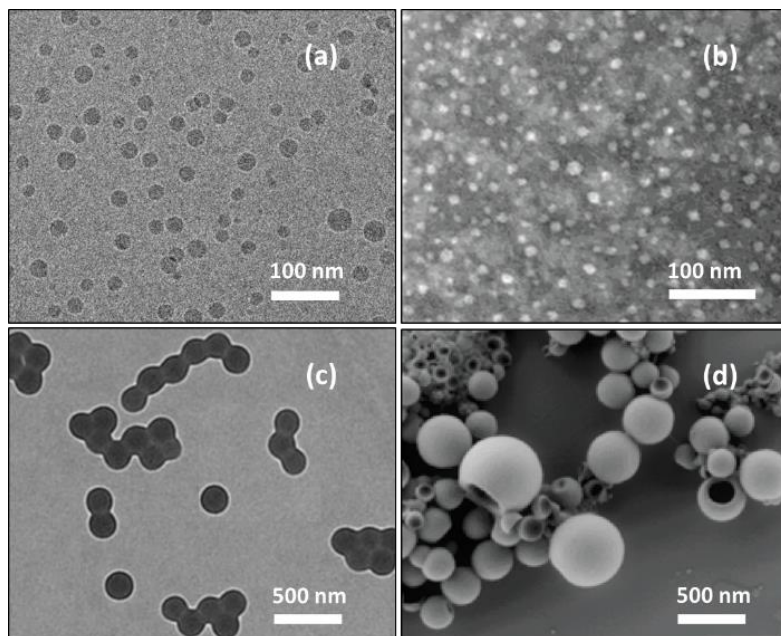


Figure 1.6. Images of PNPs produced by following emulsion-based designs (a) Poly(ethyl acrylate) NPs [78], (b) PEI-PAA NPs via emulsion-polymerization method [79], (c) PLA NPs [80], (d) PMMA NPs via emulsion-evaporation method [81]. PNPs produced with monomers (a, b) and with pre-formed polymers (c, d) solubilized in dispersed phase before emulsification process.

In miniemulsion-based designs, it's possible to directly form PNPs from monomers that the dispersed phase contains followed by polymerization, where the solvent evaporation is not mandatory, however, an excessive and multi-step purification is required to eliminate toxic and unreacted chemicals from PNPs (Figure 1.6.a, 1.6.b). Another method of fabricating PNPs by emulsion-based design is emulsion-evaporation, here a preformed polymer is dissolved in the dispersed phase followed by one of the solvent removal approaches [24], and PNPs fabricated by this approach

(Figure 1.6.c, 1.6.d) can either be directly applied or followed by a mild purification step to remove surfactant (if required).

Non-emulsion-based design

Methods in the non-emulsion-based design neither follow the specific solvent immiscibility property nor the emulsification process. Methods like diffusion and convection nanoprecipitation [50] refer to the diffusion of polymer solvent into miscible polymer non-solvent. This is different from emulsion methods, where two phases are supposed to be immiscible (for instance, cyclohexane and water) or partially miscible (ethyl acetate and water) [24], [82].

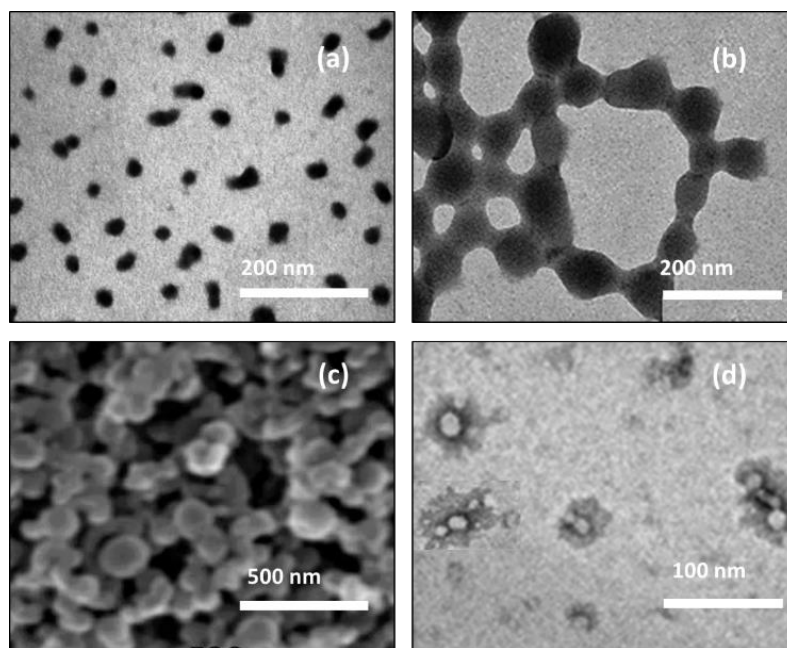


Figure 1.7. Images of PNPs produced by following non-emulsion-based designs (a) CS-PEG NPs [6] via ionic gelation, (b) CS-PMAA via polymerization [83], (c) PMMA NPs [84], and (d) Eudragit RS100 NPs via microfluidic nanoprecipitation method [85]. PNPs produced via synthetic methods (a, b) and with pre-formed polymers (c, d) solubilized in a polymer solvent before nanoprecipitation in a polymer non-solvent.

In non-emulsion-based design there are two classes that can be found to fabricate PNPs. These are the methods where a chemical synthesis like ionic gelation or polymerization is involved (Figure 1.7.a, 1.7.b). In the second class, no chemical reaction is taking place (Figure 1.7.c, 1.7.d). Nanoprecipitation can be realized by using impact-jet micromixers to fabricate drug-encapsulated PNPs [53], [84]. Initially, non-emulsion-based design can stand highly promising for involving less complex and efficient methods, however, it can be very challenging to control the mixing parameters of the two phases to form narrowly distributed PNPs [24].

1.2.4 Applications of polymeric nanoparticles

Since the early 1990s, drug deliveries have been widely developed through NPs [86], [87]. When compared to liposomes, PNPs are found to be more reproducible, stable, and more convenient for material surface modification, and to have better release properties. They can be categorized into two: nanospheres and nano- or micro-capsules. Here nanospheres are “matrix type,” where all the drug molecules are distributed throughout the matrix, differently from microcapsules, where drug molecules are located in a core, surrounded by a polymer shell [87]–[89]. PNPs made of PLGA-PEG diblock copolymer are an effective carrier for docetaxel hydrophobic drug, which is noncovalently encapsulated and released from the PNPs [84]. By using the ionic gelation method, Chitosan-PEG, Chitosan-PEG-Biotin, and conjugated NPs are produced with sizes of around 300 nm for encapsulation and release applications [6], [12], [90].

Produced PNPs, especially engineered ones can be applied in a variety of applications in food industries to protect and prolong the lifetime of products like fruits, cheese, and meat [11], [87], in the cosmetic industry to encapsulate and deliver biocompounds at high efficiencies [9], [35]. These ingredients include curcumin, polyphenols, β -Carotene, essential oils, etc. [52]. In vehicle manufacturing, nanocomposite materials are made of polymers, also for car engines, PNPs provide excellent boundary lubrication performance for low-viscosity engine oils [12], [25], [36]. Before diving into the applications some PNPs are required to be separated from their suspension and dried into powder form. PNPs produced with preformed polymers by emulsification method are going through solvent removal either by evaporation or diffusion [24]. To avoid solvent evaporation, nanoprecipitation can be used to fabricate PNPs for suitable applications [84].

PNPs' size is important for the circulation half-life, biodistribution, and cellular uptake, particularly in DD [24], [88]. The advantage of PNPs for the last application is to adapt the PNPs' formulations to control drug release depending on a requirement such as a rapid or interrupted release within several hours, or a slow release up to a month [53]. The need for drug encapsulation is emerged on the bases of the therapeutic amount of drug required to treat a specific kind of disease in an organ without leaving a harmful side-effect on other organs. For instance, an increased dosage due to the limited targeting will both favor the side effects, and increase the treatment costs, however, through encapsulation of a drug, the exposure of other organs to undesired biocompounds can be reduced, as Paul Ehrlich predicted a century ago, the increased amount of a drug was accompanied by undesirable effects on the rest of the body [53]. In another study, to reduce the number of injections during prostate cancer treatment, and improve drug targeting, cisplatin and docetaxel are co-encapsulated in a blend of PLA and PLGA-PEG NPs with reactive hydroxyl functional groups. The

surface functionalization by using the A10 RNA aptamer is maintained on the PNP surface by using the microfluidic approach to play the role of binding PNPs to the prostate-specific membrane antigen in the next steps. PNPs of 100 nm are produced by adding the functionalized polymer solution dropwise into the water phase, and then the drug release is studied. PNPs are able to deliver both cisplatin and docetaxel simultaneously within 3 days (Figure 1.8), and this approach can also be applied in solid tumor targeting of breast or lung cancers [23] [90].

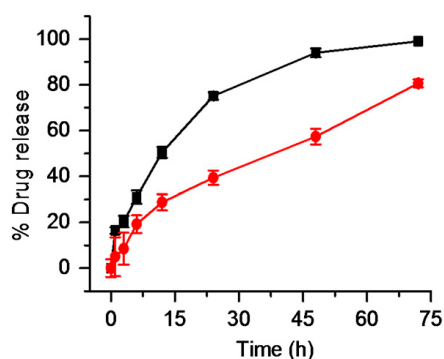


Figure 1.8. In vitro release study of prodrug (red circle) and docetaxel (square) encapsulated in PNPs within three days under sink conditions (PBS at 37 °C) [23].

Derivatives of polylactide (PLA) having pendant hydroxyl groups are prepared, then conjugated to a platinum (IV) prodrug. Following this, 80% encapsulation efficiency (EE) at 1% initial docetaxel load is achieved. The release of docetaxel from biodegradable PNPs is studied under sink conditions showing approximately 90% release (Figure 1.8) within 3 days [23]. Chitosan NP [90], which is a cationic polysaccharide in nature, is used to efficiently transport the inhibitor. To deliver the caspase-3, the chitosan NPs are coated with caspase-3, the requested ingredient, and also with monoclonal antibodies, to facilitate the delivery across the blood-brain barrier [91]. It is demonstrated that after the PNPs injection into a mice, it takes only 10 minutes for PNPs to enter the brain parenchyma to deliver an active pharmaceutical ingredient (API) [22]. PNPs made of PMMA by emulsification and polymerization method is introduced for applications where electrochemical interactions and also encapsulation of a fluorescent PNPs inside larger particles can be requested [41]. It is demonstrated that PMMA NPs can be employed to encapsulate superparamagnetic iron-oxide to produce nanohybrids for biodendrimer application [92]. Other applications like a nanocoating agent having a specific flavor or color can be found in literature. Edible enzymes, antimicrobials, or antioxidants incorporated in PNPs can be used in dairy products such as cheese, ice cream, yogurt, fruits or vegetables to protect and prolong their shelf life [11], [53].

1.3 MINIEMULSION-BASED PRODUCTION DESIGNS

1.3.1 Towards polymeric nanoparticles via miniemulsions

An emulsion can be defined as a two-phase system prepared by mixing of two immiscible liquids where one phase is dispersed within the second phase yielding a biphasic system called “dispersed phase” in “continuous phase”, or the oil in water (o/w). This can be found in a form where water is dispersed in the oil phase, referred to as w/o emulsions. In emulsions, to define which phase is continuous and which phase is dispersed, in 1913, Bancroft formulated the rule describing that in a hydrophilic colloid, where water phase is more than the oil phase, colloid will tend to make water the continuous phase. Oppositely, a hydrophobic colloid, where oil is more, will tend to make water the dispersed phase. According to this rule, phase which contains most of the surfactant simply becomes the continuous phase [93]. Additionally, regarding their average droplet size, emulsions can be classified into macroemulsions (>400 nm), miniemulsions (100-400 nm), also referred as nanoemulsions, and microemulsions (≤ 100 nm). Compared to macro- and miniemulsions, microemulsions are more thermodynamically stable and they can freely pass the visible light to appear translucent due to an extremely small droplet size [62].

Generally, miniemulsions can be divided into three types, these are oil in water (o/w), water in oil (w/o), and bicontinuous or so-called emulsion of emulsions, as water in oil in water (w/o/w) and oil in water in oil (o/w/o). It's been near a century since both w/o/w or o/w/o emulsions were introduced [44], [67]. Oils as soybean, sunflower, cottonseed oil, and sesame oil are digestible and widely used in production to especially encapsulate lipophilic compounds. While homogenizing the two immiscible phases containing polymer molecules, these systems do not necessarily require a typical organic solvent such as cyclohexane, acetone, or chloroform for instance, where the second phase can be replaced by edible oils like “Bixa Orellana” or “Copaifera langsdorffii” to avoid material contamination due to the solvent, or for the specific applications [94]. By using edible oils and homogenizing them several ingredients have been encapsulated such as paclitaxel, curcumin, polyenetaxel, retinoic acid including other anti-tumor drugs [86], and studies of entrapping essential oils, nutrients, etc. can be found reported [87].

In emulsions, the dispersed phase can be imagined as separate spherical droplets conserving their individuality throughout the process, thanks to the stabilizers (Figure 1.9) [76]. The production of these systems is fast and can be easy, however, maintaining their stability can be challenging because emulsions are thermodynamically unstable systems of two immiscible phases continuously trying to separate from each other to reach an equilibrium state [82].

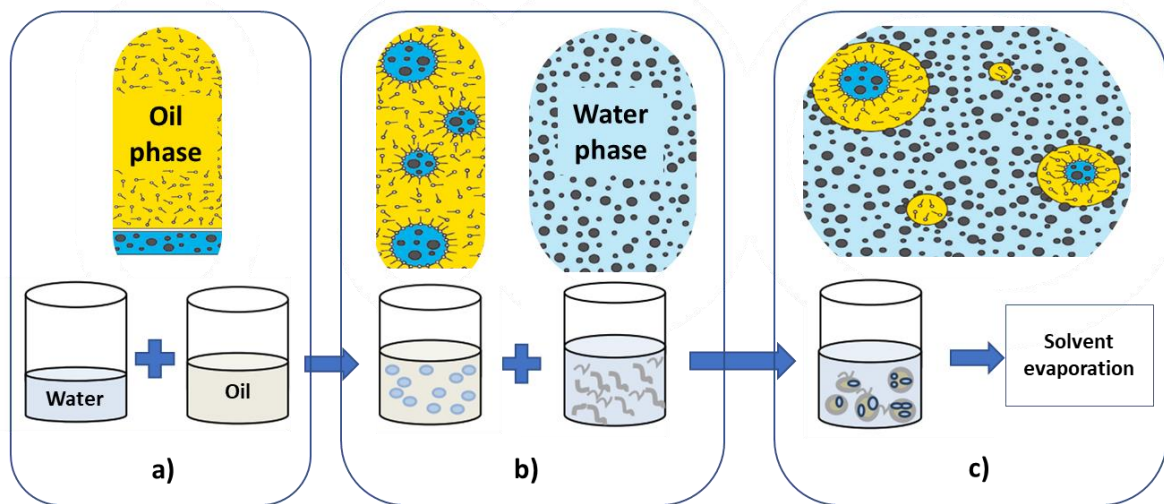


Figure 1.9. Formation steps of double-emulsion made of water and oil phases in presence of surfactant molecules in oil phase, and co-stabilizer in water phase through a) w/o emulsification, b) w/o/w emulsification, c) double emulsion evaporation. Reprinted after modifications [71], [95]

Emulsion instability is the main factor to be controlled in order to avoid the phase separation, i) during the emulsification, where the surface energy opposes the droplet break-up, and ii) after the emulsification, where smaller droplets show higher surface free energy which accelerates the formation of the larger droplets and finally phase separate. Following this, the thermodynamic instability starts to intensify under influence of an increased interfacial free energy, which indirectly leads to droplet coalescence [47], [77]. To better understand emulsion destabilization, the base w/o emulsions composed of water, sweet almond oil, and 6% v/v Span 80/Tween 80 emulsifiers at Hydrophilic-Lipophilic Balance (HLB) range of 4 to 9 were elaborated with the high-pressure homogenizer (HPH) and reported to valorize w/o emulsions made of natural compounds [96]. Stability can be reached by using additional materials like emulsion stabilizers, or surfactants, and in some scenarios, other methods or principles like the Ouzo effect [54] to reach a near-stable emulsion, and many more, detailed in Table 1.1.

Table 1.1. List of the miniemulsion-based polymeric nanoparticle fabrication methods.

PNPs	Fabrication method	Number of production steps	Advantages	Disadvantages
Janus 200 nm, ≤ 0,2 PDI [21]	Emulsification- solvent evaporation	One-step	No chemical reaction, Biodegradable nature, Anisotropy	Residual solvent and surfactant
Polycaprolactone (PCL) 235 nm, ≥ 0,2 PDI [71]	Double emulsification- evaporation	Two-steps: w/o emulsification (sonicator), w/o/w emulsification (stirring mixer) and evaporation	No chemical synthesis involved, Highly capable for maximum encapsulation	Incomplete PNPs' solidification Limited control over size and size distribution Residual impurities.
Eudragit S100 250 - 350 nm [9]	Emulsification- solvent diffusion	Two-steps: High-speed homogenization (Ultra-Turrax) and stirring for solvent diffusion	High reproducibility No chemical reaction Easy to operate	Residual solvent and surfactant High solvent consumption Poor encapsulation, large size
Eudragit L100-55 256 nm, 0,2 PDI [97]	Emulsification- solvent diffusion	Two-steps: High-frequency homogenization (Sonicator) and stirring for solvent diffusion	pH responsive drug release, no interaction between polymer and drug	Residual toxic solvent and surfactant, Additional solvent used
Polystyrene-SiO ₂ 200 nm, ≤ 0,2 PDI [98]	Emulsification- polymerization	Multi-step: High-shear homogenization, Miniemulsion polymerization, Thermal separation or calcination	High thermal and mechanical stabilities, hollow structure, no residual impurities	Chemical reaction, High temperature, Low efficiency Retained chemicals inside the PNP

PMMA, 200 nm, ≤ 0,2 PDI [41], [99]–[101]	Emulsification polymerization	Two-steps: emulsification, and mini-emulsion polymerization	Narrow size, high stability, Continuous-flow operability	Retained chemicals inside the PNP, High-shear requirement, frequent clogging
Poly (trifluoroethyl methacrylate) 270 nm ≥ 0,2 PDI [102], [103]	Surfactant-free emulsification- polymerization	High-shear homogenization, RAFT polymerization	No surfactant	Highly polydisperse and instable system Not environmental-friendly Long purification
Poly(pentaerythritol triacylate) 130-460nm, ≥1 PDI [54]	Ouzo driven self- emulsification and polymerization	One-step process: Microfluidic mixing and free-radical polymerization	Easy to implement Low energy consumption No surfactant	High solvent consumption Chemical synthesis at 60°C, Agglomeration
Eudragit S100 210 nm [104], [105]	Emulsification- salting out	Multi-step: High-shear homogenization, Salting out	Highly efficient, Easy to implement, Applicable with DNA, RNA, proteins	Intensive purification requirement, Retained salt inside the PNP

For some applications like in food industries, it's necessary to provide high emulsion stability [11], thus, several parameters are considered to maintain highly stable systems. In this context, William Seifriz introduced double-emulsions in 1925, where the oil density influence on the emulsion characteristics was also investigated. Here, an emulsion made of straw oil (having a density of 0.882 kg.L⁻¹) showed a different behavior by encapsulating smaller water droplets inside while itself being in the form of big oil droplets in water, which appeared to be the first-ever double-emulsion model [67]. However, the first time ever double-emulsion that William Seifriz demonstrated was unstable, and not applicable. This instability was due to the osmotic pressure difference based on different solute concentrations, which limited this emulsion to be applied for encapsulation. Then, it was possible to use these emulsions in drug encapsulation only after more than three decades of research [31], [47], and thanks to these studies, it's much easier to control these colloidal systems in our modern-life [31], [106]. In the literature, a T-junction microreactor can be found in a miniemulsification process of methyl methacrylate (MMA) monomer followed by the thermal

polymerization to produce 400 nm PNPs [41]. For this purpose, two immiscible phases got emulsified before polymerization by using T-junction microreactor in the presence of monomer in the dispersed phase before emulsification. Here, the aqueous phase contained the cationic surfactant cetyltrimethylammoniumbromide (CTAB) during the emulsification for generating 110 nm PMMA NPs having a positive surface charge and four different fluorescence colors. The same device was then used to achieve the continuous phase and was concentrated with polyvinyl pyrrolidone to fabricate PNPs with a flower shape and a negative surface charge [41]. The microfluidic-based device was also used to produce biodegradable Janus PNPs with a negative charge on one side, and a neutral charge in another side *via* the emulsion-evaporation method [27].

In their biomedical applications, PNPs have a huge challenge to deliver drugs having poor solubility properties while inflation hits the drug market. A drug used against parasitic infections, Daraprim, had spiked from \$14 to \$750 in the 2015 year. The price of EpiPen increased 6-folds in the 2016 year, where a full Hepatitis C treatment requires \$80,000 for a single DD with no side effects [17]. In this context, emulsification-based PNP fabrication designs can be a promising way of delivering poorly soluble materials through improved API delivery properties, and reduced production, and therapy costs [107].

1.3.2 Production techniques

Two major emulsification designs, classified according to the energy consumed during the process are known: high- and low-energy methods. High energy methods include rotor-stator mixing [82], sonication [26], high-pressure homogenization [44] [96], static mixing [108], [109] or membrane emulsification [110], [111]. It should be noted that the most referred high-energy method is the shear mixing method using rotor-stator mixers. In brief, the rotor-stators are used for the preparation of liquid-liquid dispersions of oil and water phases at rotation speeds of a minimum of 1000 rpm [112]. Several examples in industrial fields including food [51], [113], and the high-energy homogenizers to produce double emulsions in two-step processes [31], [44] can be found in the literature. Another frequently referred to high-energy method is the ultrasound method which uses ultrasound generators. These tools convert an oscillating electric field into high-energy mechanical vibrations [69], [114]. The driving force in this method is the power dissipation-induced cavitation creating bubbles that implode to generate shock waves, thus breaking the droplets [115]. For example, it was possible to reduce the size of a sunflower oil emulsion by increasing residence time, amplitude and decreasing the processing volume [26]. However, at increased emulsification time a strong heat emission can be observed, which can be considered as an undesired property for bio-applications. In low-energy methods, a process involves complex interfacial hydrodynamic

phenomena, here the process results depend on the material composition properties at a lower amount of energy input when compared to high-energy methods. The well-known low-energy methods are solvent displacement, spontaneous emulsifications, phase inversion, and the microfluidic approach [44], [62]. All the major high- and low-energy methods were investigated and discussed in detail. Following this, the high-energy methods can be found below with detailed information on working principles, efficiency, and applications.

1.3.2.1 High-energy methods

Large disruptive forces are provided in high-energy methods to reduce size of the produced material while controlling the amount of a given energy and residence time in the equipment [116].

High-pressure emulsification

In high-pressure homogenization processes, a mixture of components (oil phase, water phase, surfactant) is pushed through a small gap to prepare the emulsion at high pressure [49], [117]. This method is widely used in the food industries for high-pressure homogenization and miniemulsion production. After long-term stability tests, a part of the miniemulsion where creaming occurred was again processed by the microfluidizer to redisperse the cream layer of the miniemulsion [11]. Another good example of this method for the fabrication of emulsions can be the high-pressure microfluidic device called the Microfluidizer, which is a high-pressure device operating at 1200 psi and is considered the efficient technique for production where the oil and aqueous phases are premixed and coarse emulsion is injected into the chamber before homogenization [44].

Static mixing

Static mixing is the type of mixing method where the only driving force is the pressure difference between the inlet and outlet of the specially designed tubes which are called static mixers [118]. These mixers are mainly used to mix both miscible and immiscible liquid systems, or gas streams [109]. Static mixers started being commercially in the 1965, when Arthur D. Little Company introduced their new motionless mixing tool, a new way of mixing two liquids or one liquid with one gas with a hollow cylindrical tube that contains several thin flat, and curved sheets in the inner tube. To improve dispersions to be produced, these elements can be located in different shapes and angles. Their main use was to blend two viscous liquids that react with each other and create either a viscous or solid product, for example, synthetic resin [108], [118]. The first company to install static mixers as micromixers in a production plant was Merck, Germany, (Figure 1.10) for the synthesis of metallo-organics with 23% higher yield than in the conventional batch processes [119], [120].

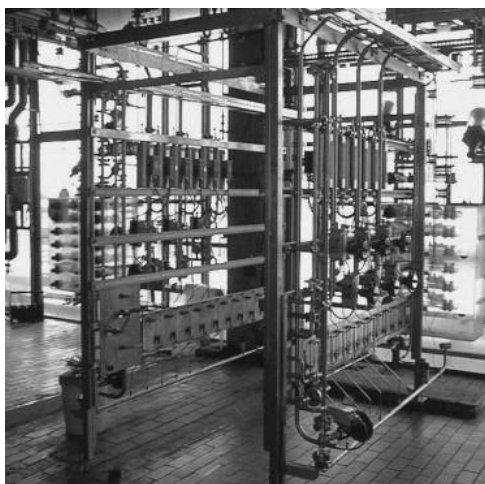
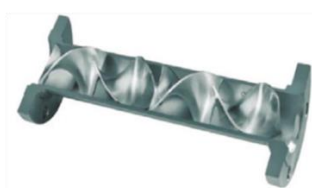


Figure 1.10. Production plant using static mixers as micromixing elements for a metallo-organic compound fabrication (Merck, Germany) [120].

Static mixing was demonstrated to be a cost-effective method that provides in-depth mixing at low pressure drop. Several static mixers can be found under the brand names of Kenics® and Sulzer® and others (Figure 1.11) in the market, which can provide laminar or turbulent flow depending on the application.



SMX (Sulzer, Inc.)



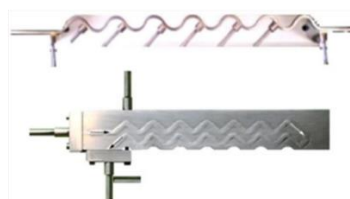
Kenics KM (Chemineer, Inc.)



KMX-V (Chemineer, Inc.)



Standard LPD (Ross Engineering, Inc.)



Corrugated channel reactors
(Laboratory pilots)

Figure 1.11. Examples of commercially available static mixers [121].

The biggest advantage is no requirement for external power apart from the energy needed to pump and flow the fluids through the mixer. However, the conversion is lower with high flow rate than in conventional stirred batch reactors and increasing the residence time requires higher pressure. Static mixers can be frequently found in the form of shell and tube heat exchangers in industries [119], [120]. Static mixers are applied in homogenization [108] [121], for instance, corn oil-in-water

emulsion was produced with a helical type of static mixer equipped with 20 elements [108]. It was demonstrated during a static mixing experiment even at very low residence time, emulsion droplets were smaller and more uniformly distributed at 4 μm size than the results received from a conventional mechanical mixing (11 μm) method [108].

Membrane emulsification

Membrane emulsification uses pressure to pass the first phase through membrane pores into the second immiscible phase. The membrane emulsification method to fabricate monodispersed emulsions was first introduced in 1986 by Nakashima and Shimuzu [110]. In this method, the shear force is applied to break the droplets inside the membrane after the liquid reaches the membrane surface, and passes through the pores at micro scales [122]. The mechanism of membrane emulsification (Figure 1.12.a), and a commercial laboratory scale membrane emulsification device (Figure 1.12.b) are given in the next figure.

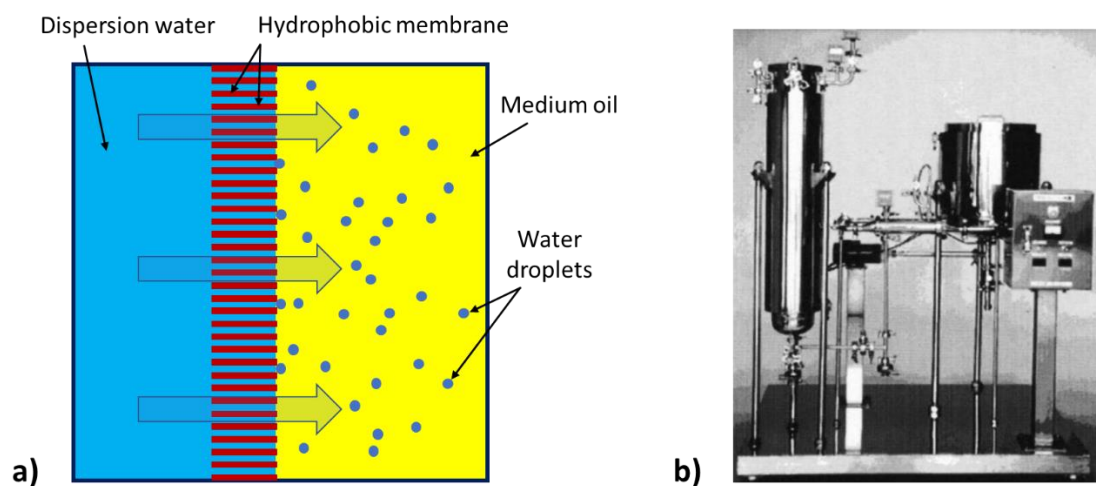


Figure 1.12. a) Schematic preparation of a w/o emulsion using a hydrophobic membrane and b) view of the laboratory scale membrane emulsification device developed in [110].

Here, the dispersed phase containing materials like polymer, surfactant, and API passes through the membrane pores which are hydrophobic in nature, and enters the oil medium by forming a dispersion. The dispersed phase is pushed with the help of a pump to flow across the membrane into the continuous phase flows to form the droplets. In membrane emulsification, due to a large number of pores, the process can be realized without further heat emission [122]. This technique has low energy consumption, however, it has a production rate lower than in the conventional methods [110], [111]. Additionally, the membrane should be replaced with a hydrophilic one to avoid membrane clogging, in case o/w emulsions are required to be prepared.

Ultrasonic emulsification method

In the list of high-energy methods, the sonication methods can be found. It was reported for the first time for emulsification in the 1927 year [123]. In general, this method uses devices called (ultra)sonicator, which converts electric energy into high-frequency ultrasonic oscillations mainly by using an ultrasound generator and a specially designed probe (Figure 1.13). The classic sonication method for miniemulsions production uses 50% of the power cycle for 2 minutes long to yield polystyrene NPs of around 110 nm diameter [124]. The mechanism of the droplet formation can be explained by the unstable interfacial waves generated by the acoustic field. Also, the bubbles induced by acoustic cavitation collapse which leads to extreme localized turbulence, where the primary droplets break into smaller ones. Recently, synthetic polystyrene@SiO₂ NPs produced by ultrasound emulsification method are reported by the addition of hyperbranched poly(ethoxysiloxane) as a stabilizer during the process to fabricate thermally stable NP dispersions [98]. Also, 200nm PLA NPs are fabricated by using a two-step ultrasonication emulsification [31].

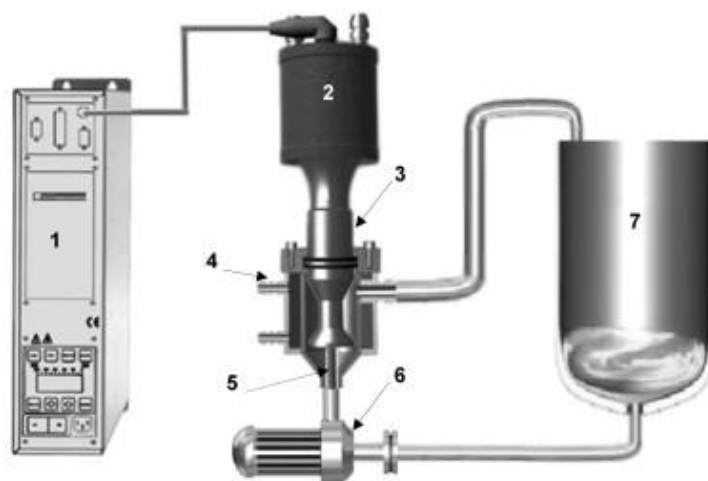


Figure 1.13. Pilot-scale ultrasonic technique miniemulsion production 1200W ultrasonic generator with (1), piezoelectric transducer (2), half-wave Barbell horn (3), reactor chamber (4), inlet tube (5), pump (6), storage/mixing beaker (7) [26].

Barbell Horn Ultrasonic Technology (Figure 1.13) is used to elaborate NPs at approximately 65 °C, and a series of premixed 50 mL samples are re-circulated for complete w/o emulsification for an average of 10 min at the ultrasonic amplitude of 90 μ_{pp} [26]. However, the titanium contamination sourced from the horn is reported. But 9-fold improved results compared to previous works of ultrasound emulsifications is achieved due to its new semi-continuous production design. The pilot-scale production is reported at the productivity rate of 100 mL/min with the energy density input of 690 J/mL for an emulsion size of below 100 nm. In another study, the exposure time of sonication is studied, and compared to the vortex mixing emulsification while producing PNPs. It is explained that, if the given energy is lower than the minimum required energy, which is called the low-energy

threshold, then the droplet doesn't break. Oppositely, it can result in a very high PDI if the given energy is too high or non-uniform [31]. Fessi *et al.* demonstrated a two-step emulsification-based PNP production, where PCL NPs reached the minimum of 219 nm size [71].

Shear-mixing methods

The most frequently referred high-energy methods in industries are shear-mixing methods [51], [112], [113], [125]. Rotor-stator mixers (RSM) are the one of the most conventional devices used in emulsification processes, and widely studied since the 1880s until reaching its modern design that was frequently used in different productions [82], [86], [112]. The mechanical and shear stress that is generated in the turbulent flow at high-speed rotation is the main principle by which droplets break-up is obtained in this method [116]. Here, homogenization takes place due to the kinetic energy given to the system. The kinetic energy is generated by the high-speed rotation of an internal part inside the stationary part resulting in turbulences between the two parts. Due to the small volume the system is induced to a quite high shear, which ruptures the droplets to yield miniemulsion [51]. The gap size between rotor and stator part (50 to 1000 μm) will define the given stress. The given shear stress can also be increased by increasing the rotation speed and/or the operating time [115]. With the rotor-stator mixing device (VirtishearTM), it was possible to homogenize an aqueous bovine serum albumin solution (BSA) with DCM to produce droplets of 1000 nm diameter. The following parameters of 24,000 rpm, and 10 mm of a rotor diameter allowed to maintain 12.5 m/s tip speed. At the end of the first emulsification minute, it was possible to reach the highest size dispersity. However, at 15,000 rpm, time was delayed to 3 minutes in order to reach the highest dispersity of 1000 nm droplets [86]. This experimental results are a good example of shear-force to droplet diameter relationship, thus in this experiment higher rotation speed reduced the droplets' polydispersity.

A larger rotor-stator system, One Silverson, was used to develop silicone oil & water emulsion. Here droplet sizes around 3000 nm were produced at 11,000 rpm (36 m/s rotor tip speed) and their size decreased down to 1000 nm at higher given shear rate, and by reducing the silicon oil viscosity. The highest shear rate was achieved with Micra D27 rotor-stator system at 36,000 rpm (5 minutes) allowing to reach 135 nm droplets with narrow size distribution [113]. RSM can be found operable in both batch mode (Figure 1.14.a), and also with complementary parts which allow it to be operated in continuous mode (Figure 1.14.b) to produce emulsions [86], [126].

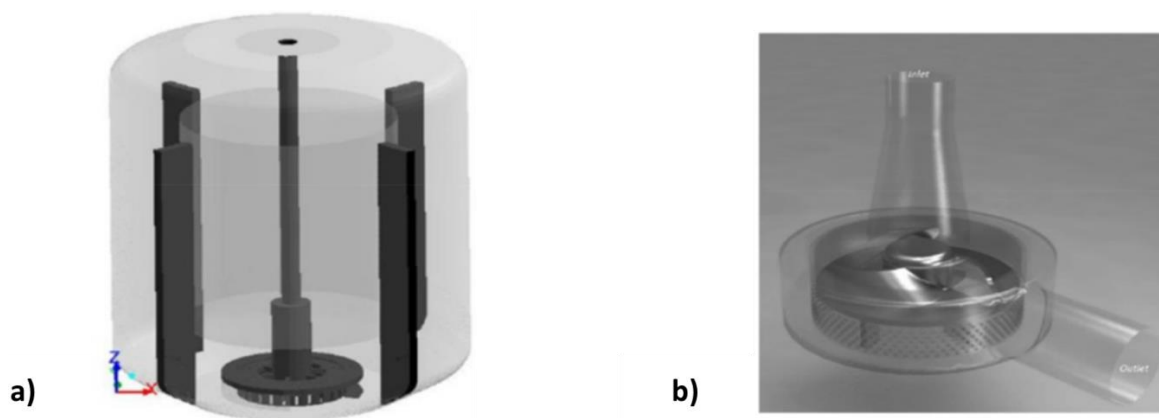


Figure 1.14. RSMs devices in batch (a) and continuous (b) mode of operation [112].

Considering both batch and continuous mode RSM operations, it's often challenging to achieve the same emulsion results, since in the continuous operations one more operating parameter, flow rate plays role to control the droplet size.

In this part, we described the devices which use high energy density to break-up the emulsion droplets. However, in order to consume less electrical energy, for instance, it can be interesting to use low-energy methods.

1.3.2.2 Low energy methods

Low-energy methods for emulsification are found to provide laminar flow and low energy dissipation conditions. Using this method has an important economic advantage due to near zero energy consumption. Additionally, it has the advantage to encapsulate fragile molecules, which cannot be encapsulated in high-energy emulsification. Differently from high-energy methods applying shear forces, in low-energy methods, the primary force controlling the droplet formation is the physicochemical properties of the system including the materials used. Here, the behavior of the surfactants, co-surfactants, solvents, and all their combinations require careful considerations. [116]. Low-energy emulsifications can be found in literature with examples of spontaneous emulsification [54], [127], phase-inversion temperature [128], phase inversion composition [129], and microfluidic emulsification [63].

Spontaneous emulsification

Spontaneous emulsification was introduced by Johannes Gad in 1879, where there was no requirement of external force to prepare emulsion. When an oil and water phases, which are not in thermodynamic equilibrium, are added together, the spontaneous emulsification (Figure 1.15) can occur [127]. This effect was then completely described and referred as “Ouzo effect” by Vitale and

Katz [130]. They demonstrated that, once the anis oil is dissolved into water, small droplets spontaneously nucleated and formed the emulsion [131]. Here, the dispersed phase was an oil containing surfactant and also another miscible soluble solvent (ethanol). When the contact of these two phases were maintained, the first prepared phase together with the solvent diffused rapidly into the aqueous phase. Following this diffusion, a high turbulence at the oil-water interface was observed. This fast diffusion accelerates the growth of an oil-water interfacial area and oil droplets spontaneously appear in the aqueous phase. In another study, 100 nm monomodal marble NPs were fabricated based on cluster chemistry *via* the simple solvent shifting “Ouzo” method [132]. This method is still valid if one works with w/o emulsions.

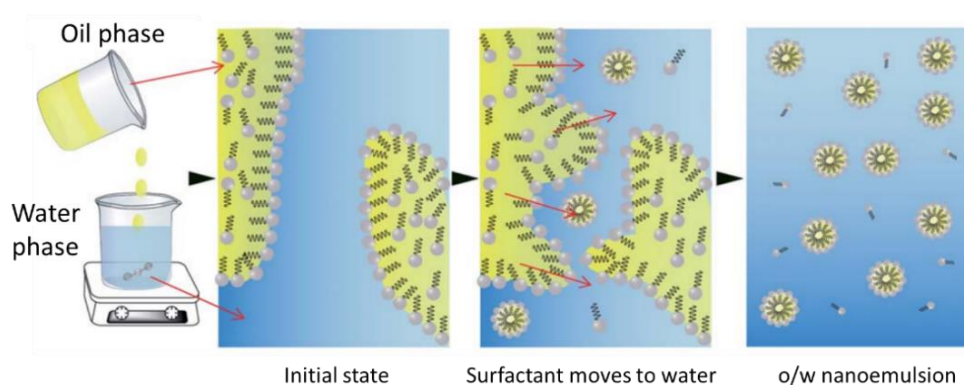


Figure 1.15. Schematic representation of the spontaneous emulsification: oil droplets are spontaneously formed when an oil phase containing a water-dispersible substance is mixed with an aqueous phase. The underlying mechanism is the movement of the water-dispersible substance from the oil phase to the water phase (red arrows), leading to interfacial turbulence and oil droplet formation [127].

For spontaneous emulsifications, three main principles play important roles in the control of the particles’ formation: i) the selection of the used materials, ii) the environment temperature, pH and ionic strength conditions, and iii) the speed with which the second phase is added to the first one [127]. The drawback can be the fact that large amounts of synthetic surfactants are required. However, a recent study showed that it’s also possible to realize spontaneous emulsification for polymerization to fabricate PNPs without using surfactants [54]. However, the process can be improved to reduce its size, and PDI value (Table 1.1).

Phase inversion Temperature

Phase inversion temperature (PIT) is a type of low-energy emulsification method that allows to produce emulsion droplets. Regarding of the “Ouzo” effect, the PIT was described by Shinoda and Saito after approximately a century in the 1969 year [133]. They demonstrated that simply mixing oil

with a non-ionic surfactant solution under low stirring can yield to an emulsion. However, a single condition had to be maintained. This was a temperature that had to be increased progressively to get emulsion droplets formed by following a phase inversion. This low-energy emulsification method can be used for producing both oil-in-water and water-in-oil emulsions due to a change in the physicochemical properties of the surfactant used including its HLB value [134]. When the temperature is low, the surfactant is highly soluble in water, increasing the temperature dehydrates the surfactant end group and lowers its solubility in water with the goal of reaching equal solubilities in both oil and water phases. At a certain temperature which is referred as PIT, the surfactant molecules are equally soluble in both phases. It was later reported that the higher surfactant hydrophilicity yield higher PIT, and when the surfactant was more hydrophobic, the PIT decreased [128], which allowed the system to be tuned for selective applications [135]. In this method, oil selection plays a major role to control the process, for example, Förster *et al.* [128] explained that with less polar oil lower PIT was achieved.

Phase Inversion Composition

The main difference between PIT and phase inversion composition (PIC) is the absence of heat input to the system, and the fact that the PIT method is restricted to the use of the amphiphiles. Here, the surfactant molecule is not required to be thermoresponsive [129]. PIC can be conducted at room temperature, and the main key parameter here is the composition change of the system [127] (Figure 1.16). To achieve an emulsion, a big volume of water is added to a water and oil mixture in order to dilute and reach a critical point above which an oil-in-water emulsion will be formed. When more water is added, the surfactant micelles of the water phase swell while the water diffuses and forms a sponge-like phase. When the addition of water continues, it leads to the phase inversion followed by the oil droplet nucleation inside the sponge phase, and the rest of the sponge phase forms spherical water-soluble micelles. Eventually, when micelles are formed the oil droplets and micelles separate yielding a bimodal particle size distribution [129]. The starting point of the PIC method is a water-in-oil micellar phase, which is an equilibrium phase of a ternary system, in which the surfactant is already at the water/oil interfaces with a curvature turned toward water (Figure 1.16).

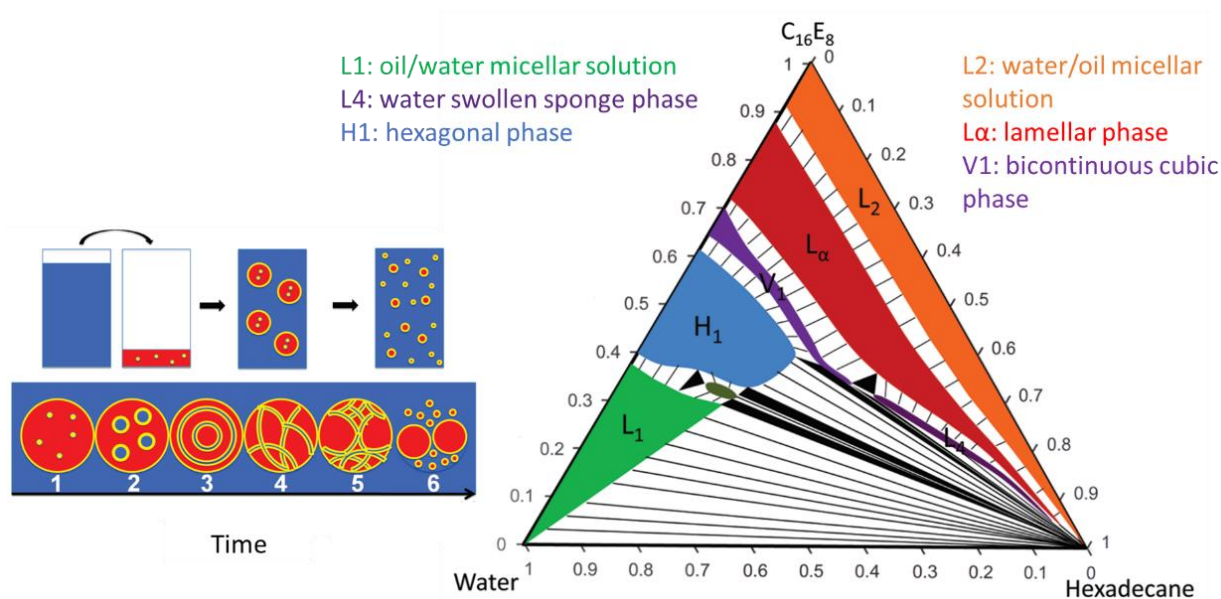


Figure 1.16. Ternary phase diagram of the C16E8 surfactant/hexadecane/water system. Six main transformations occur as water diffuses in. (1) The drop (oil and surfactant) is surrounded by water. (2) The drops swell with water and swollen reverse micelles form. (3) Further swelling leads to a decrease in the curvature and a lamellar phase form. (4) The lamellar phase connects to form a sponge phase as the curvature turns toward the oil. (5) Emulsion droplets nucleate within the sponge phase with a diameter that matches the spontaneous curvature. (6) The system transforms into a biphasic combination of small micelles, and the large droplets [129].

The method then proceeds with a large addition of water, which causes an inversion of the spontaneous curvature of the surfactant film, now turned toward the oil. It is found that for certain compositions and with some constraints on the process a homogeneous metastable emulsion, with diameters in the 100 nm range, can be obtained [127] [129].

Microfluidic emulsification

One of the main advantages of microfluidic systems is their continuous-flow operability for both emulsion-based and non-emulsion-based PNPs fabrication [50]. Especially, in the last few years, by providing a precise mixing rate of materials, such as solvent with non-solvents at nanoliters, this field also opened its doors to the complex and targeted PNP fabrication where a strong size control and narrow distribution can be maintained [19], [27], [136]. This field has been widely accepted in analytical chemistry, chemical synthesis, cell analysis, tissue engineering, etc. [136]. Microfluidic systems appeared in different chromatographic systems since the 50s [18], then they were designed for emulsification. These systems are vastly used for microdroplets production [31], [53], [137], [138], but also to produce polymeric nanoparticles (PNPs) [19]. They allow the production of PNPs with both top-down (polymerization then emulsification) or bottom-up (emulsification followed by polymerization) methods [57].

To produce a miniemulsion of methyl methacrylate (MMA), a T-junction microreactor was used and then the emulsion passed through the thermal polymerization step to yield polymethylmethacrylate (PMMA) NPs of below 400 nm [41].

Another example of microfluidic emulsification is the production of PNPs, in Serra's team, with a very small reagent amount (around 1w% in the dispersed phase) by using elongational-flow microreactor and mixers (RMX, Figure 1.17.a), using two electromechanical piston pumps [19], [21], [27].

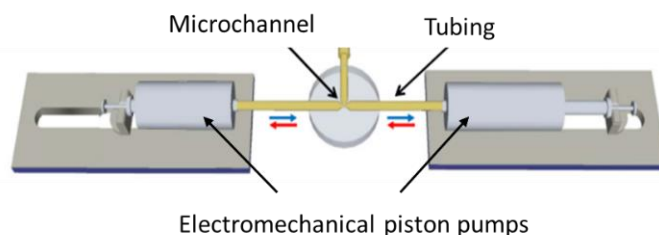


Figure 1.17. Schematic illustration of the a) microfluidic RMX [27].

The fundamental review of PNP fabrication with the bottom-up approaches by using different microchannel designs like “T”, “Y”, “Y”-serpentine, and techniques of reagent mixing like “co-flow”, “multijet”, “cross-flow”, “capillary-based”, “co-capillary based” are described in Figure 1.18 [24], [33].

Moreover, since solvent diffusion is the main driving force of nanoprecipitation [50] and it can take place within a few milliseconds (depending on the width of the lamella, more precisely, the microchannel width), it becomes crucial to control it. In this context, microfluidic systems and especially micromixers are powerful devices to produce PNPs (Figure 1.18). By using these micromixers, it has been shown that different PNPs, such as PLGA (350 nm), β -carotene copolymer, poly- ϵ -caprolactone (200-600 nm), or PMMA (250 nm) NPs can nanoprecipitate with narrow size distributions by solvent diffusion [136]. Overall, PNPs can be produced also with methods that don't include emulsification processes. Under certain requirements, this can be economically efficient

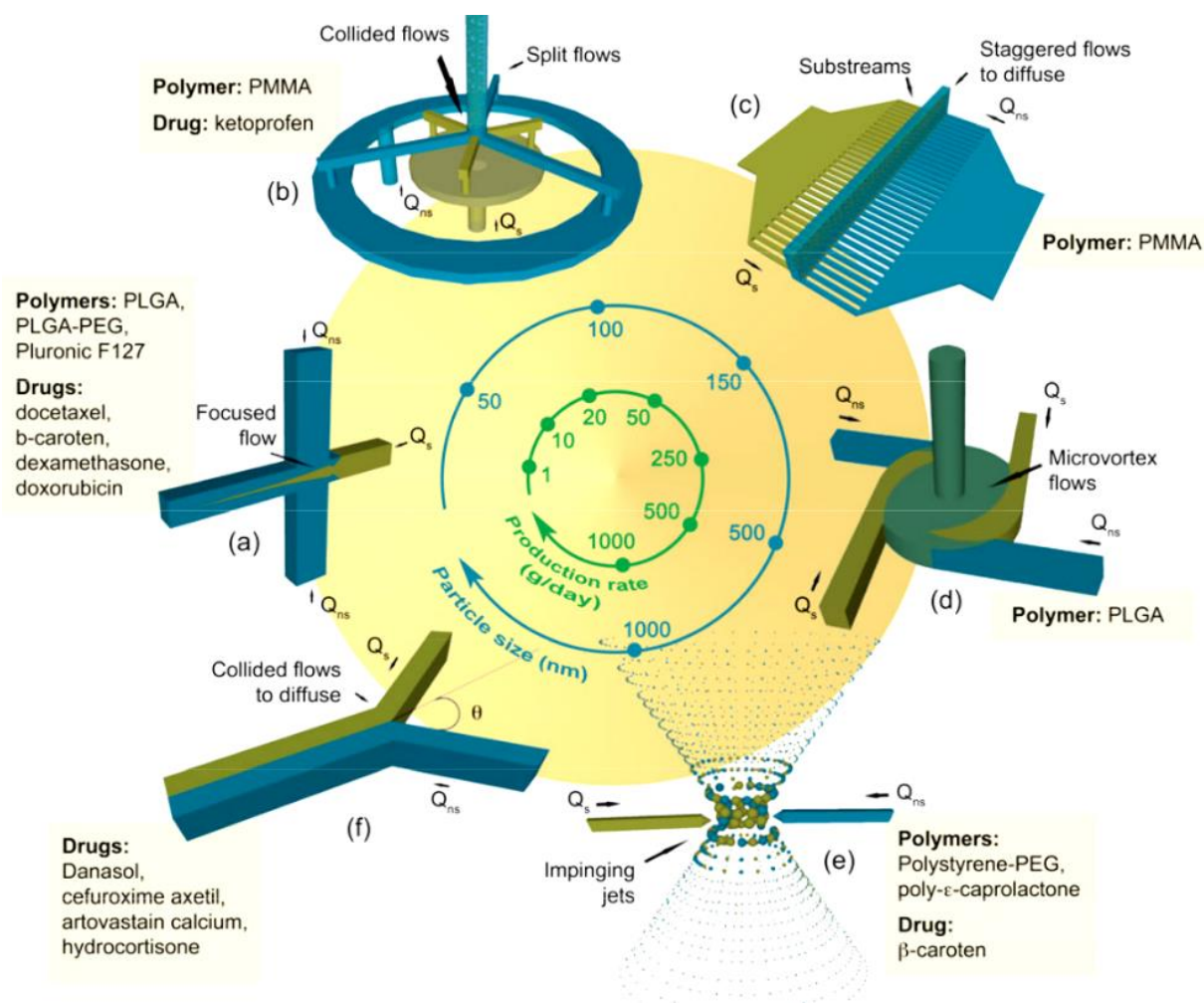


Figure 1.18. Microfluidic mixers used in different NP fabrications, Q_s and Q_{ns} represent the solvent and non-solvent flows respectively; (a) hydrodynamic flow focusing micromixer, (b) combination kinetic energy and molecular diffusion micromixer, (c) molecular diffusion microchannel, (d) multi-inlet vortex mixer, (e) confined impinging jets micromixer, (f) collided flows micromixer [136].

By using the “co-capillary” microfluidic technique, for instance, it is possible to produce droplets of MMA and to polymerize, with UV light, the droplets in a single step to obtain PMMA microparticles [139]. In another study, 100 nm PMMA NPs are fabricated by micromixer-assisted nanoprecipitation by pumping pre-formed PMMA solubilized in THF and water phases using impact-jet micromixer, and encapsulation of Ketoprofen drug in PNPs are demonstrated [84]. This low-energy method consumes a lower amount of energy (syringe pumps) when compared to high-energy methods.

Several advantages of microfluidic fabrication can be listed as improved accuracy, cost efficiency considering the microliter quantities and lower consumption, etc. Additionally, advantages like a uniform miniemulsion size and identical reaction conditions with high reproducibility can be added to the list [18], [27], [33].

Other homogenizers

In order to produce miniemulsions, similar to the methods like shear-mixing [82], ultrasonication [26], there are also other less-popular methods of emulsification. One of these methods is a bubble bursting method, where mass transfer from a lower liquid phase to an upper gas phase drives the formation of nanosized droplets. Interestingly, this is one of the non-stop processes that occur in sea waters due to the systems trying to reach their thermodynamical equilibrium state. Also, a reverse transport form of a bubble bursting method from outer air/hexadecane phase to a surfactant solution was reported for the first time only a few years ago [140]. This is a new type of low-energy emulsification method capable of producing 100 nm sized NPs applicable in drug delivery and food science. This method is limited to very small scales; however, the method is only at its starting point. There are also other homogenizers like a “narrow-gap” homogenizer (Figure 1.19), which operates at high driving pressure and yields micro-sized droplets due to a pressure drop [141].

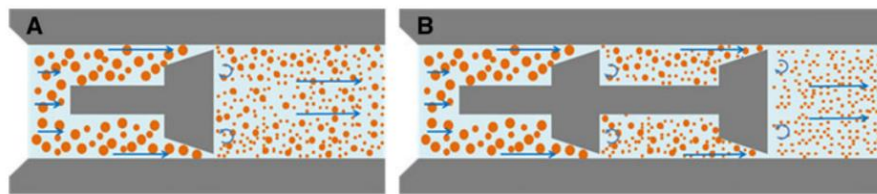


Figure 1.19. Schematic illustration of a “narrow-gap” homogenizer with a single gap (a) and two gaps (b) [116].

In “narrow-gap” homogenizer, the valve geometry, gap size, and the number of gaps highly influence the emulsion droplet size [142]. These parameters initially influence flow rate, varying the hydrodynamic conditions, which consequently influence the average power density given by the emulsification device [141]. Experimentally, this was demonstrated by Tcholakova *et al.* [143], where increasing the gap width from 75 to 395 μm increased flow rate from 3.42 to 7.8 L/min and mixing volume from 2.4×10^{-9} to $17.2 \times 10^{-9} \text{ m}^3$ in a “narrow-gap” homogenizer (Figure 1.19). Later, it was verified that the reduced flow rate resulted in final emulsions with larger droplet size by Steiner *et al.* [141]. The same team also studied the relationship between number of gaps and the emulsion properties in a “narrow-gap” homogenizer. Smaller droplet diameters (15 % lower) with 3 μm size at 8.7 L/min flow rate were observed with two gaps compared to results of a single gap homogenization, explained due to increased turbulence. However, due to additional frictional forces, two gaps require higher pressure to reach the same flow rate as a single gap homogenization.

1.3.2.3 Process and pre-process parameters

Operating parameters

Process parameters including the energy input or residence time within the equipment can be controlled directly in order to tune the particles' size: increasing them might lead to the formation of smaller particles [116], [144]. For example, in high-pressure homogenizers, pressure is one of the main process parameters, thus, increasing pressure may lead to faster and less polydisperse emulsion production [44]. In static mixers, it is more dependent on the mixer design, pressure drop across the mixer, and flow rate [108]. While using sonicator, the overall pressure doesn't appear important to be considered, however, the major process parameters here are the ultrasound amplitude, temperature, and residence time [26]. Also, in rotational shear mixing devices these are the rotation speed, fluid turbulence, and residence time [112]. Regardless of the process parameters being applied for each method, the pre-process parameters appear similar in all methods. These are the interfacial tension, material concentrations, fluid viscosity, volume and C/D ratio, applied in all emulsification methods.

Material parameters

One of the pre-process parameters is the HLB value of the surfactant used during the emulsification process. Emulsion stability can be ameliorated and controlled through the surfactants added to the initial feed materials resulting in better-stabilized interfaces and also a controlled particle size [31], [47], [62]. Additionally, the molecular structure of a surfactant should be considered, where a high unsaturation degree and solubility in a second phase (oil or water) can be directly affected by the ending groups (especially aliphatic group compatibility with an oil nature) of the surfactant molecule. [31]. It's been also demonstrated that dissolving polymers in monomer solutions where polymerization will take place later, lead to emulsion droplets with an improved stability [76] since increasing the hydrophobicity of the dispersed phase improved droplet nucleation. For instance, PLGA and PLGA-PEG NPs were produced by the emulsification-evaporation method in the presence of PVA as an emulsifier. The polymer in ethyl acetate as an organic phase was dispersed into the surfactant-containing water phase and emulsified by a high-shear homogenizer at 11.000 rpm speed. Following the homogenization process, ethyl acetate was removed by a rotary evaporator to then obtain 271 nm monomodal PNPs suspensions in water [7]. Regardless of how surfactants were vastly used in emulsion-based PNP fabrication designs, some researcher reported surfactant-free emulsion-based PNP production like emulsion-polymerization, emulsion-precipitation, which refers to direct polymerization or precipitation of a prepared emulsion [98], [100], [145].

Overall, by controlling process and pre-process parameters and maintaining appropriate operating conditions, PNPs can be produced via emulsion-based fabrication designs. There are also post-homogenization parameters that are essential to consider.

1.3.3 Theoretical aspects

PNPs produced by emulsion polymerization or dispersion polymerization are shown to self-assemble while particle growth follows a homogeneous nucleation mechanism [24], [33], [76]. There are several factors that are crucial to consider before diving into the emulsification process. These are interfacial free energy, hydrophilic-lipophilic balance, critical capillary number, emulsion stability, etc. [74].

1.3.3.1 Interfacial free energy

An important property required for stable emulsion is the immiscibility of the two phases. In some cases, the first phase is slightly soluble in the second phase where solvent diffusion can lead to the imbalance of droplet. So, the main emulsion stabilization can be understood by considering the interfacial energy [47], [62]. Interfacial energy is generated at interfaces based on imbalance of the molecular forces [31], [47]. In terms of an energy balance at droplet surface, an osmotic pressure is being affected by the hydrophobic agent which is previously dissolved in the solvent. This phenomenon can be demonstrated by ($P_{Laplace}$) the Laplace pressure, defined as the differential pressure of inner and outer parts of a given droplet of spherical droplets (Equation 1.1).

$$P_{Laplace} = \frac{2\gamma_L}{R} \quad \text{Equation 1.1}$$

$$\gamma_L = \frac{A_d}{A_{surf}} \gamma_d + \left(1 - \frac{A_d}{A_{surf}}\right) \gamma \quad \text{Equation 1.2}$$

with γ_L (mN/m) the oil droplet surface tension, R droplet radius. Then, the oil droplet surface tension correlates with A_d the surface area of the droplets, A_{surf} the surface area covered by the surfactant molecules, γ (mN/m) the interfacial tension between aqueous & organic phases, and γ_d (mN/m) the interfacial tension of aqueous & oil droplet covered with the surfactant molecules [76].

Due to their high surface energy, after emulsification, the nanodroplets are unstable in the continuous phase, however, there are some results showing that charged ligands are capable to improve miniemulsion stability by generating a repulsive force between the nanodroplets. For example, poly-ionic electrolytes can also provide a charge density that leads to surface repulsions

evolved from the nanodroplet surface charge [41], [62]. An ionic surfactant can also limit droplets' coalescence *via* electrostatic repulsions after covering the surface of droplets [76].

Moreover, considering both Laplace and osmotic pressures, it's important to reach the equilibrium state between them to stabilize the droplet [48], [76]. By reaching an optimum surfactant or polymer concentration, it is thus possible to distribute the given energy equally after reaching Laplace and osmotic pressures equilibrium, however the given emulsification energy should be high enough to treat all the droplets equally [76].

1.3.3.2 Utility of surfactants

As previously reported, emulsions are hydrodynamically unstable systems kept at their maximum metastable condition following addition of the stabilizing agents. Depending on the desired emulsion properties, the surfactant must be wisely chosen. [34]. Indeed, the emulsion properties are indirectly correlated with the surfactant thermodynamics *via* hydrophilic-lipophilic balance (HLB) value. HLB is a value to determine the hydrophilic or lipophilic degree of the surfactant as described by Griffin in 1945 [146]. HLB value gives information of the hydrophilic and lipophilic moieties' size and strength, and scales from 0 to 20. For example, surfactant HLB value of between 3.5 to 6.0, is more suitable for use in w/o emulsions [147].

When two immiscible phases are emulsified, the surfactant which is more soluble in water migrates into the water phase, this can be as fast as the turbulence is usually generated, yielding nano-sized droplets of colloid [44]. Particularly, to avoid collisions of droplets in miniemulsions and also to limit the mass exchange (Ostwald ripening), surfactants are used to stabilize the system [46], [48], [82]. In double emulsion, which is also called emulsion of emulsions [24], HLB value become even more crucial and complex. For example, to start with a w/o emulsion HLB value of below 7 (preferably 3-4), and for the second emulsification, HLB value should be kept above 10 in order to avoid droplet instabilities. Eventually, choosing correct emulsifier and controlling HLB value is one of the main properties to produce stable emulsions and also to control a droplet size [31]. Instead of moving to the higher emulsifier concentrations, tuning the average HLB value to later obtain stable emulsion can be applied through combining emulsifiers of different water-oil loving indexes. For instance, 6% v/v Span 80/Tween 80 emulsifiers at HLB ranging from 4 to 9 were used to produce stable water & sweet almond oil miniemulsion, and this was later reported as the emulsion made of natural compounds for selective applications [47], [96]. In a previous work with w/o/w double emulsion, at higher surfactant (Tween 80) concentrations, EE dramatically decreased which was induced by the rupture of internal droplets [24], [147]. However, the efficiency can be improved by combining a number of emulsifiers owing different HLB values, the ionic or non-ionic surfactant properties, and a

selective molecular structure for miniemulsion tailoring [47], [94]. Besides controlling HLB value, it was demonstrated that ionic surfactants can also change the surface properties of PNPs. Thus, while producing PMMA NPs the cationic surfactant cetyl-trimethylammonium bromide (CTAB) was added to the aqueous phase to generate PNPs with the positive surface charges through emulsification and polymerization (Figure 1.20) [41].

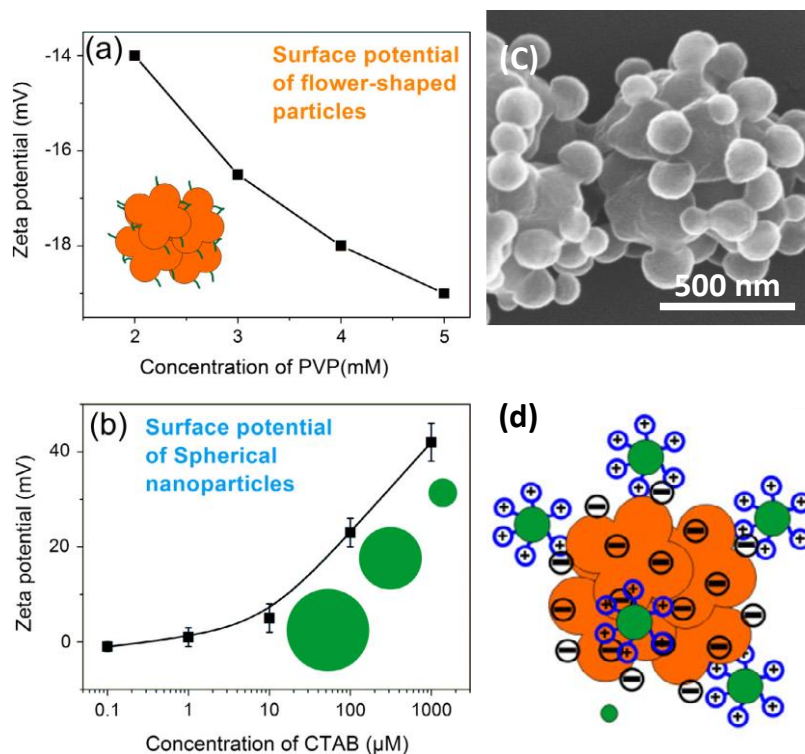


Figure 1.20. Surface charge results of the SDS based (a) and CTAB based (b) PMMA NPs, and two PNPs (c) attached by the electrostatic interactions (d) induced by the surfactants used during the fabricated by the emulsification and polymerization method [41].

For building an electrochemical interaction between two PNPs later, sodium dodecyl sulfonate (SDS) containing aqueous phase was emulsified with the same device to produce another PMMA NPs with a negative surface charge. Both systems were prepared at different ionic surfactant concentrations, and the surface potential was measured to compare the two different surface charges (Figure 1.20) of the two PMMA NPs [41].

1.3.3.3 Energy density and critical capillary number

Energy density

The energy density (E_v) describes the energy per unit volume (J/m^3) allowing to estimate the average droplet size of an emulsion. E_v depends on the power density (P_v) and the residence time t , both controlling the droplet size [115]. A significant amount of energy deposition is required to produce miniemulsion where shearing forces can overcome the viscous forces [26]. When the minimum required energy is reached, the droplet can be expected to break into smaller droplets. For example, in high-frequency ultrasonic emulsification, it is possible to reach 100 nm emulsion droplet size (100 mL/min) at the energy density input of 690 J/mL [31]. In another method, the high-pressure homogenization, the energy density E_v can be estimated by considering the pressure difference Δp of the micromixer (pressure difference between inlet and outlet) where the droplet is induced to shear or elongational-flow forces [115] [148]. In general, the energy density (J/m^3) can be expressed in the following Equation 1.3.

$$E_v = \frac{P}{\dot{V}} = \Delta p \quad \text{Equation 1.3}$$

Where P the power input (W), and ($\dot{V} = dV/dt$) volume flow rate (m^3/s), which equals to (Δp) the pressure difference (pressure drop across a restriction) depending on the device design, and may also be applied to compare energy densities of different high-energy emulsification processes.

For example, Zidouni *et al.* demonstrated how to compare different emulsification devices according to their energy densities (Figure 1.21).

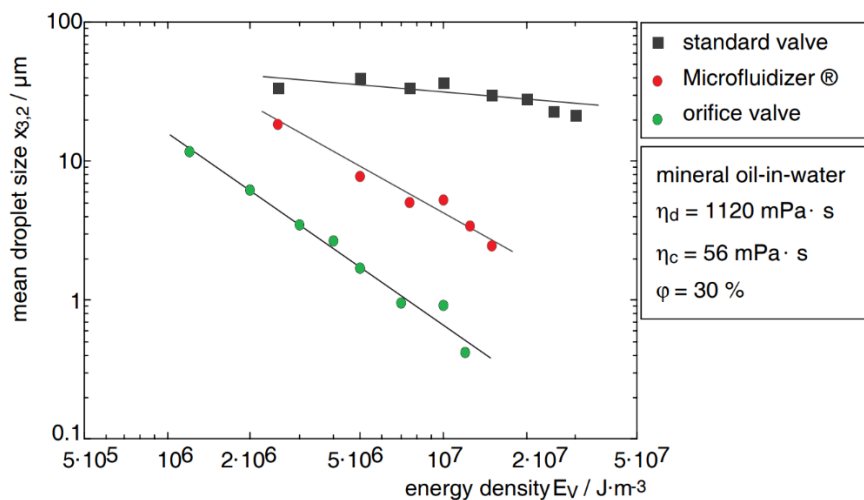


Figure 1.21. Comparison of homogenization efficiency of various homogenization valves for an o/w emulsion with a high viscosity D/C ratio η_d/η_c [148].

It was reported that three different emulsification results varied according to the provided energy density at constant viscosity, and 30% D/C ratios. The smallest emulsion droplet size of approximately 500 nm was achieved at energy density of 10^7 J/m³ according to the pressure difference at the orifice valve.

Capillary number

While producing a controlled size miniemulsion, the ratio between viscous forces and interfacial tension of the two immiscible phases is also considered to be crucial to generate (nano)droplets [24], [47]. The capillary number (Ca) is a dimensionless number defining this ratio and expressed by Equation 1.4.

$$Ca = \frac{\mu v}{\gamma} \quad \text{Equation 1.4}$$

where μ (cm² s⁻¹) is the fluid viscosity, v (m/s) the fluid velocity, and γ (mN/m) the interfacial tension between the two immiscible phases.

According to the Taylor theory, when the viscous forces are higher than the interfacial forces, the capillary number reaches its critical value, which is referred as the critical capillary number (Ca_c). At this range of Ca, the shear stress applied to fluids reaches a sufficient level to i) deform the immiscible phases high enough to form the emulsion droplet and ii) break it into smaller droplets. However, the lower the diameter of the droplets, the higher is Ca_c. This mean that breaking the smallest droplets requests higher energy. This theory also proves that in the simple shear, droplets break up when the viscosity ratio between dispersed and continuous phases is lower than 4. At a higher viscosity ratio, the Ca_c is not reached, and the shear force is not enough to rupture the droplet. On the contrary, in the two-dimensional extensional flow, the droplets rupture at viscosity ratios higher than 4, under the evolution of time.

Overall, regardless of how much work is done on the fluid, below Ca_c the emulsion droplets are not experiencing the force enough to rupture. In practice, the viscous forces of the surrounding liquid deform the second liquid in flow, forming the emulsion droplet, thus these droplets break down every time when they reach their Ca_c until the process is complete [149]. This force appears under the fluid flow conditions. Here, the phase ratio and polymer concentration also influence the final product size, due to the reason that they influence the phase viscosity, and the process requires more energy to generate smaller droplet at higher viscosity ratios [31].

1.4 NON-EMULSION-BASED PRODUCTION DESIGNS

1.4.1 List of the non-emulsion methods

PNP fabrication designs for the large-scale production have been hampered due to the reason that complex multi-step processes can limit the production efficiency. To fabricate PNPs by avoiding additional materials in the systems, some methods like the dropping nanoprecipitation [43], surface atomic wave (SAW) atomization [24], hydrodynamic flow focusing nanoprecipitation [49], [50], electrohydrodynamic co-jetting and phase separation [42], ionic gelation [6], [90], [150], complex coacervation (liquid–liquid phase separation that can occur in solutions of oppositely-charged macromolecular species) [12], microbial method (with bacteria) [151], and thermally induced phase separation (TIPS), that is induced by cooling the polymer solution can be used. The major non-emulsion based PNP fabrication methods are listed with their production steps, advantages and disadvantages (Table 1.2).

Nanoprecipitation

Nanoprecipitation is the production process of a colloidal nanosuspension made of a polymer solution dispersed into a precipitating medium [50]. In general, nanoprecipitation can be divided into three main stages (Figure 1.24.b): (I) the polymer nucleation where the polymer molecule experiences a solvent change, (II) the already formed nanoparticles start growing through aggregation to the nuclei, and (III) these NPs kinetically lock after reaching the aggregation time. The third stage is extremely slow compared to other stages. For example, to produce polyetherimide (PEI) NPs, it was dissolved in DMSO at 90°C, then temperature was gradually decreased and the solution was added dropwise to a polytetrafluoroethylene (PTFE) film to evaporate the solvent yielding a powder form PEI NPs [66]. In another study, by using microfluidic flow focusing synthesis it was possible to fabricate biodegradable PNPs having reactive hydroxyl functional groups, then the A10 RNA aptamer was used to surface functionalize these NPs, here this functional groups bind to the prostate-specific membrane antigen extracellular domain to reach the prostate cancer cells later. Before adding PLGA-PEG solution into an aqueous solution for generating NPs via nanoprecipitation, a diblock copolymer is dissolved into a solvent (acetonitrile) which is miscible with water [23]. However, even if this method is very efficient to develop engineered living materials like bacteria with polysaccharides, it is also extremely expensive. There are also methods using the main principle of nanoprecipitation with different approaches to fabricate PNPs.

The dropping nanoprecipitation

The majority of the studies introduce the dropping nanoprecipitation to fabrication PNPs, such as Wallyn *et al.* who produced PNPs of 170 ± 30 nm diameter size to deliver iodine, following the radical polymerization of 2-methacryloyloxyethyl(2,3,5-triiodobenzoate) monomer (MAOTIB) [43]. After successful polymer synthesis, 50 mg poly(MAOTIB) homopolymer and PEGylated surfactant were dissolved in 10 mL THF and then dispersed dropwise into 40 mL ethanol at 500 rpm magnetic stirring for 3 hours (Figure 1.22).

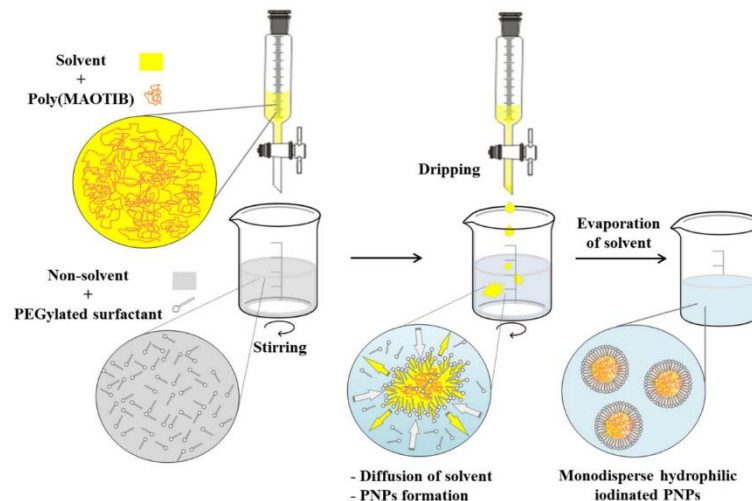


Figure 1.22. Poly(MAOTIB) nanoparticles fabrication via dropping nanoprecipitation technique based on the nanoprecipitation process

Then obtained PNPs (Figure 1.22) were washed via centrifugation to remove surfactant after diluting in water [43]. This method allows producing PNPs in batch process conditions, however, there are other nanoprecipitation methods that maintains a continuous production of PNPs.

Microfluidic nanoprecipitation

As a second example, microfluidic approaches can be used in this case due to its rapid and tunable mixing advantages [24], [56], [78]. For example, Poly (lactide-co-glycolic acid) (PLGA) and a block copolymer composed of poly (lactic-co-glycolic acid) and poly (ethylene glycol) (PLGA-b-PEG) nanoparticles were produced by microfluidic approach. They suggested that, the polymer concentration near the channel walls can influence the aggregation, and clogging can be avoided through the polymer concentration [24]. These kind of biocompatible materials have then been used to obtain RNA-functionalized surface (Figure 1.23) [53], [56].

Crystalline danazol, a hydrophobic compound with poor oral bioavailability, was used to produce drug NPs by a precipitation method: Y-shape microchannel was used to form 364 nm particles,

characterized by Fourier transform infrared spectroscopy (FTIR) to understand if the material remained stable after the process. This was reported to increase the specific surface area from 0.66 m²/g to 14.37 m²/g, and 100% drug dissolution achieved compared to traditional 35% raw danazol dissolution in 5 minutes while the drug molecules remained unaffected [18].

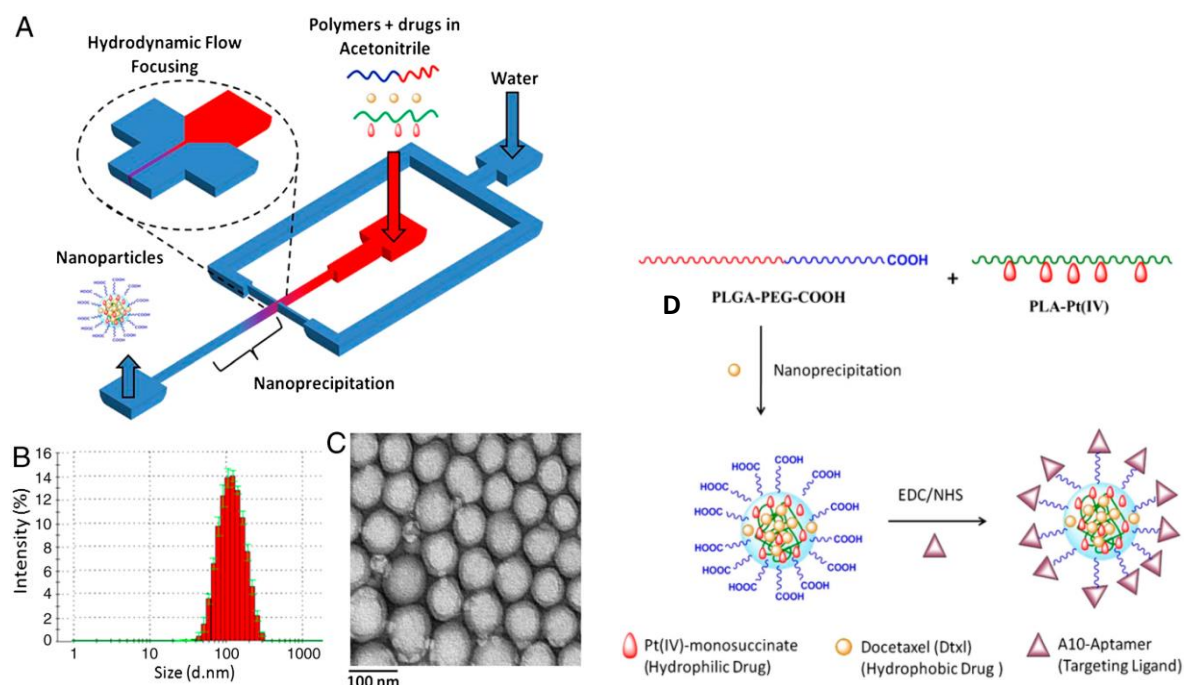


Figure 1.23. Microfluidic synthesis of PNPs (A), characterization via DLS (B), TEM (C) and surface functionalization with A10-Aptamer of hydrophilic platinum prodrug encapsulated PNPs [23].

The surface atomic wave atomization

Moreover, surface atomic wave (SAW) atomization method was used to produce PNPs followed by the microfluidic droplet generation. This microdroplet was induced to SAW atomization which resulted in PCL PNPs through rapid evaporation where aggregates reached 200 nm when dispersed into solution. This method consists from the droplet generation by using a microfluidic approach followed by the wave atomization to form PNPs in batch. It has been described that, with this method, the PNPs easily aggregate while collecting the solution after the wave atomization [24].

Hydrodynamic flow-focusing nanoprecipitation

In hydrodynamic flow-focusing nanoprecipitation (Figure 1.24), due to the diffusion of the polymer solvent into non-solvent, polymer self-assembly takes place yielding the PNPs' growth. In order to accelerate the last "lock" stage of nanoprecipitation, the fluid stream is mixed by the meeting two polymer non-solvent streams flowing at flow rates (Figure 1.24.a). The central stream is getting squeezed, yielding to a narrow stream allowing the rapid mixing. [24], [49], [56], [76]. It was

explained that layers can be generated on PNP's surfaces also by introducing polyelectrolytes and forming electrostatic nanoassembly in a controlled manner [41].

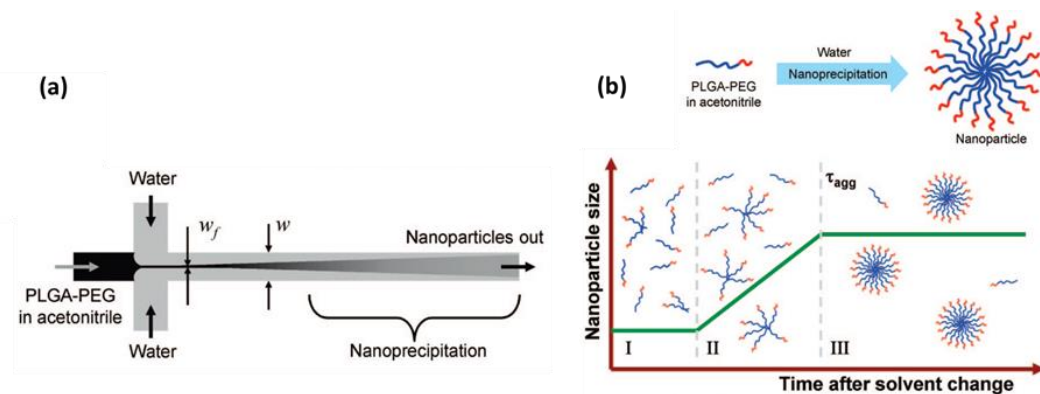


Figure 1.24. The process of mixing (a), and PNP self-assembly mechanism (b) in the hydrodynamic flow-focusing PLGA-PEG nanoprecipitation. Adapted from [49].

Hydrodynamic flow-focusing nanoprecipitation is also one of the microfluidic approaches, and overall, in non-emulsion PNPs' fabrication design microfluidic systems have a very important role and potential due to precise control over flow rates and mixing parameters.

Electrohydrodynamic co-jetting

In another microfluidic approach, co-jetting was used to generate PNPs to encapsulate biomolecules. In this context, Kyung-Ho *et al.* used the Taylor cone to produce PNPs with Janus structure through applying the electrical field, which distorts the liquid drop into a narrow line at the tip of the nozzle [152]. The electrical field leads to the formation of a polymeric particles at near nanorange, where a conjunction with solvent evaporation contributes to the size reduction (Figure 1.25).

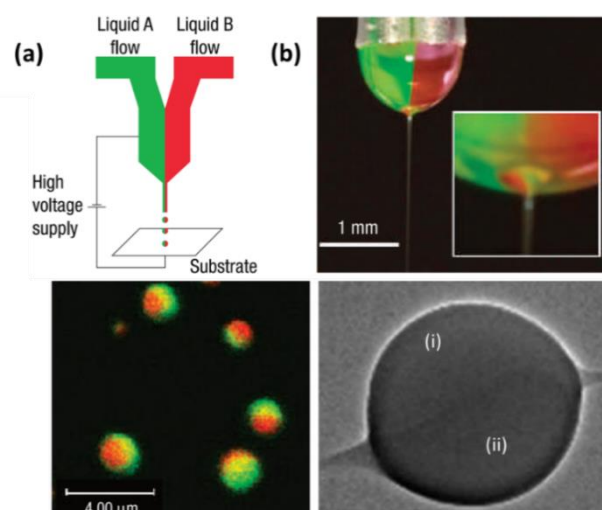


Figure 1.25. PNPs fabrication via electrohydrodynamic co-jetting method (a). Digital image of the setup with a typical Taylor cone (b). Colored image taken by confocal micrograph and TEM image of the particles produced

by electrohydrodynamic co-jetting with (i) first polymer, and (ii) second polymer forming a Janus particle of around 500-2000 nm size [152].

When exposed to an electric potential (5–15 kV), an electrical field between the liquid and the collecting substrate induces the bipolar jetting liquid into narrow line and forms Janus NPs. Thus, with this approach PEO-PAA biphasic carriers were successfully fabricated with a size range of 500-2000 nm (Figure 1.25), and were able to encapsulate color-encoded biomolecules for further characterization [152].

All the described non-emulsion-based PNP fabrication methods, and other recently developed methods can be found listed in Table 1.2 with PNP examples, their applications, advantages and disadvantages.

Table 1.2. List of the non-emulsion-based polymeric nanoparticle fabrication methods.

PNP material	Fabrication method	Number of production steps	Applications	Advantages	Disadvantages
PLGA NPs 225 nm, ≤0,2 PDI [153]	Nanoprecipitation	Two steps; Ultrasonic nanoprecipitation, solvent removal	Doxorubicin hydrochloride encapsulation	Rapid encapsulation High polymer concentration (≥ 3% w/v)	Limited process control High solvent consumption for purification
Poly(MAOTIB) NPs 163 nm, 0,1 PDI [43]	Dropping nanoprecipitation,	Two-step; radical polymerization, and the dropping nanoprecipitation	Iodine delivery, preclinical imaging	High iodine delivery High potential for co- delivery	Large volume of solvents (including toxic ones) used, purification, possible PNP agglomeration, batch operation
Chitosan-TPP NPs 300 nm [154]	Spray drying	Two steps; magnetic stirring, then spray drying	Pulmonary administration	High purity No organic solvents involved	High process temperature Low drug encapsulation Agglomeration
Chitosan NPs 600-800 nm, ≤0,2 PDI [155]	Desolvation nanoprecipitation	Both sonication and blade stirring in one- step batch operation	Antitumor agents	No organic solvents involved	Limited control Synthesis Need for an excessive washing

PCL NPs 150-200 nm, ≤0,2 PDI [24]	Surface atomic wave (SAW) atomization	Two steps; Microdroplet generation, then internal recirculation and rapid evaporation	Encapsulation and release of pDNA	Quick fabrication Few materials used No purification	Limited process control Aggregates
PLGA-PEG NPs 150 nm, ≤0,2 PDI [23]	Hydrodynamic flow focusing nanoprecipitation	One step rapid mixing	Docetaxel delivery	Narrow size, high stability Continuous process	Low encapsulation Low process volume Organic solvent
PEI-PSS NPs 100-400 nm [152]	Electrohydrodynam ic co-jetting	One-step jet ejection from a Taylor cone	Potential medical applications	Janus structure can be observed	Electrified jetting requirement Low process yield
AMB PEC NPs 600-800 nm, [156]	Polyelectrolyte complex (PEC) Method	Two steps; stirring, then dropwise addition of chitosan solution	Medical applications, >2 sulfate groups per glucosyl residue	Absence of harsh conditions Spontaneous NP formation	PNP size and size distribution can be reduced
Chitosan-TPP NPs 142 nm, ≤0,2 PDI [157]	Ionotropic gelation	One-step magnetic stirring	Protein, peptide delivery	No organic solvents	Large aggregates Unreacted polymer removal
CS-PMAA 60 nm, ≤0,2 PDI [83]	Polymerization nanoprecipitation	Two steps; Thermal stirring, and separation	Self-assembled films	No organic solvents involved	Agglomeration at normal pH, Thermal reaction
Chitosan NPs 512–820 nm [158]	Complex coacervation	Vortex mixing	DNA delivery	High encapsulation No organic solvents	Moderately high process temperature (55°C) Large particle size and size distribution
Hyaluronate ≤100 nm, [159], [160]	Microbial synthesis	Multi-step: capture, enzymatic reduction, and capping	Bone mineralization, mitigation of arthritis pain	Ecofriendly Biocompatible Reduced aggregation Reduced toxicity	Low production yield Long processing time High costs
PEI NPs 193 nm, ≤0,2 PDI [66]	Thermally induced phase separation	Two-steps; Droplet generation, then temperature induced evaporation	Not reported	Does not involve a chemical synthesis	High temperature Agglomeration

1.4.2 Process and pre-process parameters

While producing PNPs and designing their fabrication methods, the control over the final product properties can be classified into two fundamental parameters. These are process (temperature, pressure, duration, reaction kinetics, flow rate) and material which are (miscibility, interfacial tension, kinematic viscosity, phase ratio, polymer, surfactant, initiator, inhibitor, cross-linker, catalysis and other material concentrations). Such as in emulsion production, it's necessary to control the solvent and polymer non-solvent ratio, polymer concentration, diffusion and residence time, etc. [50]. It was for instance possible to tune PNPs' diameter from 80 to 200 nm by simply changing PLGA concentration from 1% w/v up to 5% w/v, which strongly influenced the size with a single pre-process parameter [24], [47].

As it was previously mentioned, in PNP fabrication two main strategies are employed to deliver the product. The first strategy is the polymerization of monomers, where the emulsion polymerization method is widely used and can be considered as of the methods of the first strategy. The second strategy is a dispersion of preformed polymers, more precisely, dispersion of a readily available synthetic or natural polymer in a polar or non-polar solvent. According to PNPs' application, raw materials and resources, one of these strategies can become more efficient than the other one.

PLGA NPs were fabricated by diffusive nanoprecipitation and it was demonstrated that the higher polymer concentration increased the average diameter of the produced PNP [24].

1.4.3 Theory behind the non-emulsion-based PNP formation

1.4.3.1 Diffusion-advection relations by Peclet number

While using microfluidic devices, flow is generally laminar which allows a controlled diffusion or convection [137]. In general, it becomes crucial to estimate whether the system is dominated by diffusion or advection, this is why (P_e) the Peclet number is necessary (Equation 1.5). P_e increases when the flow rate increases and decreases when diffusion coefficient is increased. Thus, a higher P_e means an advection dominated contribution. To reduce P_e for an improved diffusion contribution, the fluid velocity reduced. As reported in the literature, this can be done by enlarging the fluid cross-section area or by splitting this single flow into several channels [161].

$$P_e = \frac{L_c \nu}{D_c} \quad \text{Equation 1.5}$$

with L_c (m) the characteristic length, ν ($\text{m}\cdot\text{s}^{-1}$) the fluid's average velocity, and D_c ($\text{m}^2 \text{s}^{-1}$) the diffusion coefficient [161].

1.4.3.2 Mixing time

In non-emulsion based PNPs' fabrication methods, the key principle is a fast mixing of two miscible solutions (polymer solution/non-solvent). Here, the material which is going to form the NPs should be soluble in the solvent, however, the same material should stay insoluble in the non-solvent [136]. The solvent transfer, which takes place while mixing, can be underlined as the main driving process parameter to control the nanoprecipitation, and this is directly influenced by the physicochemical parameters of two solvents. It's been demonstrated that this transfer phenomenon can be controlled by referring to the microfluidics [136]. For example, a high-pressure interdigital multilamination micromixer (HPIMM) was used to realize the nanoprecipitation with controlled mixing [50]. Diffusion that takes place in the hydrodynamic flow focusing zone of this device where the width of each fluid to be mixed is in micron range (L_c). Thus, geometries of the channel but also a ratio between aqueous and organic phases may control the time of diffusion. All these factors can be expressed in the following equation (Equation 1.6).

$$\tau_{mix} \sim \frac{w_f^2}{4D_c} \approx \frac{w^2}{9D_c} \frac{1}{\left(1+\frac{1}{r}\right)^2} \quad \text{Equation 1.6}$$

With τ_{mix} (s) the mixing time, D_c ($\text{m}^2 \text{s}^{-1}$) diffusion coefficient, w_f (m) the width of a flowing stream, w (m) the channel width, and (r) the ratio of two flowing streams flow rates [49].

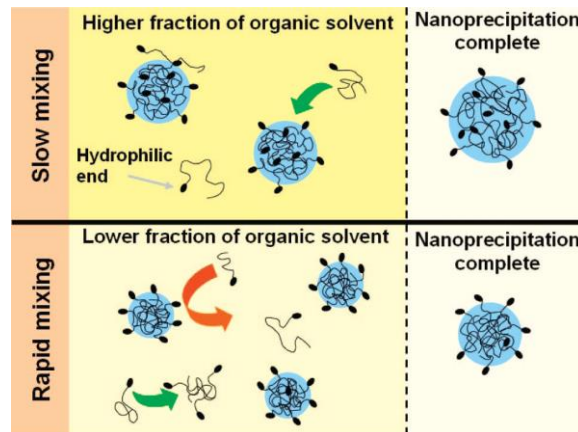


Figure 1.26. Two different self-assembly mechanisms depending on a rate of mixing during NPs formation by nanoprecipitation [49].

In this diffusion/precipitation method, NPs are formed only if the mixing time is greater than the intrinsic aggregation time (Figure 1.26). Here the organic phase is kept at high fraction that polymers can grow by adsorbing into nanoparticle aggregates driven by the hydrophilic end groups. Controversially to the slow mixing, at high mixing rates, a small organic fraction is enough to form

NPs through aggregation of polymer, and molecules don't have enough residence time to adsorb into nanoparticle matrix and grow larger with the hydrophilic end groups attached inside the nanoparticle [49].

To design the nanoprecipitation, spontaneous self-assembly of polymers can be expressed by a supersaturation ratio when the solvent quality is selectively altered [56]. Rapid self-assembly of polymers can be characterized by critical attributes like solvent content and temperature, which are driving the nucleation to reach an initial supersaturation ratio, $S_0 = C_p / C_{cmc} > 10^2$, where the unimer concentration in an initial state is C_p , the final micelle concentration following the NP nucleation and growth C_{cmc} . The homogenous mixing kinetics can be achieved when the mixing time is less than the aggregation time [56]. In this context, lower particle size can be achieved by increasing the jet velocity until particle size becomes stable, which is called a breakpoint and corresponds to (Da_p) Damkohler number (Equation 1.7) [56], [162].

$$Da_p = T_{mix} / T_{agg} \quad \text{Equation 1.7}$$

Where time ratios of mixing and aggregation are considered. Processes involving both reaction and mixing can be correlated by Da_p number [162]. On one hand, under homogeneous conditions ($Da_p < 1$), NPs are formed following polymer molecule nucleation and diffusion limited growth mechanism [162]. If we compare it with the normal crystallization process, polymers here self-assemble due to the entropic shifts following the internal degrees of freedom, which is not always the case for the crystallization of small molecules [56], [76]. It was demonstrated that, when $Da_p < 1$, only the solvent ratio can affect the critical aggregation number because mixing time is short, and agglomeration takes place very slow. For instance, different concentrations of polystyrene (10)-b-polyethylene oxide in tetrahydrofuran were mixed with a water stream. Here, the critical water content was near 20% and the initial supersaturation ratio was $S_0 > 100$ when the particle size remained stable over time after reaching a breakpoint [56].

On the other hand, when $Da_p > 1$, *i.e.* the time to homogenize the solvent and non-solvent phases is very long, the time to form polymeric structures is too short. In this case, the slow exchange and diffusion of the solvents will prolong the time of fusion leading to higher aggregation.

1.5 POST-PRODUCTION POSSIBILITIES WITH PNPs

1.5.1 Stability of polymeric nanoparticles

One of the stability challenges in nanoparticles is the particle agglomeration in nanosuspensions. Agglomeration is adhesion of particles by weak forces leading to formation of larger species. These interactions between PNPs are much weaker than the interactions in aggregation. The agglomeration is an inevitable chain auto-process of the system, and it is minimized thanks to the Brownian motion that is continuously active above zero Kelvin. No matter the efforts of the particles moving by the Brownian theory, several factors can be considered when it comes to the stability of colloidal suspensions [62], [73], [80]: (i) surfactant molecules adsorbed onto (or desorbed from) the nanoparticles' surface, (ii) nanoparticle size or charge, measured by zeta potential, (iii) the solution's pH and (iv) the eventual molecule encapsulated into the PNPs. These factors can become more crucial in the industrial application of PNPs, in prolonged storage periods with low physicochemical stability. For example, curcumin-loaded oil-in-water emulsions produced with different surfactants like arabic gum, saponins, tween, sodium caseinate and their different concentrations were studied, and demonstrated that the thermal stability of the emulsion, degradation and also curcumin retention time varies according to these parameters. Emulsion droplet was larger with the arabic gum, also impact of pH to emulsion stability varied when compared to others. The excess of an emulsifier at lower pH increased the particle size, however, in some cases, it improved the thermal stability [59].

To minimize or limit these physicochemical challenges, lyophilization (freeze-drying) after NPs' fabrication [163] and spray drying was demonstrated [73] were suggested to dry nanodispersions and thus to improve the stability of the polymeric nanoparticles.

1.5.2 Drug release studies

Drug targeting can be classified as active or passive targeting. The first targeting is fulfilled following a direct interaction of PNPs or drug with the cell. This interaction is due to the presence of specific targeting group at the surface of the PNPs dedicated to reach the cell, where the drug should be released. The passive targeting is based on an accumulation of PNPs in solid tumor cell by penetration, which is induced by enhanced permeation retention (EPR). Regardless of the drug targeting, the systems should follow four important requirements: retaining, evading, targeting and releasing [53].

Certain PNPs made of cationic polymers have been reported to be applied in a specific treatment as these nanocarriers can cross the blood-brain barrier (BBB) [6], [89]. From the cationic polymers' family, chitosan can be given as a good example because it is one of the frequently used polysaccharides in PNPs' production due to its high biodegradability and biocompatibility [12]. In the literature, a considerable amount of estradiol was delivered to the central nervous system *via* intranasal delivery from estradiol-loaded chitosan nanoparticle conjugates of around 300 nm produced by ionic gelation method [90]. Another team has reported the possibility of delivering peptides, caspase inhibitors (a family of protease enzymes) and dopamine directly to the central nervous system by using chitosan nanospheres (150-600 nm) conjugated with PEG [22], [150]. Moreover, surface modification of chitosan-based nanoparticles is easy, as reported by Aktas *et al.* for tailoring PNPs with different ligands to bypass the brain-blood barrier, and receptor antibodies [6], [17]. Indeed, chitosan was surface modified with biotin-PEG in the presence of NHS and N-(3-dimethylaminopropyl)-N'-ethylcarbodiimide hydrochloride under 24 hours stirring, then CS-PEG-Bio modified polymer foam with 83% grafting yield was received [164]. A nucleic acid delivery has been seeming more efficient since chitosan amino groups got protonated through manipulations over the molecule [12], [89]. In practice, to prolong the drug release period PAA or bovine serum albumin (BSA) were used to create a layer on a micro-droplet surface with hydrophobic poloxamer molecules [31].

It was also reported that the particle/drug pair has to be carefully chosen in order to control the drug's release kinetics. For instance, while studying the release of drugs such as docetaxel and cisplatin, the first drug was released faster than the second one under similar conditions, and this difference was explained by cisplatin being covalently bonded to the carrier's poly(acrylamide) matrix, where docetaxel is attached non-covalently [53]. In another similar study, poly(acrylamide) (PAA) was incorporated with poly(ethylenimine) (PEI) to compare cisplatin loading. The published results showed that cisplatin total release amount increased from 15% to around 25% when the PEI quantity was increased [79]. Considering the fact that PEI and PAA are oppositely charged polymers, this can reduce a covalent bond formation with cisplatin as a result of an already reduced polymer reactivity (Figure 1.27). Overall, a drug release can be improved by reducing possible covalent bonds between an active ingredient and a charged polymer matrix.

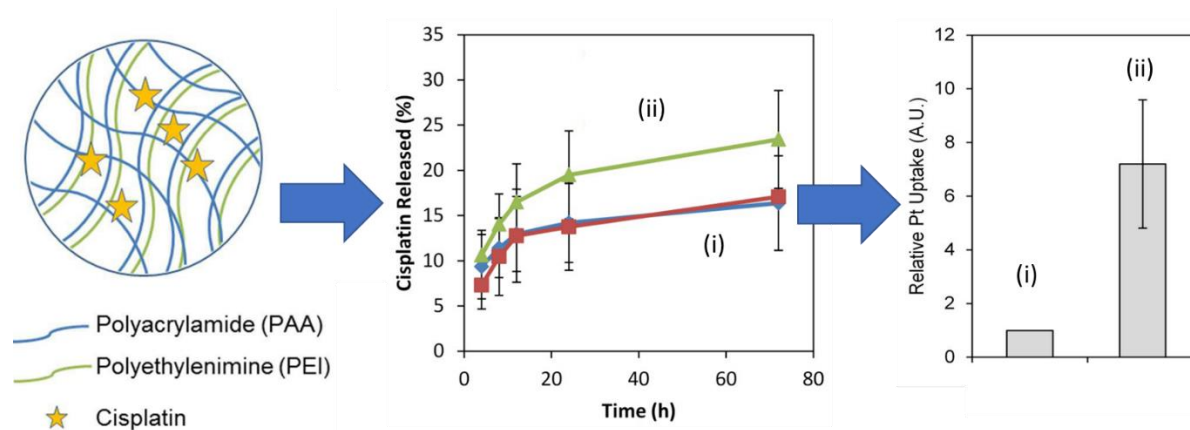


Figure 1.27. Comparison of (i) cisplatin-loaded poly(acrylamide) and (ii) poly(ethylenimine)-based poly(acrylamide) NPs with their cisplatin release kinetics, and on the right hand side, Pt uptake by a healthy model cell from cisplatin loaded NPs [79].

1.5.3 Safety of polymeric nanoparticles

Considering the fact that both emulsion and non-emulsion designs can include materials like drugs, polymer or surfactant micelles, and excess of unreacted monomers, initiators, or stabilizers following the PNP fabrication, these materials, especially the toxic ones are required to be eliminated from the system. However, this may require a very long and costly trials. In general, new methods for PNPs toxicity assessments are highly demanded [87]. Recent advances in NPs were demonstrated through different applications such as improved pharmacokinetics, also tailored biodistribution of active pharmaceutical ingredients (APIs) [6], [84]. It's also possible to deliver peptides and proteins for gene therapy with ameliorated toxicity parameters. Here NPs' parameters such as size, size distribution, surface charge, and quality factors like bioavailability, biocompatibility, degradation, and encapsulation capacity are crucial parameters that directly affect the material's performance *in vivo*. [165].

PNPs produced by methods that don't involve polymerization are considered as versatile approaches in medical [6], [9], and food industries [11] for their purity and biocompatibility. [24].

In medical applications, for long-term safety goals, the drug carriers are designed to be temporarily eliminated or reduced after the drug is completely released [6]. For this reason, preferably biodegradable materials, such as peptidyl- [166], amide- [29], [78], hydrazine- or carbonate-based PNPs [167], are chosen for their degradability with time and their no accumulation in the body, by avoiding renal filtration and potentially evolving long-term side effects.

PNPs made of the chitosan-alginate biodegradable polymers loaded with lutein revealed neither mortality nor morphological or clinical changes in rats at 10 mg/kg dose [168]. In general, the safety-

evaluation studies are limited in numbers for different applications, for instance, in food industries leaving a need for safety studies [11], [87]. Also compared to the traditional pollutants, nearly no data is available regarding NNP and ENP toxicity in water applications [25]. The toxicity assessments can be done with PNPs in DD, for example, highly DOX-loaded NPs showed higher cytotoxicity than the NPs with adjacent drug loading.

PNPs at a range of 20-200 nm size were frequently used as carriers for delivering active cosmeceutical biocompounds into the skin by penetrating skin pores. Fluorescent polystyrene NPs, Nile Red-loaded poly (ϵ -caprolactone) (PLC) were cooperated into skin pores to study its distribution [35]. In a recent study, retinol, against acne, wrinkles type of skin conditions, was encapsulated inside Eudragit RS 100 by emulsification-solvent evaporation method to fabricate 350 nm cationic PNPs for cosmeceutical applications to reduce retinols' toxicity due to its high reactivity [9].

As generally accepted, some organic solvents, such as DCM, tetrahydrofuran, chloroform, or cyclohexane, can promote toxicity and environmental risks, so, in cases of contamination, solvent residues must be eliminated from the final product through post-treatment steps. To overcome this, in all the possible scenarios, these solvents have been replaced with ethyl acetate, which was classified as GRAS (generally regarded as safe) by the FDA. Considering the entry of ethyl acetate into the market it has been shown a better toxicological profile than the other nanomaterials that use highly toxic solvents, especially for bio applications [73], [169].

1.6 CONCLUSION

In this chapter, various polymeric nanoparticles (PNPs) were discussed with their methods of fabrication, including operation conditions, pre- and post-process parameters influencing their size, size distribution, stability, etc. Applications in biomedicine, cosmetics, and food industries have evolved a large demand for PNPs fabrication, where morphology need to be fully controlled through the process design and parameters (mixing conditions, time, compositions, ratios, etc.). Thus, it is essential to consider various fabrication methods to maintain these properties with high reproducibility. It was demonstrated that, there were different methods to produce PNPs having a controlled size and size dispersity, including microfluidic devices which were found to be effective and reproducible. It can be concluded that PNPs produced by microfluidic, high-shear mixing and acoustic methods can particularly be found scalable and robust in design. Particularly found in medical, and cosmeceutical industries where these methods were used frequently to deliver active ingredients from PNPs. Also, it was demonstrated that some of shear mixing and sonication methods required the accompanying devices to maintain their continuous operability. It would be interesting

to study operating parameters like flow rate and operating volume to elaborate PNPs with these continuous processes.

In this work we compared and suggested that PNPs can be fabricated with both emulsion and non-emulsion design. According to the design, the processes were also characterized as one-step or multi-step, in small or industrial scale, where the physicochemical properties of PNPs were controlled according to the final material properties. Here, as the main difference it can be concluded that some emulsification processes require additional compounds like surfactants, stabilizers to promote stability and smaller droplet size. However, the non-emulsion design allows choosing methods of fabrication that have no emulsion stability requirements. When comparing PNPs' fabrication with pre-formed polymers, microfluidics appeared promising for being able to be used in both emulsion and non-emulsion-based designs to achieve the required PNPs' properties. For example, microfluidic synthesis of PNPs can give an access to control morphology and size which are important in the emerging field of nanomedicine. These methods offer exciting avenues to understand and control nanoprecipitation, also for tailoring PNPs' properties through controlling NPs self-assembly. For this reason, following parts of the current manuscript are dedicated to the elaboration of PNPs by shear mixing, ultrasonic and microfluidic techniques.

Additionally, there is an open window to develop one-step PNPs production methods, especially for biomedical applications. Also, most of the processes using toxic and environmentally dangerous solvents, and other materials can be avoided through improved or fundamentally new methods of fabrication. It should be noted that there is a gap between the number of produced nanomaterials and their cytotoxicity assessments as many newly developed systems lack these assessments due to the long-lasting and costly trials of cytotoxicity procedures. Following this, other solutions, such as the development of the data to estimate the most probable PNPs systems to be cytotoxic in different environments through artificial intelligence can be a future perspective of the field.

1.7 BIBLIOGRAPHY

- [1] O. Bondarenko, K. Juganson, A. Ivask, K. Kasemets, M. Mortimer, and A. Kahru, "Toxicity of Ag, CuO and ZnO nanoparticles to selected environmentally relevant test organisms and mammalian cells in vitro: A critical review," *Arch. Toxicol.*, vol. 87, no. 7, pp. 1181–1200, 2013, doi: 10.1007/s00204-013-1079-4.
- [2] M. Alam, "Photocatalytic activity of biogenic zinc oxide nanoparticles: In vitro antimicrobial, biocompatibility, and molecular docking studies," *Nanotechnol. Rev.*, vol. 10, no. 1, pp. 1079–1091, 2021, doi: 10.1515/ntrev-2021-0069.
- [3] J. Allan *et al.*, "Regulatory landscape of nanotechnology and nanoplastics from a global

- perspective," *Regul. Toxicol. Pharmacol.*, vol. 122, no. October 2020, p. 104885, 2021, doi: 10.1016/j.yrtph.2021.104885.
- [4] J. C. Cazotti, A. T. Fritz, O. Garcia-Valdez, N. M. B. Smeets, M. A. Dubé, and M. F. Cunningham, "Graft modification of starch nanoparticles using nitroxide-mediated polymerization and the grafting from approach," *Carbohydr. Polym.*, vol. 228, no. September 2019, p. 115384, 2020, doi: 10.1016/j.carbpol.2019.115384.
- [5] H. H. Liu and Y. Cohen, "Multimedia environmental distribution of nanomaterials (MendNano)," *Tech. Proc. 2012 NSTI Nanotechnol. Conf. Expo, NSTI-Nanotech 2012*, pp. 304–306, 2012.
- [6] Y. Aktaş *et al.*, "Development and brain delivery of chitosan-PEG nanoparticles functionalized with the monoclonal antibody OX26," *Bioconjug. Chem.*, vol. 16, no. 6, pp. 1503–1511, 2005, doi: 10.1021/bc050217o.
- [7] C. Hacettepe, R. K. Farmas, T. Program, and S. Tez, "Serbest Radıkal Temgzleyıgı Madde ıçeren Nanopartıküler Tađiyici Sđstemlerđn Tasari Mi Ve Deđerlendırđlmesđ," 2010.
- [8] K. Hörmann and A. Zimmer, "Drug delivery and drug targeting with parenteral lipid nanoemulsions - A review," *J. Control. Release*, vol. 223, pp. 85–98, 2016, doi: 10.1016/j.jconrel.2015.12.016.
- [9] F. Goudon, Y. Clément, and L. Ripoll, "Controlled release of retinol in cationic co-polymeric nanoparticles for topical application," *Cosmetics*, vol. 7, no. 2, pp. 1–9, 2020, doi: 10.3390/COSMETICS7020029.
- [10] A. Nasir, A. Kausar, and A. Younus, "A Review on Preparation, Properties and Applications of Polymeric Nanoparticle-Based Materials," *Polym. - Plast. Technol. Eng.*, vol. 54, no. 4, pp. 325–341, 2015, doi: 10.1080/03602559.2014.958780.
- [11] M. I. Guerra-Rosas, J. Morales-Castro, L. A. Ochoa-Martínez, L. Salvia-Trujillo, and O. Martín-Belloso, "Long-term stability of food-grade nanoemulsions from high methoxyl pectin containing essential oils," *Food Hydrocoll.*, vol. 52, pp. 438–446, 2016, doi: 10.1016/j.foodhyd.2015.07.017.
- [12] K. Nagpal, "Chitosan Nanoparticles: A Promising System in Novel Drug Delivery," *Chem. Pharm. Bull.*, vol. 58, no. November, 2010.
- [13] T. Pulingam, P. Foroozandeh, J. A. Chuah, and K. Sudesh, "Exploring Various Techniques for the Chemical and Biological Synthesis of Polymeric Nanoparticles," *Nanomaterials*, vol. 12, no. 3, 2022, doi: 10.3390/nano12030576.
- [14] N. J. Hunt, P. A. G. McCourt, Z. Kuncic, D. G. Le Couteur, and V. C. Cogger, "Opportunities and Challenges for Nanotherapeutics for the Aging Population," *Front. Nanotechnol.*, vol. 4, no. January, pp. 1–15, 2022, doi: 10.3389/fnano.2022.832524.

- [15] R. P. Felton, M. Y. Jones, K. J. Davis, and G. R. Olson, "in vivo," *ToxSci Adv. Access*, 2016.
- [16] S. Sharma, R. Parveen, and B. P. Chatterji, "Toxicology of Nanoparticles in Drug Delivery," *Curr. Pathobiol. Rep.*, vol. 9, no. 4, pp. 133–144, 2021, doi: 10.1007/s40139-021-00227-z.
- [17] Y. H. Bae and K. Park, "Advanced drug delivery 2020 and beyond: Perspectives on the future," *Adv. Drug Deliv. Rev.*, vol. 158, pp. 4–16, 2020, doi: 10.1016/j.addr.2020.06.018.
- [18] I. U. Khan, C. A. Serra, N. Anton, and T. F. Vandamme, "Production of nanoparticle drug delivery systems with microfluidics tools," *Expert Opin. Drug Deliv.*, vol. 12, no. 4, pp. 547–562, 2015, doi: 10.1517/17425247.2015.974547.
- [19] W. Yu *et al.*, "Development of an Elongational-Flow Microprocess for the Production of Size-Controlled Nanoemulsions: Application to the Preparation of Monodispersed Polymer Nanoparticles and Composite Polymeric Microparticles," *Macromol. React. Eng.*, vol. 11, no. 1, pp. 1–10, 2017, doi: 10.1002/mren.201600025.
- [20] S. Sur, A. Rathore, V. Dave, K. R. Reddy, R. S. Chouhan, and V. Sadhu, "Recent developments in functionalized polymer nanoparticles for efficient drug delivery system," *Nano-Structures and Nano-Objects*, vol. 20, p. 100397, 2019, doi: 10.1016/j.nanoso.2019.100397.
- [21] M. Vauthier, M. Schmutz, and C. A. Serra, "One-step elaboration of Janus polymeric nanoparticles: A comparative study of different emulsification processes," *Colloids Surfaces A Physicochem. Eng. Asp.*, vol. 626, no. June, p. 127059, 2021, doi: 10.1016/j.colsurfa.2021.127059.
- [22] T. Esch and T. Esch, "This week in the journal," *J. Neurosci.*, vol. 41, no. 44, p. 9064, 2021, doi: 10.1523/JNEUROSCI.twij.41.44.2021.
- [23] N. Kolishetti *et al.*, "Engineering of self-assembled nanoparticle platform for precisely controlled combination drug therapy," *Proc. Natl. Acad. Sci. U. S. A.*, vol. 107, no. 42, pp. 17939–17944, 2010, doi: 10.1073/pnas.1011368107.
- [24] C. A. Serra *et al.*, "Coupling microreaction technologies, polymer chemistry, and processing to produce polymeric micro and nanoparticles with controlled size, morphology, and composition," *Macromol. React. Eng.*, vol. 7, no. 9, pp. 414–439, 2013, doi: 10.1002/mren.201300101.
- [25] P. Westerhoff *et al.*, "Low risk posed by engineered and incidental nanoparticles in drinking water," *Nat. Nanotechnol.*, vol. 13, no. 8, pp. 661–669, 2018, doi: 10.1038/s41565-018-0217-9.
- [26] A. S. Peshkovsky, S. L. Peshkovsky, and S. Bystryak, "Scalable high-power ultrasonic technology for the production of translucent nanoemulsions," *Chem. Eng. Process. Process Intensif.*, vol. 69, pp. 77–82, 2013, doi: 10.1016/j.cep.2013.02.010.
- [27] M. Vauthier and C. A. Serra, "One-step production of polyelectrolyte nanoparticles," *Polym.*

- Int.*, vol. 70, no. 6, pp. 860–865, 2021, doi: 10.1002/pi.6178.
- [28] B. Y. Liu, C. Wu, X. Y. He, R. X. Zhuo, and S. X. Cheng, “Multi-drug loaded vitamin E-TPGS nanoparticles for synergistic drug delivery to overcome drug resistance in tumor treatment,” *Sci. Bull.*, vol. 61, no. 7, pp. 552–560, 2016, doi: 10.1007/s11434-016-1039-5.
- [29] M. Sheikhpour, L. Barani, and A. Kasaeian, “Biomimetics in drug delivery systems: A critical review,” *J. Control. Release*, vol. 253, pp. 97–109, 2017, doi: 10.1016/j.jconrel.2017.03.026.
- [30] T. Wei *et al.*, “Anticancer drug nanomicelles formed by self-assembling amphiphilic dendrimer to combat cancer drug resistance,” *Proc. Natl. Acad. Sci. U. S. A.*, vol. 112, no. 10, pp. 2978–2983, 2015, doi: 10.1073/pnas.1418494112.
- [31] S. Ding, C. A. Serra, T. F. Vandamme, W. Yu, and N. Anton, “Double emulsions prepared by two-step emulsification: History, state-of-the-art and perspective,” *J. Control. Release*, vol. 295, no. December 2018, pp. 31–49, 2019, doi: 10.1016/j.jconrel.2018.12.037.
- [32] M. Rahman, S. Laurent, N. Tawil, L. Yahia, and M. Mahmoudi, “Nanoparticle and Protein Corona,” pp. 21–44, 2013, doi: 10.1007/978-3-642-37555-2_2.
- [33] K. Amreen and S. Goel, “Review—Miniaturized and Microfluidic Devices for Automated Nanoparticle Synthesis,” *ECS J. Solid State Sci. Technol.*, vol. 10, no. 1, p. 017002, 2021, doi: 10.1149/2162-8777/abdb19.
- [34] M. Yerramilli and S. Ghosh, “Long-term stability of sodium caseinate-stabilized nanoemulsions,” *J. Food Sci. Technol.*, vol. 54, no. 1, pp. 82–92, 2017, doi: 10.1007/s13197-016-2438-y.
- [35] D. Bahamonde-Norambuena, A. Molina-Pereira, M. Cantin, M. Muñoz, K. Zepeda, and C. Vilos, “Polymeric Nanoparticles in Dermocosmetic,” *Int. J. Morphol.*, vol. 33, no. 4, pp. 1563–1568, 2015, doi: 10.4067/s0717-95022015000400061.
- [36] M. J. Derry, T. Smith, P. S. O’Hora, and S. P. Armes, “Block Copolymer Nanoparticles Prepared via Polymerization-Induced Self-Assembly Provide Excellent Boundary Lubrication Performance for Next-Generation Ultralow-Viscosity Automotive Engine Oils,” *ACS Appl. Mater. Interfaces*, vol. 11, no. 36, pp. 33364–33369, 2019, doi: 10.1021/acsami.9b12472.
- [37] D. Bennet and S. Kim, “Polymer Nanoparticles for Smart Drug Delivery,” *Appl. Nanotechnol. Drug Deliv.*, 2014, doi: 10.5772/58422.
- [38] R. Singh and J. W. Lillard, “Nanoparticle-based targeted drug delivery,” *Exp. Mol. Pathol.*, vol. 86, no. 3, pp. 215–223, 2009, doi: 10.1016/j.yexmp.2008.12.004.
- [39] G. G. Pitt, M. M. Gratzl, G. L. Kimmel, J. Surles, and A. Sohindler, “Aliphatic polyesters II. The degradation of poly (DL-lactide), poly (ϵ -caprolactone), and their copolymers in vivo,” *Biomaterials*, vol. 2, no. 4, pp. 215–220, 1981, doi: 10.1016/0142-9612(81)90060-0.
- [40] G. Birrenbach and P. P. Speiser, “Polymerized micelles and their use as adjuvants in

- immunology," *J. Pharm. Sci.*, vol. 65, no. 12, pp. 1763–1766, 1976, doi: 10.1002/jps.2600651217.
- [41] N. Visaveliya, A. Knauer, W. Yu, C. A. Serra, and J. M. Köhler, "Microflow-assisted assembling of multi-scale polymer particles by controlling surface properties and interactions," *Eur. Polym. J.*, vol. 80, pp. 256–267, 2016, doi: 10.1016/j.eurpolymj.2016.03.015.
- [42] Z. Rahiminezhad, A. M. Tamaddon, S. Borandeh, and S. S. Abolmaali, "Janus nanoparticles: New generation of multifunctional nanocarriers in drug delivery, bioimaging and theranostics," *Appl. Mater. Today*, vol. 18, p. 100513, 2020, doi: 10.1016/j.apmt.2019.100513.
- [43] J. Wallyn *et al.*, "A new formulation of poly(MAOTIB) nanoparticles as an efficient contrast agent for in vivo X-ray imaging," *Acta Biomater.*, vol. 66, pp. 200–212, 2018, doi: 10.1016/j.actbio.2017.11.011.
- [44] S. Ding *et al.*, "A new method for the formulation of double nanoemulsions," *Soft Matter*, vol. 13, no. 8, pp. 1660–1669, 2017, doi: 10.1039/c6sm02603f.
- [45] J. Xu, B. Xu, D. Shou, X. Xia, and Y. Hu, "Preparation and evaluation of vancomycin-loaded N-trimethyl chitosan nanoparticles," *Polymers (Basel)*, vol. 7, no. 9, pp. 1850–1870, 2015, doi: 10.3390/polym7091488.
- [46] L. Katharina and R. Montenegro, "Semiconducting Polymer Nanospheres in Aqueous Dispersion Prepared by a Miniemulsion Process," *J. Vinyl Addit. Technol.*, vol. 4, no. 2, pp. 117–125, 2002, doi: 10.1002/vnl.10028.
- [47] J. Jiao, D. G. Rhodes, and D. J. Burgess, "Multiple emulsion stability: Pressure balance and interfacial film strength," *J. Colloid Interface Sci.*, vol. 250, no. 2, pp. 444–450, 2002, doi: 10.1006/jcis.2002.8365.
- [48] D. Zwicker, A. A. Hyman, and F. Jülicher, "Suppression of Ostwald ripening in active emulsions," *Phys. Rev. E - Stat. Nonlinear, Soft Matter Phys.*, vol. 92, no. 1, pp. 1–13, 2015, doi: 10.1103/PhysRevE.92.012317.
- [49] R. Karnik *et al.*, "Microfluidic Platform for Controlled Synthesis of Polymeric Nanoparticles Rohit," *Nano Lett.*, vol. 8, No. 9, no. 2906–2912, 2008.
- [50] F. Bally, C. A. Serra, C. Brochon, N. Anton, T. Vandamme, and G. Hadziioannou, "A continuous-flow polymerization microprocess with online GPC and inline polymer recovery by micromixer-assisted nanoprecipitation," *Macromol. React. Eng.*, vol. 5, no. 11–12, pp. 542–547, 2011, doi: 10.1002/mren.201100047.
- [51] J. James *et al.*, "Scale-up of batch rotor–stator mixers. Part 1—power constants," *Chem. Eng. Res. Des.*, vol. 124, pp. 313–320, 2017, doi: 10.1016/j.cherd.2017.06.020.
- [52] A. Taha *et al.*, "Ultrasonic emulsification: An overview on the preparation of different emulsifiers-stabilized emulsions," *Trends Food Sci. Technol.*, vol. 105, pp. 363–377, 2020, doi:

- 10.1016/j.tifs.2020.09.024.
- [53] I. U. Khan *et al.*, "Microfluidic conceived Trojan microcarriers for oral delivery of nanoparticles," *Int. J. Pharm.*, vol. 493, no. 1–2, pp. 7–15, 2015, doi: 10.1016/j.ijpharm.2015.06.028.
- [54] H. Kempe and M. Kempe, "Ouzo polymerization: A bottom-up green synthesis of polymer nanoparticles by free-radical polymerization of monomers spontaneously nucleated by the Ouzo effect; Application to molecular imprinting," *J. Colloid Interface Sci.*, vol. 616, pp. 560–570, 2022, doi: 10.1016/j.jcis.2022.02.035.
- [55] G. M. Nabar *et al.*, "Micelle-templated, poly(lactic-co-glycolic acid) nanoparticles for hydrophobic drug delivery," *Int. J. Nanomedicine*, vol. 13, pp. 351–366, 2018, doi: 10.2147/IJN.S142079.
- [56] B. K. Johnson and R. K. Prud'homme, "Mechanism for rapid self-assembly of block copolymer nanoparticles," *Phys. Rev. Lett.*, vol. 91, no. 11, pp. 1–4, 2003, doi: 10.1103/PhysRevLett.91.118302.
- [57] P. Iqbal, J. A. Preece, and P. M. Mendes, "Nanotechnology: The 'Top-Down' and 'Bottom-Up' Approaches," *Supramol. Chem.*, 2012, doi: 10.1002/9780470661345.smc195.
- [58] V. Lohmann, M. Rolland, N. P. Truong, and A. Anastasaki, "Controlling size, shape, and charge of nanoparticles via low-energy miniemulsion and heterogeneous RAFT polymerization," *Eur. Polym. J.*, vol. 176, no. June, p. 111417, 2022, doi: 10.1016/j.eurpolymj.2022.111417.
- [59] M. Kharat, G. Zhang, and D. J. McClements, "Stability of curcumin in oil-in-water emulsions: Impact of emulsifier type and concentration on chemical degradation," *Food Res. Int.*, vol. 111, no. April, pp. 178–186, 2018, doi: 10.1016/j.foodres.2018.05.021.
- [60] "View of Emulsion types, stability mechanisms and rheology.pdf." .
- [61] D. S. Kolotova, Y. A. Kuchina, L. A. Petrova, N. G. Voron'ko, and S. R. Derkach, "Rheology of water-in-crude oil emulsions: Influence of concentration and temperature," *Colloids and Interfaces*, vol. 2, no. 4, 2018, doi: 10.3390/colloids2040064.
- [62] D. J. McClements, "Nanoemulsions versus microemulsions: Terminology, differences, and similarities," *Soft Matter*, vol. 8, no. 6, pp. 1719–1729, 2012, doi: 10.1039/c2sm06903b.
- [63] S. Ding, C. A. Serra, N. Anton, W. Yu, and T. F. Vandamme, "Production of dry-state ketoprofen-encapsulated PMMA NPs by coupling micromixer-assisted nanoprecipitation and spray drying," *Int. J. Pharm.*, vol. 558, no. December 2018, pp. 1–8, 2019, doi: 10.1016/j.ijpharm.2018.12.031.
- [64] J. Abdurahim, C. A. Serra, C. Blanck, and M. Vauthier, "One-step production of highly monodisperse size-controlled poly(lactic-co-glycolic acid) nanoparticles for the release of a hydrophobic model drug," *J. Drug Deliv. Sci. Technol.*, vol. 71, no. May, p. 103358, 2022, doi:

- 10.1016/j.jddst.2022.103358.
- [65] Q. Mei *et al.*, "Formulation and in vitro characterization of rifampicin-loaded porous poly (ϵ -caprolactone) microspheres for sustained skeletal delivery," *Drug Des. Devel. Ther.*, vol. 12, pp. 1533–1544, 2018, doi: 10.2147/DDDT.S163005.
- [66] P. Zhu, H. Zhang, and H. Lu, "Preparation of polyetherimide nanoparticles by a droplet evaporation-assisted thermally induced phase-separation method," *Polymers (Basel)*, vol. 13, no. 10, 2021, doi: 10.3390/polym13101548.
- [67] W. Seifriz, "STUDIES IS EMULSIONS by William Seifriz," *Chem. Eng.*, 1925.
- [68] T. O. Ch *et al.*, "Insulin: Intestinal absorption as water-in-oil emulsions," vol. 219, pp. 856–857, 1968.
- [69] K. Zhang *et al.*, "Ultrasonic assisted water-in-oil emulsions encapsulating macro-molecular polysaccharide chitosan: Influence of molecular properties, emulsion viscosity and their stability," *Ultrason. Sonochem.*, vol. 64, p. 105018, 2020, doi: 10.1016/j.ultsonch.2020.105018.
- [70] R. C. Mundargi, V. R. Babu, V. Rangaswamy, P. Patel, and T. M. Aminabhavi, "Nano/micro technologies for delivering macromolecular therapeutics using poly(d,l-lactide-co-glycolide) and its derivatives," *J. Control. Release*, vol. 125, no. 3, pp. 193–209, 2008, doi: 10.1016/j.jconrel.2007.09.013.
- [71] M. Iqbal, J. P. Valour, H. Fessi, and A. Elaissari, "Preparation of biodegradable PCL particles via double emulsion evaporation method using ultrasound technique," *Colloid Polym. Sci.*, vol. 293, no. 3, pp. 861–873, 2015, doi: 10.1007/s00396-014-3464-9.
- [72] R. I. Pinhassi *et al.*, "Arabinogalactan-folic acid-drug conjugate for targeted delivery and target-activated release of anticancer drugs to folate receptor-overexpressing cells," *Biomacromolecules*, vol. 11, no. 1, pp. 294–303, 2010, doi: 10.1021/bm900853z.
- [73] N. Venkatesh *et al.*, "Polymeric Nanoparticles: Production, Characterization, Toxicology and Ecotoxicology," *Molecules*, vol. 25, p. 3731, 2020.
- [74] T. M. Squires and S. R. Quake, "Exact cnoidal solutions of the extended KdV equation," *Acta Phys. Pol. A*, vol. 133, no. 5, pp. 1191–1199, 2018, doi: 10.12693/APhysPolA.133.1191.
- [75] S. Ding, N. Anton, T. F. Vandamme, and C. A. Serra, "Microfluidic nanoprecipitation systems for preparing pure drug or polymeric drug loaded nanoparticles: an overview," *Expert Opin. Drug Deliv.*, vol. 13, no. 10, pp. 1447–1460, 2016, doi: 10.1080/17425247.2016.1193151.
- [76] K. Ouzineb, C. Graillat, and T. F. McKenna, "Study of compartmentalization in the polymerization of miniemulsions of styrene and butyl methacrylate," *J. Appl. Polym. Sci.*, vol. 91, no. 1, pp. 115–124, 2004, doi: 10.1002/app.13181.
- [77] S. Slomkowski *et al.*, "Terminology of polymers and polymerization processes in dispersed

- systems (IUPAC recommendations 2011),” *Pure Appl. Chem.*, vol. 83, no. 12, pp. 2229–2259, 2011, doi: 10.1351/PAC-REC-10-06-03.
- [78] I. U. Khan *et al.*, “Microfluidic conceived Trojan microcarriers for oral delivery of nanoparticles,” *Int. J. Pharm.*, vol. 493, no. 1–2, pp. 7–15, 2015, doi: 10.1016/j.ijpharm.2015.06.028.
- [79] T. Shirakura, A. Ray, and R. Kopelman, “Polyethylenimine incorporation into hydrogel nanomatrices for enhancing nanoparticle-assisted chemotherapy,” *RSC Adv.*, vol. 6, no. 53, pp. 48016–48024, 2016, doi: 10.1039/c6ra02414a.
- [80] S. Lazzari, D. Moscatelli, F. Codari, M. Salmona, M. Morbidelli, and L. Diomedea, “Colloidal stability of polymeric nanoparticles in biological fluids,” *J. Nanoparticle Res.*, vol. 14, no. 6, 2012, doi: 10.1007/s11051-012-0920-7.
- [81] R. H. Staff, K. Landfester, and D. Crespy, “Recent advances in the emulsion solvent evaporation technique for the preparation of nanoparticles and nanocapsules,” *Adv. Polym. Sci.*, vol. 262, no. October, pp. 329–344, 2013, doi: 10.1007/12_2013_233.
- [82] S. Hall, A. W. Pacek, A. J. Kowalski, M. Cooke, and D. Rothman, “The effect of scale and interfacial tension on liquid-liquid dispersion in in-line Silverson rotor-stator mixers,” *Chem. Eng. Res. Des.*, vol. 91, no. 11, pp. 2156–2168, 2013, doi: 10.1016/j.cherd.2013.04.021.
- [83] M. R. de Moura, F. A. Aouada, and L. H. C. Mattoso, “Preparation of chitosan nanoparticles using methacrylic acid,” *J. Colloid Interface Sci.*, vol. 321, no. 2, pp. 477–483, 2008, doi: 10.1016/j.jcis.2008.02.006.
- [84] N. Anton *et al.*, “A new microfluidic setup for precise control of the polymer nanoprecipitation process and lipophilic drug encapsulation,” *Soft Matter*, vol. 8, no. 41, pp. 10628–10635, 2012, doi: 10.1039/c2sm25357g.
- [85] S. Yus, Cristina. Manuel, Arruebo. Silvia, Irusta. Victor, “Microflow Nanoprecipitation of Positively Charged Gastroresistant Polymer Nanoparticles of Eudragit[®] Chemical Parameters,” 2020.
- [86] Y. F. Maa and C. Hsu, “Liquid-liquid emulsification by rotor/stator homogenization,” *J. Control. Release*, vol. 38, no. 2–3, pp. 219–228, 1996, doi: 10.1016/0168-3659(95)00123-9.
- [87] H. Lu, S. Zhang, J. Wang, and Q. Chen, “A Review on Polymer and Lipid-Based Nanocarriers and Its Application to Nano-Pharmaceutical and Food-Based Systems,” *Front. Nutr.*, vol. 8, no. December, pp. 1–13, 2021, doi: 10.3389/fnut.2021.783831.
- [88] M. Zhang, Q. Xiong, J. Chen, Y. Wang, and Q. Zhang, “A novel cyclodextrin-containing pH-responsive star polymer for nanostructure fabrication and drug delivery,” *Polym. Chem.*, vol. 4, no. 19, pp. 5086–5095, 2013, doi: 10.1039/c3py00656e.
- [89] T. Patel, J. Zhou, J. M. Piepmeier, and W. M. Saltzman, “Polymeric nanoparticles for drug

- delivery to the central nervous system," *Adv. Drug Deliv. Rev.*, vol. 64, no. 7, pp. 701–705, 2012, doi: 10.1016/j.addr.2011.12.006.
- [90] X. Wang, N. Chi, and X. Tang, "Preparation of estradiol chitosan nanoparticles for improving nasal absorption and brain targeting," *Eur. J. Pharm. Biopharm.*, vol. 70, no. 3, pp. 735–740, 2008, doi: 10.1016/j.ejpb.2008.07.005.
- [91] Y. H. Bae and K. Park, "Advanced drug delivery 2020 and beyond: Perspectives on the future," *Adv. Drug Deliv. Rev.*, vol. 158, pp. 4–16, 2020, doi: 10.1016/j.addr.2020.06.018.
- [92] S. Ding *et al.*, "Microfluidic-Assisted Production of Size-Controlled Superparamagnetic Iron Oxide Nanoparticles-Loaded Poly(methyl methacrylate) Nanohybrids," *Langmuir*, vol. 34, no. 5, pp. 1981–1991, 2018, doi: 10.1021/acs.langmuir.7b01928.
- [93] E. Ruckenstein, "Microemulsions, macroemulsions, and the Bancroft rule," *Langmuir*, vol. 12, no. 26, pp. 6351–6353, 1996, doi: 10.1021/la960849m.
- [94] G. R. Leonardi, M. M. Silva, C. M. Guimarães, F. de A. Perrechil, and S. Friberg, "Janus Emulsions of Bixa Orellana Oil," *J. Dispers. Sci. Technol.*, vol. 37, no. 12, pp. 1718–1723, 2016, doi: 10.1080/01932691.2016.1138230.
- [95] T. S. H. Leong, M. Zhou, N. Kukan, M. Ashokkumar, and G. J. O. Martin, "Preparation of water-in-oil-in-water emulsions by low frequency ultrasound using skim milk and sunflower oil," *Food Hydrocoll.*, vol. 63, pp. 685–695, 2017, doi: 10.1016/j.foodhyd.2016.10.017.
- [96] G. Colucci, A. Santamaria-Echart, S. C. Silva, I. P. M. Fernandes, C. C. Sipoli, and M. F. Barreiro, "Development of water-in-oil emulsions as delivery vehicles and testing with a natural antimicrobial extract," *Molecules*, vol. 25, no. 9, pp. 5–7, 2020, doi: 10.3390/molecules25092105.
- [97] S. Hao, B. Wang, Y. Wang, L. Zhu, B. Wang, and T. Guo, "Preparation of Eudragit L 100-55 enteric nanoparticles by a novel emulsion diffusion method," *Colloids Surfaces B Biointerfaces*, vol. 108, pp. 127–133, 2013, doi: 10.1016/j.colsurfb.2013.02.036.
- [98] Y. Zhao, Z. Chen, X. Zhu, and M. Möller, "A Facile One-Step Approach toward Polymer@SiO₂ Core-Shell Nanoparticles via a Surfactant-Free Miniemulsion Polymerization Technique," *Macromolecules*, vol. 49, no. 5, pp. 1552–1562, 2016, doi: 10.1021/acs.macromol.6b00038.
- [99] J. C. de La Cal, J. R. Leiza, J. M. Asua, A. Buttè, G. Storti, and M. Morbidelli, "Emulsion Polymerization," *Handb. Polym. React. Eng.*, no. June 2016, pp. 249–322, 2008, doi: 10.1002/9783527619870.ch6.
- [100] J. Faucheu, C. Gauthier, L. Chazeau, J. Y. Cavallé, V. Mellon, and E. B. Lami, "Miniemulsion polymerization for synthesis of structured clay/polymer nanocomposites: Short review and recent advances," *Polymer (Guildf.)*, vol. 51, no. 1, pp. 6–17, 2010, doi: 10.1016/j.polymer.2009.11.044.

- [101] D. Crespy and K. Landfester, "Miniemulsion polymerization as a versatile tool for the synthesis of functionalized polymers," *Beilstein J. Org. Chem.*, vol. 6, pp. 1132–1148, 2010, doi: 10.3762/bjoc.6.130.
- [102] J. Zhou, H. Yao, and J. Ma, "Recent advances in RAFT-mediated surfactant-free emulsion polymerization," *Polym. Chem.*, vol. 9, no. 19, pp. 2532–2561, 2018, doi: 10.1039/c8py00065d.
- [103] S. Bilgin, R. Tomovska, and J. M. Asua, "Surfactant-free high solids content polymer dispersions," *Polymer (Guildf.)*, vol. 117, pp. 64–75, 2017, doi: 10.1016/j.polymer.2017.04.014.
- [104] I. M. Valente *et al.*, "An Insight on Salting-out Assisted Liquid–Liquid Extraction for Phytoanalysis," *Phytochem. Anal.*, vol. 28, no. 4, pp. 297–304, 2017, doi: 10.1002/pca.2676.
- [105] A. M. Hyde, S. L. Zultanski, J. H. Waldman, Y. L. Zhong, M. Shevlin, and F. Peng, "General Principles and Strategies for Salting-Out Informed by the Hofmeister Series," *Org. Process Res. Dev.*, vol. 21, no. 9, pp. 1355–1370, 2017, doi: 10.1021/acs.oprd.7b00197.
- [106] M. Iqbal, N. Zafar, H. Fessi, and A. Elaissari, "Double emulsion solvent evaporation techniques used for drug encapsulation," *Int. J. Pharm.*, vol. 496, no. 2, pp. 173–190, 2015, doi: 10.1016/j.ijpharm.2015.10.057.
- [107] Y. Singh *et al.*, "Nanoemulsion: Concepts, development and applications in drug delivery," *J. Control. Release*, vol. 252, pp. 28–49, 2017, doi: 10.1016/j.jconrel.2017.03.008.
- [108] P. Sungwornpatansakul, J. Hiroi, Y. Nigahara, T. K. Jayasinghe, and K. Yoshikawa, "Enhancement of biodiesel production reaction employing the static mixing," *Fuel Process. Technol.*, vol. 116, pp. 1–8, 2013, doi: 10.1016/j.fuproc.2013.04.019.
- [109] F. Theron and N. Le Sauze, "Comparison between three static mixers for emulsification in turbulent flow," *Int. J. Multiph. Flow*, vol. 37, no. 5, pp. 488–500, 2011, doi: 10.1016/j.ijmultiphaseflow.2011.01.004.
- [110] T. Nakashima, M. Shimizu, and M. Kukizaki, "Particle control of emulsion by membrane emulsification and its applications," *Adv. Drug Deliv. Rev.*, vol. 45, no. 1, pp. 47–56, 2000, doi: 10.1016/S0169-409X(00)00099-5.
- [111] S. Van Der Graaf, C. G. P. H. Schroën, and R. M. Boom, "Preparation of double emulsions by membrane emulsification - A review," *J. Memb. Sci.*, vol. 251, no. 1–2, pp. 7–15, 2005, doi: 10.1016/j.memsci.2004.12.013.
- [112] A. Håkansson, "Rotor-stator mixers: From batch to continuous mode of operation-A review," *Processes*, vol. 6, no. 4, pp. 1–17, 2018, doi: 10.3390/pr6040032.
- [113] P. Scholz and C. M. Keck, "Nanoemulsions produced by rotor-stator high speed stirring," *Int. J. Pharm.*, vol. 482, no. 1–2, pp. 110–117, 2015, doi: 10.1016/j.ijpharm.2014.12.040.

- [114] W. Li, T. S. H. Leong, M. Ashokkumar, and G. J. O. Martin, "A study of the effectiveness and energy efficiency of ultrasonic emulsification," *Phys. Chem. Chem. Phys.*, vol. 20, no. 1, pp. 86–96, 2017, doi: 10.1039/c7cp07133g.
- [115] S. M. Jafari, E. Assadpoor, Y. He, and B. Bhandari, "Re-coalescence of emulsion droplets during high-energy emulsification," *Food Hydrocoll.*, vol. 22, no. 7, pp. 1191–1202, 2008, doi: 10.1016/j.foodhyd.2007.09.006.
- [116] R. C. Santana, F. A. Perrechil, and R. L. Cunha, "High- and Low-Energy Emulsifications for Food Applications: A Focus on Process Parameters," *Food Eng. Rev.*, vol. 5, no. 2, pp. 107–122, 2013, doi: 10.1007/s12393-013-9065-4.
- [117] O. D. H. Jasmina, "Preparation of Nanoemulsions by High-energy and Low-energy emulsification methods," *Springer Nat. Singapore*, vol. 62, pp. 317–322, 2017, doi: 10.1007/978-981-10-4166-2.
- [118] F. Zidouni, E. Krepper, R. Rzehak, S. Rabha, M. Schubert, and U. Hampel, "Simulation of gas-liquid flow in a helical static mixer," *Chem. Eng. Sci.*, vol. 137, pp. 476–486, 2015, doi: 10.1016/j.ces.2015.06.052.
- [119] Z. Anxionnaz, M. Cabassud, C. Gourdon, and P. Tochon, "Heat exchanger/reactors (HEX reactors): Concepts, technologies: State-of-the-art," *Chem. Eng. Process. Process Intensif.*, vol. 47, no. 12, pp. 2029–2050, 2008, doi: 10.1016/j.cep.2008.06.012.
- [120] R. Bierbaum, M. Nüchter, and B. Ondruschka, "Mikrowellenassistierte Reaktionsführung: Mikrowellenapparatur im Miniplant-Maßstab mit Online-Analytik," *Chemie-Ingenieur-Technik*, vol. 76, no. 7, pp. 961–965, 2004, doi: 10.1002/cite.200403417.
- [121] A. Ghanem, T. Lemenand, D. Della Valle, and H. Peerhossaini, "Static mixers: Mechanisms, applications, and characterization methods - A review," *Chem. Eng. Res. Des.*, vol. 92, no. 2, pp. 205–228, 2014, doi: 10.1016/j.cherd.2013.07.013.
- [122] M. M. Dragosavac, R. G. Holdich, G. T. Vladisavljević, and M. N. Sovilj, "Stirred cell membrane emulsification for multiple emulsions containing unrefined pumpkin seed oil with uniform droplet size," *J. Memb. Sci.*, vol. 392–393, pp. 122–129, 2012, doi: 10.1016/j.memsci.2011.12.009.
- [123] "Philosophical Magazine Series 7 XXXVIII . The physical and biological effects of high-frequency sound-waves of great intensity," no. September 2012, pp. 37–41, 2009.
- [124] K. Landfester, N. Bechthold, F. Tiarks, and M. Antonietti, "Formulation and stability mechanisms of polymerizable miniemulsions," *Macromolecules*, vol. 32, no. 16, pp. 5222–5228, 1999, doi: 10.1021/ma990299+.
- [125] A. Håkansson and F. Innings, "The dissipation rate of turbulent kinetic energy and its relation to pumping power in inline rotor-stator mixers," *Chem. Eng. Process. - Process Intensif.*, vol.

- 115, pp. 46–55, 2017, doi: 10.1016/j.cep.2017.01.007.
- [126] “The Royal Society is collaborating with JSTOR to digitize, preserve, and extend access to Proceedings of the Royal Society of London. ® www.jstor.org,” *Society*, 1880.
- [127] D. J. McClements, “Edible nanoemulsions: Fabrication, properties, and functional performance,” *Soft Matter*, vol. 7, no. 6, pp. 2297–2316, 2011, doi: 10.1039/c0sm00549e.
- [128] W. von R. Engels, T, “Lyotrope fliissigkristalline Phasen,” no. 1, pp. 1–2, 1999.
- [129] K. Roger, B. Cabane, and U. Olsson, “Emulsification through surfactant hydration: The PIC process revisited,” *Langmuir*, vol. 27, no. 2, pp. 604–611, 2011, doi: 10.1021/la1042603.
- [130] S. A. Vitale and J. L. Katz, “Liquid droplet dispersions formed by homogeneous liquid-liquid nucleation: ‘The ouzo effect,’” *Langmuir*, vol. 19, no. 10, pp. 4105–4110, 2003, doi: 10.1021/la026842o.
- [131] D. Carreau, D. Bassani, and I. Pianet, “The ‘Ouzo effect’: Following the spontaneous emulsification of trans-anethole in water by NMR,” *Comptes Rendus Chim.*, vol. 11, no. 4–5, pp. 493–498, 2008, doi: 10.1016/j.crci.2007.11.003.
- [132] F. Sciortino *et al.*, “The Ouzo effect to selectively assemble molybdenum clusters into nanomarbles or nanocapsules with increased HER activity,” *Chem. Commun.*, vol. 54, no. 95, pp. 13387–13390, 2018, doi: 10.1039/c8cc07402j.
- [133] K. Shinoda and H. Saito, “The effect of temperature on the phase equilibria and the types of dispersions of the ternary system composed of water, cyclohexane, and nonionic surfactant,” *J. Colloid Interface Sci.*, vol. 26, no. 1, pp. 70–74, 1968, doi: 10.1016/0021-9797(68)90273-7.
- [134] M. Parent, C. Nouvel, M. Koerber, A. Sapin, P. Maincent, and A. Boudier, “PLGA in situ implants formed by phase inversion: Critical physicochemical parameters to modulate drug release,” *J. Control. Release*, vol. 172, no. 1, pp. 292–304, 2013, doi: 10.1016/j.jconrel.2013.08.024.
- [135] K. Shinoda and H. Saito, “The Stability of O/W type emulsions as functions of temperature and the HLB of emulsifiers: The emulsification by PIT-method,” *J. Colloid Interface Sci.*, vol. 30, no. 2, pp. 258–263, 1969, doi: 10.1016/S0021-9797(69)80012-3.
- [136] S. Ding, N. Anton, T. F. Vandamme, and C. A. Serra, “Microfluidic nanoprecipitation systems for preparing pure drug or polymeric drug loaded nanoparticles: an overview,” *Expert Opin. Drug Deliv.*, vol. 13, no. 10, pp. 1447–1460, 2016, doi: 10.1080/17425247.2016.1193151.
- [137] C. Serra, N. Sary, G. Schlatter, G. Hadziioannou, and V. Hessel, “Numerical simulation of polymerization in interdigital multilamination micromixers,” *Lab Chip*, vol. 5, no. 9, pp. 966–973, 2005, doi: 10.1039/b500440c.
- [138] C. A. Serra and Z. Chang, “Microfluidic-assisted synthesis of polymer particles,” *Chem. Eng. Technol.*, vol. 31, no. 8, pp. 1099–1115, 2008, doi: 10.1002/ceat.200800219.

- [139] L. B. Braun, T. Hessberger, C. A. Serra, and R. Zentel, "UV-Free Microfluidic Particle Fabrication at Low Temperature Using ARGET-ATRP as the Initiator System," *Macromol. React. Eng.*, vol. 10, no. 6, pp. 611–617, 2016, doi: 10.1002/mren.201600015.
- [140] J. Feng *et al.*, "Nanoemulsions obtained via bubble-bursting at a compound interface," *Nat. Phys.*, vol. 10, no. 8, pp. 606–612, 2014, doi: 10.1038/nphys3003.
- [141] H. Steiner, R. Teppner, G. Brenn, N. Vankova, S. Tcholakova, and N. Denkov, "Numerical simulation and experimental study of emulsification in a narrow-gap homogenizer," *Chem. Eng. Sci.*, vol. 61, no. 17, pp. 5841–5855, 2006, doi: 10.1016/j.ces.2006.04.016.
- [142] A. P. Yong, M. Aminul ISLAM, and N. Hasan, "a Review: Effect of Pressure on Homogenization," *Nat Sci*, vol. 35, no. 1, pp. 1–22, 2017, [Online]. Available: <http://www.eds.yildiz.edu.tr/AjaxTool/GetArticleByPublishedArticleId?PublishedArticleId=2390>.
- [143] S. Tcholakova, N. D. Denkov, D. Sidzhakova, I. B. Ivanov, and B. Campbell, "Langmuir 2003 Tcholakova Interrelation between drop size and protein adsorption at various emulsification conditions," no. 13, pp. 5640–5649, 2003.
- [144] S. Ding, C. A. Serra, T. F. Vandamme, W. Yu, and N. Anton, "Double emulsions prepared by two-step emulsification: History, state-of-the-art and perspective," *J. Control. Release*, vol. 295, no. September 2018, pp. 31–49, 2019, doi: 10.1016/j.jconrel.2018.12.037.
- [145] S. M. M. Modarres-Gheisari, R. Gavagsaz-Ghoachani, M. Malaki, P. Safarpour, and M. Zandi, "Ultrasonic nano-emulsification – A review," *Ultrason. Sonochem.*, vol. 52, pp. 88–105, 2019, doi: 10.1016/j.ultsonch.2018.11.005.
- [146] A. Honciuc, *Chemistry of Functional Materials Surfaces and Interfaces: Fundamentals and Applications*. 2021.
- [147] M. F. Ficheux, L. Bonakdar, F. Leal-Calderon, and J. Bibette, "Some stability criteria for double emulsions," *Langmuir*, vol. 14, no. 10, pp. 2702–2706, 1998, doi: 10.1021/la971271z.
- [148] H. Schubert, R. Engel, and L. Kempa, "Principles of Structured Food Emulsions: Novel Formulations and Trends," *Glob. Issues Food Sci. Technol.*, pp. 3–19, 2009, doi: 10.1016/B978-0-12-374124-0.00001-6.
- [149] G. DeBruijn and S. M. Whitton, "Fluids," *Appl. Well Cem. Eng.*, pp. 163–251, 2021, doi: 10.1016/B978-0-12-821956-0.00012-2.
- [150] A. Trapani *et al.*, "Characterization and evaluation of chitosan nanoparticles for dopamine brain delivery," *Int. J. Pharm.*, vol. 419, no. 1–2, pp. 296–307, 2011, doi: 10.1016/j.ijpharm.2011.07.036.
- [151] P. Q. Nguyen, N. M. D. Courchesne, A. Duraj-Thatte, P. Praveschotinunt, and N. S. Joshi, "Engineered Living Materials: Prospects and Challenges for Using Biological Systems to Direct

- the Assembly of Smart Materials,” *Adv. Mater.*, vol. 30, no. 19, pp. 1–34, 2018, doi: 10.1002/adma.201704847.
- [152] K. H. Roh, D. C. Martin, and J. Lahann, “Biphasic Janus particles with nanoscale anisotropy,” *Nat. Mater.*, vol. 4, no. 10, pp. 759–763, 2005, doi: 10.1038/nmat1486.
- [153] T. Betancourt, B. Brown, and L. Brannon-Peppas, “Doxorubicin-loaded PLGA nanoparticles by nanoprecipitation: Preparation, characterization and in vitro evaluation,” *Nanomedicine*, vol. 2, no. 2, pp. 219–232, 2007, doi: 10.2217/17435889.2.2.219.
- [154] A. Grenha, B. Seijo, C. Serra, and C. Remuñán-López, “Chitosan nanoparticle-loaded mannitol microspheres: Structure and surface characterization,” *Biomacromolecules*, vol. 8, no. 7, pp. 2072–2079, 2007, doi: 10.1021/bm061131g.
- [155] X.-X. Tian and M. J. Groves, “ Formulation and Biological Activity of Antineoplastic Proteoglycans Derived from Mycobacterium vaccae in Chitosan Nanoparticles ,” *J. Pharm. Pharmacol.*, vol. 51, no. 2, pp. 151–157, 2010, doi: 10.1211/0022357991772268.
- [156] W. Tiyaboonchai and N. Limpeanchob, “Formulation and characterization of amphotericin B-chitosan-dextran sulfate nanoparticles,” *Int. J. Pharm.*, vol. 329, no. 1–2, pp. 142–149, 2007, doi: 10.1016/j.ijpharm.2006.08.013.
- [157] Q. Gan, T. Wang, C. Cochrane, and P. McCarron, “Modulation of surface charge, particle size and morphological properties of chitosan-TPP nanoparticles intended for gene delivery,” *Colloids Surfaces B Biointerfaces*, vol. 44, no. 2–3, pp. 65–73, 2005, doi: 10.1016/j.colsurfb.2005.06.001.
- [158] A. Bozkir and O. M. Saka, “Chitosan Nanoparticles for Plasmid DNA Delivery: Effect of Chitosan Molecular Structure on Formulation and Release Characteristics,” *Drug Deliv. J. Deliv. Target. Ther. Agents*, vol. 11, no. 2, pp. 107–112, 2004, doi: 10.1080/10717540490280705.
- [159] M. F. Moradali and B. H. A. Rehm, “Bacterial biopolymers: from pathogenesis to advanced materials,” *Nat. Rev. Microbiol.*, vol. 18, no. 4, pp. 195–210, 2020, doi: 10.1038/s41579-019-0313-3.
- [160] S. Ghosh, R. Ahmad, M. Zeyauallah, and S. K. Khare, “Microbial Nano-Factories: Synthesis and Biomedical Applications,” *Front. Chem.*, vol. 9, no. April, 2021, doi: 10.3389/fchem.2021.626834.
- [161] F. Noël, C. A. Serra, and S. Le Calvé, “Design of a novel axial gas pulses micromixer and simulations of its mixing abilities via computational fluid dynamics,” *Micromachines*, vol. 10, no. 3, pp. 1–16, 2019, doi: 10.3390/mi10030205.
- [162] A. J. Mahajan and D. J. Kirwan, “Micromixing Effects in a Two-Impinging-Jets Precipitator,” *AIChE J.*, vol. 42, no. 7, pp. 1801–1814, 1996, doi: 10.1002/aic.690420702.
- [163] A. Ziaee, A. B. Albadarin, L. Padrela, T. Femmer, E. O’Reilly, and G. Walker, “Spray drying of

- pharmaceuticals and biopharmaceuticals: Critical parameters and experimental process optimization approaches," *Eur. J. Pharm. Sci.*, vol. 127, pp. 300–318, 2019, doi: 10.1016/j.ejps.2018.10.026.
- [164] M. Yemisci, S. Caban, E. Fernandez-megia, Y. Capan, P. Couvreur, and T. Dalkara, "Chitosan Nanoparticles for Targeted Delivery," vol. 1727, pp. 443–454.
- [165] S. Garg, G. Heuck, S. Ip, and E. Ramsay, "Microfluidics: a transformational tool for nanomedicine development and production," *J. Drug Target.*, vol. 24, no. 9, pp. 821–835, 2016, doi: 10.1080/1061186X.2016.1198354.
- [166] S. Saranya and K. V. Radha, "Review of Nanobiopolymers for Controlled Drug Delivery," *Polym. - Plast. Technol. Eng.*, vol. 53, no. 15, pp. 1636–1646, 2014, doi: 10.1080/03602559.2014.915035.
- [167] I. Vroman and L. Tighzert, "Biodegradable polymers," *Materials (Basel)*, vol. 2, no. 2, pp. 307–344, 2009, doi: 10.3390/ma2020307.
- [168] V. Toragall, N. Jayapala, M. S P, and B. Vallikanan, "Biodegradable chitosan-sodium alginate-oleic acid nanocarrier promotes bioavailability and target delivery of lutein in rat model with no toxicity," *Food Chem.*, vol. 330, p. 127195, 2020, doi: 10.1016/j.foodchem.2020.127195.
- [169] V. R. Sinha and A. Trehan, "Biodegradable microspheres for protein delivery," *J. Control. Release*, vol. 90, no. 3, pp. 261–280, 2003, doi: 10.1016/S0168-3659(03)00194-9.

Chapter 2: Materials and Methods

PREFACE	99
2.1 MATERIALS	99
2.1.1 Solvents	99
2.1.1.1 Polar solvents	100
2.1.1.2 Non-polar solvents	100
2.1.2 Polymers	101
2.1.3 Emulsifiers	103
2.1.4 Rifampicin	104
2.1.5 Other materials	105
2.2 METHODS OF PREPARATION	105
2.2.1 Emulsion methods	105
2.2.1.1 Elongational-flow reactor and mixer	106
2.2.1.2 Shear-mixing	111
2.2.1.3 Sonication	113
2.2.2 Solvent removal	115
2.2.3 Non-emulsion method	118
2.2.4 Polymeric nanoparticle purification	119
2.3 METHODS OF CHARACTERIZATION	120
2.3.1 Analyses by spectroscopic methods	120
2.3.1.1 Dynamic Light Scattering & Zeta Potential	120
2.3.1.2 UV-visible Spectroscopy	122
2.3.1.3 Fourier Transform Infrared	123
2.3.1.4 Nuclear Magnetic Resonance	123
2.3.2 Methods of microscopic characterization	124
2.3.2.1 Transmission Electron Microscopy	124
2.3.2.2 Scanning Electron & Keyence Microscopies	124
2.3.2.3 Atomic Force Microscopy	124
2.3.3 Interfacial Tension Measurements	125
2.3.4 Other characterization methods	126
2.4 METHODS OF APPLICATION	126
2.4.1 Drug delivery studies	126
2.4.2 Stability	127
2.5 BIBLIOGRAPHY	128

Chapter 2

Materials and Methods

PREFACE

In this chapter, materials used for both emulsion and non-emulsion-based polymeric nanoparticles (PNP) fabrication designs, the protocols, and the characterization methods are described. Emulsion-based PNP fabrication design was built in three different, rotor-stator mixing, sonication, and elongational-flow micromixing emulsification approaches to later elaborate a suitable design for drug delivery application (Figure 2.1).

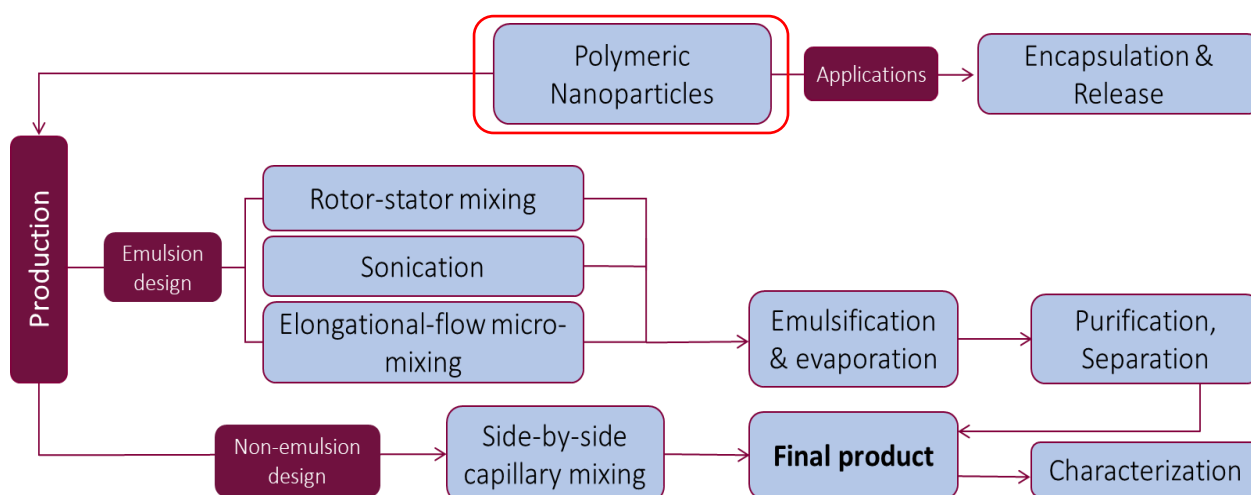


Figure 2.1. Polymeric nanoparticle production strategy through the emulsion- and non-emulsion-based fabrication designs by using different methods.

2.1 MATERIALS

2.1.1 Solvents

Substances that were used in this research to dissolve solutes, namely, solvents can be classified into polar and non-polar groups regarding their polarity-based solubility factor. These materials were used for either producing PNPs through emulsification, nanoprecipitation, and diffusion or for PNPs' post-production treatment like dilution and purification.

2.1.1.1 Polar solvents

Due to a large dipole moment driven by the electronegativity difference between atomic bonds, solvents can be polar. Several polar solvents used in this research are listed in Table 2.1. with their boiling points at atmospheric pressure, dynamic viscosities, and densities at 20°C temperature.

Table 2.1. Polar solvents used

Solvent name (and supplier)	Boiling point (°C)	Dynamic Viscosity at 20°C (cP)	Density at 20°C (g/mL)
Water*	100°C	1 cP	0.99
Ethanol (Merck)	78°C	1.14 cP	0.79
Isopropanol (Merck)	82°C	2.4 cP	0.78
Polyethylene glycol (Merck)	250°C	67 cP	1.2
Trimethylol propane (Sigma-Aldrich)	295°C	90 cP	1.1

*Milli-Q water obtained with a Merck-Millipore (Molsheim, France) filtration system

The given solvents were used in this thesis for different purposes. Water was used as a continuous phase in o/w emulsions, and a dispersed phase in w/o emulsions. Alcohols were used mainly in the last chapter, where isopropanol was used as a continuous phase fluid, and ethanol was used in the purification of nanoparticles. Poly(ethylene glycol) and trimethylol propane were used as viscosifying agents in water. All the solvents were received and used in an analytical grade.

2.1.1.2 Non-polar solvents

The hydrophobicity of materials is correlated with their non-polar molecular structure. The majority of the non-polar solvents presented in Table 2.2 were used in this project for their hydrophobicity-based immiscible or partially soluble nature with water. This property of the listed solvents allowed them to represent either a dispersed emulsion droplet or a continuous phase fluid.

Table 2.2. Non-polar solvents used

Solvent name (and supplier)	Boiling point (°C)	Dynamic Viscosity at 20°C (cP)	Density at 20°C (g/mL)
Dichloromethane (Aldrich)	40°C	0.44 cP	1.32
Ethyl acetate (Merck)	77°C	0.45 cP	0.9
Chloroform (Aldrich)	61°C	0.57 cP	1.49
Toluene (Fisher)	110°C	0.6 cP	0.86
Cyclohexane (Fisher)	81°C	1 cP	0.78
Hexadecane (Merck)	287°C	3.4 cp	0.77
Paraffin oil (VWR)	370°C	15 cp	0.84
Miglyol® 812 (Caelo)	250°C	33 cp	0.94
Olive oil (Carapelli)	180°C	84 cp	0.91
Silicone oil (Aldrich)	315°C	970 cp	0.97

More precisely, ethyl acetate and hexadecane were frequently referred in processes like emulsification. Miglyol® 812 was used in drug encapsulation to reduce the burst release, and chloroform was used in sample preparation for characterization. Other non-polar solvents were used to prepare and optimize the w/o emulsions in Chapter 5.

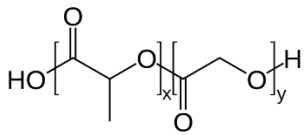
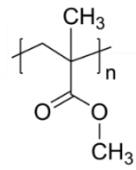
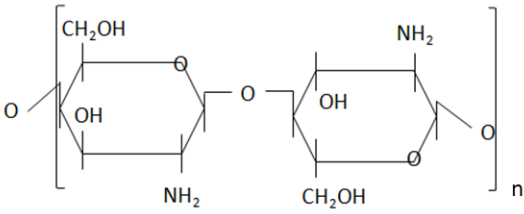
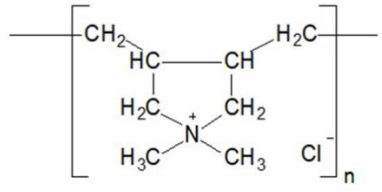
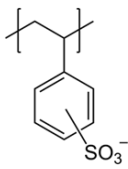
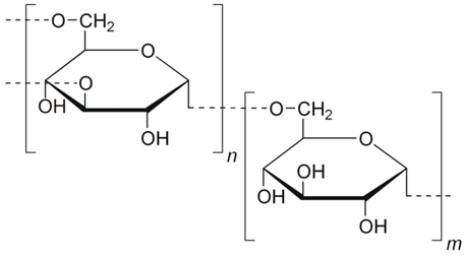
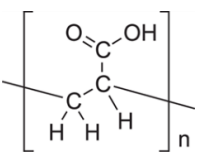

Miglyol® 812, a medium-chain triglyceride was used as received to prepare the emulsions and improve drug delivery-related properties, like burst release phenomenon during the cumulative drug release studies. Other non-polar solvents were used to understand the emulsification process, as some emulsions were highly unstable to proceed without hydrophilic lyophilic balance (HLB) value control.

2.1.2 Polymers

Poly(lactic-co-glycolic acid) 50:50 (PLGA) block copolymer Resomer® RG 504 H (Merck, 64,000 g/mol) (Table 2.3.a) with approved biocompatibility by Food and Drug Administration (FDA), complete degradation and wide-range of biological applications are used in this thesis for PNPs' fabrication and drug encapsulation.

Poly (methyl methacrylate) (PMMA) (Table 2.3.b), is a linear chain polymer (Merck, 120,400 g/mol) soluble in most non-polar solvents from this research to fabricate PNPs. This material is nonbiodegradable, however, it can undergo photodegradation or oxidative degradation.

Table 2.3. Polymers used

	Polymer name	Chemical formula
a)	PLGA	
b)	PMMA	
c)	Chitosan	
d)	PDADMAC	
e)	PSS	
f)	Dextran	
g)	PAA	
h)	PEI	

Other polymers, classified as polyelectrolytes due to their ionic structure, were also used. From the cationic polymers' family poly(D-glucosamine), with a brand name Chitosan (Merck, 200,000 g/mol) was used to form polyelectrolyte complexes following its cationic nature. Chitosan (Table 2.3.c) is a naturally occurring biodegradable, biocompatible polysaccharide, and is widely used in PNPs production due to its properties. Poly(diallyldimethylammonium chloride) (PDADMAC) (Merck, 20-35% solutions in water, 35% of 100,000 g/mol, 20% of 500,000 g/mol and 45% of 1,000,000 g/mol) is a cationic polymer (Table 2.3.d) and was used to produce surface charged PNPs, and polyelectrolyte complexes. Poly (styrene sulfonate) (PSS) (Sigma, 70,000 g/mol) is an anionic polymer (Table 2.3.e), used to form anisotropic PNPs. Dextran (Table 2.3.f) is a glucose polymer (Merck, 110,000 g/mol) used to fabricate complex polyelectrolyte NPs following its anionic nature. Poly (acrylic acid) (PAA) (SCF Floerger, 450,000 g/mol (102g/mol), 4,000,000 g/mol, 18,000,000) is an anionic polymer (Table 2.3.g.) with a formula of $(C_3H_4O_2)_n$. A linear poly (ethylenimine) (PEI) (Merck, 10,000 g/mol), used as surface modification agent for silicon wafer (Chapter 4), since it is a polyanion (Table 2.3.h).

2.1.3 Emulsifiers

Similar to sodium caseinates acting as a stabilizing agent in milk, cheese, or ice creams, in this research, some emulsifiers, also known as surfactants, were requested to achieve long-term miniemulsion stability. Indeed, surfactants are required to avoid thermodynamic instabilities influenced by i) the interfacial free energy and ii) the osmotic pressure difference based on different solute concentrations, which both lead to droplet coalescence. To produce stable emulsions and to have improved control of droplet size, a given amount of a chosen surfactant was added to the continuous phase under gentle stirring to equally distribute molecules for the following emulsification process.

Pluronic® F-127 (Merck, 12,500 g/mol), a non-ionic, non-toxic, biodegradable block copolymer (Figure 2.2.a) was used as received to prepare oil-in-water (o/w) emulsions. According to the number of x and y groups, this polymer can be either more hydrophobic or more hydrophilic. Here, the polymer we used had x = 95 polypropylene oxide (PPO) groups and y = 62 polyethylene oxide (PEO) groups at both edges, with an HLB value of 22, which makes this material more hydrophilic, or water-soluble in nature.

Another non-ionic emulsifier, sorbitan ester, sorbitan mono-9-octadecenoate (Figure 2.2.b) with a commercial name of Span® 80 (Merck, 429 g/mol) and HLB value of 4.3 was used to prepare w/o emulsions.

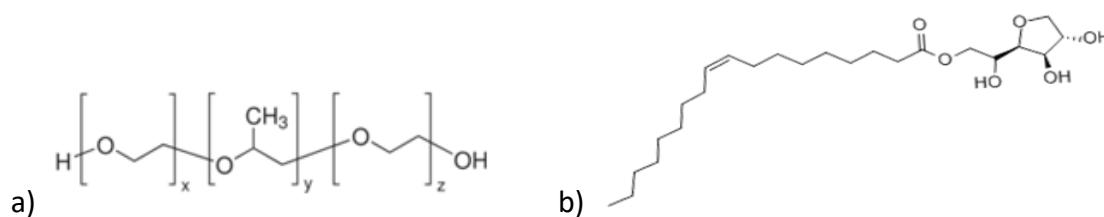


Figure 2.2. Schematic representation of a) Pluronic® F-127 and b) Span® 80.

2.1.4 Rifampicin

A few selective materials that were used in this research can be listed starting with rifampicin (TCI, Figure 2.3), a hydrophobic antibiotic.

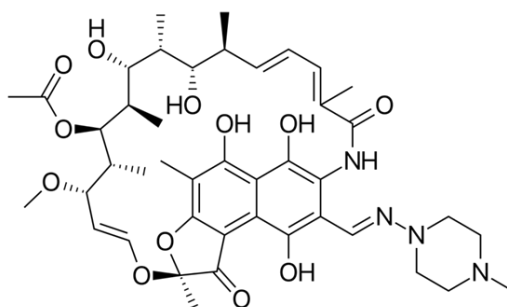


Figure 2.3. Schematic representation of rifampicin.

The high frequency of pulmonary tuberculosis (TB) diseases demands the development of novel drug delivery approaches that can enhance the bioavailability of drugs in the lungs [1]. Following this, we used Rifampicin as a model drug to apply in our drug encapsulation and release studies. Rifampicin was received in an analytical grade and stored at 4°C temperature before being employed to fabricate drug-loaded PNPs. Rifampicin, a member of the ansamycin antibiotic family, was discovered in 1965, and accepted by FDA in 1971 [2]. This drug has then been widely used in bacterial infection treatments like Legionnaires' disease, Mycobacterium avium [1], or TB [2]. Rifampicin is hydrophobic in nature (Log P = 3.179) with low solubility, and it is a member of a class II drug in the Biopharmaceutical Classification System (BCS) [3]. Besides its hydrophobic nature, one of the main challenges of using this drug is its high rate of degradation, and instability (Table 2.4) [5].

Table 2.4. Percentage recoveries of rifampicin at 25°C and 37°C during 72 hours [3]

Time (hours)	Rifampicin recovery (%)			
	25°C		37°C	
	1 mg/ml	0.01 mg/ml	1 mg/ml	0.01 mg/ml
0	99.9 ± 0.95	96.9 ± 2.4	101.9 ± 4.4	97.3 ± 1.8
6	96.7 ± 1.05	93.5 ± 0.1	99.6 ± 4.6	92.6 ± 1.8
24	94.3 ± 1.42	86.5 ± 1.9	96.7 ± 4.2	68.7 ± 1.2
48	91.6 ± 1.92	72.5 ± 0.5	92.9 ± 4.4	59.1 ± 4.5
72	88.3 ± 2.14	66.0 ± 2.1	89.7 ± 4.6	54.6 ± 8.0

This data was used to estimate Rifampicin loss during the drug release studies.

2.1.5 Other materials

Citric acid monohydrate (Merck), and anhydrous sodium carbonate (Merck) were used to maintain a buffer solution. Silicon wafers with 200 mm diameter were purchased from WaferNet Inc. (San José, CA, USA) for substrate preparation through cutting at the desired size and form. Spectrum™ Spectra/Por™ 4 RC (Fisher Scientific, USA) dialysis bag tubing with molecular weight cut-off between 12,000 and 14,000 g/mol were used for the drug in vitro release studies.

2.2 METHODS OF PREPARATION

2.2.1 Emulsion methods

In this research, PNPs were produced by methods that do not involve post polymerization for being a versatile approach due to their purity and biocompatibility. In emulsion methods, firstly, a preformed polymer was dissolved in the dispersed phase. Then samples at various continuous/dispersed phases (C/D) volume ratios were emulsified at room temperature with homogenizers. Two types, o/w, and w/o emulsions were used to fabricate PNPs. In all processes, except in the non-emulsion method, a significant amount of energy was given to the system to produce miniemulsions. Then, following the solvent removal, and PNP formation *via* polymer self-assembly, the PNPs were further purified (Figure 2.4).

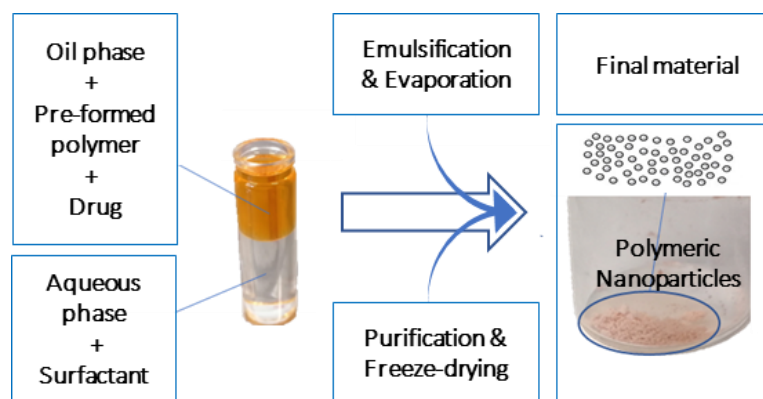


Figure 2.4. Overview of the emulsification of two immiscible phases to fabricate PNPs.

The surfactant was solubilized in either deionized water or in an oil phase of w/o emulsions following the addition of 1-3% w/v emulsifier in the continuous phase before emulsification. Simultaneously, the dispersed phase contained 1% w/v of polymer (and rifampicin 1-10% w/w of polymer, when required) solubilized in an oil phase followed by emulsification.

2.2.1.1 Elongational-flow reactor and mixer

One of the most advanced devices used in microfluidic emulsification is the elongational-flow reactor and micromixer (μ RMX). For the production of nanoemulsions, this device was equipped with two mid-pressure (2.5 bar) syringe pumps (neMESYS[®] Mid Pressure Module, Cetoni), two 25 mL stainless steel syringes (Cetoni), and one polyetheretherketone tee (Valco Vici). The syringe pumps were connected with an interface cable to be operated by the supplier's software. As such, it is possible to set the flow rate for both pumps at the same value and to run them under reciprocating cycles. The supplier's software also allows monitoring of the pressure inside the tubes (see below). Different elongational-flow micromixers differing from their microchannel diameter (0.15, 0.25, 0.50 and 0.75 mm) were used in this study to proceed the emulsification. These micromixers had four ports, while two were linked to the stainless-steel syringes by two poly(tetrafluoroethylene) PTFE tubing (1.06 mm ID, 1.68 mm OD). While two PTFE tubings were connected in opposite port directions (180°) of the micromixer, the other two ports of the micromixer were isolated. Two additional ports of the pistons were closed during the experiment by using two 3-way on/off valves, which were controlled by the computer software (Figure 2.5).

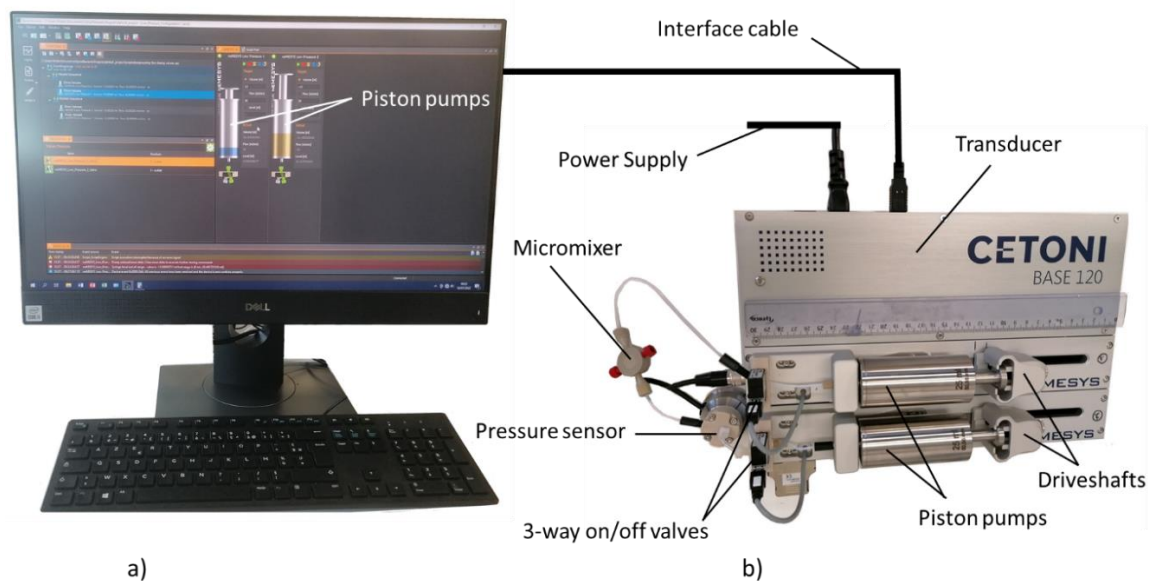


Figure 2.5. Overview of the elongational-flow reactor and micromixer with its control unit (a) and the mixing unit (b) connected.

Since the whole system including the microchannel is exposed to different solvents and surfactants, polymers, and monomers, PTFE, PEEK, and stainless-steel parts are used for their resistance to the most aggressive compounds and can be used for the reaction and the elongation of the droplets in the presence of different materials. The elongational-flow reactor and micromixer is a microfluidic device providing a precise mixing rate of materials inside the microchannel.

The mechanism of droplet deformation was studied since the 1934 year when Taylor reported two possible deformations of the fluid. These were simple deformation induced by the rotational shear, and two-dimensional extensional deformation, which was observed with irrotational shear [4]. Theoretically, to deform the droplet, it must be first distorted from its spherical shape. Following the distortion at a given stress, now two deformation types can be considered to break the droplet. In the first scenario, this deformation depends upon the instantaneous conditions, and due to a round motion in rotational stress, the droplet deforms at a 45° angle, where the increasing viscous drag limits the droplet rupture. This kind of limited deformation was quite different from the horizontal elongation observed in the two-dimensional extension. Here, the shape of the slightly elongated droplet continued elongating in the same direction, and the breaking point was no longer dependent on instantaneous conditions. This was since the viscous drag on the droplet surface didn't limit the horizontal elongation according to the theory of Geoffrey I. Taylor [4]. Then, in the 1980th P. Taylor and H. Grace experimentally proved that in the simple deformation, after a viscosity ratio of 4 the emulsion droplets were not able to rupture at constant stress. However, in the two-dimensional extension, there was no limit for the droplet deformation.

To understand the droplet break-up mechanism, which is opposed by the viscous drag forces, the capillary number (Ca) can be expressed as the ratio of the viscous forces to the interfacial forces.

$$Ca = \frac{\mu \dot{\epsilon} D_d}{2\gamma} \quad \text{Equation 2.1}$$

With the viscosity of emulsion μ , the elongational strain rate $\dot{\epsilon}$, the droplet diameter D_d and the interfacial tension between the two phases γ can be calculated.

According to the Taylor theory, the droplet will rupture when the critical capillary number Ca_c is reached. The newly formed droplets have a diameter that differs from the previous droplet, meaning the Ca now is equal or higher to the Ca_c . The droplet rupture in this condition will continue until the Ca_c value cannot be reached, this is when the droplet size doesn't change anymore [5].

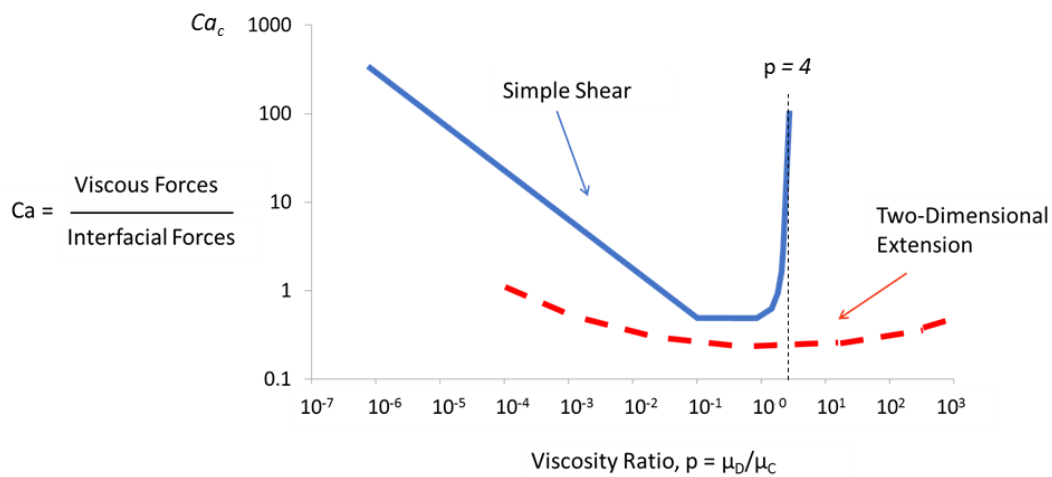


Figure 2.6. Droplet deformation at two different conditions; simple shear (rotational shear) and two-dimensional extension (irrotational shear) according to the Taylor theory.

Simple shear devices (Figure 2.6) require a tremendously high energy density due to the high critical Capillary number Ca_c required above the viscosity ratios of 4, however, two-dimensional systems allow droplet deformation at high viscosity ratios without demanding increased energy inputs. Thus, following this theory, the droplet deformation became more efficient at high viscosity ratios and high flow rates via a selective emulsification design.

In general, droplets are passing through the microchannel several times, in some cases up to 500 times (2 passes/cycle) (Figure 2.7). Considering the droplet size changing at each cycle, the newly formed droplets will have a different Ca than before. Thus, when Ca_c is reached again, the already ruptured droplets (in the previous cycle) will break up. This will continue the same until the moment when Ca stands below Ca_c . As such, droplet rupture is no longer possible and the size of droplets is no further changing.

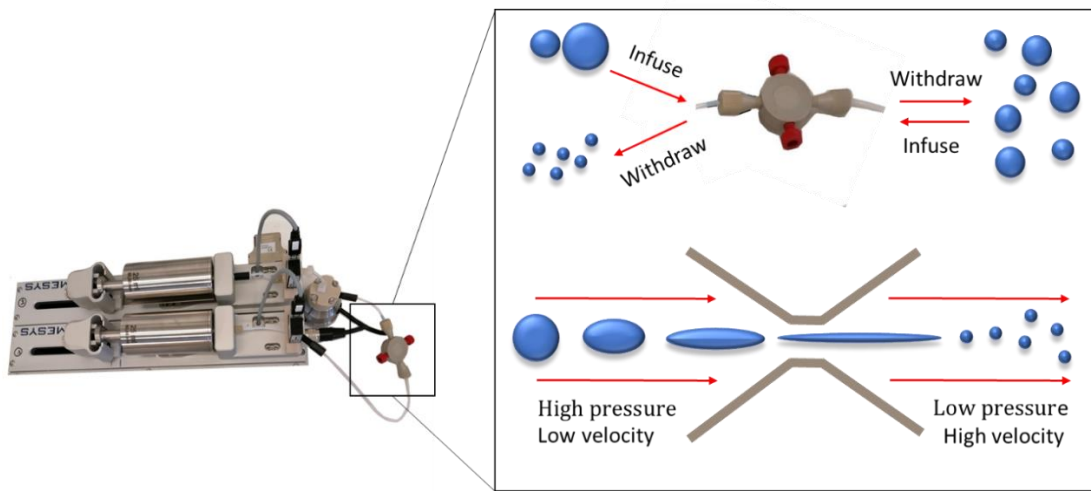


Figure 2.7. Illustration of the droplet break-up, and formation of the smaller droplets at elongational-flow strain inside the micromixer, the two-dimensional deformation according to the Taylor theory. The fluid passing through the restriction area loses its pressure and gains higher velocity, leading to droplet elongation.

As shown in Figure 2.7, in an elongational-flow based device the restriction plays an important role since the diameter is much smaller than the inlet and outlet channels. Thus, when the liquid passes from the tight channel its velocity increases leading to a strong local elongational strain rate of the droplets. The droplets also undergo a simple shear due to a restricted flow, however, this form of shear force is very negligible compared to the elongational force. The sum of these forces yields smaller droplets through the deformation and break-up of the larger droplets. The elongational strain rate can be calculated according to the Cogswell analysis for the Newtonian systems [6] by Equation 2.2.

$$\dot{\epsilon} = \frac{2\tau_w\gamma_{\dot{w}}}{3\Delta P_e} \quad \text{Equation 2.2}$$

where τ_w is the shear at the restriction wall, ΔP_e the pressure drop at the restriction entrance, and $\gamma_{\dot{w}}$ the shear at the restriction wall.

In the present case, $\gamma_{\dot{w}}$ can be calculated as indicated in Equations 2.3, and 2.4, i.e. for cylindrical shape restrictions.

$$\gamma_{\dot{w}} = \frac{\tau_w}{\mu} \quad \text{Equation 2.3}$$

$$\tau_w = \frac{D_h\Delta P_h}{4L_h} \quad \text{Equation 2.4}$$

Here, D_h and L_h are the diameter and the length of the restriction, respectively, and ΔP_h , the pressure drop across the restriction. Given the laminar flow in the microchannel (typically $Re = 1650$), and assuming that the fluid is Newtonian, the pressure drop across the microchannel length (ΔP_h) is given by the Hagen-Poiseuille law (Equation 2.5).

$$\Delta P_h = \frac{128 \mu L_h q}{\pi D_h^4} \quad \text{Equation 2.5}$$

$$\Delta P_h = \frac{32 f L_h \rho q^2}{\pi^2 D_h^5} \quad \text{Equation 2.6}$$

Where q and D_h are the flow rate of emulsion and the restriction diameter respectively. The Fanning friction factor is a function of the Reynolds number (Re) and the relative roughness e of the restriction wall.

The pressure drop at the restriction entrance can be expressed considering the loss coefficient K_f of the restriction and the mean velocity $\langle u \rangle = \frac{4q}{\pi D_h^2}$ through the restriction:

$$\Delta P_e = K_f \frac{\rho \langle u \rangle^2}{2} = 0.45 \left[1 - \left(\frac{D_h}{D_t} \right)^2 \right] \frac{\rho \langle u \rangle^2}{2} \quad \text{Equation 2.7}$$

where D_t is the inner diameter of the cylindrical restriction, this is connected to the restriction.

Considering all these equations it can be concluded that there are multiple factors including the geometries that affect droplet deformation and rupture. For example, a higher flow rate, and reduced microchannel size improves the elongational stress leading to smaller droplet size. Also, the shear rate at the restriction wall or the lower value of the interfacial tension can help in reaching the Ca_c required to rupture the droplet. In this context, microfluidic devices are highly efficient considering the precise parameters and highly controlled reaction conditions that are reproducible [7].

2.2.1.2 Shear-mixing

In this study, a rotor–stator mixer (Ultra-Turrax® T 25 basic, 800 W, IKA®) having a 13 mm diameter arm, shown in Figure 2.8, was employed for high-energy homogenization. Six different rotational speeds, from 9 to 24 krpm, of the shear-mixing device, were available for the process.

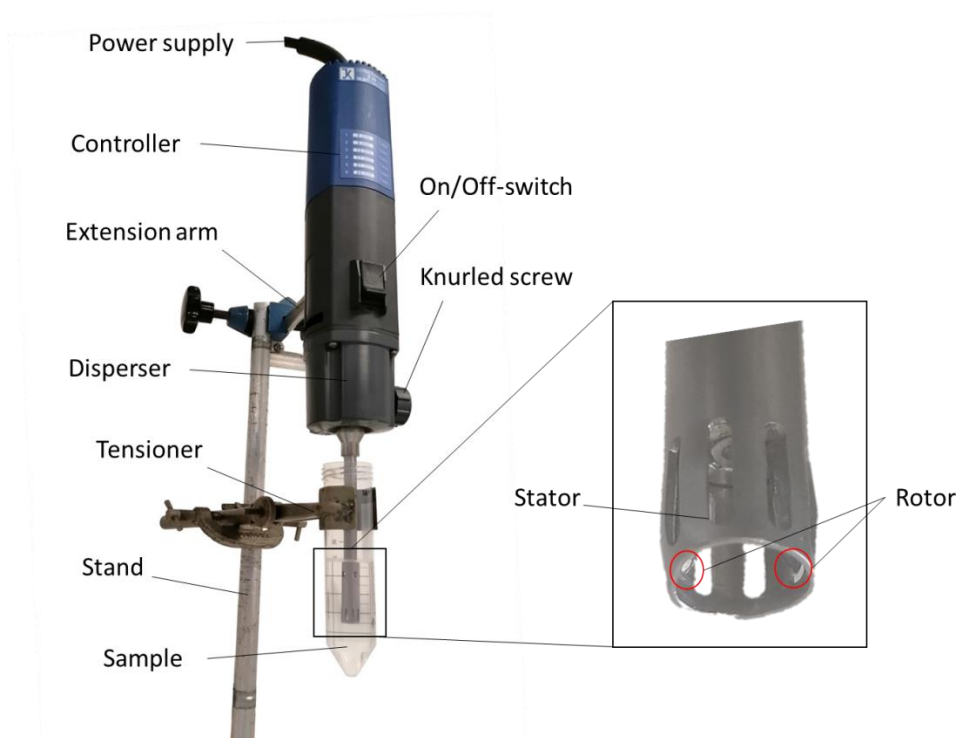


Figure 2.8. Overall view of the Ultra-Turrax® T 25 basic showing its main parts.

While the rotor moves at a high rotation speed, the liquid which is going to be homogenized is automatically moving towards the dispersion head by axial force, then radially forced to penetrate through the slots of the rotor/stator parts. In general, the higher the acceleration stronger the shear and thrust forces applied to the material to rupture the droplet. The continuous and the dispersed phases were homogenized at different speeds for a given emulsification time at 20°C, to then produce polymeric nanoparticles (PNPs). The given device has dimensions of 87 x 106 x 271 mm on the disperser part, and 13 x 160 mm on the rotor-stator part with 2.5 kg weight, which operates at 220 V design voltage, 50/60 Hz frequency with 800 W of power consumption. The given geometries and power consumption yield the rotor speed range of 3000 – 25000 rpm, and noise level of 75 dbA. In shear-mixing, the droplets generation takes place due to the kinetic energy given to the fluid. This energy is generated by the high-speed rotation of an internal part inside a stationary part which creates high turbulences between the two parts. Due to the small sample volume, the system is induced to a quite high energy dissipation, which deforms and ruptures the droplet. According to the

Kolmogorov-Hinze theory, the shear-mixing is directly dependent on a rotor speed (N), and rotor diameter (d), and can be expressed by the global Weber (We) number (Equation 2.8) [8].

$$We = \frac{\rho N^2 d^3}{\gamma} \quad \text{Equation 2.8}$$

with the fluid density (ρ), rotor speed (N), rotor diameter (d), the interfacial tension (γ). Following the Weber number, the droplet diameter is found in the Ohnesorge (Oh) number, which is the ratio of viscous forces to interfacial and inertia forces [9]. Oh number is expressed with the Weber number and the Reynolds number (Equation 2.9).

$$Oh = \frac{\mu}{\sqrt{\rho\gamma D}} = \frac{\sqrt{We}}{Re} \quad \text{Equation 2.9}$$

With the fluid viscosity (μ), fluid density (ρ), the interfacial tension (γ), and the droplet diameter (D). The droplet breakup mechanism with Ultra-Turrax® T 25 basic can be illustrated as shown in the following Figure 2.9.

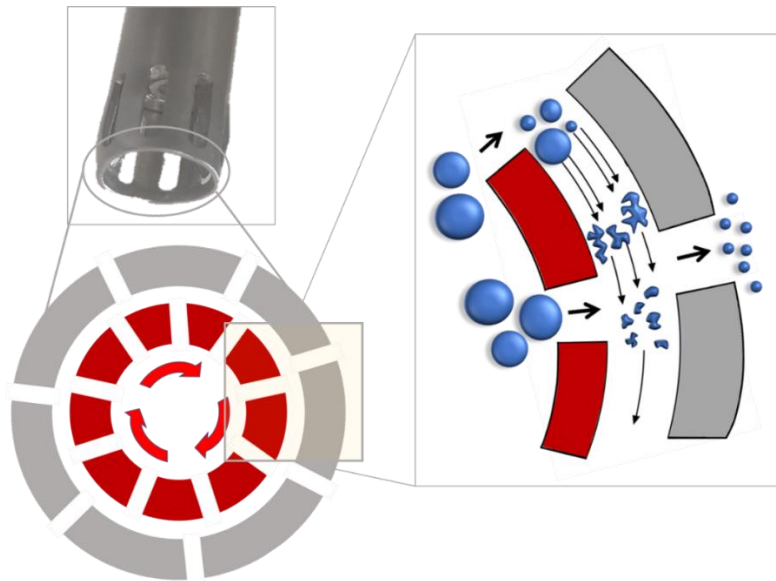


Figure 2.9. Illustration of the droplet rupture mechanism between the rotor (red) and stator (gray) at a high rotation speed of the Ultra-Turrax® T 25 basic.

It should be noted that parallely with the given high shear, the effectiveness of the homogenization is also highly dependent on the time that the particles are exposed to deformation in the shear zone. The Ultra-Turrax® T 25 basic can operate between the range of approximately 2-17 m/s rotation velocity (at d=13 mm), At the optimum rotation a few minutes of processing time is usually sufficient

to reach the desired particle size, however, long processing times can act oppositely by decreasing the efficiency yielding to an insignificant particle size improvement but an increased temperature [8].

2.2.1.3 Sonication

Emulsification of two immiscible phases was conducted by using an ultrasonic homogenizer (Bandelin Sonopuls HD2200) having a 3 mm diameter tip during a given time at different amplitudes (t_{on}/t_{total}) to produce stable emulsions. A cooling water bath was applied to maintain the temperature at 20°C. The illustration of the Sonopuls HD2200 sonicator with its generator & control unit for high-frequency (HF) and the resonator with its insulation box is displayed in Figure 2.10.

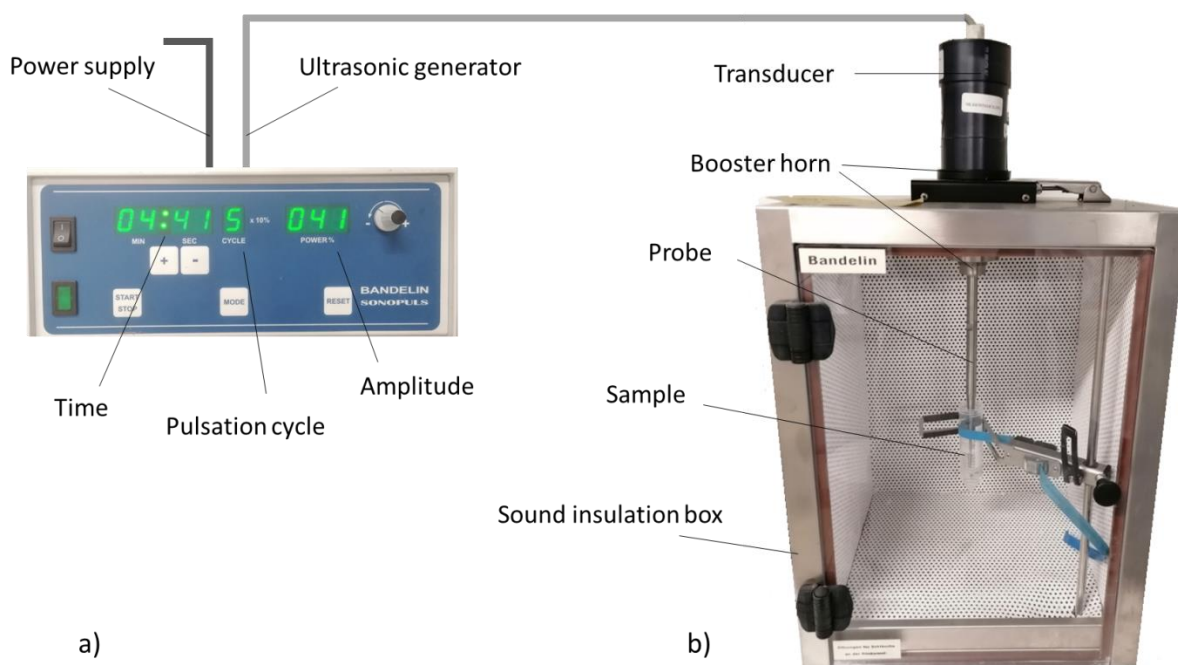


Figure 2.10. Standard Bandelin Sonopuls HD2200 for lab routine with HF generator & control unit (a) and the resonator unit (b).

HF generator & control unit aims at transforming electrical energy into HF signal in a controlled way and transmitting it to the resonator unit. This unit has dimensions of length, width, and height 257 × 180 × 115 mm respectively, with a maximum HF output of 200 kHz (W_{eff}). And it's capable of controlling the given transducer but also transducers with other dimensions. Transducer, also called converter or oscillator, dimensions of 70 × 150 mm titanium probe of 3 mm tip end-point radius. Considering tip diameter, operation volume is between 2 mL to 50 mL at a processing frequency of 20 kHz ±500 Hz, main connection of 230 V~ (±10 %). Under the given power density, the unstable waves generated in the interface induced by the acoustic field deform the droplets. These waves also

generate cavitation bubbles induced by the interior or exterior pressure fluctuations, and the cavitation bubbles implode leading to extreme localized turbulence, which creates additional pressure to deform the droplets. However, the surface energy of the droplet is one of the factors keeping the droplet with its minimum surface area and minimizing the droplet breakup. Also, the recoalescence of the droplets is one of the factors which is considered while ultrasonic emulsification. Thus, considering all these factors, the critical stable droplet diameter (d_{crit}) for a low dispersed phase viscosity ($\eta_d < 10 \text{ mPa}\cdot\text{s}$) can be expressed (Equation 2.10).

$$d_{crit} = C \varepsilon^{-2/5} \gamma^{3/5} \rho_c^{-3/5} \quad \text{Equation 2.10}$$

With C a constant value, ε the power density ($\text{W}\cdot\text{kg}^{-1}$), γ the interfacial tension and ρ_c the continuous phase density. The power density is the average power dissipated per mass unit of emulsion.

When the residence time (τ), and the processing volume (V) of the emulsion exposed to the given power (P) are considered, the energy density is calculated (Equation 2.11).

$$E_v = P \tau / V \quad \text{Equation 2.11}$$

The energy density is the energy given (J) per unit volume (J/m^3). Here, the energy density must be higher than the minimum required energy to rupture the droplets. It's also referred to as the low-energy threshold when E_v is not sufficient enough to break the droplets, and it can yield also a very high PDI at non-uniform E_v , [10], [11]. According to E_v , at a lower volume, it's possible to reach a minimum droplet size with Sonicator, described in the 3rd Chapter.

The exterior pressure (p_E) to a given cavitation bubble with a radius R is correlated to the interior pressure (p_I), and the particle geometries change depending on the p_E and p_I . By considering the γ interfacial tension, this can be expressed (Equation 2.12).

$$p_I - p_E = \frac{2 \gamma \Delta T}{R} \quad \text{Equation 2.12}$$

where R is the cavitation bubble radius, and ΔT the temperature difference.

The size starts growing when the exterior pressure is less than the interior pressure. Following the size growth, the bubble implodes when the outer pressure becomes higher than the internal pressure due to the resonance in amplitude (Figure 2.11). This implosion is followed by massive pressure fluctuations and heat, that rupture the emulsion droplets. In practice, a higher interfacial tension value requires a higher pressure difference to achieve the implosion, this also requires higher

resonance in amplitude. The general mechanism of the droplet breakup at different given factors is illustrated in the following figure (Figure 2.11).

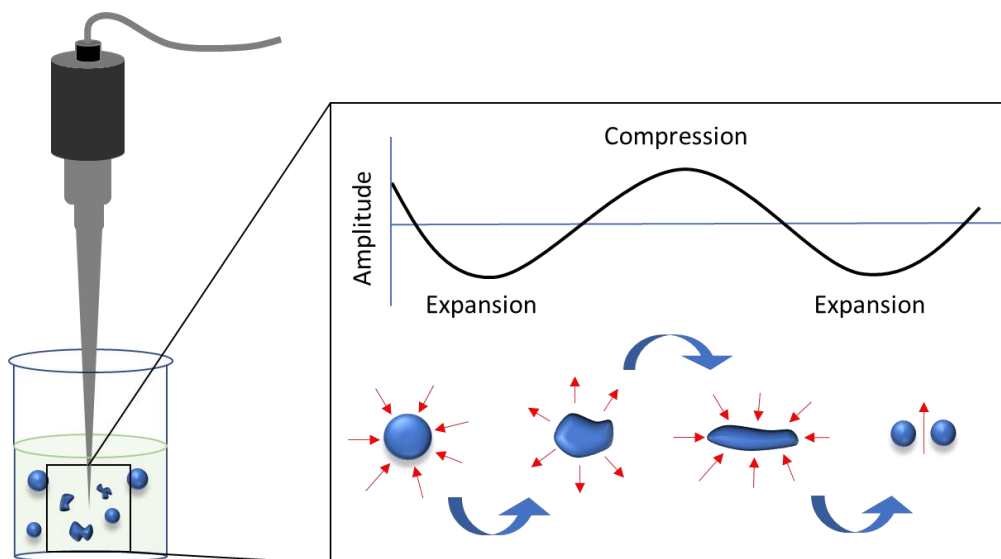


Figure 2.11. Droplet breakup mechanism during ultrasonic waves.

There is a heat emission in the process that is determined by measuring the temperature variations of the fluid and referred to as the calorimetric power (Equation 2.13).

$$P_{calo} = \frac{cm\Delta T}{t} \quad \text{Equation 2.13}$$

In the given equation, P_{calo} (W) is dependent on the heat capacity c (J/K), mass of the liquid m , and the temperature difference ΔT (K), generate during the process [11]. Higher temperature, and liquid mass increase P_{calo} , and thus increases the power converted to heat energy.

2.2.2 Solvent removal

In this research, four different solvent removal approaches were employed; evaporation, diffusion, forced convection, and lyophilization.

Evaporation

In this approach, ambient temperature of 20°C, an atmospheric pressure, and surface area of a sample induced to evaporation were maintained constant within 24 hours of slow solvent separation to yield PNPs of various polymers.

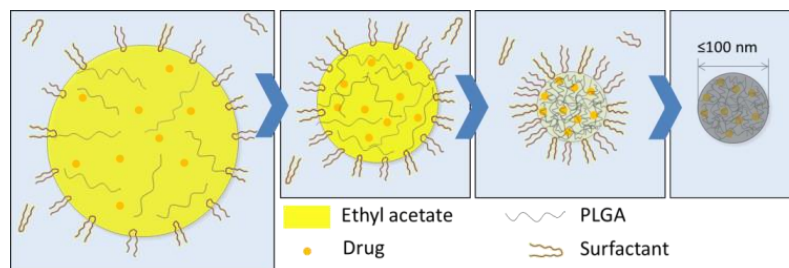


Figure 2.12. Formation of spherical PNP by solvent evaporation from a miniemulsion droplet.

The formation mechanism of a PNP through solvent evaporation from a miniemulsion droplet is shown in Figure 2.12. This takes place following the migration of a solvent out of the droplet, which leads the polymer molecules to reach a supersaturation point to self-assemble. This approach doesn't require specific equipment and device.

Diffusion

In diffusion-type separation, evaporation doesn't play a major role. Here, the main principle is to add a solvent (ethanol) into the continuous oil phase in order to facilitate the water extraction from the dispersed polymer phase. Here, the dispersed phase solvent diffuses into the 3rd solvent (ethanol), leaving polymer molecules precipitated inside the droplet. This method is considered to consume large volumes of water or other solvents, however, doesn't require specific equipment and can be applicable in some specific scenarios like rapid solvent removal. In this study, some polyelectrolyte NPs are produced *via* the emulsification and solvent diffusion method.

Forced convection

The third approach, forced convection requires a specific device called rotary evaporator (Rotavapor R-210) illustrated in (Figure 2.13).

Following the w/o emulsification process, 10 mL of miniemulsion sample was added to a 50 mL boiling flask connected to the flask adapter and the rotavapor unit. The temperature set point at the heating unit's controller was given at range of 25-50°C to evaporate water whilst the electrical vacuum pump maintained the vacuum pressure range of 70-350 mbar controlled by the rotavapor unit. The chiller unit was used to maintain condensation of an evaporated water and collection in the receiving flask while the process time ranged from 2-6 hours at 10 rpm (Figure 2.13.c).

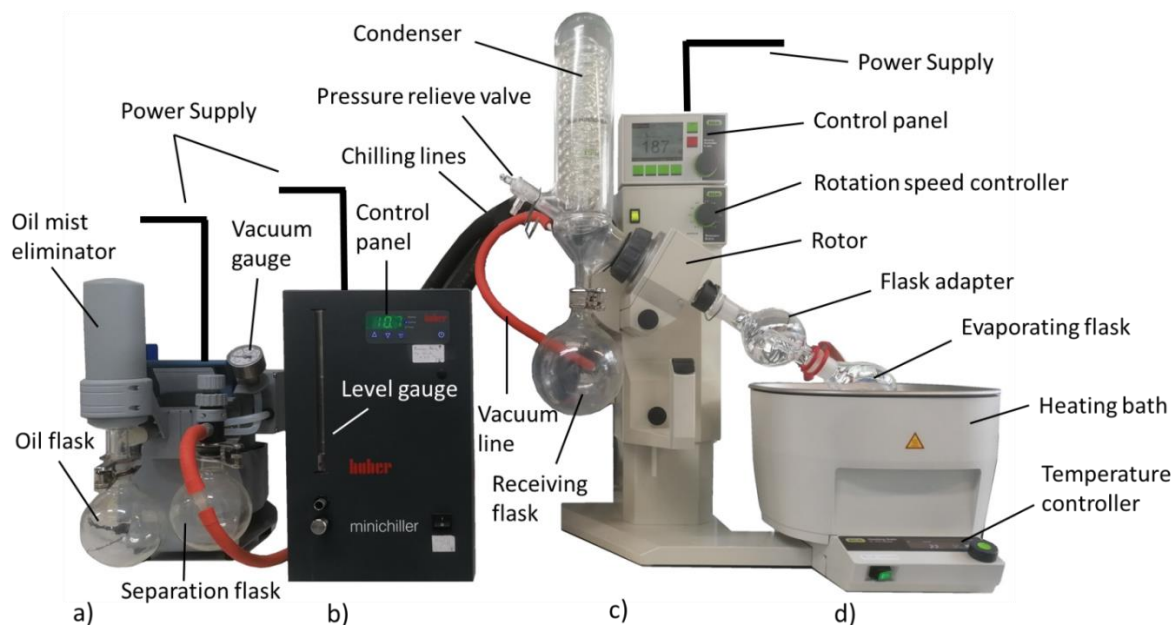


Figure 2.13. Rotary evaporation system used in PNP fabrication; a) electric vacuum pump, b) chiller, c) rotavapor, d) heating unit

Sample weights (with flask) were measured before, during, and after the evaporation to initially optimize the evaporation time. This time was set since the sample started weighting constant for the last three measurements at constant operating parameters.

Lyophilization

During PNP's separation from water, one of the limits is nanoparticle agglomeration due to hydrogen bonds of water molecules. To minimize or limit this physicochemical challenge, lyophilization (freeze-drying) with a (Lebconco, FreeZone 2.5) was used to separate water from PNPs by avoiding particle agglomeration. Nanosuspension was frozen in liquid nitrogen before connecting to the lyophilization system, then water was gradually eliminated by sublimation process for 24-72 hours to avoid hydrogen bond driven agglomeration.

To remove the water, an electric vacuum pump (Edwards) was used to maintain a stable vacuum inside the drying chamber (Figure 2.14.a). The refrigeration unit contains a compressor inside the metallic box which operates to reduce the temperature of the drying chamber (Figure 2.14.b).

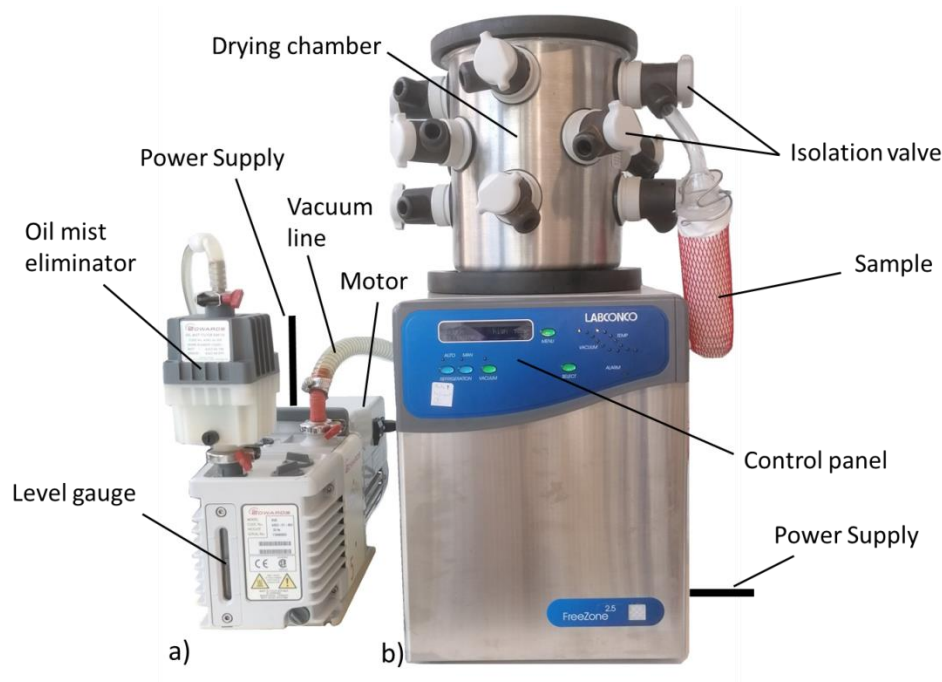


Figure 2.14. Overview of the lyophilization system used in PNP purification; a) electric vacuum pumping unit, b) refrigeration unit

Following the dispersed phase solvent evaporation and purification, PNPs were inserted into liquid nitrogen for 15 minutes to freeze the sample. Then, samples were connected to the drying chamber by maintaining the vacuum pressure range of 200-500 mbar, and -50°C during the process. Samples were collected in powder form for the next characterization.

2.2.3 Non-emulsion method

Non-emulsion-based methods differ from the emulsion-methods in their design, as described in the 1st Chapter. In non-emulsion methods, there are no specific solvent immiscibility requirements and emulsification processes. Thus, in this method, the surface-active ingredients are not used. The principle of the process is the diffusion of polymer solvent (water) into a miscible polymer non-solvent (e.g. ethanol), differently from the previously discussed emulsion method, where two immiscible or partially miscible (ethyl acetate and water) phases were used. This non-emulsion-based method will turn out to be more time efficient than previous (emulsion) method.

This method relies on the capillary co-flow of two streams of oppositely charged polymers dissolved in a common solvent (water) and surrounded by the flow of a polymer non-miscible fluid (propanol) in which water is miscible. Upon the in-flow diffusion of water in propanol, two physical phenomena may arise, as discussed in chapter 5, namely precipitation and electrostatic aggregation of the two polymers leading to the production of polyelectrolyte complex (PEC) nanoparticles.

The setup to implement this non-emulsion-based method is composed of three syringe pumps (PHD2000, Harvard Apparatus) connected to a microfluidic setup comprising two side-by-side glass capillaries and a PTFE tubing of 30 cm length and inner diameter equals to 0.5, 1 or 1.6 mm (Figure 2.15).

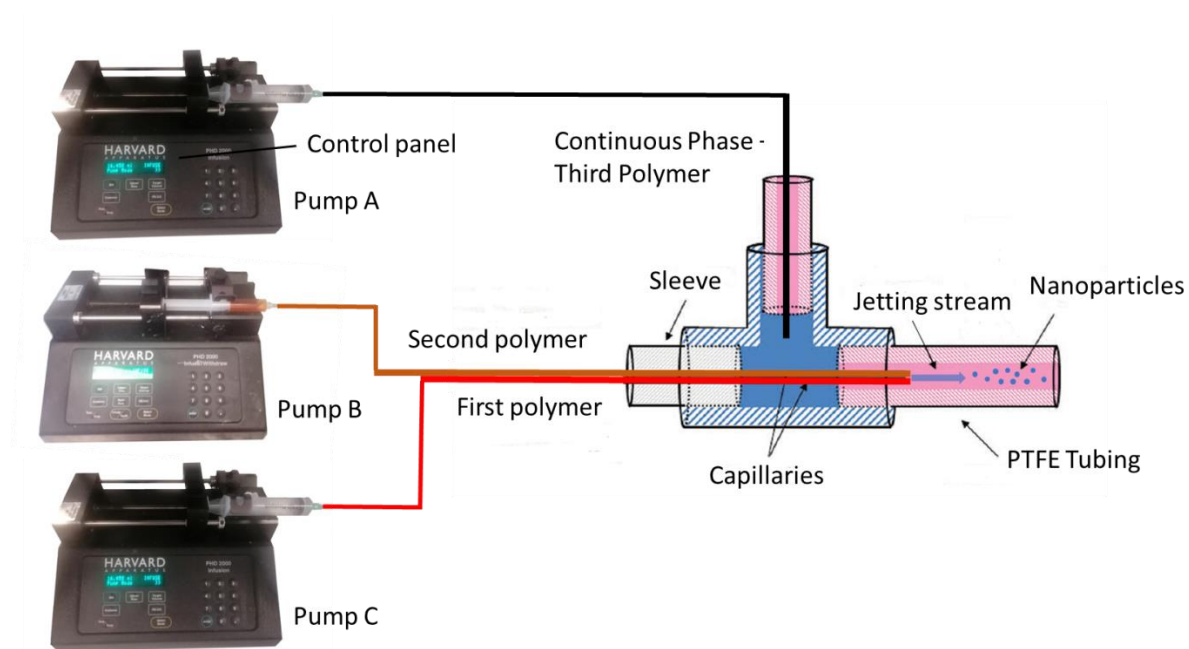


Figure 2.15. Overview of the one-step non-emulsion-based PEC NPs fabrication device.

Here, Pump A injects the continuous alcohol phase. Pump B and C inject the two different aqueous polymer solutions at a concentration of 0,1 – 20 % w/v through two capillaries of same but variable inner and outer diameters (ID: 40 and 75 μm ; OD: 100 and 350 μm). Both polymeric fluids are injected at the same flow rate ranging from 100 – 10,000 nL/min. All the samples are collected at the exit of PTFE tubing at ambient temperature and characterized without further purification.

Upon, diffusion of water in propanol, it is expected that PNPs are formed by precipitation and or electrostatic interactions.

2.2.4 Polymeric nanoparticle purification

To study the drug release at 37°C from previously produced DNPs, they were isolated from the solution by centrifugation (9500 rpm, 30 min) and filtration (filter diameter = 0.2 μm) before being introduced into a dialysis tube containing a 7.4 pH-controlled buffer solution. To separate the DNPs from the water phase, to calculate the encapsulation efficiency and to study the cumulative drug release from the DNPs under sink condition, nanosuspensions were first centrifuged at 9500 rpm for

30 min at 20°C (Rotina 420R Hettich Zentrifugen) to eliminate surfactant and then lyophilized (Labconco Freezone freeze dryer) at 0.4 mbar during 24 h at -50°C.

Here, it's necessary to consider the process yield, especially during the purification steps due to the material loss. Both production and purification processes are followed by the process yield estimations (Equation 2.14).

$$\text{Process yield (\%)} = \frac{\text{particles weight}}{\text{weight of total components}} \quad \text{Equation 2.14}$$

To calculate the drug load, the final PNP weight was estimated following the 30 minutes of centrifugation and lyophilization.

2.3 METHODS OF CHARACTERIZATION

Due to their critically small geometries, PNP characterization required specific techniques such as Dynamic light scattering (DLS), Transmission electron microscopy (TEM) [7], Ultraviolet Spectroscopy (UV), Surface tension tracking (Tracker) for pre-fabrication. For verification, additional techniques such as atomic force microscopy (AFM), Scanning Electron Microscopy (SEM) and, Infrared Spectroscopy (FTIR) were used. The morphology characterization of PNPs was demonstrated by mainly DLS and TEM techniques in triplicates to confirm the particle's size, size distribution and shape.

2.3.1 Analyses by spectroscopic methods

Since Isaac Newton was able to split light with a prism, spectroscopy has become the field of interrelations between electromagnetic radiation and matter, which provided an opportunity to study material properties. In this part of the chapter, we explain the spectroscopic methods that were used to characterize the produced materials.

2.3.1.1 Dynamic Light Scattering & Zeta Potential

Following the previously explained processes of fabrication, the average size and size distribution of the PNPs were characterized by using the dynamic light scattering (DLS) a non-invasive technique (Malvern Nano ZetaSizer) applied for measuring particles in suspension and macromolecules in solution. For this purpose, the helium-neon laser at 4 mW emitted at 633 nm with a scattering angle of 173° at a constant temperature of 25°C was maintained to characterize diluted samples of the

nanosuspension. This measurement is giving two different, however correlated results of particle size and the polydispersity index (PDI), a measure of the modality of the size distribution. In general, PDI values are required to be always below 0.2, which corresponds to a monomodal distribution of particles [15]. To perform the analyses 0.02 mL of the nanosuspensions are poured dropwise into 1 mL of deionized water located inside a 3.5 mL 10 x 10 x 45 mm plastic cuvette, and further inserted into the sample holder of the spectrometer before starting the measurement. An average of 30 values were calculated by the device at each run.

To characterize a sample, the ZetaSizer technique can be interpreted by understanding its working principle. In general, this technique treats the scattered light intensity signals sourced from the time-dependent fluctuations that occur inside the sample. These fluctuations are based on the Brownian motion that particles are undergoing due to the bombardment by the solvent molecules. More clearly, particles are randomly (uncontrolled) moving to reach their thermodynamically stable state, and disturbing the passing light intensity which is converted into a value of the particle diameter. Since Robert Brown observed grains moving in water in 1827 [12], it was possible to calculate the velocity of moving objects driven by mainly entropic forces and referred to as the translational diffusion coefficient D . It was explained that when the particles are large, they move slower, thus, a slower Brownian motion they have. However, smaller particles move faster due to being "kicked" further away by solvent molecules, thus, a higher Brownian motion they experience [12]. Approximately a century later, following the Stokes-Einstein equation (Equation 2.15), it was possible to convert the translational diffusion coefficient D into a hydrodynamic diameter D_H .

$$D_H = \frac{k T}{3\pi\mu D} \quad \text{Equation 2.15}$$

With μ the viscosity, T the absolute temperature of the system, D translational diffusion coefficient of the particle, and the Boltzmann's constant.

Since these measurements are well established for the systems ranging in size for having a better Brownian motion visualization, for highly monodisperse particles, the exponential decaying function of the correlator time delay τ was used:

$$G(\tau) = A [1 + B \exp(-2\Gamma\tau)] \quad \text{Equation 2.16}$$

This calculation was processed automatically depending on the light scattering reports by considering A the correlation function baseline, B intercept of the correlation function, and Γ a number representing Dq^2 where $q = (4 \pi n / \lambda_0) \sin (\theta/2)$, and D is the translational diffusion coefficient derived from the Brownian motion. Here, q is found from n the refractive index of dispersant, λ_0 the

wavelength of the laser, and θ its scattering angle. The given calculations are found in the format of volume, number, and intensity values of the particles at the end of multiple measurements. In this study, only the number average of the particles will be discussed, which provides precise information on different particle diameter populations.

The same device (Malvern Zeta Potential) was also employed for the measurement of the zeta potential. This was performed by first measuring a quantity known as electrophoretic mobility, which is the particle velocity in a unit electrical field. By using a specific design (cathode, anode), the given electrical field is directly passing through the sample, which is later correlated to the electrophoretic mobility. In practice, when the given electric field is high, the accuracy of the analysis increases, as the electrophoretic mobility is derived from the relationship of the Mobility = Velocity/Electric field [12]. Here, either positive or negative signs of the mobility can be found depending on the travel direction under the given electric field. Velocity is obtained from the light scattered by the particles, which is known as the 'Doppler Effect'. The frequency comparison of the scattered signal with a reference signal, which allows also very small frequency shifts to be measured, was processed to obtain the velocity results. The frequency was maintained between 250 and 320 Hertz to detect signals above and below the given numbers, then the electric field was applied leading to higher frequencies corresponding to the positively charged particles and lower frequencies to correspond to negatively charged particles. The given electrical field was reversed periodically (every 26 to 45 milliseconds), and the changes were reported as a function of time.

2.3.1.2 UV-visible Spectroscopy

Ultraviolet-visible spectroscopy (Perkin Elmer – Lambda 25) with a wavelength ranging from 2500 nm to 190 nm was used to quantify the drug concentration that was encapsulated inside the nanoparticles and released from the drug-loaded nanoparticles. A 3.5 mL standard quartz cuvette with a 10 mm light path was used for all characterizations. First, the calibration curve was established by dissolving the drug crystals into deionized water up to 1-20 μ g/mL at 1 hour cold (4°C) stirring at 300 rpm. Following the calibration curve, encapsulated and released drug quantities were calculated according to the ultraviolet light absorbance (A) with Beer Lambert law (Equation 2.17).

$$A = \epsilon bC \qquad \text{Equation 2.17}$$

With ϵ the molar absorptivity, b the light path length, C the molar concentration.

2.3.1.3 Fourier Transform Infrared

Materials were characterized by the Fourier transform infrared spectroscopy (FTIR, Bruker) to understand if the polymer molecules remained stable or if degradation took place during and after the process. By using this technique, the infrared region of the electromagnetic radiation spectrum was obtained. Compared to visible light, the infrared region shows a longer wavelength with a lower frequency. Followed by the given infrared radiation (IR) in a sample, the absorbed light spectrum at different frequencies that occur in the bonds between existing elements of PNPs was measured. In other words, the material's molecular composition was determined thanks to the sample's ability to absorb infrared light.

In this context, Vertex 70 from Bruker Optics was used to record FTIR spectra equipped with MCT (mercury cadmium telluride) detector and a black-body source. The spectra of the solids were measured on the diamond through ATR (attenuated total reflectance). Following an intensive purification and lyophilization, prepared PNP powder was brought to contact with the diamond surface of the FTIR spectroscopy and the measurements were recorded.

2.3.1.4 Nuclear Magnetic Resonance

Obtained PNPs were analyzed for their quality by using the Nuclear magnetic resonance (^1H NMR) spectra recorded on a Bruker Advance DPX400 I 400 MHz spectrometer equipped with UltraShieldTM magnets. This technique was used to observe local magnetic fields around atomic nuclei. The signals providing access to details of the molecular structure of the sample were detected with sensitive radio receivers located inside the device. The main purpose of this analysis was to detect any alternations in the molecular structure of biodegradable polymer during the PNP fabrication. To prepare samples for the liquid-state NMR analysis, following the emulsification-evaporation step, Poly (lactic-co-glycolic acid) PLGA, Poly (methyl methacrylate) PMMA, and PLGA-PMMA NPs were rigorously purified in 5 steps of centrifugation in water to eliminate the surfactant and the solvent molecules. After the purification steps, the samples were freeze-dried (Figure 2.14) with a Freeze dryer (Lebconco, FreeZone 2.5) at 200 mbar and -50°C for the sublimation of the water for 48 hours. 15 mg of powder PNP was dissolved in 0.6 mL of deuterated chloroform (CDCl_3) and added to an NMR thin-walled glass tube before inserting to the device, then, the received signals were analyzed using MestReNova software. NMR chemical shifts were reported as the δ scale in ppm relative to the solvent peak ($\delta = 7.26$) in CDCl_3 . The terms m, s, d, t, q, and dd represent multiplet, singlet, doublet, triplet, quadruplet, and doublet of doublet respectively. Coupling constants (J) are given in Hertz (Hz).

2.3.2 Methods of microscopic characterization

Because all the fabricated products in this research were 1000 times narrower than the average human hair, we tried to measure these nanomaterials by using all the available high-resolution microscopic techniques. These include transmission electron microscopy (TEM), scanning electron microscopy (SEM), and atomic force microscopy (AFM).

2.3.2.1 Transmission Electron Microscopy

To analyze the morphology and shape of the nanoparticles, transmission electron microscopy (TEM) experiments were performed. 5 μL of the nanosuspensions were deposited onto a freshly glow-discharged carbon-covered grid (400 mesh). The suspension was left for 2 minutes and then the grid was negatively stained with 5 μL of uranyl acetate (2v% in water) for another minute before being dried using filter paper. The grids were observed at 200 kV with a Tecnai G2 (FEI) microscope. Images were acquired with an Eagle 2k (FEI) sCCD camera.

2.3.2.2 Scanning Electron & Keyence Microscopies

Scanning Electron Microscope (SEM) SU8010 (Hitachi, Japan) has been used with a detector at an accelerating voltage of 1.0 kV for collecting the secondary electrons (SE). In this technique, electrons are first generated at the top of the column (electron gun), followed by the acceleration and passage through diverse lenses to produce a focused electron beam. When the given beam interacts with the sample surface, a range of electrons are backscattered (BSE) to provide information about the sample. Films of self-assembled PNPs were prepared by casting the water/particles suspension (1 mg/mL) on silicon wafer substrates (1 cm \times 1 cm) dried at 25 $^{\circ}\text{C}$, and glued with conductive carbon adhesive tape (Agar Scientific, UK), followed by the sample imaging of the top surface.

2.3.2.3 Atomic Force Microscopy

To verify the previously analyzed samples, AFM (Bruker, USA) was used to characterize the morphology of PNPs in size and shape. The study was realized at a free amplitude of 500 mV, a free vibration frequency of 179 kHz by tapping mode at room temperature. Silicon cantilevers with a spring constant of 13-77 $\text{N}\cdot\text{m}^{-1}$ and a silicon tip ACT-50 were used for the measurements. Before starting the morphological characterization, the silicon wafer was purified through 15 minutes of washing in KOH solution, 15 minutes in an ethanol solution, and 3 minutes in a Plasma Cleaner PDC-

002 (Harrick Plasma, USA) at high RF power (~ 30 W). Following the substrate purification, 1% w/v PEI solution was added dropwise (10 drops) to the substrate surface by spin coating technique at 5000 rpm before washing it with the deionized water. In the last step, purified and diluted 0.1 mL nanosuspension was added dropwise by spin coating at 7000 rpm and was then fixed on metallic support using super glue (Loctite Super Glue-3) before starting AFM imaging.

2.3.3 Interfacial Tension Measurements

For producing miniemulsions with controlled parameters, the interfacial tension of the immiscible phases was studied to improve the droplet generation based on the capillary number. The interfacial tensions (mN/m) between oil and water phases were measured by employing a Teclis Scientific Tracker technique. This technique operates with the help of a control unit, an A25 Refrigerated Circulation (Thermo Scientific, USA) unit to maintain requested temperature conditions, and an operations unit connected to the “Wdropdata” software (Figure 2.16). According to the rising bubble method, first, the water phase (deionized water and surfactant) in a 25 mL glass cuvette was placed inside the temperature-controlled chamber at 20°C. The oil phase was then continuously injected from a 500 μ L glass syringe directly to the center of the water solution to create and maintain a 3 μ L droplet.

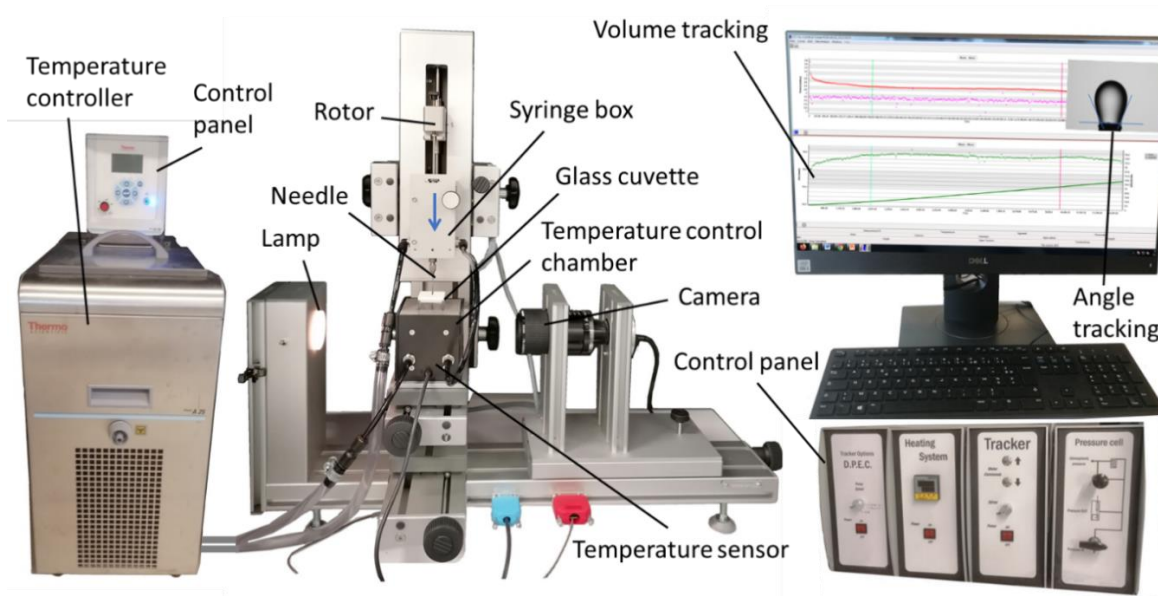


Figure 2.16. Overview of the Teclis tracking system used to characterize the interfacial tension of two phases with the rising-bubble method.

The glass cuvette and syringe were used as a carrier of the given samples, and due to micro-volumes used during measurements, these two parts were purified step-by-step in acid-base solutions,

acetone, and alcohol solution for 30 minutes for each step inside the ultrasonication bath. The needle of the syringe was heated above 250°C temperature following the ultrasound purification steps before starting the measurements to avoid impurities which can later limit the angle tracking. The droplet tracking with the rising bubble method was video recorded during the 500 minutes for each sample in triplicates with a total number of 30 successful measurements.

2.3.4 Other characterization methods

Other characterization devices like weighting balance (Thermo Fisher, USA) to precisely balance and estimate the materials, digital microscopic imaging technique (Keyence, France) to observe evaporation phenomenon in large emulsion droplets, temperature detector (RS-232 Data Logger thermometer) to follow the heat effects in processes. Also, a density meter (Mettler Toledo) to determine solution densities, and a kinematic viscosity measurement device (Ubbelohde viscometer) to viscosities of the samples at room temperature were used to understand the pre-process parameters. Also, visual emulsion stability in time tests were performed by storing prepared emulsions and observing their phase separation phenomenon at normal conditions. All the characterization methods were realized at Institute Charles Sadron (ICS).

2.4 METHODS OF APPLICATION

2.4.1 Drug delivery studies

To start encapsulation, a given amount of drug (rifampicin) was first mixed with 10 µL of Miglyol® 812 and then added to 1w% PLGA in ethyl acetate, the resulting solution composing the oil dispersed phase. The continuous phase was composed of water saturated with 8.7% ethyl acetate to prevent drug diffusion from oil to the aqueous phase [13]. After the successful production of nanoemulsions, all samples were left overnight in a fume hood to let the solvent evaporate and a nanosuspension of drug-loaded PLGA NPs in water was recovered.

To separate the drug-loaded nanoparticles (DNPs) from the water phase, to calculate the encapsulation efficiency and to study the cumulative drug release from the DNPs under sink condition, nanosuspensions were first centrifuged at 9500 rpm for 30 min at 20°C (Rotina 420R Hettich Zentrifugen) to eliminate surfactant and then lyophilized (Labconco Freezone freeze dryer) at 0.4 mbar during 24 h at -50°C.

Then, the drug load (DL) and the encapsulation efficiency (EE) were calculated (Equation 2.18, 2.19) [14]. DL corresponds to the drug weight percentage in the final product, EE is the weight ratio of encapsulated drug to the total weight of the drug introduced in the feed.

$$DL = \frac{\text{weight of encapsulated drug}}{\text{weight of DNPs}} \quad \text{Equation 2.18}$$

$$EE = \frac{\text{weight of encapsulated drug}}{\text{weight of drug introduced in the device}} \quad \text{Equation 2.19}$$

Following the drug encapsulation, cumulative release studies were carried out to understand the relationship between process, pre-process parameters, and drug release kinetics.

DNPs were first loaded into a dialysis bag tubing. then the bag was immersed in 60 mL of pH-controlled phosphate buffer solution (pH = 7.4). Then, rifampicin release from polymeric DNPs was carried out in an incubator (PolyMax 1040, 330 W, Heidolph) equipped with a temperature control system (37°C), a sample collection platform, and a rotational speed controller (50 rpm).

The amount of drug (μg) released from DNPs was determined by UV-visible spectroscopy at 332 nm by taking into account the rifampicin possible degradation (Equation 2.20) considering the rifampicin degradation kinetics (Table 2.4). Cumulative drug release was calculated by the ratio of the released drug (μg) to the initially loaded drug (μg) (Equation 2.21).

$$T_n = (\lambda_{n332} / \lambda_{332}) C_0 + L \quad \text{Equation 2.20}$$

with T the total released drug (μg) at time n , λ_{n332} the absorbance at time n , λ_{332} absorbance at certain drug quantity ($\mu\text{g}/\text{mL}$) C_0 obtained from the calibration curve, and L , total loss of drug at phosphate buffer solution replacement (μg).

$$\text{Drug release} = \frac{T_n}{\text{Weight of drug loaded}} \quad \text{Equation 2.21}$$

2.4.2 Stability

Two types of physicochemical stabilities were discussed in this research; miniemulsion stability against phase separation, and nanosuspension stability against agglomeration. The miniemulsion stability against phase separation was observed depending on the time required for the solvent

removal, explained in the solvent removal section. The second instability, the agglomeration in nanosuspensions is an inevitable auto-process, and driven by weak adhesive forces, especially during the intensive purification steps, however, it can be minimized thanks to the Brownian motion that is continuously active above the zero Kelvin. Some physicochemical parameters such as drug content, and residence time were the control strategies of nanosuspension stability. These factors can become more crucial in the industrial application of PNPs, in prolonged storage periods.

PNPs were washed via centrifugation to remove surfactant and other impurities followed by the dilution in water. As previously explained, a size of below 200 nm is a guarantee of stability by avoiding immune system attacks in physiological media, thus, PNPs were maintained at this size range during the purification.

Because materials like the surfactant and other molecules like hydrophobic agents directly control the osmotic pressure, the miniemulsion instability was avoided by keeping the osmotic pressure equal to or above the droplet's Laplace pressure. Here, the emulsion stability was maintained during the process, and also during the post-homogenization solvent-removal period through these concentrations.

In medical applications, for long-term safety goals, the drug carriers are designed to be temporarily eliminated or reduced after the drug is completely released. For this reason, initially, biodegradable materials were chosen to be expected to degrade in time and not accumulate in the body to potentially evolve long-term side effects.

2.5 BIBLIOGRAPHY

- [1] M. Me, "Rifampin," *Tuberculosis*, vol. 88, no. 2, pp. 151–154, 2008, doi: 10.1016/S1472-9792(08)70024-6.
- [2] J. Van Ingen *et al.*, "Why do we use 600 mg of rifampicin in tuberculosis treatment?," *Clin. Infect. Dis.*, vol. 52, no. 9, 2011, doi: 10.1093/cid/cir184.
- [3] F. Sadouki, "Micro-encapsulated poly (vinyl alcohol) nanoparticles for rifampicin delivery to the lungs," *King's Coll. London*, 2020.
- [4] G. I. Taylor and P. R. S. L. A, "The formation of emulsions in definable fields of flow," *Proc. R. Soc. London. Ser. A, Contain. Pap. a Math. Phys. Character*, vol. 146, no. 858, pp. 501–523, 1934, doi: 10.1098/rspa.1934.0169.
- [5] P. Taylor and H. P. Grace, "Dispersion Phenomena in High Viscosity Immiscible Fluid Systems and Application of Static Mixers As Dispersion Dispersion Phenomena in High Viscosity Immiscible Fluid Systems and Application OF Static Mixers As Dispersion

- Devices in Such Systems,” *Science (80-.)*, vol. 6445, no. 912873516, pp. 37–41, 2009, doi: 10.1080/00986448208911047.
- [6] M. Vauthier, M. Schmutz, and C. A. Serra, “One-step elaboration of Janus polymeric nanoparticles: A comparative study of different emulsification processes,” *Colloids Surfaces A Physicochem. Eng. Asp.*, vol. 626, no. June, p. 127059, 2021, doi: 10.1016/j.colsurfa.2021.127059.
- [7] S. Ding *et al.*, “A new method for the formulation of double nanoemulsions,” *Soft Matter*, vol. 13, no. 8, pp. 1660–1669, 2017, doi: 10.1039/c6sm02603f.
- [8] A. Håkansson, “Rotor-stator mixers: From batch to continuous mode of operation-A review,” *Processes*, vol. 6, no. 4, pp. 1–17, 2018, doi: 10.3390/pr6040032.
- [9] G. DeBruijn and S. M. Whitton, “Fluids,” *Appl. Well Cem. Eng.*, pp. 163–251, 2021, doi: 10.1016/B978-0-12-821956-0.00012-2.
- [10] E. Cell and H. Sample, “High-power ultrasound in laboratories Cleaning – Degassing – Emulsifying Cell disruption – Homogenizing Company Profile.”
- [11] W. Li, T. S. H. Leong, M. Ashokkumar, and G. J. O. Martin, “A study of the effectiveness and energy efficiency of ultrasonic emulsification,” *Phys. Chem. Chem. Phys.*, vol. 20, no. 1, pp. 86–96, 2017, doi: 10.1039/c7cp07133g.
- [12] Malvern and M. Instruments, “Dynamic Light Scattering: An Introduction in 30 Minutes,” *Tech. Note MRK656-01*, pp. 1–8, 2011, [Online]. Available: <http://scholar.google.com/scholar?hl=en&btnG=Search&q=intitle:Dynamic+Light+Scattering+:+An+Introduction+in+30+Minutes#3>.
- [13] C. Wischke and S. P. Schwendeman, “Principles of encapsulating hydrophobic drugs in PLA/PLGA microparticles,” *Int. J. Pharm.*, vol. 364, no. 2, pp. 298–327, 2008, doi: 10.1016/j.ijpharm.2008.04.042.
- [14] I. U. Khan, C. A. Serra, N. Anton, and T. Vandamme, “Continuous-flow encapsulation of ketoprofen in copolymer microbeads via co-axial microfluidic device: Influence of operating and material parameters on drug carrier properties,” *Int. J. Pharm.*, vol. 441, no. 1–2, pp. 809–817, 2013, doi: 10.1016/j.ijpharm.2012.12.024.
- [15] C. Dhrisya *et al.*, “Therapeutic efficacy of nanoparticles and routes of administration” *Biomaterials Research*, vol. 23, 2019, doi: <https://doi.org/10.1186/s40824-019-0166-x>

Chapter 3: One-step Production of Highly Monodisperse size-controlled Poly(lactic-co-glycolic acid) nanoparticles for the release of a hydrophobic model drug

3.1	INTRODUCTION	133
3.2	PROCESS ELABORATION RESULTS	134
3.2.1	Influence of the operating parameters on the PLGA nanoparticles	134
3.2.2	Polydispersity index of the produced PNPs	137
3.2.3	Heat emission during the process of emulsification	138
3.2.4	Process volume influence on PNP fabrication	139
3.3	PLGA NANOPARTICLES AS DRUG CARRIERS	140
3.3.1	Rifampicin's calibration curve	141
3.3.2	PLGA size and size distribution influenced by the drug encapsulation	143
3.3.3	Understanding the size reduction at different material concentrations	145
3.3.4	Coherence of results from two different characterization techniques	147
3.4	DRUG RELEASE FROM PLGA NANOPARTICLES	148
3.4.1	Influence of the initial drug weight content on the drug release	148
3.5	CONCLUSION	152
3.6	BIBLIOGRAPHY	153

Chapter 3

One-step Production of highly monodisperse size-controlled poly(lactic-co-glycolic acid) nanoparticles for the release of a hydrophobic model drug

Adapted from JDDST.2022.103358

3.1 INTRODUCTION

The need for a new drug delivery system is requested by the pharmaceutical industry [1], [2]. Indeed, the number new drugs having a continuous dose requirement for treatment, without harming organs, have triggered the need for alternative drug delivery strategies [3], [4]. Some diseases request to maintain an effective therapeutic drug concentration over time and thus to develop formulations that allow the prolonged delivery of an active pharmaceutical ingredient [5], [6]. Previous studies suggest that drugs having delivery issues could be encapsulated in biodegradable polymeric nanoparticles (PNPs) of diameters as low as 200 nm to improve stability of drugs and to tune their release profiles [7]–[9]. Moreover, based on the control over their morphology, size, bioavailability and high biostability, PNPs are promising candidates as drug carriers [10]–[12]. Indeed, biodegradable polymers have the capacity of being cleaved into biocompatible byproducts through enzymatic degradation and enzyme-catalyzed hydrolysis process, thus delivering drugs in a controlled release manner [5], [13], [14]. Poly(lactic-co-glycolic acid) block copolymer (PLGA) is one of the carrier candidates for drug delivery systems since European Medicine Agency and Food and Drug Administration approved it for its bioavailability [13]–[15]. This biocompatible polymer can protect drugs from degradation until their release starts [3], [10], [16]. In this context, drug-loaded PLGA microspheres (57 μm of diameter) can easily be fabricated by the emulsification-evaporation method and encapsulation efficiency of 92% (1.5% w/w drug load) can be reached at optimum conditions [6], [10]. Also, the presence of glycerides, such as Miglyol, can reduce diffusion of drug out of the polymer molecules [17] because of its adhesive property to act as a diffusion barrier throughout the PNP matrix. While various methods such as emulsification-evaporation, salting-out or nanoprecipitation have been studied to produce PNPs [18]–[20], microfluidic-assisted processes appear to be an asset for the production of PNPs with biological-related applications [11], [21]. Indeed, size-controlled droplets can be generated even with highly viscous solutions (e.g. polymers)

with viscosity ratios higher than 4, which is the limiting value according to Taylor’s theory for shear devices [22]–[24]. Using these methods, the required drug carrier mass can be reduced to decrease production costs [7], [9]. For instance, some of these systems have been developed by a two-step process to produce ketoprofen-loaded PNPs (45% of encapsulation efficiency) with controlled size (100 to 200 nm). Selecting an appropriate encapsulation technique is an important stage while working with biodegradable polymers. However, the techniques presented in the literature for emulsification are still usually multistep, multiplying risks of contaminations and drug alteration [9], [11], [18].

Moreover, compared to previous works done with PNPs [11], [20], [25], in this work the continuous phase pre-saturation is applied for the first time to the microfluidic-assisted emulsification and solvent-evaporation method to i) increase the amount of encapsulated hydrophobic model drug (rifampicin) and ii) improve the control over PNPs’ diameter and size distribution.

3.2 PROCESS ELABORATION RESULTS

3.2.1 Influence of the operating parameters on the PLGA nanoparticles

Desired poly(lactic-co-glycolic acid) (PLGA) NPs properties, *i.e.* the average PNP size below 200 nm, and the size distribution of below 0.2 value, were achieved following the process elaboration according to the drug delivery application. In this first part, the production of biodegradable PNPs with PLGA was conducted with three different devices described in Chapter 2 (rotor-stator mixer, sonicator and elongational-flow micromixer- μ RMX) at given operating parameters (Table 3.1). The goal here was thus to assess the effect of operating processing parameters (emulsification time and mixing parameter) and chemical parameters (continuous to disperse phase C/D volume ratio) on the PNPs’ size and size dispersity. Emulsification time was ranging from 5 to 40 minutes and mixing parameters (MP) of rotation speed, power amplitude, flow rates according to the provided energy density of each device to break up the emulsion droplets into smaller droplets.

Table 3.1. Parameters used to produce PLGA NPs with three different emulsification devices.

Device	Emulsification times (min)	Mixing parameter (MP)	C/D volume ratio
Rotor-stator mixer	5 to 25	6,500 to 24,000 rpm	60/40 and 85/15
Sonicator	1 to 12	10% to 90% of amplitude	60/40 and 85/15
μ RMX	20 to 100 [†]	10 to 40 mL/min	60/40 and 85/15

[†]60 min corresponds to 150 cycles

Following the emulsification of 1,5 w/v Pluronic® F127 in water as the continuous phase, and 1% w/v PLGA solution in ethyl acetate as the dispersed phase, the dispersed solvent was evaporated at room temperature and atmospheric pressure, and at a constant surface area of $78,5 \times 10^{-6} \text{ m}^2$ within 24 hours of slow separation to yield PLGA NPs ((Figure 3.1).

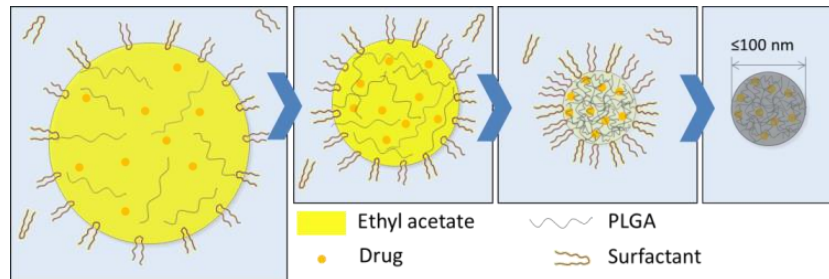


Figure 3.1. Ethyl acetate evaporation and formation of spherical PLGA nanoparticles from the miniemulsion droplets dispersed in water.

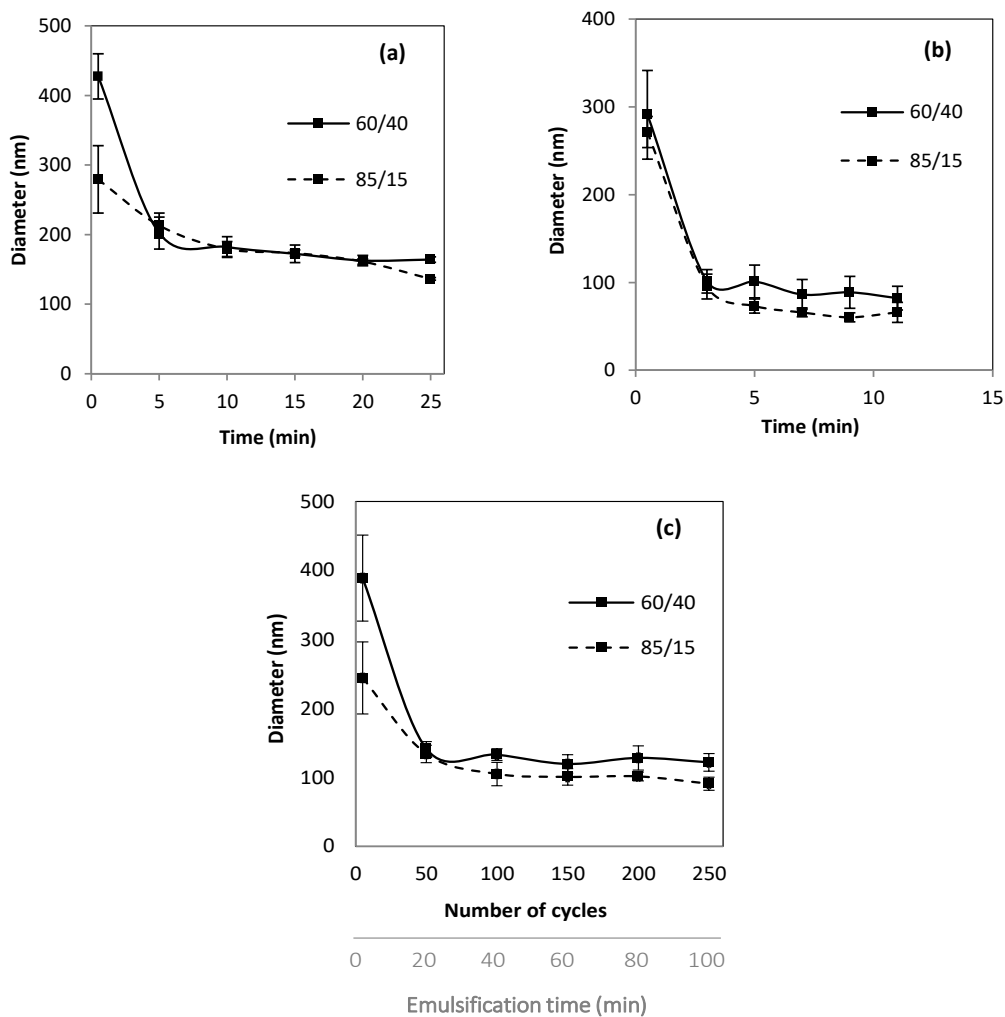


Figure 3.2. Evolution of PLGA nanoparticles' size at 85/15 and 60/40 volume ratios. The PLGA NPs were produced by a) rotor-stator mixing, b) sonication or c) elongational-flow micromixer.

After emulsification and solvent evaporation, the size and monomodality of these PNPs depending on operating parameters were analyzed by dynamic light scattering (DLS) and discussed (Figure 3.2, Figure 3.3). As observed in Figure 3.2, after a short emulsification time (less than 5 min), there were huge size differences between the three devices. With C/D = 60/40 for example, highly polydisperse particles of 430 nm, 300 nm and 400 nm were produced by the rotor-stator mixer, the sonicator and the elongational-flow reactor and micromixer (μ RMX) respectively. These results, due to the different mechanisms of particle formation, were coherent with previous studies carried out by our team [9], [21], [22]. Indeed, rotor-stator produced particles by shear effect applied by external rotational force, sonication process produced particles by water gas bubble implosion (known to lead to smaller particles) and μ RMX mainly used a flow focusing mechanism in order to produce nanodroplets.

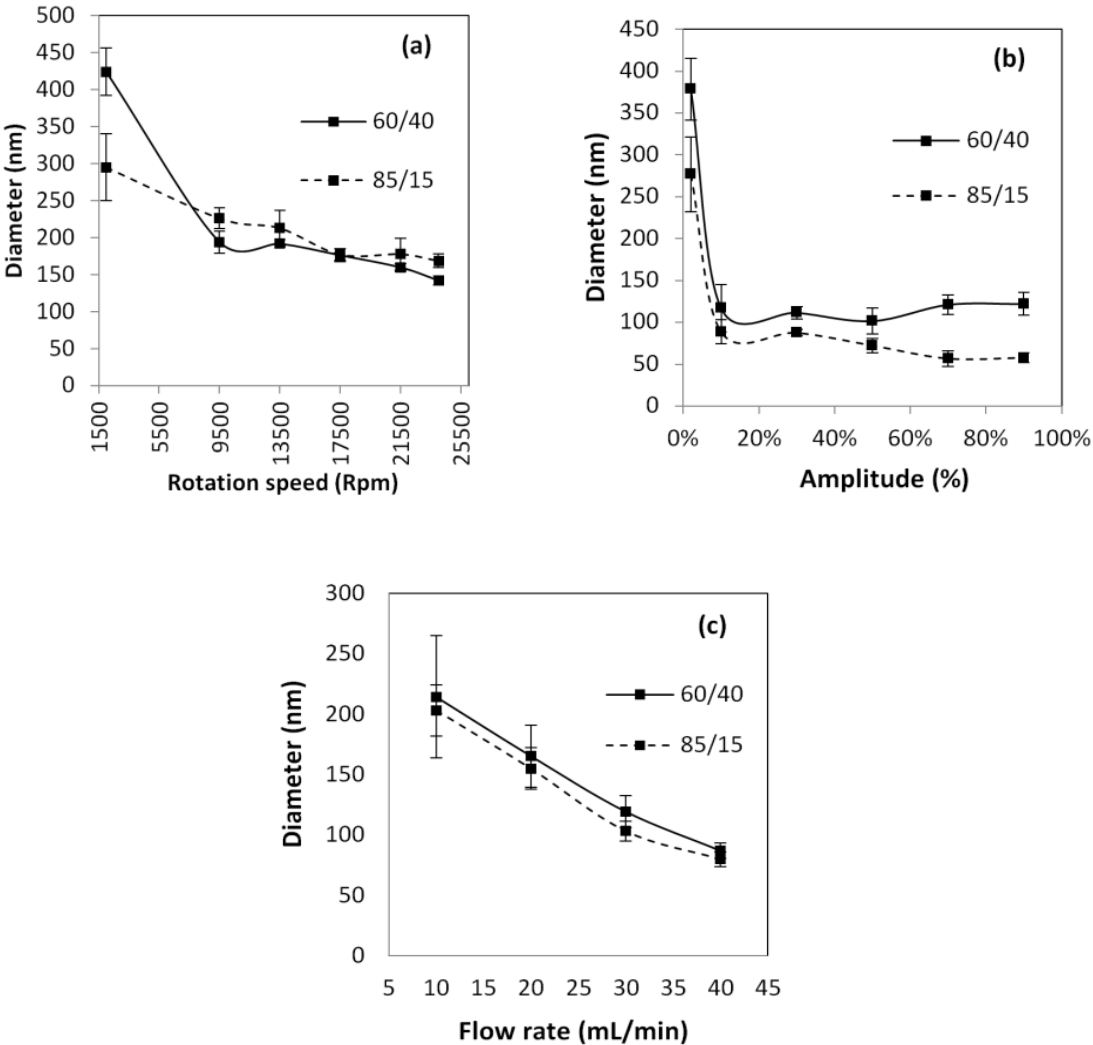


Figure 3.3. Evolution of PLGA nanoparticle size at 85/15 and 60/40 volume ratios. The PLGA NPs were produced by a) rotor-stator mixing, b) sonication or c) elongational-flow micromixing

After a longer emulsification time, a plateau value was obtained at lower sizes: 150 nm (shear mixer) and 100 nm (sonicator and elongational-flow reactor and micromixer). The operating parameters of shear mixer (rotational speed), sonicator (power amplitude) and elongational-flow reactor and micromixer (flow rate) also allowed optimizing NPs' size (Figure 3.3), and PDI value (Figure 3.4). As expected, increasing these parameters lead to a decrease of the PNPs' size. The minimum size was 136 nm with the rotor-stator mixer (25 min, 17500 rpm), 57 nm with sonicator (5 min, 70% amplitude) and 80 nm with the elongational-flow reactor and micromixer (60 min, 40 mL/min). Noteworthy, the emulsification with sonicator at 5 minutes, 70% amplitude conditions reached 70°C temperature without an external cooling condition, which will be discussed in the next part.

Moreover, with a higher C/D volume ratio (85/15), the average particle size decreased more than 20% in size, as reported in Figure 3.2. and in Figure 3.3. This was coherent with previous studies demonstrating that decreasing the polymer concentration, *i.e.* increasing the C/D volume ratio, decreased the system's viscosity which lead to the production of smaller particles [22], [26].

Following the elaboration, it was possible to achieve PNP size of below 150 nm, and it was described. In the next part, the size distribution of the produced PNPs can be found in details.

3.2.2 Polydispersity index of the produced PNPs

As shown in Figure 3.4, all devices allowed the production of monomodal nanoemulsions that can mainly be controlled by operating parameters allowing to yield monomodal (PDI below 0.2 [27]) PLGA NPs with a size below 150 nm.

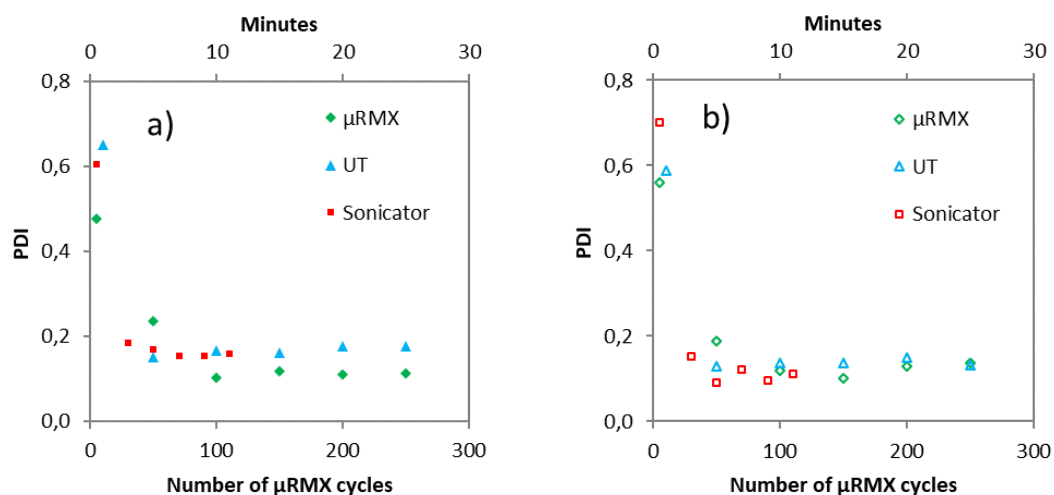


Figure 3.4. Polydispersity index results of PLGA nanoparticles produced by three emulsification devices: sonicator, rotor-stator mixer (UT), elongational-flow micromixer (μ RMX) at a) 85/15, and b) 60/40 C/D volume ratios. Process parameter are 50% amplitude, 17.500 rpm, and 150 cycles for the given devices respectively.

In Figure 3.4, PDI values of PLGA NPs were in the range of 0,05 and 0,2 (Figure 3.4) following an increasing emulsification time. For a very short emulsification time as 1 minute, similarly to the average size results (Figure 3.2, Figure 3.3), the size distribution of PLGA NPs was broad and at given production conditions. This can be explained by the insufficient residence time of the emulsion droplets induced to the shear and elongational-flow forces.

In conclusion, after few minutes, all the devices allowed the production of monomodal PNPs. However, we need to keep in mind that shear mixing lead to bigger size. Thus, in order to choose between sonication and elongational flow for drug encapsulation experiments, the heat released during emulsification needed to be investigated.

3.2.3 Heat emission during the process of emulsification

As previously discussed in the “Materials and Methods” chapter, the high-energy methods, *i.e.* sonication and shear mixing, can increase the systems temperature by emitting heat (Figure 3.5). During the sonication process, ultrasound effects like cavitation occurs. Cavitation leads to high temperatures ($T \geq 60\text{ }^{\circ}\text{C}$) that can later affect the drug stability and accelerate the polymer degradation by reaching their glass transition temperatures.

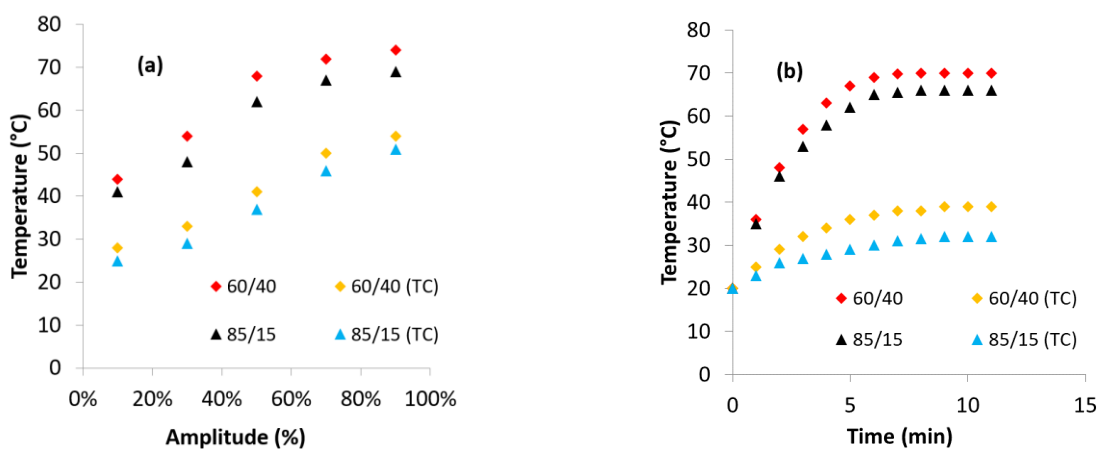


Figure 3.5. Evolution of the PLGA emulsions' (C/D ratios of 60/40 and 85/15) temperatures with and without temperature control (TC); (a) within 5 minutes of sonication, (b) at 50% power input.

In Figure 3.5, it was demonstrated that, at starting from a very low power amplitude and the emulsification time (20% and 1 minute respectively) the systems temperature already reached above the ambient temperature. This was coherent with the previous report that explained an extremely high heat emission (5,000 K) during the sonication process [28]. Two additional parameters were studied in this part: emulsions continuous and dispersed phase ratio, and presence of the temperature control (TC). First, at C/D volume ratio equal to 85/15, the temperature was

approximately 10% lower than with the 60/40 volume ratio emulsification at same conditions. Considering the lower viscosity value of the oil phase, at C/D ratio of 85/15 the total average viscosity was higher than the 60/40 emulsion viscosity. Indeed, considering the same given energy densities in both emulsions, the temperature increase can be explained by the amount of energy transformed into a mechanical energy which ruptured the emulsion droplet, where higher viscosity systems require higher critical capillary number, thus, higher energy according to the Taylor Grace theory. The second factor while changing C/D volume ratio is the number of surfactant molecules in the process: the number of molecules in a unit emulsion volume was maximum at C/D volume ratio equal to 85/15. Thus, the transfer of surfactant molecules onto the droplet surface (Marangoni effect) was maximum, leading an accelerated droplet break-up and thus, decreasing the system's temperature at the beginning of the emulsification.

It should also be noted that, temperature increase lowers the viscosities, which indirectly decreases the critical capillary number, eventually reducing the time required for the emulsification. However, this was not required in the drug encapsulation that was studied later. It was possible to control temperature for the shear mixing with an external cold water, however, in sonication TC reduced the process temperature maximum of a 50%, leaving the emulsion temperature above 30°C.

On the opposite, the μ RMX did not induce any temperature increase and thus was the only device chosen to further study the one-step encapsulation of rifampicin.

3.2.4 Process volume influence on PNP fabrication

Another interesting point to investigate, before focusing on drug encapsulation, was the impact of the total emulsion's volume, at constant process operating parameters, on the PNPs' size. In the previous chapter, it was indeed discussed that the power density E_v is the average power dissipated per unit of mass of the emulsion ($W\ kg^{-1}$). When the residence time (τ) and the power (P) are kept constant, and the processing volume (V) of the emulsion increased, the energy density will decrease according to Equation 2.11 (Chapter 2).

Following this relationship, at reduced power density E_v , the emulsification process slows down, yielding larger emulsion droplets at a given residence time. This was the case for both shear and ultrasound processes, where the average PLGA NPs' size increased by 128% and 250% emulsification, respectively, when the total volume V was multiplied by 4 (Figure 3.6). Moreover, PNPs produced by both techniques were highly polydisperse at high operational volumes.

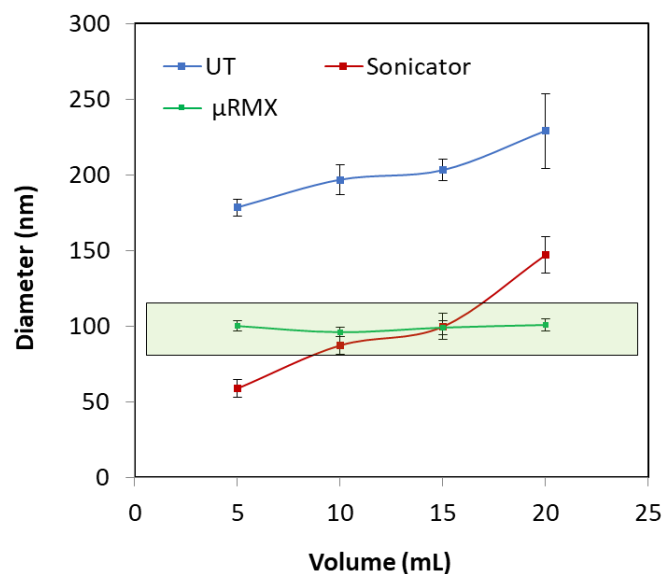


Figure 3.6. Evolution of the PLGA NP size produced with three different techniques; Shear-mixing at 17,500 rpm for 10minutes, sonication 50% power for 5 minutes of sonication, and μ RMX 150 cycles at 30 mL/min flow rate.

However, the elongational-flow emulsification showed the fixed size of 101 nm for all operational volumes between 5 mL and 20 mL. Additionally, PLGA NPs at each operational volume had a similar particle size distribution of below 0,15, which is a monomodal size distribution. This was coherent with Grace Taylor theory, where the elongational-flow type of droplet breakup mechanism was different from the simple shear force mechanism.

This property of elongational-flow emulsification to yield PNP sizes at constant values was another strong reason to follow the drug encapsulation with this technique. Also, the ability of elongational-flow emulsification to operate at higher operational volumes yielding constant material properties can be the key parameter for shifting to the larger scale production.

3.3 PLGA NANOPARTICLES AS DRUG CARRIERS

In the previous part, three different devices have been studied to produce biodegradable NPs, showing suitable size and dispersity features for drug delivery systems. However, by shear mixing and by sonication unnecessarily high particle size changes and heat effects occurred. Since μ RMX performed no excess heat release and produced monomodal PNPs, this device has been chosen (150 cycles, 30 mL/min) for the following investigation concerning drug encapsulation by PLGA NPs.

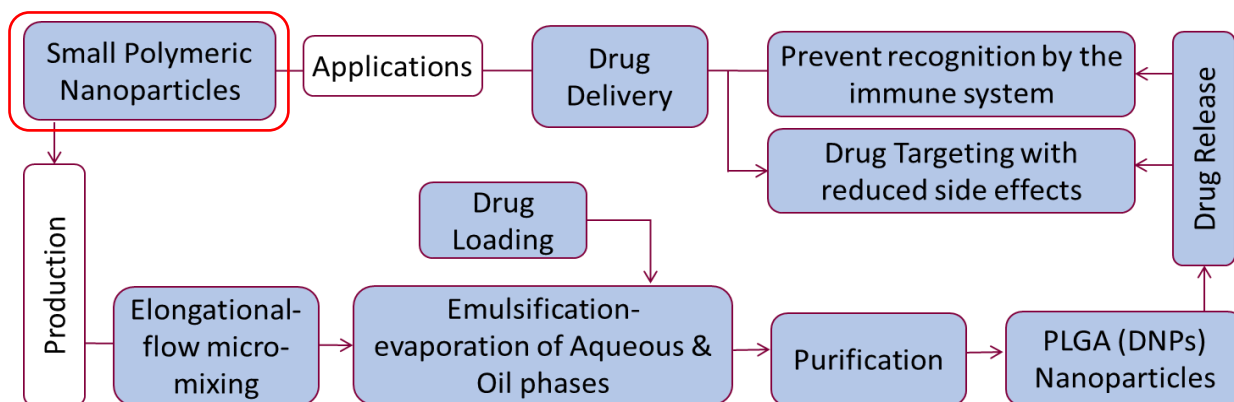


Figure 3.7. Schematic representation of PLGA nanoparticles' production and drug delivery strategy through the elaborated emulsification-evaporation method. "DNPs" stands for drug-loaded nanoparticles.

In Figure 3.7, the drug loading was carried out when the emulsification was processed. Then, following 24 hours of solvent evaporation at room temperature, drug-loaded PLGA nanosuspensions were purified to eliminate the drug content that was not encapsulated to later study the encapsulation efficiency and the drug released from drug-loaded nanoparticles (DNPs).

3.3.1 Rifampicin's calibration curve

First of all, it was important to quantify the rifampicin content in a solution to later estimate the drug (rifampicin) concentration while studying encapsulation and release. The drug was quantified by solubilizing the drug in water at different concentrations before measuring it with a UV spectrometer. However, rifampicin had two main UV absorbance regions (Figure 3.8) and could degrade through time [29], which leads to variations in final calculations. To verify this effect, two calibration curves were generated at $\lambda = 332$ nm (Figure 3.10.b) and at $\lambda = 469$ nm (Figure 3.9.a), and all the samples were left to degrade in 72 hours.

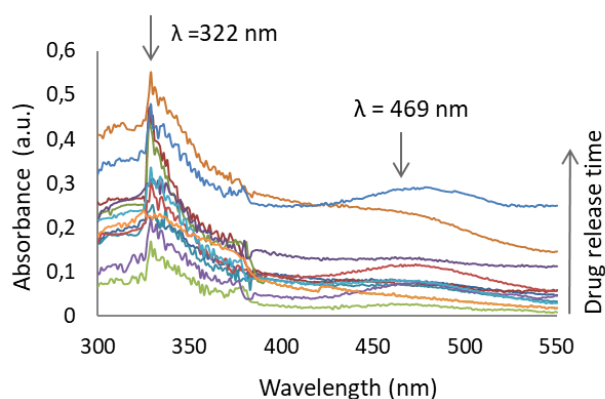


Figure 3.8. Evolution of the two UV absorbance regions at different rifampicin concentrations and time (from 1 hour to 168 hours) extracted from the PLGA NPs drug release studies.

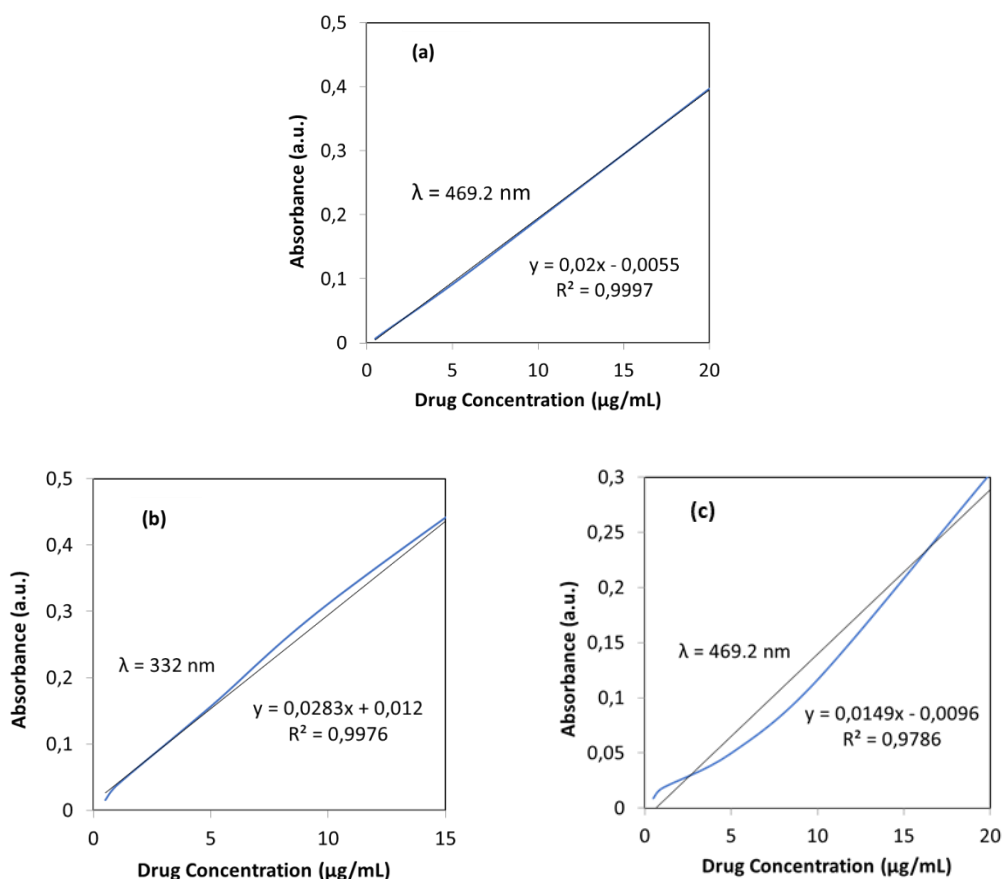


Figure 3.9. Initial UV absorbance spectra (a) from rifampicin at various concentrations in water realized in order to obtain the (b) drug degradation at $\lambda = 332$ nm, and (c) drug degradation at $\lambda = 469$ nm absorbance region at 37°C during 72 hours. Blue lines represent the real values of rifampicin absorbance, and black lines represent the correlation variables of absorbance.

When both absorbance regions were compared after 72 hours, $\lambda = 469$ nm region showed a reduced absorbance due to decreased (degradation). At lower concentrations, absorbance was found decreasing more, compared to absorbance at higher concentrations. This was verified with $R^2 = 0.98$ (Figure 3.9.c), compared to $R^2 = 0.999$ (Figure 3.9.a). Rifampicin degradation kinetics was thus coherent with the previous studies carried out at different (0.01-1 mg/mL) drug. $\mu\text{g/mL}$ concentrations [29]. Considering these results, faster and uncontrolled degradation at lower rifampicin concentrations was verified, and was the main reason to study drug encapsulation and release later according to $\lambda = 332$ nm region.

Following these results, the calibration curve for the main drug delivery studies was established at 332 nm according to Beer-Lambert law (Figure 3.10.b).

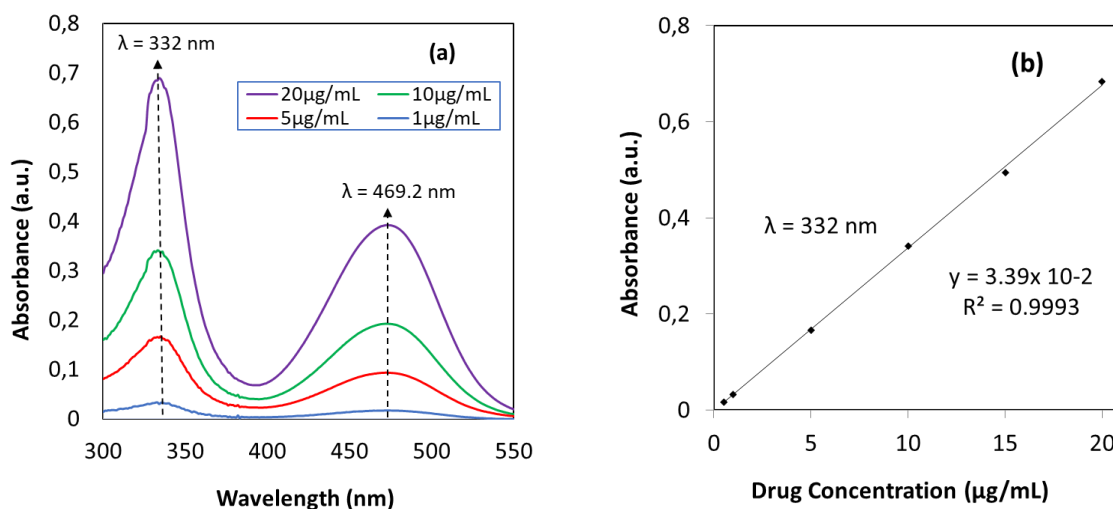


Figure 3.10. UV absorbance spectra from rifampicin at various concentrations (a) in water realized in order to obtain the (b) calibration curve at $\lambda = 332$ nm. The equation of the fitting curve is Absorbance = $3.39 \times 10^{-2} \times$ Drug Concentration ($R^2 = 0.999$).

3.3.2 PLGA size and size distribution influenced by the drug encapsulation

In this part, the influence of drug (rifampicin) concentration on encapsulation efficiency was investigated. For this purpose, the drug was introduced into the disperse phase (1w/v% of PLGA in ethyl acetate) at different weight contents with respect to PLGA, ranging from 1%/PLGA w/w to 10%/PLGA w/w (the samples were called R1 to R10 respectively). Drug load (DL), encapsulation efficiency (EE), amount of encapsulated drug and the average size of a drug carrier are reported in Table 3.2 while drug-loaded nanoparticles' (DNPs') size and PDI variations with respect to the initial drug weight content are presented in Figure 3.11.

Table 3.2 Drug loading (DL) and encapsulation efficiency (EE) for different initial drug weight contents.

Sample name	Initial drug weight content with respect to PLGA (w/w)	DL (%)	EE (%)	Encapsulated Drug (μg)	Average Size of DNP
R1	1%	2.2 ± 0.1	95 ± 3	191 ± 5	76 ± 5
R2	2%	3.6 ± 0.2	80 ± 5	319 ± 19	66 ± 4
R5	5%	4.5 ± 0.5	40 ± 3	395 ± 27	69 ± 2
R10	10%	7.2 ± 0.4	32 ± 2	634 ± 33	65 ± 2

According to the drug encapsulation results, it was possible to encapsulate bigger ratio of the drug inside PLGA NPs when the initial drug weight content was low. However, by increasing the initial drug weight it was inevitable to miss a bigger portion migrating to the continuous phase, thus, decreasing EE. This can be explained by osmotic gradient, where the drug starts migrating from highly concentrated solution to low concentrations to reach its equilibrium. In our system, this mainly took place during the emulsification, especially during the solvent migration from the droplet to the continuous phase, which eventually fastened the migration of drug molecules.

Moreover, the DL increased from 2.2% to 7.2% while increasing the initial drug concentration from 1% w/w to 10% w/w. EE reached its highest value at the lowest drug load, however the mass quantity of encapsulated drug (191 μg at 1%/PLGA w/w) was the lowest value (319 μg at 2%/PLGA w/w, 395 μg at 5%/PLGA w/w and 634 μg at 10%/PLGA w/w) among all experiments. The minimum load could be applied to minimize the loss of (non-encapsulated) drug, however the highest quantity of encapsulated drug, considering the drug/polymer ratio, can be reached only at higher initial drug loads (Table 3.2). So, it appeared that, considering the size and PDI values, 5% w/w initial drug concentration regarding to polymer weight content, led to the production of the most monomodal DNPs having a diameter below 70 nm.

Additionally, migration of materials, especially the polymer solution through diffusion can result in a disproportionately fast droplet surface hardening that occurs during emulsification, limiting the polymer shrinkage. This hardening was delayed by applying the pre-saturation method, *i.e.* by saturating the continuous phase with the disperse phase's solvent, in order to control a diffusion of the organic solvent during the emulsification and solvent evaporation. Interestingly, from the unloaded PLGA NPs to 2% w/w initial drug concentration, the particle size was still reduced by more than 25% (Figure 3.11), and similar monomodality at all drug concentrations were recorded.

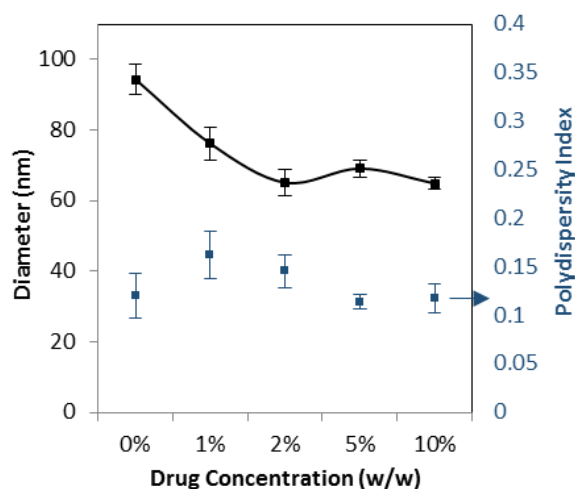


Figure 3.11. Evolution of the PLGA drug-loaded nanoparticles' diameter size and polydispersity index for different drug weight contents with respect to PLGA.

Increasing rifampicin initial weight content unexpectedly decreased the NPs' size from 94 ± 4 nm down to $69 \text{ nm} \pm 2$ nm (Figure 3.11). This result was explained by a decrease in the interfacial tension between the continuous and disperse phases without ($\sigma_{0\%} = 3.2$ mN/m) and with drug ($\sigma_{10\%} = 2.8$ mN/m), due to the intermolecular interactions that occur between PLGA and rifampicin and due to the presence of rifampicin at the surface of the droplets.

3.3.3 Understanding the size reduction at different material concentrations

Considering a large size reduction while adding rifampicin to PLGA solution, it was to study this difference in size by using the droplet tracking technique. Interfacial tension of two immiscible phases changed depending on the materials present in solution (Figure 3.12).

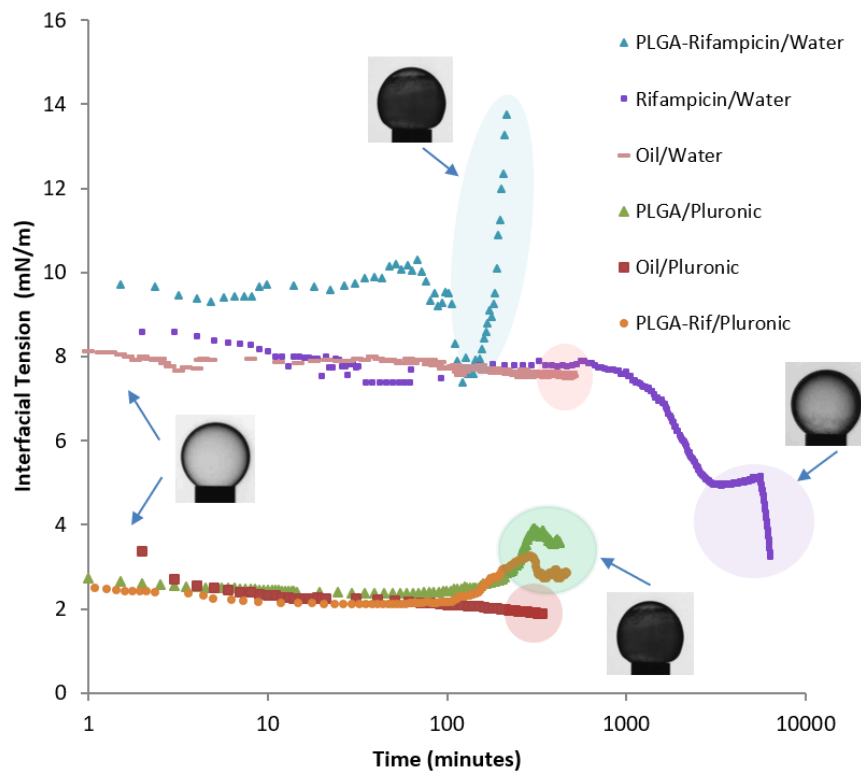


Figure 3.12. Interfacial tension measurements between ethyl acetate phase and water phase compositions with Teclis Tracker technique (see 2.3.3). The given droplets contained from different compositions of ethyl acetate (oil phase); only Rifampicin, only PLGA, and both PLGA-Rifampicin. The surrounding fluid contained from only water or Pluronic F127 surfactant in water. Two dark droplets represent oil phases containing polymer, and the bright droplet represent free oil/water or oil/Pluronic in water. Increase in the interfacial tension values represent the surface hardening of the droplet (layer).

Generally, 6 samples were measured, and when no surfactant was introduced to the surrounding phases, in the all measurements, the interfacial tension value was above 8 mN/m. In the presence of

Pluronic F127 surfactant, the interfacial tension value directly started from approximately 3.2 mN/m, and continued shifting down by reaching 2.5 mN/m within 2 hours. This means the surfactant molecules come to the interface, and slowly deposit onto the droplet surface due to the Marangoni convection. Thus, eventually the droplet and the surrounding fluid reach the minimum value of interfacial tension. This was coherent with previous study [30], verifying the measurements were comparable to nanoemulsions from previous parts.

In the oil phase (droplet), where PLGA and rifampicin can be found, the interfacial tension reduced from 8.5 mN/m to 7mN/m within less than 1 hour, then sharply decreased down to 4.3 mN/m (Figure 3.12, cyan triangles). When both surfactant and rifampicin presented in the oil phase (orange circles), interfacial tension was 0.4 mN/m lower than the oil phase without rifampicin (green triangles). This result explains why PNP size decreases when rifampicin present in the oil phase (Figure 3.11).

When all the components presented in both phases a continuous deposition of both surfactant and PLGA molecules created a thin layer on the droplet surface, leading to the dark color of the droplet, and sharp increase in interfacial tension values. This tendency was generally observed after approximately 100 minutes of measurement. These sharply increasing values (Figure 3.12) are an indication of a skin formation on the surface of the droplet. PLGA-Rifampicin composition (cyan triangles) led to the highest skin forming, however Rifampicin alone (purple squares) didn't form a fixed layer on droplet surface, it decreased interfacial tension between water and oil phases after 900 minutes in non-dynamic condition.

The formation of a thin layer on surface of the droplets, mainly during the formation of PNPs, was then confirmed with a morphological analysis of the droplet surfaces (Figure 3.13).

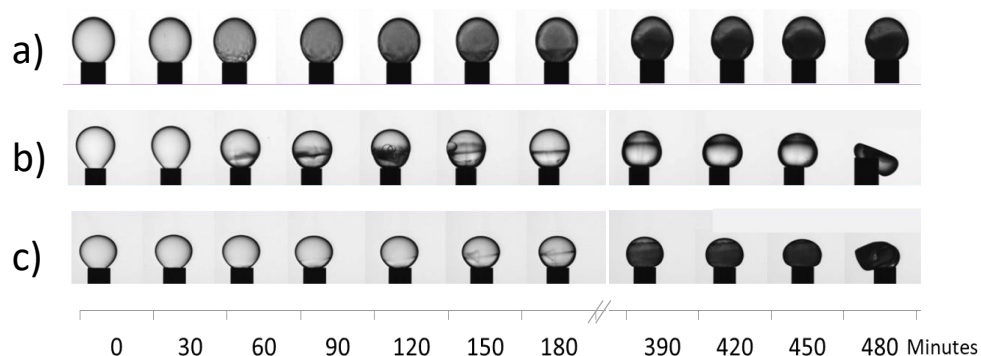


Figure 1.13. Evolution of the droplets' shape with time for a) PLGA-Rifampicin in ethyl acetate + water, b) PLGA in ethyl acetate + surfactant in water and c) PLGA-Rifampicin in ethyl acetate + surfactant in water.

It's believed that this change took place due to Rifampicin's limited solubility in water after certain time period, which in turn acts as a surfactant between water and oil phases. Moreover, any type of

reduction in an interfacial tension leads to smaller particle formation later in during the emulsification process.

In this part, the reduced interfacial tension was demonstrated as the main reason of the PNP size reduction in the presence of rifampicin. Additionally, the polymer layer was demonstrated on the surface of droplets, which can be interesting to understand PNP formation following self-assembly of the polymer molecules.

3.3.4 Coherence of results from two different characterization techniques

PLGA NP size and size distribution were characterized by using two techniques in this chapter: DLS (the number average) and TEM (statistical analysis on 500 particles). As shown in Figure 3.14, both characterization methods were coherent when compared. For instance, size reduction (91 nm for unloaded PLGA NPs, 64 nm at 5% rifampicin concentration) and narrower size distribution while adding rifampicin to the polymer solution were confirmed with both characterization techniques.

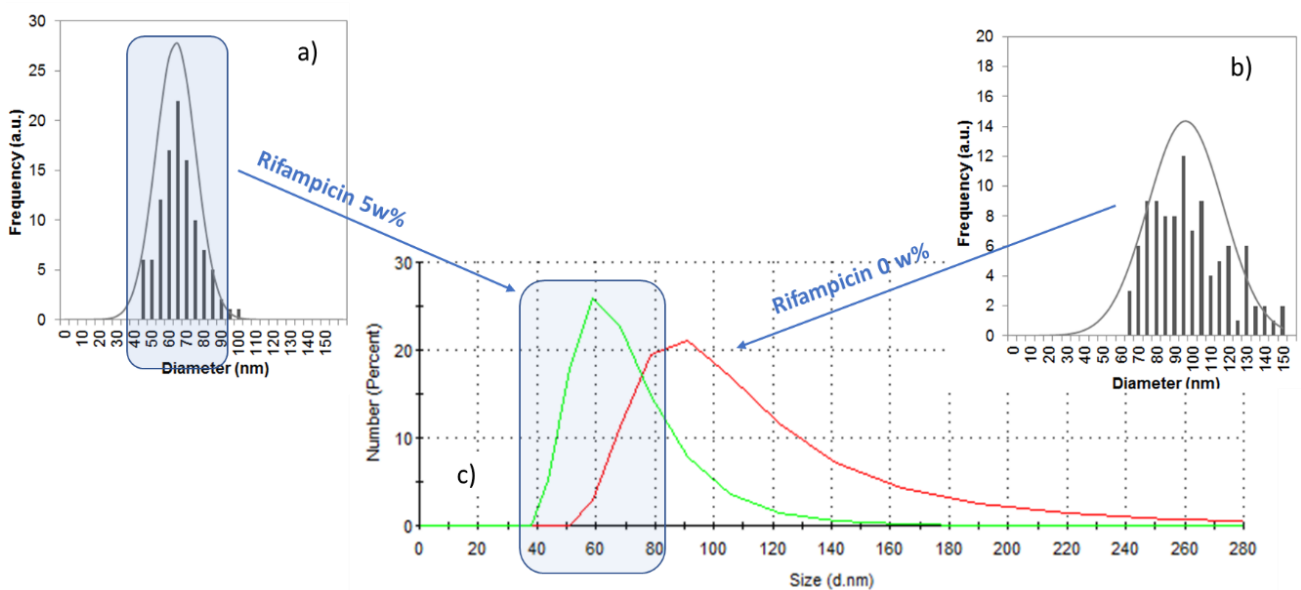


Figure 3.14. Statistical analysis based on TEM images for a) 5% w/w DNPs and b) unloaded PNPs, and the average PNPs diameter from DLS.

3.4 DRUG RELEASE FROM PLGA NANOPARTICLES

3.4.1 Influence of the initial drug weight content on the drug release

In order to study the drug release at 37°C from previously produced DNPs, they were isolated from the solution by centrifugation (9500 rpm, 30 min) and filtration (filter diameter = 0.2 μm) before being introduced into a dialysis tube in a 7.4 pH-controlled buffer solution. The amount of drug (μg) released from DNPs was determined by UV-visible spectroscopy at 332 nm by considering the rifampicin possible degradation (Equation 2.20). The cumulative drug release was then calculated by the mass ratio of the released drug to the initially loaded drug (Equation 2.21).

Drug release kinetics for different initial drug weight contents with respect to PLGA are given in μg and percentage values (Figure 3.15). It is worthy to note that the given Rifampicin released percentage values were calculated considering the encapsulated drug quantity. For example, a quantity of encapsulated drug for R5 was 395 ± 15 μg, and 175 ± 9 μg was released after 8 days, which makes 45% of drug released.

As previously indicated, R1, R2, R5 and R10 represent the samples studied at 1% w/w, 2% w/w, 5% w/w and 10% w/w of initial drug introduced in the disperse phase respectively.

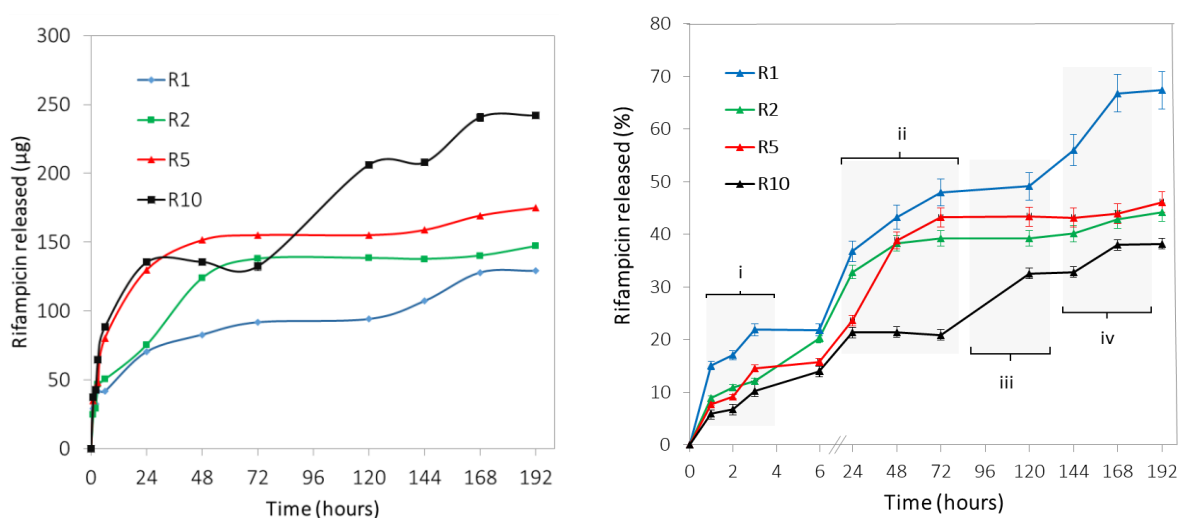


Figure 3.15. In-vitro drug release profile at 1% w/w (R1), 2% w/w (R2), 5% w/w (R5), and 10% w/w (R10) rifampicin weight content relatively to PLGA a) in micrograms and b) in percentage.

First of all, the amount of released drug increased with time, proving that the developed system achieved a sustain drug release over time. Moreover, the drug quantity released in 8 days was 129 ± 12 μg (67%), 147 ± 10 μg (46%), 175 μg ± 9 μg (45%) and 242 μg ± 9 μg (38%) for R1, R2, R5 and R10 respectively. So, different drug release kinetics occurred for a maximum amount of Rifampicin

released in 8 days equal to 242 μg . This drug delivery system can thus be adapted to various released doses. Observing the error bars, DNPs formed with the lowest initial drug concentration (R1) may be considered as a non-stable system, contrary to DNPs produced with higher drug concentrations.

More interestingly, in Figure 3.15.b, four substages were identified for drug release process:

- (i) Burst release effect was noticed within first 3 hours;
- (ii) From 6 to 72 hours, a cumulative drug release due to constant diffusion from DNPs to water was observed;
- (iii) A partial resilience occurred between 3 and 5 days, which can be explained by the drug entrapment near inner surface of DNPs;
- (iv) On last stage, the drug encapsulated in center of DNPs started to diffuse into water after reaching DNPs' surface.

These four substages were likely correlated either to the polymer degradation or to diffusion of drug across PLGA chains. In order to investigate this point, transmission electron microscopy images were carried out the first, third and eighth days of release study (Figure 3.16). DNPs investigated by TEM were at 5% w/w initial drug weight content due to high accuracy in diameter and size distribution (Figure 3.11).

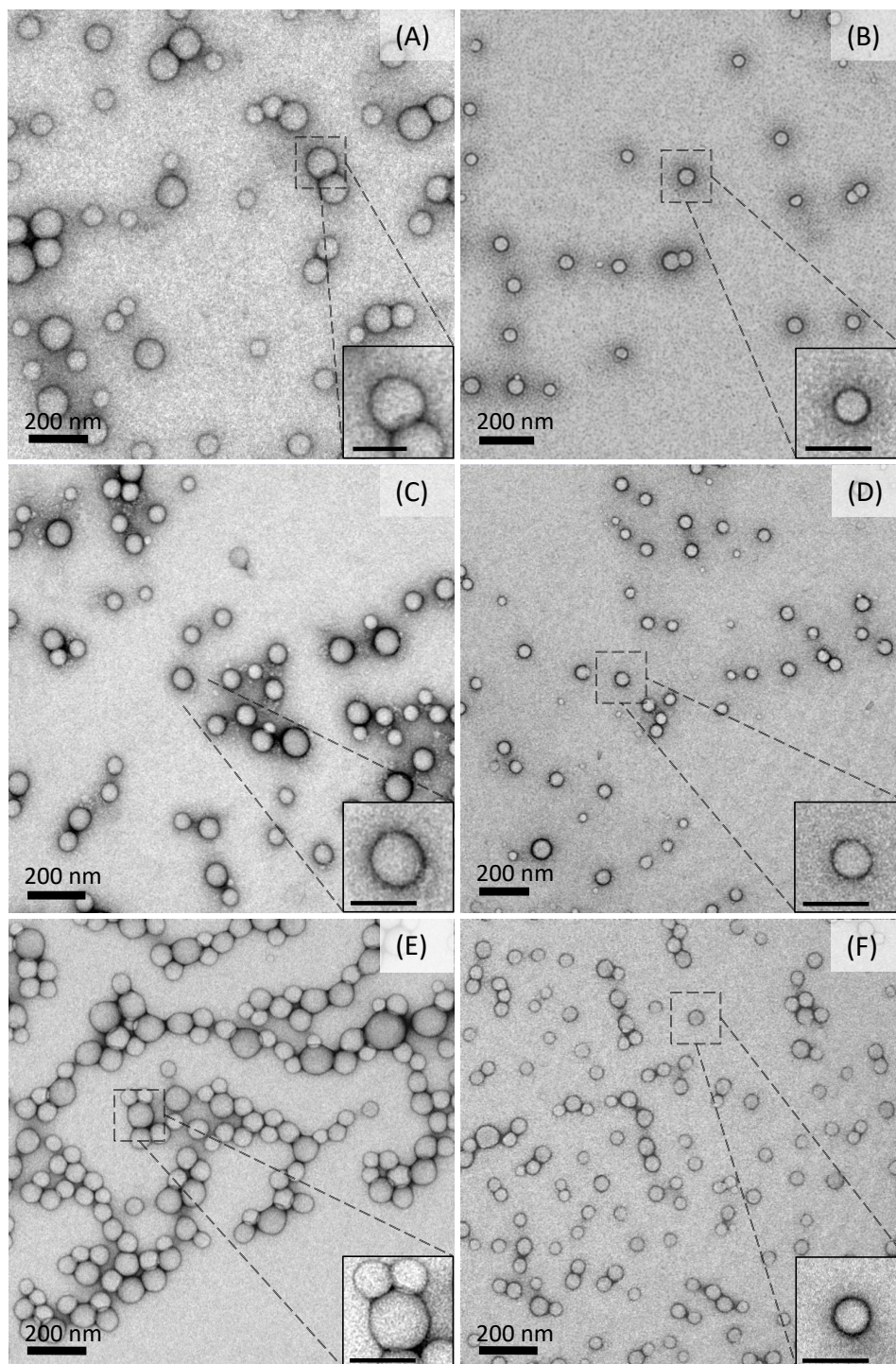


Figure 3.16. TEM images (A-F) of unloaded PLGA NPs (A, C, E) and 5% w/w drug-loaded DNPs (B, D, F) after 1st (A, B), 3rd (C, D) and 8th day (E, F) at 37°C and pH = 7.4.

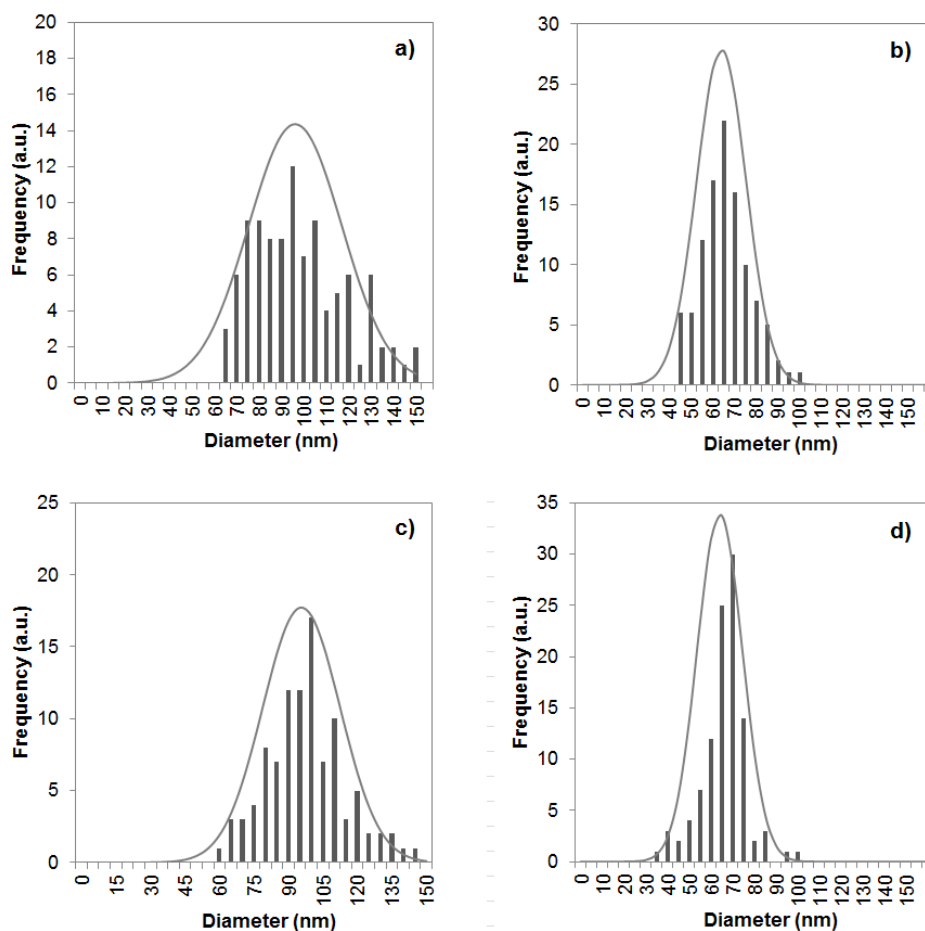


Figure 3.17. The statistical analysis of unloaded PLGA NPs (a, b) and 5% w/w drug-loaded DNPs (c, d) after 1st (a), and 8th day (b) at 37°C and pH = 7.4.

In Figure 3.16, TEM images showed spherical NPs for unloaded PLGA NPs and through all in vitro release period. From the initial stage, NPs (A) and DNPs (B) produced with the same operating parameters had a size difference of more than 30 nm. Thus, diameter size difference between unloaded NPs (Figure 3.17.a, 98 nm) and DNPs (Figure 3.17.c, 64 nm) at the first day confirmed the previously discussed DLS size results (Figure 3.11). The broader Gaussian curve obtained for the PLGA NPs (Figure 3.17) also proved the higher PDI compared to DNPs. The blank NPs at 3rd day (C), and at 8th days (E) showed, by TEM, a high morphological stability property similar to DNPs at 3rd day (D), and at 8th day (F), and the statistical analysis (Figure 3.17) confirmed these results.

As previously discussed in the literature, PLGA 50:50 degradation can start after more than 2 weeks [14] and here, PLGA-based NPs were still spherical and without physical damages after 8 days. This phenomenon made a clear understanding of the mechanism of drug release that occurred: rifampicin was released from the DNPs by diffusion between PLGA chains.

Overall, no PLGA degradation was observed within 8 days, which makes a diffusive drug release understandable. For further studies the drug release can be improved through polymer degradation.

3.5 CONCLUSION

This work proposes to implement the emulsification-evaporation method for the one-step production of PLGA drug-loaded NPs. Influence of three different emulsification devices operating parameters (emulsification time, temperature and mixing parameters) as well as chemical parameters (drug concentration) on the nanoparticles' mean diameter and drug release profiles was thoroughly studied. Emulsification-evaporation method was a reliable way to produce biodegradable, biocompatible poly(lactic-co-glycolic acid) nanoparticles (PLGA NPs). First, processes as sonication, shear-mixing and elongational flow micromixing were operated and allowed the production of smaller NPs (diameter below 150 nm). Indeed, by changing emulsification time and mixing parameters, minimum values of diameter size and size distribution (PDI below 0.2) have been obtained. The minimum size was 136 nm with the rotor-stator mixer (25 min, 17500 rpm), 57 nm with sonicator (5 min, 70% amplitude) and 80 nm with the elongational-flow reactor and micromixer (60 min, 40 mL/min). It was thus stated that elongational-flow micromixing was the most reliable way to produce biocompatible, monomodal NPs adapted for drug encapsulation with fine size control.

Rifampicin was then encapsulated into PLGA NPs at different drug loads ranging from 1% w/w to 10% w/w regarding of polymer weight content. Interestingly, the unloaded PLGA NPs and drug-loaded NPs had different diameter size values, respectively 94 nm and 63 nm. Considering DNPs diameter and size dispersity, the optimum EE of 40% at 5% w/w initial drug concentration was achieved. Additionally, the continuous phase pre-saturation method was applied to 60/40 continuous/disperse phases before elongational-flow emulsification which decreased the size of NPs from 126 nm to 94 nm without drug encapsulation. TEM images showed the difference between size, monomodality of unloaded and drug loaded NPs and a non-degradable characteristic of the PLGA matrix within 8 days.

In vitro drug release study from spherical polymeric DNPs under sink conditions showed that the drug quantity can be controlled by varying the initial drug weight content but simultaneously affects DNPs' average size. Moreover, the cumulative release reached higher values with an increasing amount of initial drug weight content. Encapsulated Rifampicin quantities inside PLGA DNPs were between 191 μg to 634 μg and the released drug quantities were equal to 129 μg (67%) and to 242 μg (38%) respectively.

This work thus opens innovative perspectives for the design of controlled drug release systems. Indeed, the influence of the polymer structure and the interrelation between the different polymer properties and the diffusion rate of a produced nanomaterial can be investigated in order to obtain

an improved drug delivery. Thus, in the next chapter we study polymer blends, and anisotropic PNPs to encapsulate rifampicin, and compare with the PLGA NPs presented in this chapter.

3.6 BIBLIOGRAPHY

- [1] A. A. Barba *et al.*, "Engineering approaches for drug delivery systems production and characterization," *Int. J. Pharm.*, vol. 581, no. March, p. 119267, 2020, doi: 10.1016/j.ijpharm.2020.119267.
- [2] F. Noël, C. A. Serra, and S. Le Calvé, "Design of a novel axial gas pulses micromixer and simulations of its mixing abilities via computational fluid dynamics," *Micromachines*, vol. 10, no. 3, pp. 1–16, 2019, doi: 10.3390/mi10030205.
- [3] H. M. Abdelaziz *et al.*, "Inhalable particulate drug delivery systems for lung cancer therapy: Nanoparticles, microparticles, nanocomposites and nanoaggregates," *J. Control. Release*, vol. 269, no. October 2017, pp. 374–392, 2018, doi: 10.1016/j.jconrel.2017.11.036.
- [4] B. J. Boyd *et al.*, "Successful oral delivery of poorly water-soluble drugs both depends on the intraluminal behavior of drugs and of appropriate advanced drug delivery systems," *Eur. J. Pharm. Sci.*, vol. 137, no. May, p. 104967, 2019, doi: 10.1016/j.ejps.2019.104967.
- [5] J. Liu *et al.*, "A modified hydrophobic ion-pairing complex strategy for long-term peptide delivery with high drug encapsulation and reduced burst release from PLGA microspheres," *Eur. J. Pharm. Biopharm.*, vol. 144, no. August, pp. 217–229, 2019, doi: 10.1016/j.ejpb.2019.09.022.
- [6] Q. Mei *et al.*, "Formulation and in vitro characterization of rifampicin-loaded porous poly (ϵ -caprolactone) microspheres for sustained skeletal delivery," *Drug Des. Devel. Ther.*, vol. 12, pp. 1533–1544, 2018, doi: 10.2147/DDDT.S163005.
- [7] C. Bulmer, "Encapsulation and Controlled Release of rHu-Erythropoietin from Chitosan Biopolymer Nanoparticles," 2012.
- [8] B. Y. Liu, C. Wu, X. Y. He, R. X. Zhuo, and S. X. Cheng, "Multi-drug loaded vitamin E-TPGS nanoparticles for synergistic drug delivery to overcome drug resistance in tumor treatment," *Sci. Bull.*, vol. 61, no. 7, pp. 552–560, 2016, doi: 10.1007/s11434-016-1039-5.
- [9] S. Ding, C. A. Serra, T. F. Vandamme, W. Yu, and N. Anton, "Double emulsions prepared by two-step emulsification: History, state-of-the-art and perspective," *J. Control. Release*, vol. 295, no. December 2018, pp. 31–49, 2019, doi: 10.1016/j.jconrel.2018.12.037.
- [10] A. Mahboubian, S. K. Hasheminein, S. Moghadam, F. Atyabia, and R. Dinarvand, "Preparation and in-vitro evaluation of controlled release PLGA microparticles containing triptoreline,"

- Iran. J. Pharm. Res.*, vol. 9, no. 4, pp. 369–378, 2010, doi: 10.22037/ijpr.2010.902.
- [11] S. Ding *et al.*, “Microfluidic-Assisted Production of Size-Controlled Superparamagnetic Iron Oxide Nanoparticles-Loaded Poly(methyl methacrylate) Nanohybrids,” *Langmuir*, vol. 34, no. 5, pp. 1981–1991, 2018, doi: 10.1021/acs.langmuir.7b01928.
- [12] J. Wallyn *et al.*, “A new formulation of poly(MAOTIB) nanoparticles as an efficient contrast agent for in vivo X-ray imaging,” *Acta Biomater.*, vol. 66, pp. 200–212, 2018, doi: 10.1016/j.actbio.2017.11.011.
- [13] Y. Sun *et al.*, “Superparamagnetic PLGA-iron oxide microcapsules for dual-modality US/MR imaging and high intensity focused US breast cancer ablation,” *Biomaterials*, vol. 33, no. 24, pp. 5854–5864, 2012, doi: 10.1016/j.biomaterials.2012.04.062.
- [14] M. Allahyari, R. Mohabati, A. Vatanara, and M. Golkar, “In-vitro and in-vivo comparison of rSAG1-loaded PLGA prepared by encapsulation and adsorption methods as an efficient vaccine against *Toxoplasma gondii*,” *J. Drug Deliv. Sci. Technol.*, vol. 55, p. 101327, 2020, doi: 10.1016/j.jddst.2019.101327.
- [15] E. M. Elmowafy, M. Tiboni, and M. E. Soliman, *Biocompatibility, biodegradation and biomedical applications of poly(lactic acid)/poly(lactic-co-glycolic acid) micro and nanoparticles*, vol. 49, no. 4. Springer Singapore, 2019.
- [16] C. E. Mora-Huertas, H. Fessi, and A. Elaissari, “Polymer-based nanocapsules for drug delivery,” *Int. J. Pharm.*, vol. 385, no. 1–2, pp. 113–142, 2010, doi: 10.1016/j.ijpharm.2009.10.018.
- [17] C. Wischke and S. P. Schwendeman, “Principles of encapsulating hydrophobic drugs in PLA/PLGA microparticles,” *Int. J. Pharm.*, vol. 364, no. 2, pp. 298–327, 2008, doi: 10.1016/j.ijpharm.2008.04.042.
- [18] S. Ding, C. A. Serra, N. Anton, W. Yu, and T. F. Vandamme, “Production of dry-state ketoprofen-encapsulated PMMA NPs by coupling micromixer-assisted nanoprecipitation and spray drying,” *Int. J. Pharm.*, vol. 558, no. December 2018, pp. 1–8, 2019, doi: 10.1016/j.ijpharm.2018.12.031.
- [19] P. Rafiei and A. Haddadi, “A robust systematic design: Optimization and preparation of polymeric nanoparticles of PLGA for docetaxel intravenous delivery,” *Mater. Sci. Eng. C*, vol. 104, no. November 2018, pp. 1–11, 2019, doi: 10.1016/j.msec.2019.109950.
- [20] Y. Singh *et al.*, “Nanoemulsion: Concepts, development and applications in drug delivery,” *J. Control. Release*, vol. 252, pp. 28–49, 2017, doi: 10.1016/j.jconrel.2017.03.008.
- [21] M. Vauthier, M. Schmutz, and C. A. Serra, “One-step elaboration of Janus polymeric nanoparticles: A comparative study of different emulsification processes,” *Colloids Surfaces A Physicochem. Eng. Asp.*, vol. 626, no. June, p. 127059, 2021, doi: 10.1016/j.colsurfa.2021.127059.

- [22] N. Anton *et al.*, “A new microfluidic setup for precise control of the polymer nanoprecipitation process and lipophilic drug encapsulation,” *Soft Matter*, vol. 8, no. 41, pp. 10628–10635, 2012, doi: 10.1039/c2sm25357g.
- [23] P. Taylor and H. P. Grace, “Dispersion Phenomena in High Viscosity Immiscible Fluid Systems and Application of Static Mixers As Dispersion Dispersion Phenomena in High Viscosity Immiscible Fluid Systems and Application O F Static Mixers As Dispersion Devices in Such Systems,” *Science (80-.)*, vol. 6445, no. 912873516, pp. 37–41, 2009, doi: 10.1080/00986448208911047.
- [24] G. I. Taylor and P. R. S. L. A, “The formation of emulsions in definable fields of flow,” *Proc. R. Soc. London. Ser. A, Contain. Pap. a Math. Phys. Character*, vol. 146, no. 858, pp. 501–523, 1934, doi: 10.1098/rspa.1934.0169.
- [25] K. Y. Hernández-Giottonini *et al.*, “PLGA nanoparticle preparations by emulsification and nanoprecipitation techniques: Effects of formulation parameters,” *RSC Adv.*, vol. 10, no. 8, pp. 4218–4231, 2020, doi: 10.1039/c9ra10857b.
- [26] F. Bally *et al.*, “Improved size-tunable preparation of polymeric nanoparticles by microfluidic nanoprecipitation,” *Polymer (Guildf)*, vol. 53, no. 22, pp. 5045–5051, 2012, doi: 10.1016/j.polymer.2012.08.039.
- [27] W. Tiyaboonchai and N. Limpeanchob, “Formulation and characterization of amphotericin B-chitosan-dextran sulfate nanoparticles,” *Int. J. Pharm.*, vol. 329, no. 1–2, pp. 142–149, 2007, doi: 10.1016/j.ijpharm.2006.08.013.
- [28] Tandiono *et al.*, “Sonochemistry and sonoluminescence in microfluidics,” *Proc. Natl. Acad. Sci. U. S. A.*, vol. 108, no. 15, pp. 5996–5998, 2011, doi: 10.1073/pnas.1019623108.
- [29] F. Sadouki, “Micro-encapsulated poly (vinyl alcohol) nanoparticles for rifampicin delivery to the lungs,” *King’s Coll. London*, 2020.
- [30] W. Yu *et al.*, “Development of an Elongational-Flow Microprocess for the Production of Size-Controlled Nanoemulsions: Application to the Preparation of Monodispersed Polymer Nanoparticles and Composite Polymeric Microparticles,” *Macromol. React. Eng.*, vol. 11, no. 1, pp. 1–10, 2017, doi: 10.1002/mren.201600025.

Chapter 4: One-step elongational-flow synthesis of anisotropic polymeric nanoparticles used as drug carriers

4.1	INTRODUCTION	159
4.2	ELABORATION OF ANISOTROPIC POLYMERIC NANOPARTICLES	160
4.2.1	Influence of the process parameters	161
4.2.2	Influence of the C/D volume ratio and the phase pre-saturation conditions	163
4.2.3	Influence on the polymers' ratio	164
4.3	SINGLE, BLEND AND JANUS STRUCTURES	167
4.3.1	Morphology analysis	167
4.3.2	Solid FTIR characterization of the produced particles	169
4.3.3	Comparison of the PNP's capacity to encapsulate a model drug	171
4.3.4	Drug release from single and anisotropic PNPs	173
4.4	ADDITIONNAL CHARACTERIZATIONS AND CONSIDERATIONS	175
4.4.1	Observations on size and size distribution	175
4.4.2	Some notes to be considered for the next studies	177
4.5	CONCLUSION	178
4.6	BIBLIOGRAPHY	179

Chapter 4

One-step elongational-flow synthesis of anisotropic polymeric nanoparticles used as drug carriers

4.1 INTRODUCTION

Triggered by a continuous dose requirement [1], [2], the pharmaceutical industry requests new drug delivery systems with controlled drug carrier profiles. More recently, assembling different materials having various properties, such as hydrophilicity or a surface charge, raised a lot of interest [3], [4]. Indeed, generating anisotropic (objects having different properties in their composing parts [5]), or Janus-like (two different compositions, shape or morphology) particles give rise to unique properties for applications such as drug co-delivery [6], colloidal surfactants [7], biological sensors [8], and potential Janus PNPs that will be studied [3], [4].

In the literature, several methods were reported for the production of anisotropic polymeric nanoparticles (aPNPs) such as double-emulsion method [9], microfluidic approach [5], [10], masking method [7], self-assembly method [6], and others [11], [12]. However, most of them presented in the literature are multistep (particles' formation followed by surface modification), multiplying risks of contaminations and drug alteration [12]–[14]. For instance, PNPs of below 100 nm consisting of two halves of different polymer compositions made of acrylic acid and styrene monomers are produced *via* emulsion RAFT polymerization [7]. It is first possible to produce aPNPs without using emulsions as Amreen *et al.* demonstrated in 2021 by producing PNPs smaller than 150 nm from poly(lactic-co-glycolic-acid) poly(ethylene glycol) PLGA-b-PEG diblock copolymer [15]. Here, a three-dimensional microfluidic system is employed. A “T” junction is used to nanoprecipitate two different polymers solubilized in a common solvent (acetonitrile) with water. In 2021, Vauthier *et al.* demonstrated the possible way to fabricate Janus PNPs having a chemical anisotropy in a single-step by emulsification-evaporation method [4]. Here, microfluidic-based device was used to produce biodegradable Janus PNPs, of a maximum of 250 nm, with a negative charge on one side poly(styrene sulfonate) and a neutral charge poly(lactic-co-glycolic acid) in another side. [4]. Another team used co-jetting with Taylor cone to produce aPNPs of poly(ethylene oxide) poly(acrylic acid) with Janus structure with a size range of 500-2000 nm [16].

To efficiently produce aPNPs with the previously described elongational-flow reactor and mixer (μ RMX), it was chosen to use polymers with different hydrophobicity (lately allowing the

encapsulation of two drugs in one particle). Moreover, it is demonstrated that poly (styrene sulfonate)-poly (methyl methacrylate) (PSS/PMMA) polymer blends had a highly immiscible character because the chains of different polymers repel each other, while the same polymer chains join together, forming two distinct phases [17]. Thus, these polymers will be used in this work, in addition to the previously used PLGA, to design new aPNPs with specific properties. In a first part, the elaboration of single, blend and Janus PNPs made of PMMA, PLGA and PSS, and their mixtures are developed *via* the microfluidic-assisted emulsification and solvent-evaporation method. Compared to previous works done with polymeric NPs [14], [18], [19], here the continuous phase pre-saturation method is applied to fabricate blend and Janus PNPs. This improves the control over PNPs' diameter and size distribution and reduces drug diffusion before the drug release starts, which is also mentioned in the previous chapter. The fabricated PNPs/aPNPs are compared by encapsulating a model drug (rifampicin) in a one-step process to later study their drug release profile.

4.2 ELABORATION OF ANISOTROPIC POLYMERIC NANOPARTICLES

Following the previously produced PLGA NPs by using the solvent pre-saturation approach, here, both single PNPs and aPNPs were fabricated with the elongational-flow reactor and mixer to achieve different PNPs' compositions and morphologies.

The continuous phase was composed of 1.5 w/v Pluronic® F127 in water and the dispersed phase was composed of 1% w/v polymer solution in ethyl acetate. Then, the dispersed solvent was evaporated at 20°C within 24 hours to yield PNPs. This procedure, illustrated in Figure 4.1, was maintained for the elaboration of all the PNPs in this part.

The effect of process parameters (emulsification time and mixing parameter) and material parameters (continuous to disperse phase C/D volume ratio, polymers ratio) on the PNPs' diameter and size distribution were assessed. The varied parameters of the μ RMX are given in Table 4.1.

Table 4.1. Parameters used to produce PNPs.

Emulsification times (min)	Flow rate (mL/min)	C/D volume ratios	Ratios between polymers (w/w)	Microchannel size (μ m)
20 to 100 [†]	10 to 50	60/40 and 85/15	85/15 to 15/85	150 to 750

[†]60 min corresponds to 150 cycles

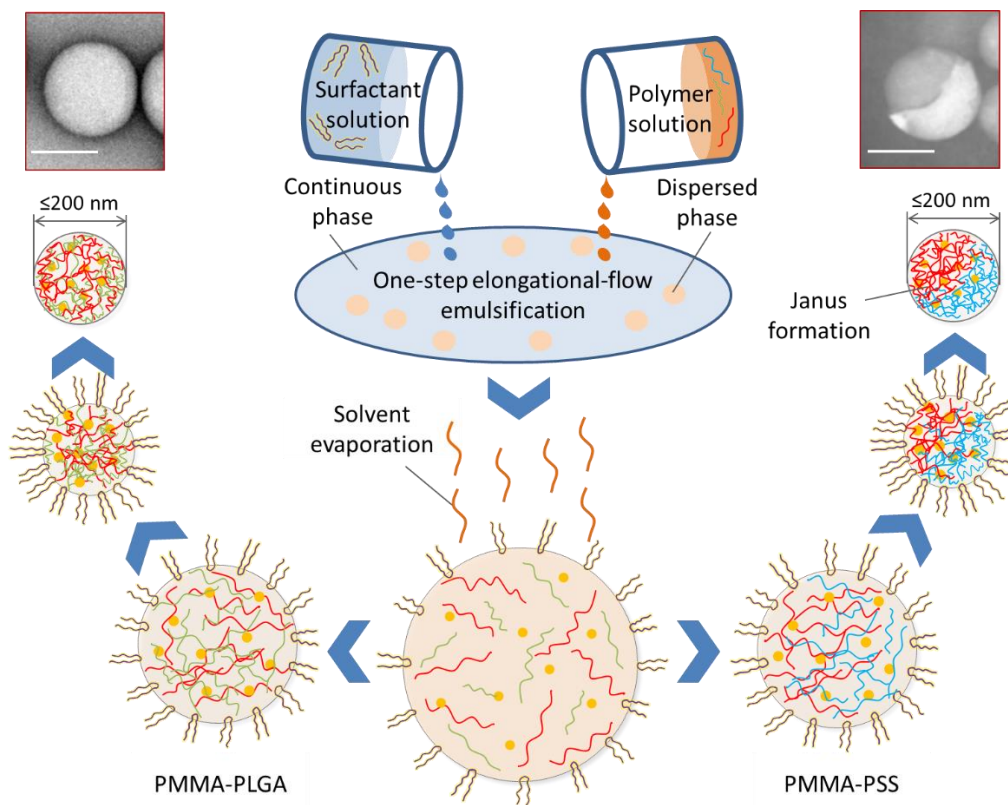


Figure 4.1. Schematic representation of PMMA-PLGA (polymer blend) and PMMA-PSS (Janus) NP formation through the one-step elongational-flow emulsification-evaporation method.

4.2.1 Influence of the process parameters

In this part, the results of the influence of the above process parameters (Table 4.1) were described. In the elaboration, PMMA-PLGA blend was used to produce PNPs. The size and monomodality of PMMA-PLGA NPs depending on operating parameters were reported in Figure 4.2 and 4.3.

PMMA-PLGA NPs' size and size distribution were directly controlled with the process parameters of the μ RMX. After a longer emulsification time (after 150 cycles) at 30 mL/min, a near plateau value was obtained at 110 nm, PDI = 0.13 (Figure 4.2.a). The flow rate itself also affected the PNP size, thus at above 20 mL/min, the final PNPs started showing the size below 200 nm, PDI \leq 0.2, and a plateau value was reached above 30 mL/min (Figure 4.2.b). Additionally, the microchannel's diameter allowed to achieve monomodal PNPs ($0.2 >$ PDI) with a highly controlled particle size (Figure 4.2.c) ranging from 110 nm (150 μ m) to 207 nm (750 μ m). Here, 150 cycles, 30 mL/min, and 150 μ m were optimum operating parameters to achieve the minimum PNP size (110 nm) and size distribution (PDI = 0.13) with the elongational-flow reactor and micromixer. The given trends of PMMA-PLGA NPs were following the results from the previously studied single PLGA NPs (See Figure 3.2.a-c), at higher elongational strain the smaller PNPs were achieved, and then the plateau value was reached.

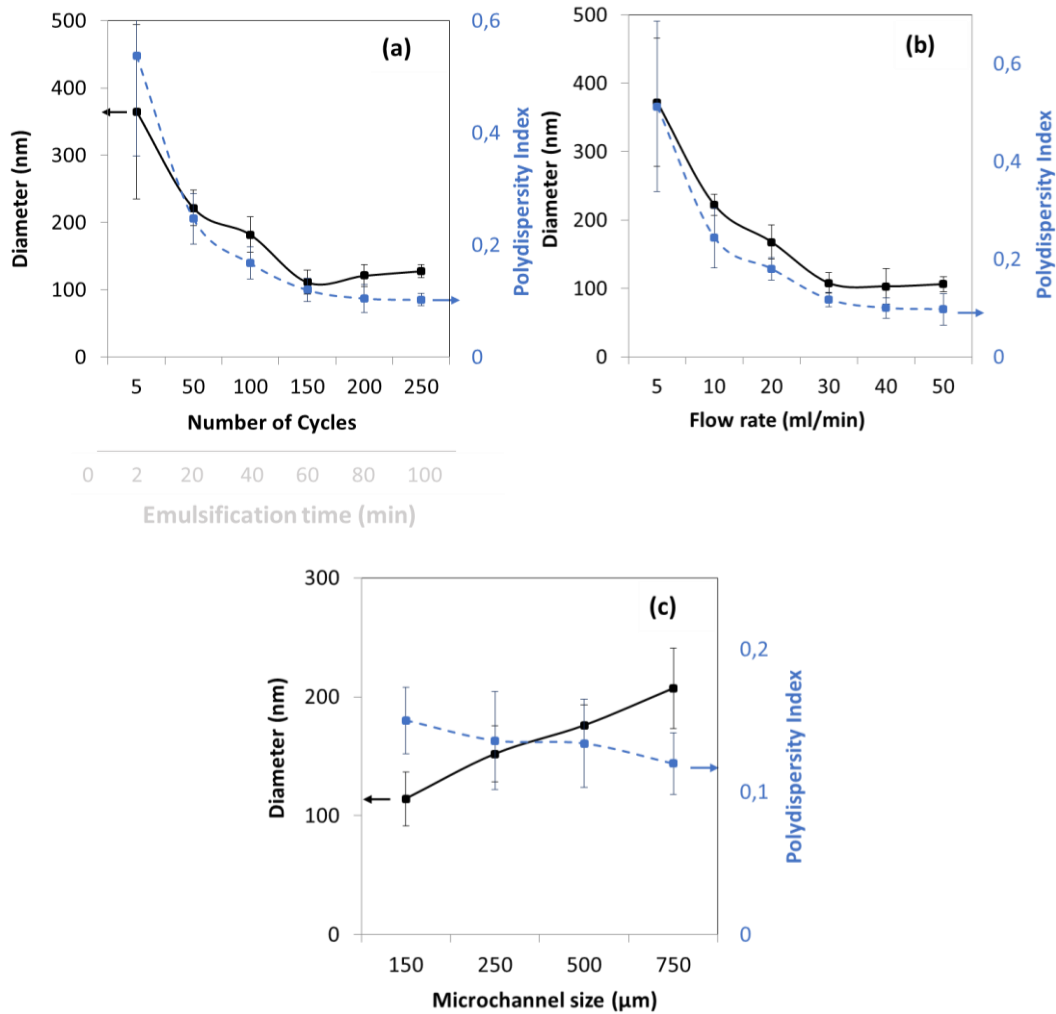


Figure 4.2. Evolution of PMMA-PLGA (50:50) nanoparticles' size and size distribution at different (a) number of cycles (30 mL/min, microchannel of 150 μm), (b) flow rates (150 cycles, microchannel of 150 μm) and (c) microchannel's diameter (30 mL/min, 150 cycles) produced with elongational-flow micromixer at 60/40 volume ratios.

Finally, the process parameters of the elongational-flow reactor and micromixer allowed the optimization PMMA-PLGA NPs' size and PDI value. The optimal process parameters used in the following parts are given in Table 4.2.

Table 4.2. Optimal process parameters used to produce aPNPs with the μRMX.

Emulsification time (min)	Flow rate (mL/min)	Microchannel size (μm)
60	30	250

In this part, the continuous to dispersed C/D volume ratio was kept constant and equal to 60/40, and the polymer's weight ratio was kept equal to 50/50 w/w to achieve the μRMX optimum process

parameters. In the next part, C/D ratios, and polymer weight ratios were elaborated to later study PNPs' cargo properties.

4.2.2 Influence of the C/D volume ratio and the phase pre-saturation conditions

In this part, it was possible to further reduce PNPs' size by varying the C/D volume ratio, and using a pre-saturated continuous phase (See chapter 2.4.1), where 8.7% ethyl-acetate was dissolved into the water before the emulsification. Since the trendline (lower size at higher elongational strain) is the same for single PNPs, PMMA-PLGA, PMMA-PSS, and PLGA-PSS NPs, only the graphs obtained for PMMA-PLGA, and single PNPs were given in Figure 4.3.

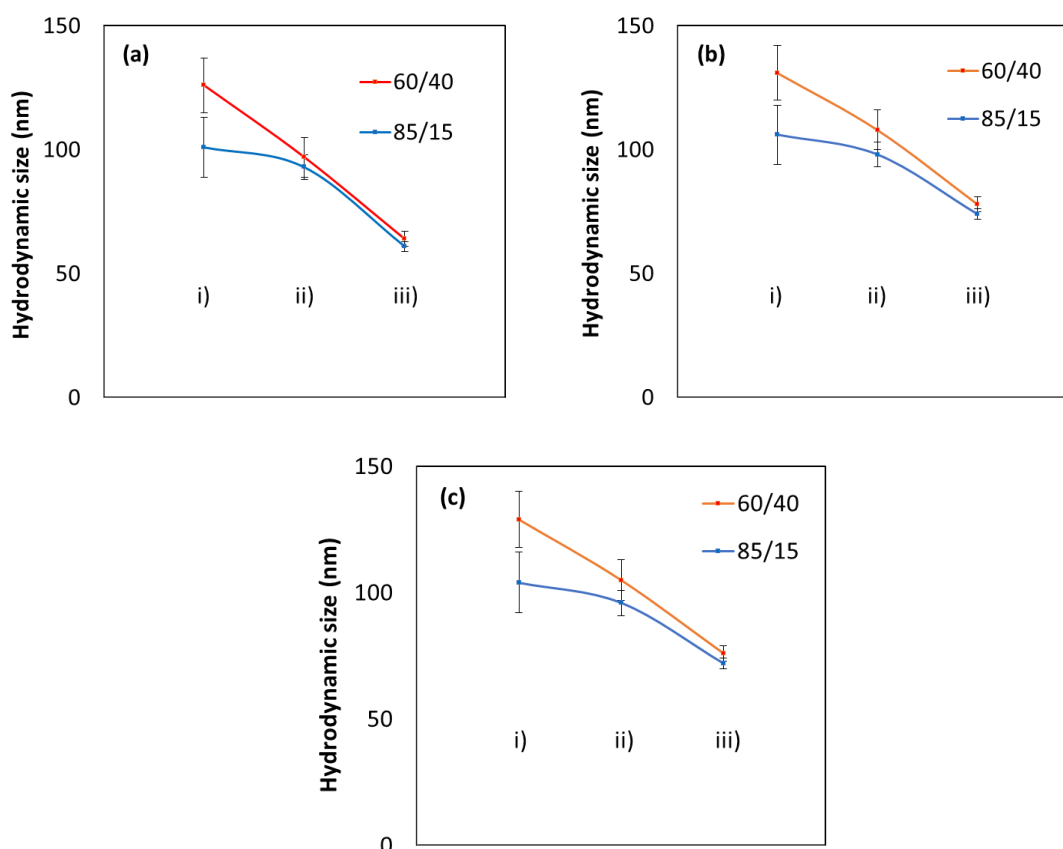


Figure 4.3. DLS average size results of (a) single PLGA, (b) PMMA and (c) blend PMMA-PLGA NPs produced at various C/D volume ratios with the elongational-flow micromixer (30 mL/min, 150 cycles, microchannel of 150 μm). Different pre-process conditions were used to compare size differences i) traditional, ii) pre-saturated solvent condition, and iii) drug-loaded and pre-saturated condition. The third condition was added since the addition of the drug (rifampicin) also reduced the size in previous parts (see 3.3.3).

All three PLGA, PMMA, and PMMA-PLGA NPs showed a similar trend of size decrease when the C/D ratio increased from 60/40 to 85/15. All results were coherent with previous studies (see chapter

3.2) demonstrating that decreasing the polymer concentration, *i.e.* increasing the C/D volume ratio, decreased the system's viscosity, leading to the production of smaller particles. Additionally, changing the pre-process condition also reduced the PNP size. The minimum PMMA-PLGA NPs' size achieved was 110 nm (PDI = 0.13) with phase pre-saturation conditions, which reduced the PNPs' size by more than 10%, compared to the first, traditional condition (Figure 4.3). Another important novelty was that at phase pre-saturation conditions C/D volume ratio was less effective as size reduction decreased from more than 15% (from 129 nm to 105 nm) to 6% (from 104 nm to 98 nm). This was induced by the reduced ethyl-acetate diffusion into the water at pre-saturation condition. When water phase was pre-saturated, no ethyl-acetate diffusion took place, however, in traditional condition, during the emulsification a self-saturation took place, which eventually altered the original C/D ratio. For example, at the C/D ratio of 85/15 in traditional condition, reaching 8.7% v/v saturation point for water, increasing the original C/D ratio resulted in lower dispersed phase volume left, which reduced the PNP size in the end. However, at a 60/40 ratio water phase self-saturated by using less amount of ethyl-acetate, that altered the C/D ratio too, but comparatively less than in 85/15 emulsions.

The third condition was studied on the basis of results reported in chapter 3.3.3, where a drug (rifampicin) addition reduced the PNP size by reducing the interfacial tension. It was interesting since here the same trend was also observed with PMMA and PMMA-PLGA NPs. The third, drug-loaded and pre-saturated condition (Figure 4.3) reduced the PNP size by around 20%. PNPs' size reached values below 85 nm for both 85/15 and 60/40 C/D volume ratios. PDI values of PNPs remained similar and below 0.2 in all three compositions and three conditions. This was due to the intermolecular interactions and rifampicin acting as a surfactant according to the interfacial tension results of ethyl acetate and water phases (Chapter 3, Figure 3.11). Rifampicin reduced the interfacial tension up to 10% after a certain period.

Overall, following the C/D volume ratio optimization, the ratio of 60/40 allowed for achieving an optimum PNPs' size when the pre-saturation condition was maintained. Thus, it allowed producing twice more (mg) PNPs in a 60/40 ratio than in an 85/15 ratio, due to the higher volume of polymer solution in the emulsion, which was important to consider in the next studies.

4.2.3 Influence on the polymers' ratio

In the previous sections, we optimized the process parameters like the number of cycles, and flow rates (Table 4.2) as well as the pre-process conditions like phase pre-saturation, and C/D volume ratio (Figure 4.3). Now, we investigate the effect, on PNPs' size and size distribution, of the two

polymer weight ratio for PMMA-PSS (Figure 4.4), and PLGA-PSS (Figure 4.5) systems while keeping the overall polymer concentration constant at 1% w/v in ethyl acetate.

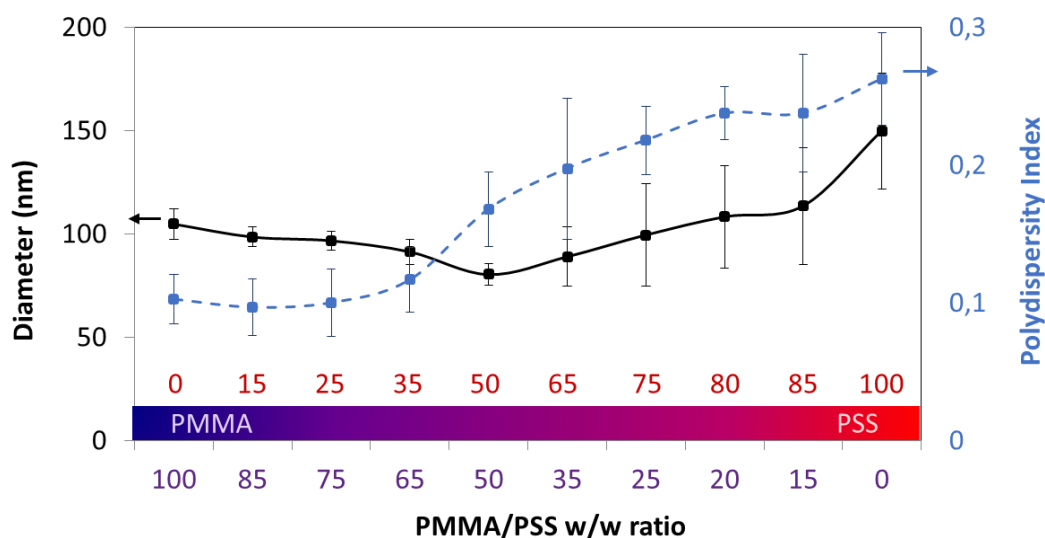


Figure 4.4. Evolution of the PMMA-PSS NPs' size and size distribution at various polymer (PMMA or PSS) mass relative percentages. PMMA-PSS NPs were produced at C/D volume ratios of 60/40, (150 cycles, 30 mL/min, microchannel size 150 μ m).

In Figure 4.4, the PMMA-PSS size ranged from 80 nm to 150 nm, and the PDI value was obtained between 0.1 and 0.3, depending on PMMA mass relative percentage (0 to 100%) PSS and PMMA were showing different solubilities in ethyl acetate. Considering the poorly soluble nature of PSS in ethyl acetate, when PMMA volume was reduced, insufficient polymer molecules were maybe present to maintain polymers' self-assembly. This may explain why PNPs' size decreased as a function of PMMA weight content in ethyl acetate, this incomplete polymer self-assembly maybe led to wider size distribution and size fluctuations (Figure 4.4). After reaching a minimum PMMA concentration the PMMA-PSS NPs became larger and non-controlled in size.

This phenomenon was observed similarly in PLGA-PSS NPs: lower PLGA/PSS mass ratio decreased the overall concentration, thus reduced aPNPs' size (Figure 4.5).

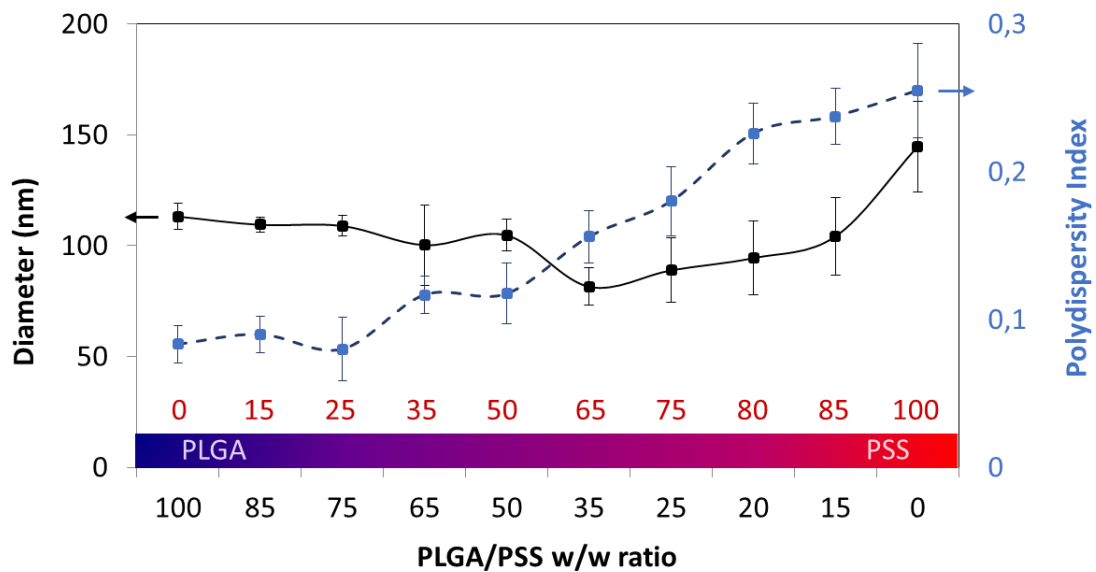


Figure 4.5. Evolution of the PLGA-PSS NPs' size and size distribution at various (PLGA or PSS) mass relative percentages. PLGA-PSS NPs were produced at C/D volume ratios of 60/40, (150 cycles, 30 mL/min).

After reaching 50% w/w PSS mass ratio, PLGA-PSS aPNPs' size sharply decreased from 110 nm to 85 nm, however, PDI value increased (Figure 4.5). The aPNP's size and monomodality at 50/50 PLGA-PSS ratio were coherent with the values reported in a recent study of our group [10].

It's worth mentioning that, in this part PMMA-PLGA blend NPs were not presented, since PMMA-PLGA blend NPs showed a similar PNP's size at (100 ± 5 nm) at all polymer ratios. This plateau value was due to the highly soluble nature of both PLGA and PMMA polymers in ethyl-acetate. However, PSS was poorly soluble in the same solvent, leading to overall polymer concentration change.

The optimal parameters for process and pre-process are thus summarized in Table 4.3.

Table 4.3. Optimal parameters are used to produce further PNPs, with the pre-saturation method.

Emulsification time (min)	Flow rate (mL/min)	C/D volume ratio	Ratios between polymers (w/w)	Microchannel size (µm)
60	30	60/40	65:35	250

4.3 SINGLE, BLEND AND JANUS STRUCTURES

4.3.1 Morphology analysis

Following the process and pre-process optimization, the morphology of the produced aPNPs were analyzed with various microscopy techniques: TEM, SEM, and AFM. Following the emulsification with the μ RMX (conditions in Table 4.3), PNPs were centrifuged at 9500 rpm for 20 minutes to reduce the surfactant concentration to limit the observation of surfactant micelles (< 15 nm) disturbing the observations in TEM characterization. Then, all the PNPs were first morphologically characterized with TEM (Figure 4.6)

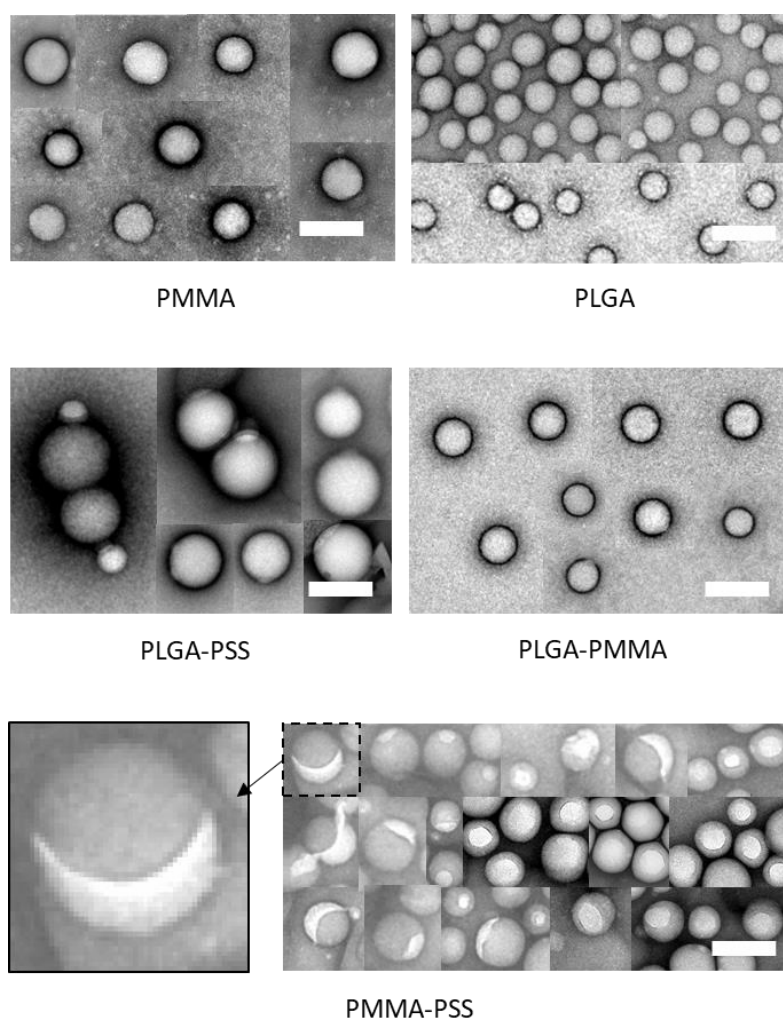


Figure 4.6. TEM images showing the evolution of the surface morphology of PNPs made of different polymeric nanoparticles produced with the μ RMX (150 cycles, 30 mL/min flow rate, 250 μ m micromixer size). The scale bars represent 200 nm.

In Figure 4.6, the single PMMA and PLGA NPs were found in 110 and 97 nm respectively with similar spherical shapes. Comparing all the PNPs, at operating parameters given in Table 4.3, the smallest size was observed in PLGA NPs among all the images, which was coherent with DLS results, and

previous results (see 3.2.1). Since PLGA and PMMA were both neutral polymers with approximately the same hydrophobicity, it was not surprising to not see any anisotropy with the PLGA-PMMA particles: both polymers were mixed in the particles without clear phase separation. Then, PLGA-PSS aPNPs were studied and appeared in the Janus form: two polymers with different natures appeared, where the PSS part was much smaller compared to the PLGA one, demonstrated in a previous study [10].

Finally, PMMA-PSS aPNPs appeared in the form of Janus with two different polymers co-existing in a single body. This anisotropy was due to the immiscible nature of PSS and PMMA, which induced the polymer separation inside the emulsion droplet during the organic solvent evaporation.

It becomes thus interesting to understand the properties of the Janus PMMA-PSS aPNPs' surface and to determine what the polymer composing the brighter part (Figure 4.6. PMMA-PSS). To do so, several rinsing steps with water were carried out on the aforementioned Janus PNPs to reduce the number of surfactant molecules surrounding the particles.

TEM images showed the reduction on the brighter side of the Janus PMMA-PSS aPNPs (Figure 4.7), proving the importance of surfactant and that the brighter side is composed of PSS.

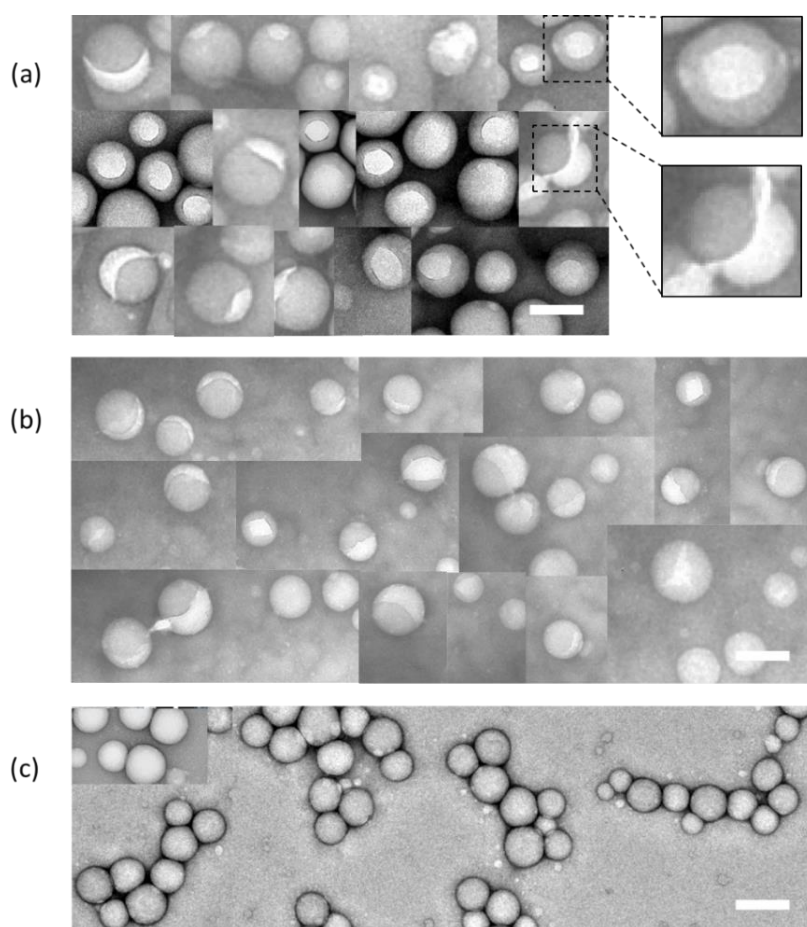


Figure 4.7. Evolution of the surface morphology of PMMA-PSS aPNPs after (a) a single wash, (b) three washing steps and (c) five washes in raw.

In the first image, a single “wash” limited the surfactant molecules to form large micelles, and allowed us to view Janus PNPs (Figure 4.7.a). For the second image, the similarly produced Janus PNPs were centrifuged and washed three times to reduce the surfactant concentration, however, it was believed that this washing did not fully eliminate the surfactant from the system. Here, Janus PNPs can be found less covered with PSS (Figure 4.7.b), due to its migration to the water phase, and leaving larger PNP surface uncovered. In the last stage, the produced Janus PNPs were washed five times to fully eliminate the surfactant molecules, where PSS fully migrated to the water phase taking away the anisotropy properties of the initial material, and leaving a single PMMA NP (Figure 4.7.c). The average surface area of the produced PNPs was measured considering 100 PMMA-PSS aPNPs, and found to be approximately $0.1 \mu\text{m}^2$. Approximately $0.015 \mu\text{m}^2$ of each aPNPs’ surface was found covered with PSS molecules at initial state (Figure 4.7.a), *i.e.* 15% of the average surface area of single aPNP. Following the rinsing process, the covered surface area was reduced to less than 10% (Figure 4.7.b), which was more than 5% “washed” surface. In the last state, all the surfaces can be found uncovered (Figure 4.7.c).

Overall, this experimental part allowed us to distinguish the two polymers, and to verify the anisotropy property of the neutral/charged particles. It was also possible to verify that the bright side of polymer was PSS, due to its hydrophilic nature. In the next part FTIR technique was used to verify the chemical composition of all the produced PNPs and aPNPs.

4.3.2 Solid FTIR characterization of the produced particles

To understand the chemical composition of each product, a solid powder form of the pure polymers PNPs/aPNPs were achieved with two-step centrifugation and freeze-drying. Then, these PNP powders were characterized with the FTIR spectroscopy, and the results were described in the next figure (Figure 4.8). Here, all the PNPs showed high absorbance in the G-I ($1000\text{-}1200 \text{ cm}^{-1}$) region representing C-O stretching. PSS showed another high absorbance in J ($600\text{-}800 \text{ cm}^{-1}$) region, which was not the case in other PNPs, and this can be found in binary-blends containing PSS.

The region E-F ($1300\text{-}1500 \text{ cm}^{-1}$) was observed in all the samples, slightly more intense absorbance can be found in PMMA NPs, and a wide region can be observed in PLGA NPs representing C-H bending. This was the least absorbance region for PSS sample.

The second highly intense absorbance was observed in C-D ($1700\text{-}1750 \text{ cm}^{-1}$) region representing C=O stretching, especially D (1722 cm^{-1}) for PMMA, and C (1752 cm^{-1}) for PLGA NPs. This region was wider representing both absorbance points when a blend PMMA-PLGA NPs were measured. In this region PSS did not absorb the IR light, which explains absence of C=O functional groups in PSS

molecule, however, it absorbed A (3300-3500 cm^{-1}) region representing O-H groups. This region was observed in all other PNPs containing PSS.

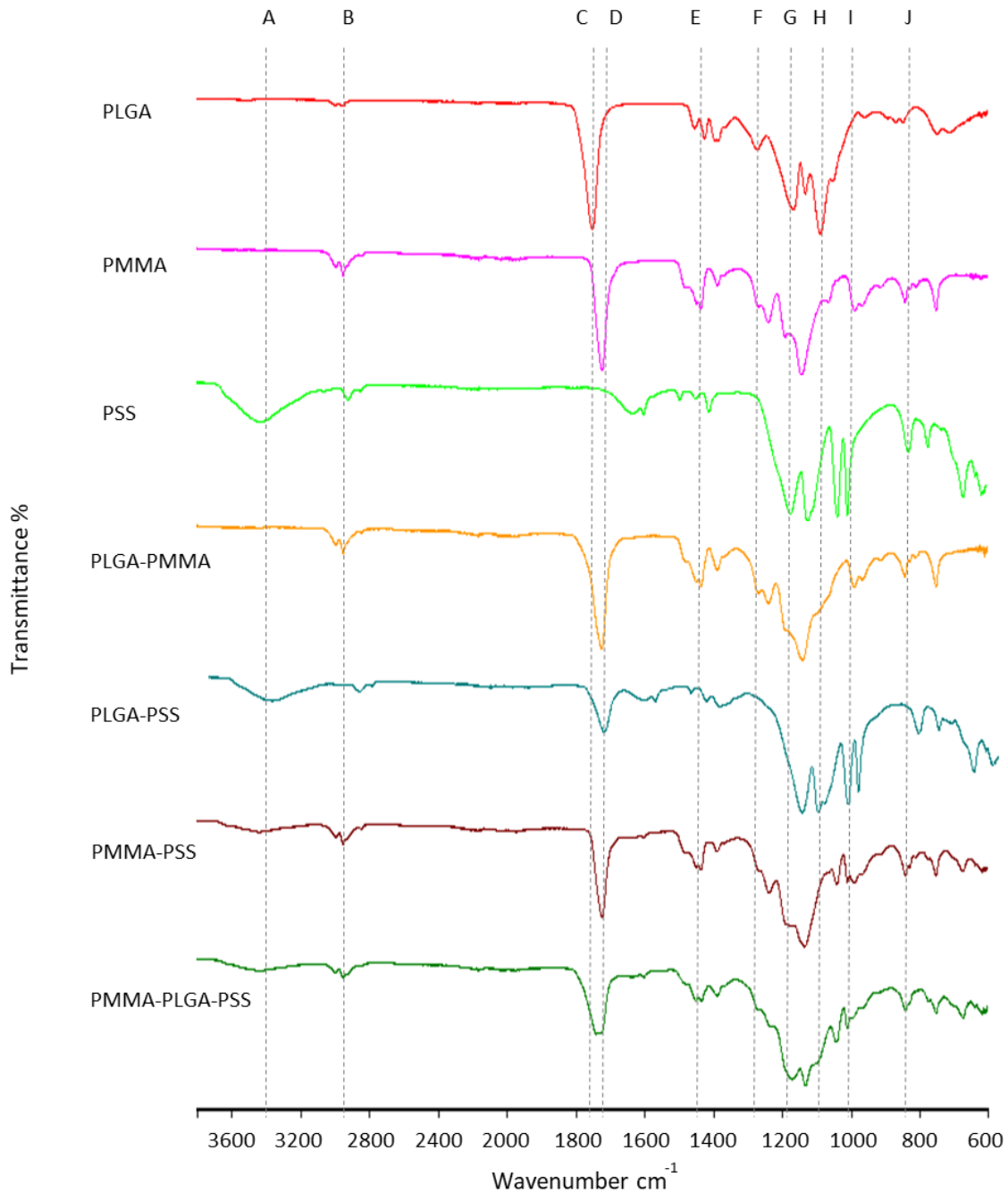


Figure 4.8. FTIR spectra of the different produced polymeric nanoparticles.

Moreover, in all samples a weak (2900-3000 cm^{-1} , B) absorbance can be observed representing -CH stretching. This analysis was helpful to understand the presence of polymers in PNP blends according to the representing functional groups of each polymer. This analysis also verifies no significant chemical shifts took place while mixing two or more different polymers. It should also be noted that the solid FTIR analysis method that was used in this study to measure IR absorbance at the surface of

a given matrix. In this case, the anisotropic PNPs could absorb two different IR regions at once. However, this would not be the case for isotropic PNPs or DNPs.

4.3.3 Comparison of the PNP's capacity to encapsulate a model drug

Produced PNPs were studied according to their capacity to encapsulate a model drug (rifampicin). As it was previously demonstrated that 5% w/w initial drug load was the optimal concentration to work with, this amount was kept constant here. For the same reason, the pre-saturation method was applied. To study encapsulation efficiency (EE) of the PNPs, the calibration curve established in chapter 3 (Figure 3.8) was used.

In the following study, the drug-loaded samples of PMMA, PLGA, PMMA-PLGA, and PMMA-PSS particles are referred as P1, P2, P3 and P4 (Table 4.4) respectively.

Table 4.4 Drug loading (DL), encapsulation efficiency (EE) and the average size for different drug-loaded particles.

Sample name	Chemical composition	Initial drug weight content with respect to polymer (w/w)	DL (%)	EE (%)	Encapsulated Drug (μg)	Average Size of DNPs
P1	PMMA	5%	4.3 ± 0.3	36 ± 4	364 ± 25	104 ± 8
P2	PLGA	5%	4.5 ± 0.5	40 ± 3	395 ± 19	69 ± 2
P3	PMMA-PLGA	5%	4.5 ± 0.6	37 ± 5	367 ± 22	91 ± 4
P4	PMMA-PSS	5%	4.2 ± 0.5	33 ± 4	333 ± 33	110 ± 15

Similar to the previous chapter, with the single PLGA DNPs, here all the drug-loaded PNPs showed a considerable decrease of the average size, from 125 nm to 110 nm for PMMA-PSS for instance.

At 5% initial drug load of rifampicin, the highest drug load (DL), and the highest EE was achieved with P2. It was possible to reach the highest encapsulated rifampicin quantity of 0.39 mg inside 69 nm PLGA DNPs at 4.5% w/w DL. This value was 30 μg lower with the sample P1, where 0.36 mg rifampicin out of 1 mg initial drug load was left inside 104 nm polymer matrix. The P3 DNPs showed a similar DL and EE with 0.37 mg, and the average size was smaller than the size of P1. The minimum DL, and EE was achieved with P4, where 333 μg drug was encapsulated inside the polymer matrix.

This difference under the same process parameters, pre-process conditions, and same initial drug load was due to the nature of polymers used. It's believed that, higher EE achieved with P2 was due

to the polymer MW (64,000 g/mol) that was lower than the other polymers (PMMA Mw = 120,000 g/mol, PSS Mw = 70,000 g/mol), and smaller molecules were more probable to entrap the drug molecules while polymer self-assembly.

The length of the polymer molecules affects the number of molecules build per PNP, thus, at higher Mw, 1% w/v polymer solution contained a smaller number of polymer molecules. This can be imagined as constructing a house with the largest building materials which are limited in numbers (due to limited total mass). Thus, the house becomes larger and large gaps can be found similar to PNPs self-assembled with large polymer molecules, where bigger pores can be expected. These pores act as a channel for drug molecules to pass through to leave the PNP matrix, however, when polymer Mw is lower, these channels become narrower, and a higher number of polymer molecules isolate this drug molecules until the solvent fully evaporated. There are also intermolecular interactions which are dependent on other polymer physico-chemical parameters like hydrophobicity, chemical affinity, dipole moment, etc.

Considering theoretically large pores of PMMA DNPs, it was interesting to understand the DNPs' purity after encapsulation, and before the release studies, since there could be possibility that drug molecules escape the DNP matrix. In order to verify, the DNPs were isolated from the impurities like surfactant, non-encapsulated drug molecules, and the solvent, FTIR analysis were carried out (Figure 4.9).

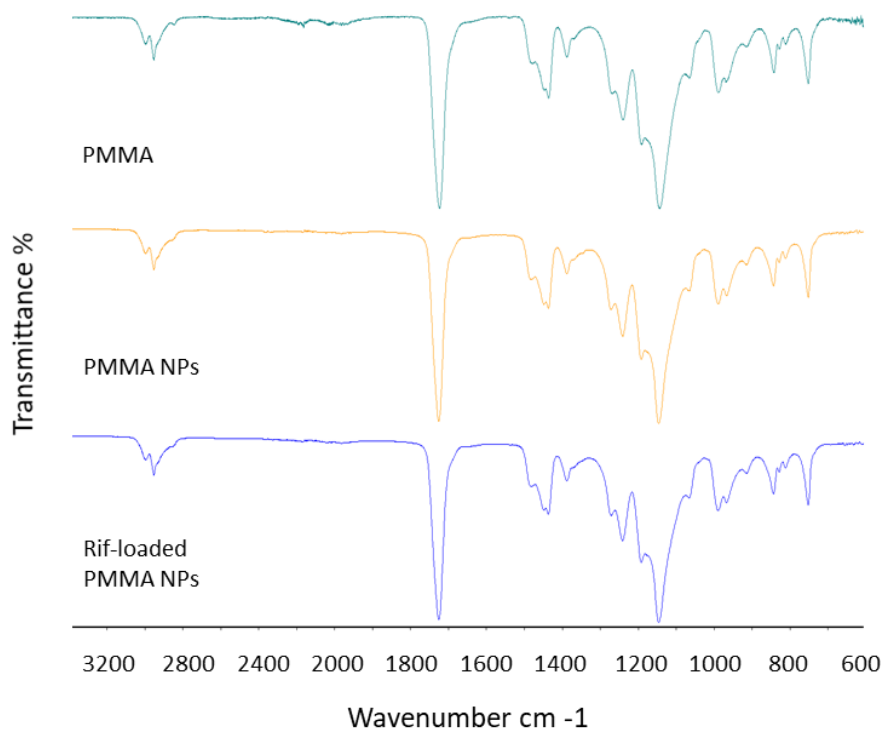


Figure 4.9. FTIR spectra of PMMA, PMMA NPs and rifampicin-loaded PMMA PNPs.

In Figure 4.9, the three FTIR spectra were similar, which means the impurities were successfully eliminated from all the samples following the drug encapsulation. Following the encapsulation and the sample purification, all the samples were ready to be studied for their drug release profiles.

4.3.4 Drug release from single and anisotropic PNPs

Following the drug encapsulation, and isolation of the impurities from P1 to P4, their drug release profile was studied in a 7.4 pH-controlled buffer solution at 37°C. The cumulative amount of drug (μg) released from P1-P4 under sink conditions was determined by UV-visible spectroscopy at 332 nm by considering the rifampicin possible degradation (Equation 2.20). Drug release kinetics for P1, P2, P3, P4 samples are given in both quantitative (μg) (Figure 4.10) and percentage values (Figure 4.11).

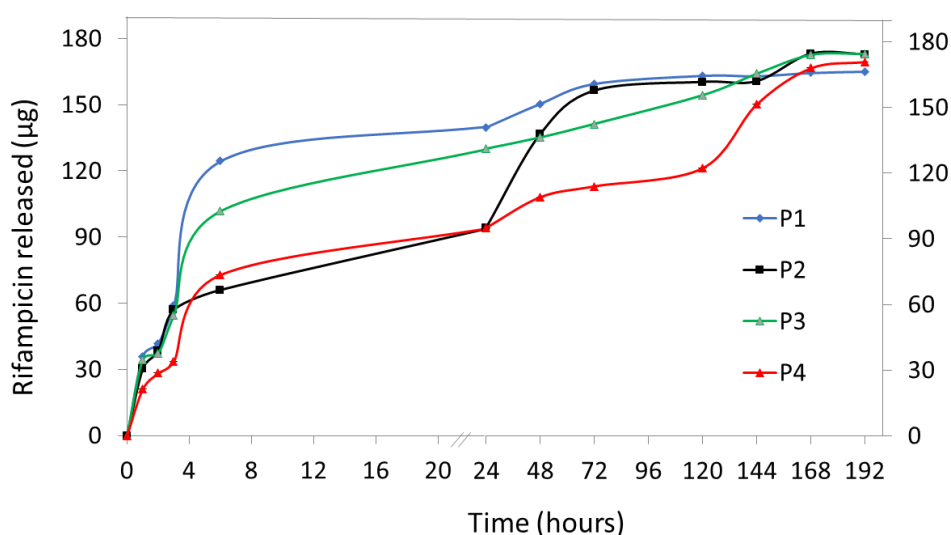


Figure 4.10. In-vitro drug release profiles (μg) from PNPs of (P1) PMMA, (P2) PLGA, (P3) PMMA-PLGA, and (P4) PMMA-PSS at 5% w/w rifampicin/polymer weight content.

In general, all the four samples demonstrated similar final released drug quantities of around $170 \pm 10 \mu\text{g}$ (47 % of $365 \mu\text{g}$ encapsulated rifampicin) within 8 days, proving the cumulative drug release over time. It can be observed that, at the first 3 hours, the burst releases of P1, P2, and P3 ($57 \pm 2 \mu\text{g}$) were more than 50% higher than the drug release of P4 ($34 \mu\text{g}$). This was described in the following part (Figure 4.11).

Moreover, the drug quantity released in 8 days was $167 \pm 12 \mu\text{g}$ (46%), $175 \pm 11 \mu\text{g}$ (45%), $175 \mu\text{g} \pm 9 \mu\text{g}$ (48%) and $171 \mu\text{g} \pm 19 \mu\text{g}$ (51%) for P1, P2, P3 and P4 respectively.

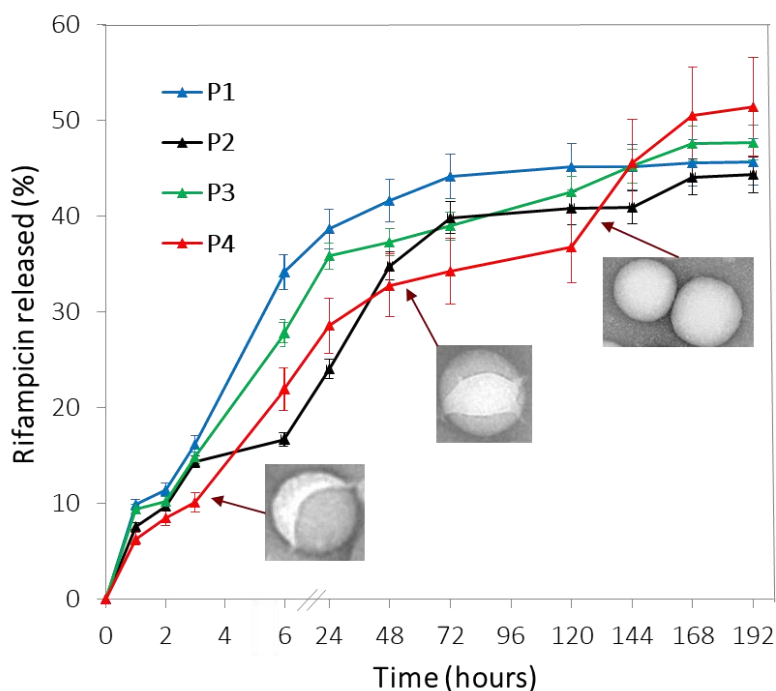


Figure 4.11. In-vitro drug release profiles (%) from PNPs of PMMA (P1), PLGA (P2), PMMA-PLGA (P3), and PMMA-PSS (P4) at 5% w/w rifampicin/polymer weight content.

In general, it can be mentioned that, all the samples experienced their major release within the first 48 hours period. At 48 hours, rifampicin release was 39%, 36%, 29%, and 24% for P1, P2, P3, and P4 respectively. Then, the release kinetics decelerated till the 6th day, and another active 48 hours of release plateau can be observed on the last day. This phenomenon was explained in our previous study (see chapter 3.4), where the drug encapsulated near DNPs center started to diffuse into water after reaching DNPs' surface. Here, comparatively low Mw (64,000 g/mol) PLGA (P2) didn't allow rifampicin to completely freely diffuse through the closely packed molecules, and the percentage value of drug release was low. However, P1 DNPs released faster due to its larger Mw (110,000 g/mol). This indicates that the polymer type and their Mw are affecting the drug release kinetics. Released rifampicin from P3, 174 μg (48%) can be considered more controlled, this can be related to its property based on two different polymer properties. Theoretically, fast diffusion was eliminated by smaller PLGA molecules filling the large channels formed between PMMA molecules. This was one example of how blend DNPs can improve drug release. The fourth and the main sample P4, Janus PMMA-PSS DNPs released the maximum percentage amount of drug 171 μg (51%) compared to other DNPs. This could be explained by first, large channels allowing faster diffusion through PMMA molecules, that was observed in single PMMA DNPs, and the second, PSS on DNP surface isolating these channels limiting their direct diffusion. The given image (Figure 4.11) of PMMA-PSS Janus NPs show how PSS covers the particles' surface. In short, rifampicin molecules accumulated between PSS layer and PMMA channels. It was described that, PSS gradually dissolves into water (Figure 4.7), by

leaving more PMMA surface, thus more drug molecules to diffuse. Overall, PNPs' nature, and structure can be considered to reach an improved release control, thus to adapt drug delivery systems to various release doses.

4.4 ADDITIONNAL CHARACTERIZATIONS AND CONSIDERATIONS

4.4.1 Observations on size and size distribution

PNP size and size distribution were additionally characterized by using several techniques to confirm some results of DLS (Figure 4.2), TEM (Figure 4.6) in this chapter. These were AFM (Figure 4.12), TEM (4.11), and SEM (Figure 4.14) techniques to observe some of fabricated PNPs. Both results were coherent when compared. AFM images were captured as was explained in the chapter 2.3.2.3.

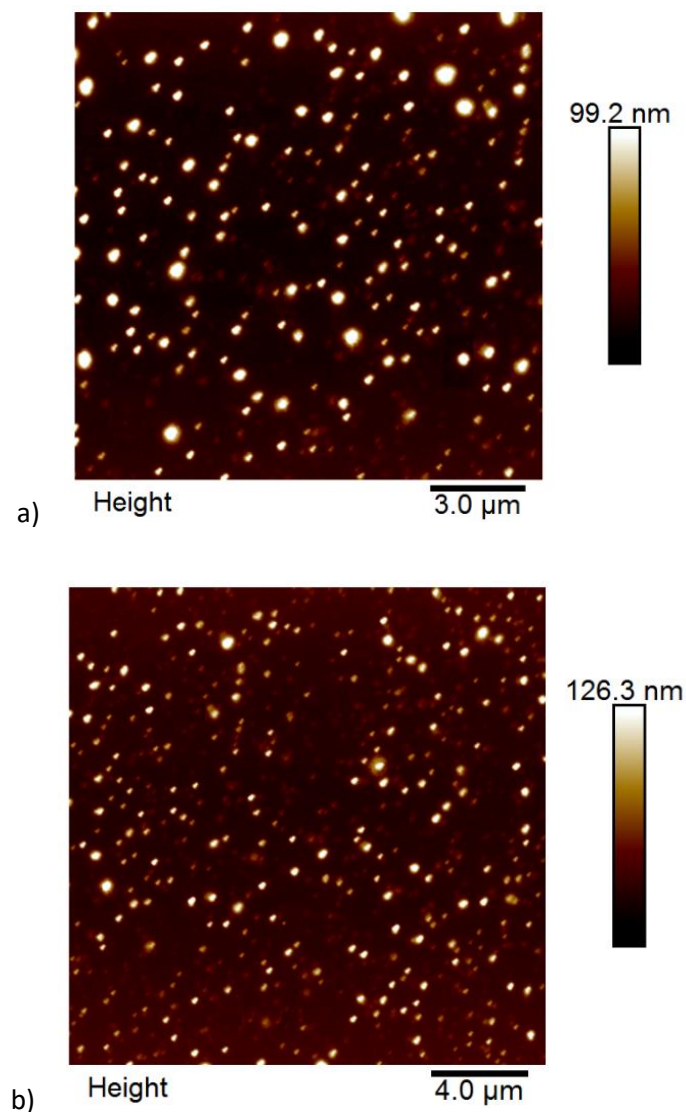


Figure 4.12. AFM images of a) PLGA-PSS (average of below 200 nm), and b) PMMA-PSS NPs (150 nm).

It can be observed that, both a) PLGA-PSS and b) PMMA-PSS aPNPs were below 200 nm. This was coherent with DLS result of aPNPs produced at similar process conditions. However, it should be noted that, preparation of sample for AFM characterization was different, and more complex than the sample for DLS characterization, since for AFM imaging, aPNPs had to be first deposited on surface modified silicon wafer by using spin coating technique to achieve a sufficient distribution of aPNPs. This could lead to loss of some aPNPs. Additionally, AFM technique revealed only aPNP size and size distribution, but not the particles' anisotropic property, considering the spherical shape of the produced PMMA-PSS aPNPs.

Then, to confirm again the size and size distribution of PNPs, TEM (Figure 4.12), and SEM (Figure 4.13) images were analyzed on the basis of measuring 500 PNP diameters. This once more confirmed all the produced PNPs being monomodal with average size below 200 nm.

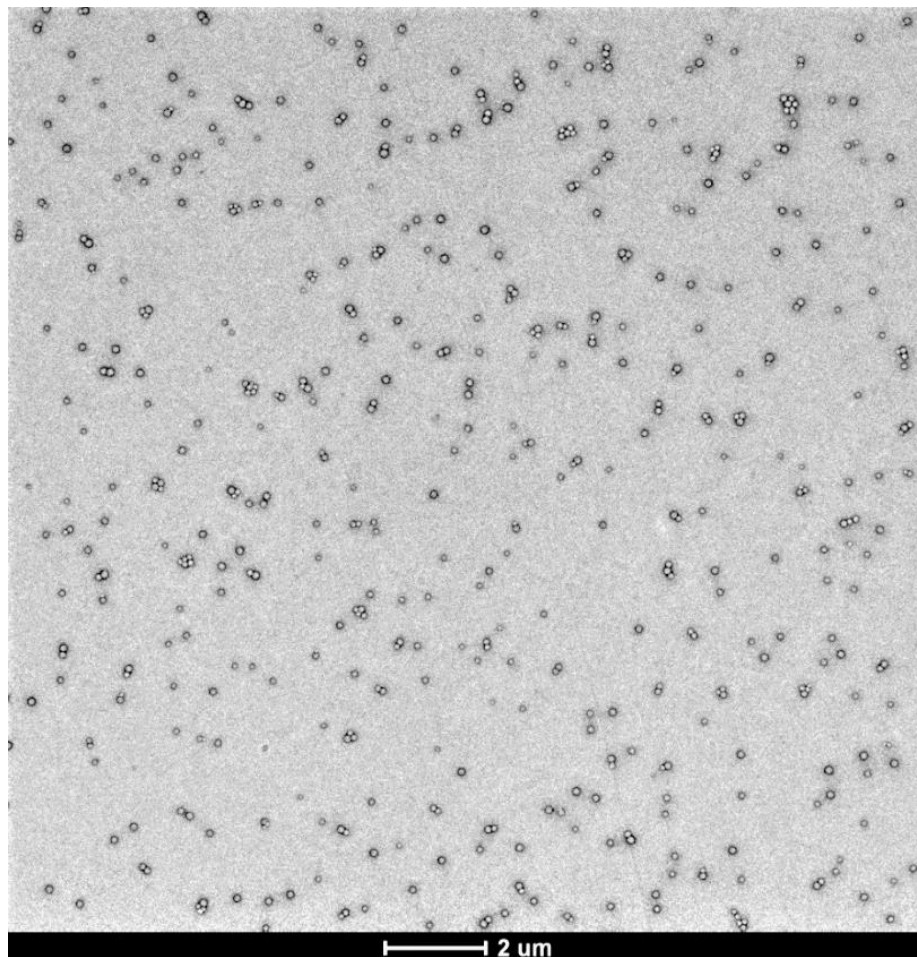


Figure 4.13. TEM image of PMMA-PLGA blend PNPs produced at 150 cycles, 30 mL/min having 100 nm diameter size and narrow size distribution (PDI = 0,1).

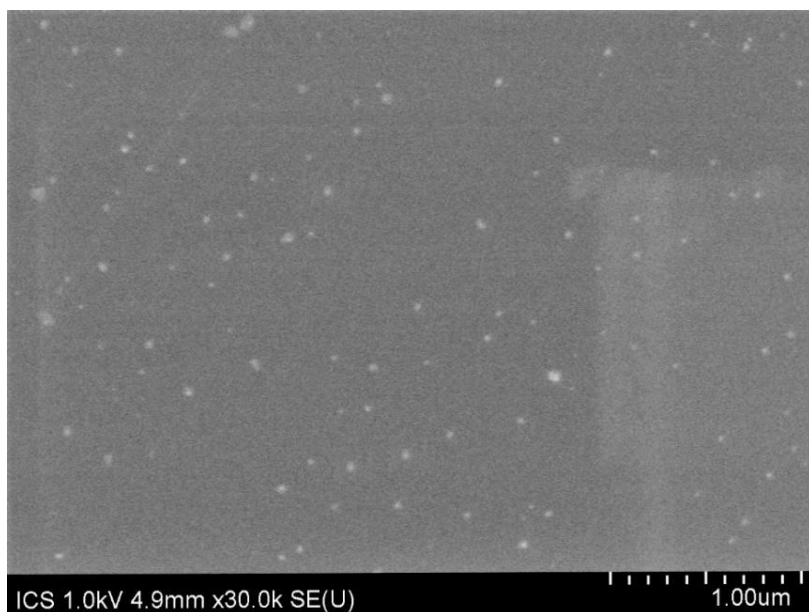


Figure 4.14. SEM image of drug loaded PMMA-PLGA blend PNPs produced at 150 cycles, 30 mL/min having 80 nm average size and narrow size distribution (PDI = 0,15).

The given images of PMMA-PLGA NPs (Figure 4.10) and DNPs (Figure 4.11) were captured by using TEM and SEM techniques respectively. When compared, it can be observed that the produced PNPs were challenging to identify in SEM image, however, the resolution was much higher with TEM, and PNPs were clearly visible. In general, the only technique that allowed to observe Janus PNPs' morphology was TEM, considering the difference in the polymer densities. AFM images allowed to verify the PNPs' size and their height, which also corresponded to a diameter of a spherical object. The PNPs' agglomeration while deposition on a substrate to receive micrographs was inevitable, especially in AFM imaging. It can be concluded that, in this study the highest resolution was achieved with TEM technique, which also allowed to observe the Janus PNPs, however, other techniques were useful to verify the size and size distribution.

4.4.2 Some notes to be considered for the next studies

In this study, we used three different polymers with different material properties to prepare single and blend PNPs. It was observed that the difference in material properties can turn to be a key factor for formulation of an anisotropic PNPs. Here, the hydrophobic nature of PMMA, and hydrophilic nature of PSS was one of the driving forces to achieve Janus structure. To our knowledge, in the literature this was the first reported anisotropic aPNPs with a hydrophilic polymer layer covering some parts of the hydrophobic polymeric sphere surface. This anisotropy was applied in PNPs washing, where PSS part left the PNPs' surface open after multi-step interventions. As a result of this

“cleaning”, the PNP became totally hydrophobic without relying on chemical synthesis methods. This property can be later used in surface modification, selective absorption and release, or a hydrophobic agent that can shift from amphoteric to hydrophobic in time.

To better control the anisotropy, and achieve desired properties, it's necessary to consider the physicochemical properties of the polymers, such as for PLGA, the effect of molecular weight and the molar ratio of lactic and glycolic acid, which controls the drug carrier properties of PNPs. As previously discussed, the hydrolysis is one of the major properties that PLGA molecule experiences, also, a drug load may lead to PLGA degradation in acidic medium, which is not the case for PMMA, PSS [21], [22]. In the present study, it was at a negligible scale due to a slow degradation of PLGA molecules [23], reported in the previous chapter. However, changing the polymer properties, can be a way for controlling the release kinetics. Similarly, PMMA can be reduced in MW to achieve a slower release, and can be increased in molar concentration to achieve higher EE. All these parameters can be tailored according to the demand, and more interestingly, in a single-step elongational-flow emulsification and evaporation.

Overall, it was possible to fabricate anisotropic PNPs in a single-step process, and this opened many other opportunities to achieve advanced polymeric nanomaterials in one step production, and without hiring multi-step chemical synthesis methods.

4.5 CONCLUSION

This work proposes to implement the emulsification-evaporation method for the one-step production of PNPs. Emulsification-evaporation method was a reliable way to achieve both single, binary-blend, and Janus PNPs. In this context, PMMA-PLGA NPs were first produced by changing emulsification time, mixing parameters to optimize the system to achieve minimum values of diameter size and size distribution for PNPs (PDI below 0.2). Then, three i) traditional, ii) pre-saturated solvent, and iii) pre-saturated & drug-loaded conditions allowed to further reduce PNPs' size and compare PMMA-PLGA NPs with single PLGA and PMMA NPs. The results showed that PNP's sizes varied dramatically, with more than 40% of size difference between the first and the third conditions. Thus, PNPs' diameters of 64 nm, 76 nm, and 78 nm were achieved for single PLGA, PMMA, and binary-blend PMMA-PLGA NPs respectively. However, the size distribution (<0.2) was similar at each condition. This was explained by the solvent diffusion, and the interfacial tension, that was also studied in chapter 3. In the end of this studies, the optimum operating parameters with the elongational-flow reactor and micromixer were found (60 min, 30 mL/min flow rate, and 250 μm microchannel size) to achieve desired PNPs' size and size distribution.

In the second part, binary-blend PMMA-PSS and PLGA-PSS NPs were investigated to optimize their concentration ratio to reach desired PNPs' properties. DLS results of the produced binary-blend PNPs showed that, above the 50% w/w PSS/PMMA ratio, binary-blend PNPs of both PMMA-PSS and PLGA-PSS became less likely to be monomodal in size. Following the polymer ratio study, in the next part, five different PNPs were morphologically characterized and compared. It was revealed that, PMMA-PSS and PLGA-PSS NPs formed a Janus structure with two distinct polymer populations forming a single spherical matrix, however, PMMA-PLGA NPs were mixed to form single body PNP matrix. This was correlated with both polymers' hydrophobic nature. Then, PMMA-PSS Janus PNPs were further studied to verify one side to be PSS, and another side to be PMMA. In this context, these PNPs were centrifuged to separate two polymers according to their difference in hydrophobicity. Due to its hydrophilic nature, PSS gradually disappeared by leaving a hydrophobic PMMA surface. This revealed that, the brighter aPNPs side was PSS, and a larger side was PMMA.

In the next part, two single, and two binary-blend PNPs were used to encapsulate a model drug, rifampicin to study and compare their cargo capacities. At 5% w/w rifampicin initial load with respect to the polymer weight content, maximum EE was achieved with single PLGA NPs (40%, 175 µg). This was correlated to a comparatively low MW (50,000) of PLGA, which improved entrapment of the drug molecules inside the polymer matrix, however, the drug release was less in percentage compared to other PNPs. In vitro drug release study of DNPs under sink conditions showed that the polymer type was affecting the drug release kinetics. Released rifampicin quantities from single PMMA, PLGA, binary-blend PMMA-PLGA, and Janus PMMA-PSS DNPs were 166 µg (46%), 175 µg (44%), 174 µg (48%) and 171 µg (51%) respectively. The highest release percentage value was achieved with the Janus PNPs, which was explained by a gradual dissolution of the PSS matrix out of the Janus structure leading to more drug molecules to escape the DNP.

Overall, this work allowed to fabricate Janus structures showing anisotropy in one-step production. This thus opened an innovative perspective for the design of new anisotropic PNPs. By changing polymer type, and properties, that can improve and control the drug release, can be a promising strategy to later develop new structures, and study more polymers for different applications. Indeed, the interrelation between the material affinity, and the diffusion out of droplet while emulsification can be also investigated in order to ameliorate the produced material performance.

4.6 BIBLIOGRAPHY

- [1] H. M. Abdelaziz *et al.*, "Inhalable particulate drug delivery systems for lung cancer therapy: Nanoparticles, microparticles, nanocomposites and nanoaggregates," *J. Control. Release*, vol. 269, no. October 2017, pp. 374–392, 2018, doi: 10.1016/j.jconrel.2017.11.036.

- [2] B. J. Boyd *et al.*, “Successful oral delivery of poorly water-soluble drugs both depends on the intraluminal behavior of drugs and of appropriate advanced drug delivery systems,” *Eur. J. Pharm. Sci.*, vol. 137, no. May, p. 104967, 2019, doi: 10.1016/j.ejps.2019.104967.
- [3] N. Visaveliya, A. Knauer, W. Yu, C. A. Serra, and J. M. Köhler, “Microflow-assisted assembling of multi-scale polymer particles by controlling surface properties and interactions,” *Eur. Polym. J.*, vol. 80, pp. 256–267, 2016, doi: 10.1016/j.eurpolymj.2016.03.015.
- [4] M. Vauthier and C. A. Serra, “One-step production of polyelectrolyte nanoparticles,” *Polym. Int.*, vol. 70, no. 6, pp. 860–865, 2021, doi: 10.1002/pi.6178.
- [5] C. Ohm, N. Kapernaum, D. Nonnenmacher, F. Giesselmann, C. Serra, and R. Zentel, “Microfluidic synthesis of highly shape-anisotropic particles from liquid crystalline elastomers with defined director field configurations,” *J. Am. Chem. Soc.*, vol. 133, no. 14, pp. 5305–5311, 2011, doi: 10.1021/ja1095254.
- [6] Z. Rahiminezhad, A. M. Tamaddon, S. Borandeh, and S. S. Abolmaali, “Janus nanoparticles: New generation of multifunctional nanocarriers in drug delivery, bioimaging and theranostics,” *Appl. Mater. Today*, vol. 18, p. 100513, 2020, doi: 10.1016/j.apmt.2019.100513.
- [7] B. T. T. Pham, C. H. Such, and B. S. Hawkett, “Synthesis of polymeric janus nanoparticles and their application in surfactant-free emulsion polymerizations,” *Polym. Chem.*, vol. 6, no. 3, pp. 426–435, 2015, doi: 10.1039/c4py01125b.
- [8] P. Yáñez-Sedeño, S. Campuzano, and J. M. Pingarrón, “Janus particles for (bio)sensing,” *Appl. Mater. Today*, vol. 9, pp. 276–288, 2017, doi: 10.1016/j.apmt.2017.08.004.
- [9] S. Ding, C. A. Serra, T. F. Vandamme, W. Yu, and N. Anton, “Double emulsions prepared by two-step emulsification: History, state-of-the-art and perspective,” *J. Control. Release*, vol. 295, no. September 2018, pp. 31–49, 2019, doi: 10.1016/j.jconrel.2018.12.037.
- [10] M. Vauthier, M. Schmutz, and C. A. Serra, “One-step elaboration of Janus polymeric nanoparticles: A comparative study of different emulsification processes,” *Colloids Surfaces A Physicochem. Eng. Asp.*, vol. 626, no. June, p. 127059, 2021, doi: 10.1016/j.colsurfa.2021.127059.
- [11] S. Ding *et al.*, “A new method for the formulation of double nanoemulsions,” *Soft Matter*, vol. 13, no. 8, pp. 1660–1669, 2017, doi: 10.1039/c6sm02603f.
- [12] S. Ding, C. A. Serra, N. Anton, W. Yu, and T. F. Vandamme, “Production of dry-state ketoprofen-encapsulated PMMA NPs by coupling micromixer-assisted nanoprecipitation and spray drying,” *Int. J. Pharm.*, vol. 558, no. December 2018, pp. 1–8, 2019, doi: 10.1016/j.ijpharm.2018.12.031.
- [13] S. Ding, C. A. Serra, T. F. Vandamme, W. Yu, and N. Anton, “Double emulsions prepared by two-step emulsification: History, state-of-the-art and perspective,” *J. Control. Release*, vol.

- 295, no. December 2018, pp. 31–49, 2019, doi: 10.1016/j.jconrel.2018.12.037.
- [14] S. Ding *et al.*, “Microfluidic-Assisted Production of Size-Controlled Superparamagnetic Iron Oxide Nanoparticles-Loaded Poly(methyl methacrylate) Nanohybrids,” *Langmuir*, vol. 34, no. 5, pp. 1981–1991, 2018, doi: 10.1021/acs.langmuir.7b01928.
- [15] K. Amreen and S. Goel, “Review—Miniaturized and Microfluidic Devices for Automated Nanoparticle Synthesis,” *ECS J. Solid State Sci. Technol.*, vol. 10, no. 1, p. 017002, 2021, doi: 10.1149/2162-8777/abdb19.
- [16] K. H. Roh, D. C. Martin, and J. Lahann, “Biphasic Janus particles with nanoscale anisotropy,” *Nat. Mater.*, vol. 4, no. 10, pp. 759–763, 2005, doi: 10.1038/nmat1486.
- [17] M. M. Alshehri, Z. A. Alothman, A. Y. Bedjah Hadj Ahmed, and T. Aouak, “New Method Based on Direct Analysis in Real-Time Coupled with Time-of-Flight Mass Spectrometry (DART-ToF-MS) for Investigation of the Miscibility of Polymer Blends,” *Polymers (Basel)*, vol. 14, no. 9, 2022, doi: 10.3390/polym14091644.
- [18] K. Y. Hernández-Giottonini *et al.*, “PLGA nanoparticle preparations by emulsification and nanoprecipitation techniques: Effects of formulation parameters,” *RSC Adv.*, vol. 10, no. 8, pp. 4218–4231, 2020, doi: 10.1039/c9ra10857b.
- [19] Y. Singh *et al.*, “Nanoemulsion: Concepts, development and applications in drug delivery,” *J. Control. Release*, vol. 252, pp. 28–49, 2017, doi: 10.1016/j.jconrel.2017.03.008.
- [20] J. Abdurahim, C. A. Serra, C. Blanck, and M. Vauthier, “One-step production of highly monodisperse size-controlled poly(lactic-co-glycolic acid) nanoparticles for the release of a hydrophobic model drug,” *J. Drug Deliv. Sci. Technol.*, vol. 71, no. May, p. 103358, 2022, doi: 10.1016/j.jddst.2022.103358.
- [21] N. Kamaly, B. Yameen, J. Wu, and O. C. Farokhzad, “Degradable controlled-release polymers and polymeric nanoparticles: Mechanisms of controlling drug release,” *Chem. Rev.*, vol. 116, no. 4, pp. 2602–2663, 2016, doi: 10.1021/acs.chemrev.5b00346.
- [22] N. Wang, X. S. Wu, C. Li, and M. F. Feng, “Synthesis, characterization, biodegradation, and drug delivery application of biodegradable lactic/glycolic acid polymers: I. synthesis and characterization,” *J. Biomater. Sci. Polym. Ed.*, vol. 11, no. 3, pp. 301–318, 2000, doi: 10.1163/156856200743715.
- [23] M. Allahyari, R. Mohabati, A. Vatanara, and M. Golkar, “In-vitro and in-vivo comparison of rSAG1-loaded PLGA prepared by encapsulation and adsorption methods as an efficient vaccine against *Toxoplasma gondii*,” *J. Drug Deliv. Sci. Technol.*, vol. 55, p. 101327, 2020, doi: 10.1016/j.jddst.2019.101327.

Chapter 5: Process design and optimization of polyelectrolyte complex nanoparticles' production

5.1	INTRODUCTION	185
5.2	POLYELECTROLYTES FORMED VIA EMULSIONS	187
5.2.1	Characterization of pre-formed polyelectrolytes and their complexes	187
5.2.2	Characterization of polyelectrolyte nanoparticles and their complexes	189
5.2.3	Sign of improved electrostatic attraction	191
5.2.4	Side-by-side capillary device to improve electrostatic interactions	193
5.3	NON-EMULSION DESIGN WITH SIDE-BY-SIDE CAPILLARY DEVICE	195
5.3.1	Process optimization	195
5.3.2	PEC NPS formation mechanism	196
5.3.3	Other polyelectrolytes capable of forming PEC NPs	198
5.3.4	Side-by-side capillary collecting tubing	199
5.3.5	Polymer molecular weight effect on final product properties	201
5.3.6	Morphological characterizations	202
5.4	CONCLUSION	204
5.5	BIBLIOGRAPHY	205

Chapter 5

Process design and optimization of polyelectrolyte complex nanoparticles' production

5.1 INTRODUCTION

Nanoparticles (NPs) compose the most important part of the sparkling field of nanotechnology, with a wide range of applications from medical [1], food [2], cosmetics [3], drug delivery with controlled active pharmaceutical ingredient (API) release profiles [4], [5], agriculture [6] to car manufacturing [7]. Especially, NPs made from polymers are found to be attractive due to their wide range of advantages [8]–[10]. Polymeric nanoparticles (PNPs) are refashioning the polymer's physicochemical characteristics, eventually highlighting the advantages of nanotechnology [11]. In the nanoscale, bulk counterparts of these polymeric nanomaterials can appear with improved physicochemical, optical, mechanical, and electrical properties [12]–[14], attributing to their nano geometries and a large surface area per unit of volume. Based on the control over their morphology, size, bioavailability, and high biostability, PNPs of diameters as low as 200 nm can be found as promising candidates in different applications, especially in drug delivery [9], [15], [16]. Also, PNPs containing two different polymers can present new physicochemical properties or shapes. Those are driven by the individual polymers properties and production process [17], [18].

In previous studies, several methods to produce PNPs are described [19]–[22], including synthetic approaches [23]. Especially, the emulsification techniques presented in the literature are still usually multistep multiplying risks of contaminations [16], [20], [24]. Additionally, some challenges like a slow translation from research to real applications of PNPs, evolve from several factors. These are poor mixing conditions, high energy consumptions, and insufficient product yields of the conventional batch methods [25], and their associated high batch-to-batch variations [14], [26]. It is still prudent to find methods that can significantly improve PNPs' fabrication and avoid the inherent limitations of conventional methods [27]. In this context, microfluidics can be found as a potential tool for the fabrication of PNPs with highly controlled mixing parameters both on small and larger scales. It allows the production of nanomaterials with geometries as low as a few tens of nanometers. To this extent PNPs' microfluidic fabrication benefits from rapid and tunable mixing [26], [28], [29]. For example, the 2D hydrodynamic flow-focusing approach allows producing poly(lactide-co-glycolic acid) (PLGA) and a bloc copolymer composed of PLGA and poly(ethylene

glycol) (PLGA-b-PEG) nanoparticles. However, it appeared that the polymer concentration induced aggregation near the channel walls [26]. In the flow focusing systems, the central stream is getting squeezed, yielding a narrow stream allowing rapid mixing [30], [31]. The microfluidic method also allows the PNPs' surface modification by introducing polyelectrolytes (PE) in a controlled manner [17]. Moreover, co-jetting can achieve the production of PNPs with Janus structure: for instance by applying an electrical field, allowing the fabrication of poly(ethylene oxide) – poly(acrylic acid) PEO-PAA biphasic carriers with a size range of 500-2000 nm [32] or without electrical field, producing monomodal PLGA-PEG NPs of 271 nm *via* emulsification-evaporation method [33]. However, all the aforementioned examples are costly due to expensive device parts and fabrication methods. Also, other limits like fouling, clogging, poor chemical compatibility, need for a cleanroom facility for the manufacture of lab-on-a-chip devices were recently reported [34], [35]. In this context, capillary-based microfluidic systems, for which the fluid(s) of interest is(are) flowing in the centerline line of the system are compatible with all aggressive solvents and can be fabricated from cheap, commercially available glass capillary tubes. These systems can have as much potential as lab-on-chip devices regarding highly controlled flow parameters [27]. Additionally, capillary-based devices allow operation by avoiding the contact of dispersed phase fluid with the collecting tubing walls, limiting the fouling, clogging, and dissolution of device components. Considering all these advantages, a side-by-side capillary device is very promising, however, this device has never been described to produce NPs (only to produce microparticles).

In this work, poly(acrylic acid)/poly(diallyldimethylammonium chloride) PAA/PDADMAC NPs have been firstly developed *via* ultrasound (see 2.2.1.3), elongational-flow emulsification (see 2.2.1.1) and solvent evaporation methods (see 2.2.2). Following the results achieved from these studies, a new non-emulsion-based polyelectrolyte complexes (PEC) method for the fabrication of NPs was developed with the side-by-side capillary device (see 2.2.3). Then, some parameters like flow rates, and device geometries were optimized to achieve different PEC NPs, of PAA/PDADMAC, Dextran/PDADMAC, PAA/Chitosan with controlled size below 100 nm and size distribution allowing future biomedical applications (PDI < 0.2).

Overall, considering the previously reported PNP fabrication methods, in this chapter we introduce a novel method of PEC NP synthesis *via* the side-by-side capillary device, that is known for achieving microdroplets.

5.2 POLYELECTROLYTES FORMED VIA EMULSIONS

5.2.1 Characterization of pre-formed polyelectrolytes and their complexes

Before diving into main experiments to achieve PNPs, 5% w/v poly(acrylic acid) (PAA) and 5% w/v poly(diallyl dimethylammonium chloride) (PDADMAC) solutions were mixed to form a PEC. This was done to demonstrate an electrostatic interaction between the two oppositely charged polyelectrolytes, leading to the formation of large sediments (Figure 5.1).

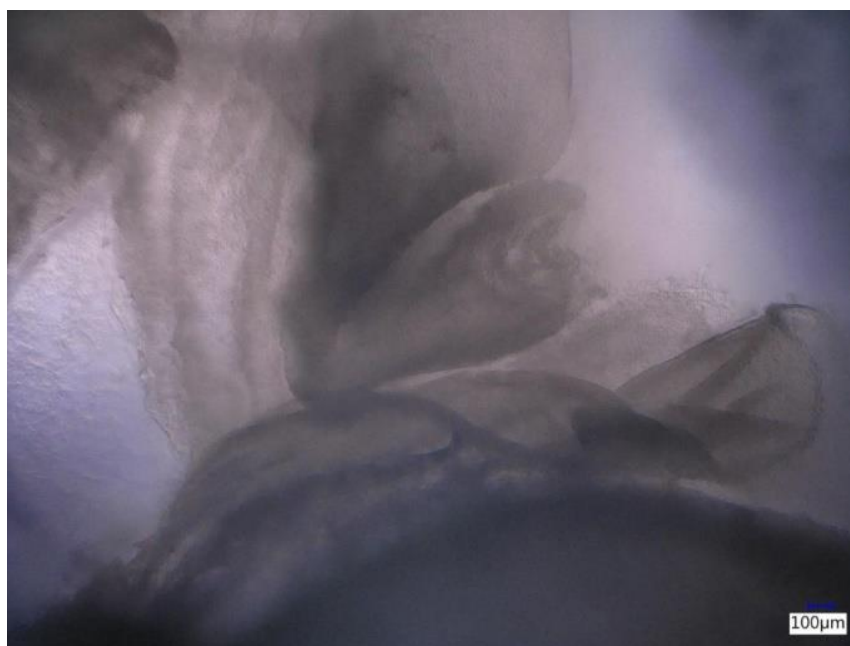


Figure 5.1. Microscopic image of PAA-PDADMAC polymer complex prepared through the dropwise addition of 5% w/v PAA solution into 5% w/v PDADMAC solution.

Figure 5.1 shows a large PEC formed following a mixing process of two polymer solutions by dropwise addition of 5% w/v PAA anionic solution to 5% w/v PDADMAC cationic solution under a pH 7 medium. However, by decreasing the pH of the solutions the PEC formation slowed down, and finally, no PEC was observed in an acidic medium. This was related to the electrochemical properties of the polymers, that was investigated by measuring the zeta potential (see 2.3.1.1), following the preparation of the polymer solutions at three different polymer concentrations and three pH conditions (Table 5.1). Thus, at pH 7, both polymers had ionic properties, and the latter changed according to their concentration and pH value. Increasing PDADMAC concentration from 1% w/v to 10% w/v increased the conductivity from 4 mS/cm to 32 mS/cm, however, electrophoretic mobility and charge (*i.e.* zeta potential) didn't change significantly. This was similar while changing pH, PDADMAC showed a positive value of charge in the range of 21 mV to 27 mV, and conductivity increased from positive 17 mS/cm to 26 mS/cm in an acidic medium. The second polymer, anionic

PAA solution, showed a strong negative value from -51 mV to -76 mV with near-zero conductivity and $-5 \pm 1 \mu\text{mcm}/\text{vs}$ electrophoretic mobility at a neutral medium (pH 7). This polymer demonstrated similar electrochemical properties at pH 10, however, in an acidic medium, no anionic property was detected, except highly enhanced conductivity (14 mS/cm). as was described in Table 5.1.

Table 5.1. Electrochemical properties of PAA and PDADMAC.

Medium	Polymer	Concentration (% w/v)	Zeta potential (mV)	Standard Deviation (mV)	Electrophoretic mobility ($\mu\text{mcm}/\text{vs}$)	Conductivity (mS/cm)
pH 7	PDADMAC	1	27	± 5	2	4
		5	27	± 1	2	17
		10	22	± 3	2	32
	PAA	1	-51	± 4	-4	0
		5	-76	± 6	-6	1
		10	-63	± 5	-5	1
pH 10	PDADMAC	5	21	± 4	2	14
	PAA	5	-62	± 5	-5	2
pH 2	PDADMAC	5	24	± 4	2	26
	PAA	5	0	0	0	14

These measurements allowed us to understand the PEC formation under certain material parameters like polymer concentration, and solvent medium. This property of the two polymers was later applied to produce PEC NPs in both emulsion and non-emulsion-based PNP fabrication methods. Contrary to PDADMAC, PAA's charge was affected by the pH value.

5.2.2 Characterization of polyelectrolyte nanoparticles and their complexes

In this part, PE NPs made of individual PAA or PDADMAC, and their complexes were produced by preparing w/o hexadecane emulsions with Sonicator and μ RMX (see 2.2.1). Then, by using rotary evaporator (see 2.2.2) the polymer solvent (water) was eliminated to yield PE NPs. Following the water elimination at each experiment, nanosuspensions in hexadecane shifted from white color to near transparent, which indicated the completion of the solvent removal process (Figure 5.2).



Figure 5.2. Image of 5/5 w/w PAA-PDADMAC polymer complex in miniemulsion (left) and nanosuspension (right) prepared *via* two-step emulsification and evaporation method reported in Table 5.2 (sample 11).

Water removal was verified by measuring the vial weight every 30 minutes until no weight loss was detected anymore, and when the nanosuspension was nearly transparent (Figure 5.2). Following this, the nanosuspension was diluted with ethanol and centrifuged to eliminate the surfactant molecules from the system (see 2.2.4). Several PNPs were produced in one-step homogenization with sonicator (see 2.2.1.3) or μ RMX (2.2.1.1), and two step homogenization and mixing by using both devices. Both PE and PEC NPs were produced and characterized for their size, monomodality, and surface charge. The list of produced NPs and their complexes can be found in Table 5.2.

In Table 5.2, it was possible to fabricate PAA, PDADMAC NPs, and PAA/PDADMAC PEC NPs, however, in most cases, the size appeared widely distributed: the PDI value was in the range of 0.2 to 0.7. Only PDADMAC NPs produced at 3% SPAN80 concentration with sonicator appeared monomodal with 53 nm size. In general, higher surfactant concentration allowed producing smaller and monomodal PNPs. Moreover, at 10% w/v polymer concentrations, the produced PNPs were multimodal. This was related to the polymer solutions' viscosity, as previously described in the Taylor Grace theory (2.2.1).

Table 5.2. Size, size distribution (PDI), and surface charge properties of PE NPs and their complexes produced under different emulsification conditions (all with a continuous to dispersed phase volume ratio equal to 85/15).

Sample	Device name	Mixing time (min)	Second mixing parameter	Polymer	Polymer concentration (% w/v)	SPAN80 (% w/v)	Diameter size (nm)	PDI	Surface Charge (mV)
1			70%	PAA	1		42	0.2	-35
2			70%	PDADMAC	1		51	0.3	+29
						1.5			
3			70%	PAA	10		34	0.3	-23
4			70%	PDADMAC	10		70	0.4	+27
5	Sonicator	5	30%	PAA	5		61	0.2	-28
6			30%	PDADMAC	5		53	0.1	+33
7			50%	PAA	5	3	60	0.2	-26
8			50%	PDADMAC	5		51	0.15	+34
9			30%	PDADMAC/ PAA	5-5		250	0.3	+14
10			30%	PDADMAC/ PAA	1-1		151	0.3	+12
11	μRMX	60 (=150 cycles)	30 mL/min	PAA	5		52	0.5	-29
12		60	30 mL/min	PDADMAC	5		72	0,3	+35
13	Sonicator and μRMX	5 + 60	50% power and 30 mL/min	PDADMAC/ PAA	5-5	3	48	0.2	+14

While comparing the PEC NPs produced in two-step emulsification, it was observed that the particle size and size dispersity decreases at higher concentrations of the surfactant (Figure 5.3), however, interestingly, the total surface charge increased (Table 5.3).

Table 5.3. Influence of the surfactant's concentration on the PDADMAC/PAA NPs' size, size distribution, and surface charge. Process: 5 min sonication of 5% w/v PAA (Table 5.2 sample 7) and 5% w/v PDADMAC (Table 5.2 sample 8) in hexadecane at 50% followed by 60 min μ RMX at 30 mL/min.

SPAN 80 concentration (% w/v)	Diameter size (nm)	PDI	Surface Charge (mV)
1	91	0.4	+5
2	67	0.3	+6
3	48	0.2	+14

Size reduction from widely multimodal 91 nm NPS to near monomodal 48 nm at higher surfactant concentration could be explained by the reduced interfacial tension between hexadecane and water phases. This eventually decreased the critical capillary number to rupture the emulsion droplets, this phenomenon was coherent with our previous studies where lower interfacial tension resulted in smaller PNPs (see 3.3). Concerning the surface charge, and especially the value of +14 mV reported in Table 5.3, two hypotheses can be proposed: i) the charge density of PDADMAC just take the lead somehow or ii) PDADMAC nanodroplets surrounds PAA nanodroplets. This will be later discussed with the help of TEM images (Figure 5.4).

5.2.3 Sign of improving electrostatic attraction

In the previous part, two w/o emulsions were produced by ultrasound emulsification at three different surfactant concentrations. Then, these two emulsions were mixed and introduced into μ RMX. Here, it was explained what happened when two emulsions mixed inside μ RMX. Initially, it was expected to form a complex structure with the elongational-flow micromixing mechanism (see 2.2.1.1). In this context, 5 mL emulsion of 5 % w/v PAA in hexadecane, and 5 mL emulsion of 5 % w/v PDADMAC in hexadecane were introduced in μ RMX, then operated at 150 cycles, 30 mL/min flow rate. Then, the collected sample was evaporated by using a rotary evaporator (see 2.2.2) to achieve the solid NPs in hexadecane (Figure 5.3).

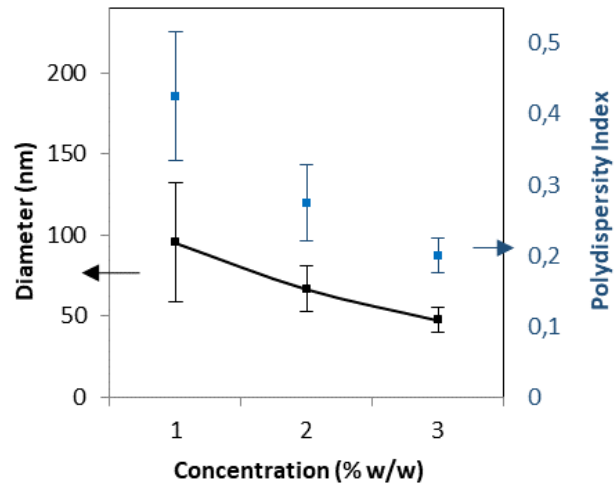


Figure 5.3. DLS average size results of PAA/PDADMAC PNPs at three different SPAN80 concentrations. PAA and PDADMAC emulsions are produced separately with ultrasound emulsification (5 minutes, 50%) at 85/15 C/D volume ratio, then both emulsions together are processed with the μ RMX (150 cycles, 30 mL/min, 75 μ m).

It can be observed that the higher the surfactant concentration, the smaller the PNPs' size (Figure 5.3), however, PEC NPs were not observed, and a layered structure was found to be formed out of individual PE NPs (Figure 5.4).

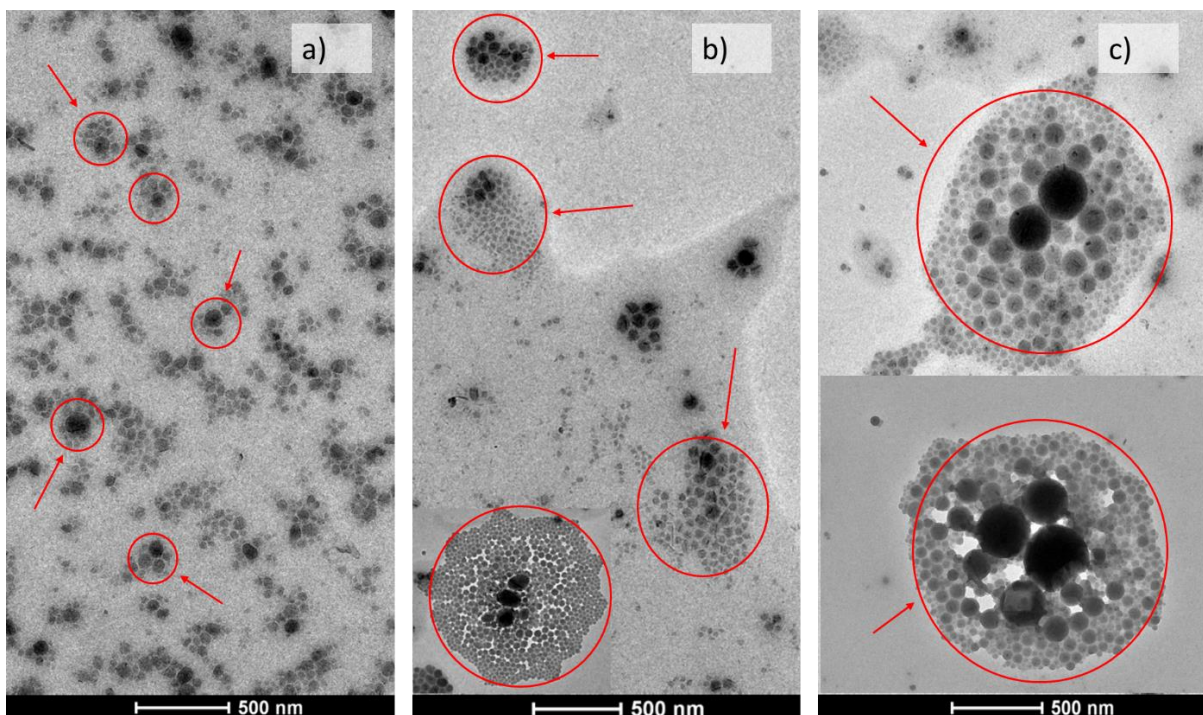


Figure 5.4. TEM images of PAA/PDADMAC NPs at SPAN80 concentrations of a) 3 % w/v, b) 2 % w/v, c) 1 % w/v. PNPs were produced with ultrasound emulsification (5 minutes, 50%) at 85/15 C/D volume ratio, then processed with μ RMX (150 cycles, 30 mL/min, microchannel of 750 μ m).

At higher (3% w/v) surfactant concentration, PE NPs were more isolated (Figure 5.4.a) compared to the systems with less surfactant concentration (Figure 5.4.b and Figure 5.4.c). Also, it was observed that at lower concentrations, the PE NP size was widely distributed, where small particles such as 30 nm can be found agglomerated to larger 170 nm PE NPs. Considering the final positive surface charge between +6 mV and +14 mV (Table 5.2, sample 13), and narrowly distributed PDADMAC NPs at 51 nm size (Table 5.2, sample 8) the outer layer in the given TEM images (brighter and smaller PE NPs) were representing PDADMAC NPs. Moreover, the surface charge of PDADMAC (Table 5.2, sample 8) decreased from + 34 mV to +14 mV (Table 5.2, sample 13), which might be an indication of the weak electrostatic interactions between two oppositely charged polymers, leading to reduced active charged groups.

5.2.4 Side-by-side capillary device to improve electrostatic interactions

To promote the electrostatic interactions between two oppositely charged polymer emulsion droplets, it was interesting to further reduce the surfactant concentration while mixing two pre-formed emulsions. This can be achieved with the side-by-side capillary device (see 2.2.3), in which two previously obtained emulsions were mixed in the presence of a continuous phase composed of pure alcohol surrounding the flow of the two emulsions and injected into the collecting tube. This additional phase also acted as a polymer anti-solvent (Propan-2-ol). This solvent was chosen i) to allow the dissolution of surfactant, for its miscibility with ii) hexadecane and iii) water. It also allowed leaving freely the polymer molecules to electrostatically interact. This goal was achieved, as the two pre-formed emulsions were mixed after leaving the side-by-side capillaries, forming the PEC NPs in the range of 80 nm to 140 nm depending on the surfactant concentration (Figure 5.5).

Interestingly, when the results obtained at the same polymer concentration (5% w/v) but different emulsification devices (μ RMX Figure 5.3 and side-by-side capillary device Figure 5.5.b) were compared, it was observed that the PNPs size increased while increasing the surfactant concentration (Figure 5.3), conversely to the μ RMX. This can be explained by the difference in mixing mechanisms. Increasing the surfactant concentration resulted in the decrease of the surface tension, which in turn, accordingly to the Taylor theory (chap 2.2.1.1) increased the capillary number allowing the easier breaking of the droplets into smaller ones. In a side-by-side capillary device, this was different, since the mixing didn't imply shear or elongational forces but relied on the diffusion of the polymer solvent into the continuous phase, and polymer aggregation. It could be assumed that during this diffusion, surfactant molecules were dragged into the continuous phase, allowing the polymer molecules of opposite charges to merge, resulting in bigger NPs. It should be also mentioned

that, at the mixing point of two oppositely charged polymers, the newly formed PE complex became also water-insoluble (Figure 5.1). However, water diffusion here can be considered to later control the final material properties as it drove the emulsion droplet to precipitate before the electrostatic interaction was complete.

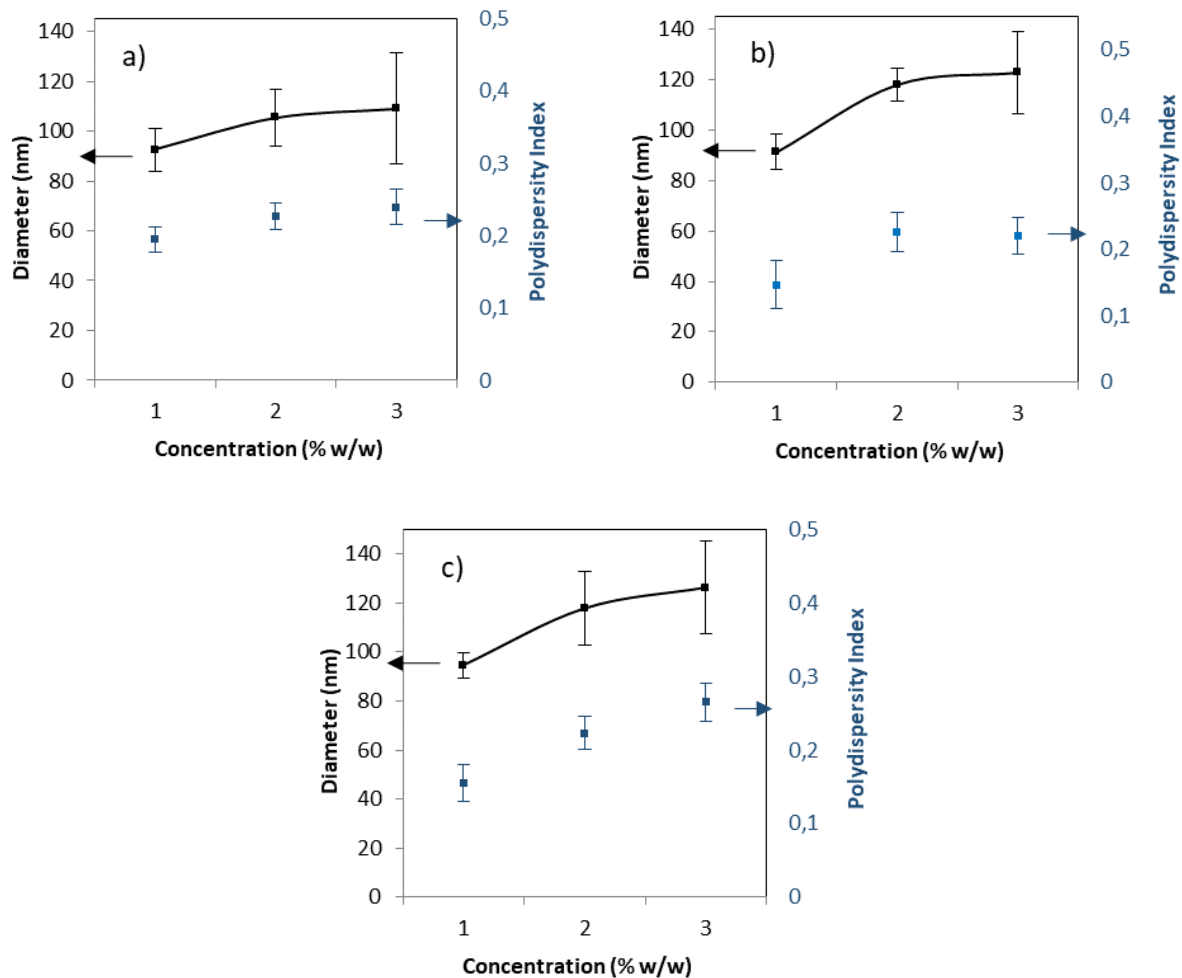


Figure 5.5. DLS average size results of PAA/PDADMAC PNPs produced from emulsion method at three different SPAN80 concentrations (1, 2 and 3 %w/w) and for different PAA/PDADMAC NPs individual polymer concentrations of a) 1 % w/v, b) 5 % w/v, and c) 10 % w/v. PAA and PDADMAC emulsions were produced with sonicator (5 minutes, 50%) at 85/15 C/D volume ratio, then processed with the side-by-side capillary device at $Q = 6/200 \mu\text{L}/\text{min}$ dispersed phases/continuous phase flow rates (75 μm capillary ID, 1.6 mm collecting tubing ID).

Following the specific mixing conditions maintained by the side-by-side capillary device, it was interesting to follow the PEC formation by directly relying on polymer solutions, as the NP formation was dependent on the electrostatic interactions. This would also appear as a new non-emulsion-based PNP production method, as fabrication of NPs by using the side-by-side capillary device has never been reported before.

5.3 NON-EMULSION DESIGN WITH SIDE-BY-SIDE CAPILLARY DEVICE

5.3.1 Process optimization

In the previous part, the emulsion-based design to achieve the PE and their NP complexes was described, which eventually brought us to a novel surfactant-free non-emulsion-based method capable to fabricate PNPs. In this context, the polymer solutions were directly used and introduced in the side-by-side capillary device to form PEC NPs. It was possible to observe the jetting stream inside the side-by-side capillary device. This stream was formed during the mixing of two dispersed (polymer) phases at controlled flow rates, and adding color to the dispersed (PAA) phase made the jetting stream visible (Figure 5.6).

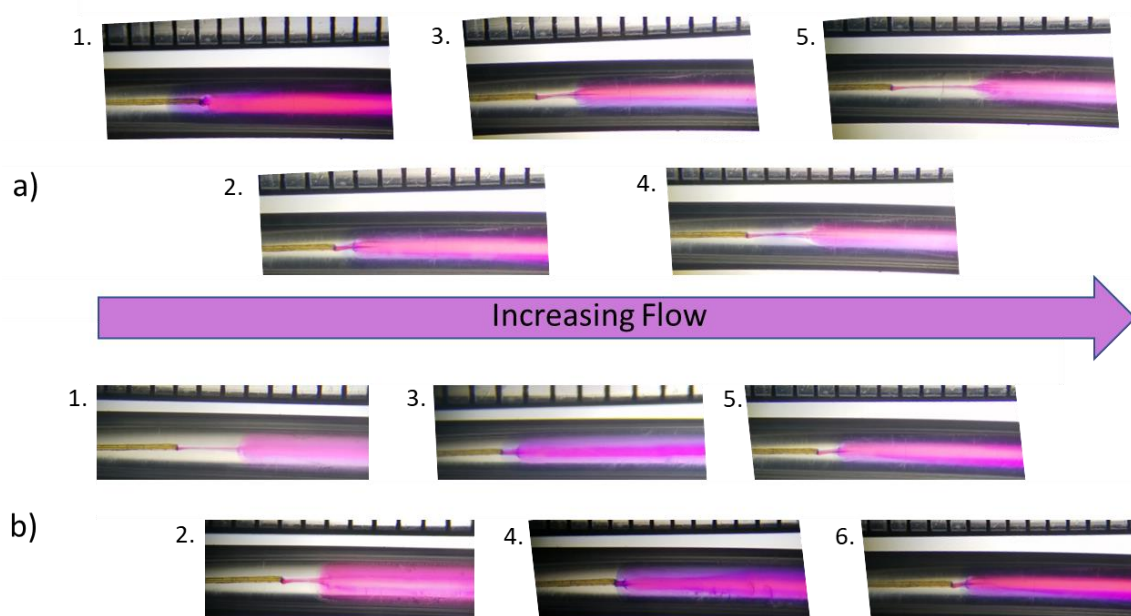


Figure 5.6. View of the mixing by using the side-by-side capillary device at a) constant dispersed phases flow rates of 6 $\mu\text{L}/\text{min}$ and variable continuous phase flow rate (100, 200, 350, 500, 650 $\mu\text{L}/\text{min}$) and b) constant continuous phase flow rate of 200 $\mu\text{L}/\text{min}$, where dispersed phase flow rates changed (1, 3, 5, 6, 8, 10 $\mu\text{L}/\text{min}$). All the given images represent less than 13 mm in length.

It can be observed that increasing the continuous phase flow rate at a constant dispersed phase flow rate lead to an elongated jetting from 1 mm to 4 mm, which was then described to affect the NP size (Figure 5.7). Initially, the continuous phase flow rate was optimized by changing the flow rates at a constant 6 $\mu\text{L}/\text{min}$ dispersed phases flow rate (Figure 5.6.a). Then, the dispersed phase flow rate was optimized at a constant 200 $\mu\text{L}/\text{min}$ continuous phase flow rate to achieve the required material properties (Figure 5.6.b). In these experiments, the two dispersed phases that were injected through

the 40 μm capillary tubes consisted of 1% w/v PAA aqueous solution, and 1 % w/v PDADMAC aqueous solution respectively. The produced PNPs at different flow rates were characterized with DLS (Figure 5.7).

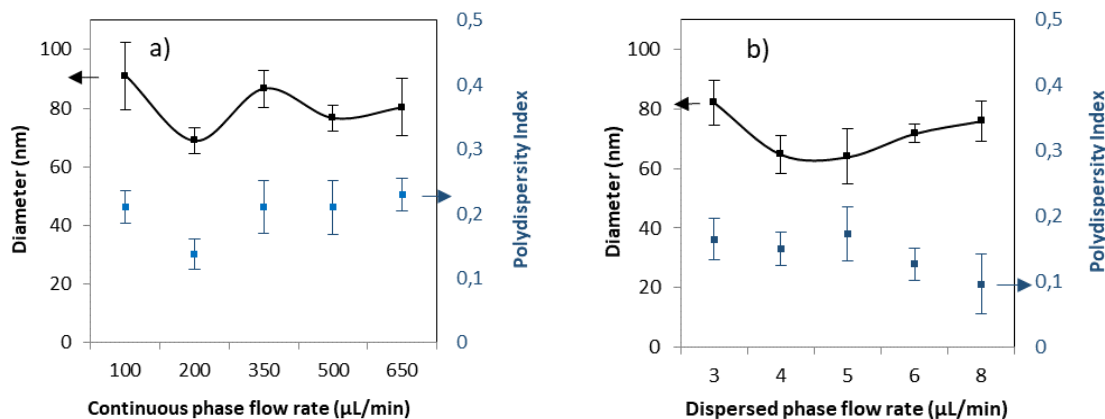


Figure 5.7. DLS average size and size distribution results of PAA/PDADMAC NPs produced with a side-by-side capillary device for non-emulsion method as a function of continuous or dispersed phase flow rates. Capillaries of 40 μm ID, collecting tubing of 1,6 mm diameter at a) 6 $\mu\text{L}/\text{min}$ dispersed phase flow rates, and b) 200 $\mu\text{L}/\text{min}$ continuous phase flow rate.

It was observed that the continuous phase flow rate not only reduces the PEC NP size but also the PDI when the flow rate was increased up to 200 $\mu\text{L}/\text{min}$. Increasing the flow rate further induced the production of less monomodal PEC nanoparticles with erratic higher sizes. This could be ascribed to a higher polymer solvent diffusion into the continuous phase, leading to faster electrostatic interaction and random precipitation given the reduction in the jet thickness observed in Figure 5.6. It should be noted that at a higher continuous flow rate the jetting stream was also longer (5 mm) and faster (Figure 5.6), which verified the highly intensified diffusion due to the higher interfacial area between two solvents and reduced residence time for PEC NPs' formation. In the next part, the formation mechanism of PEC NPs was experimentally tested and described.

5.3.2 PEC NPS formation mechanism

It was suggested that the PEC NPs in this study were formed upon the following two mechanisms: i) electrostatic interactions between two oppositely charged polymer molecules, and ii) nanoprecipitation of the polymer molecules after diffusion of the polymer solvent into the continuous phase. To better understand the formation mechanism, one of the mechanisms can be eliminated by injecting only one polyelectrolyte solution within the side-by-side capillary device as illustrated in Figure 5.8.

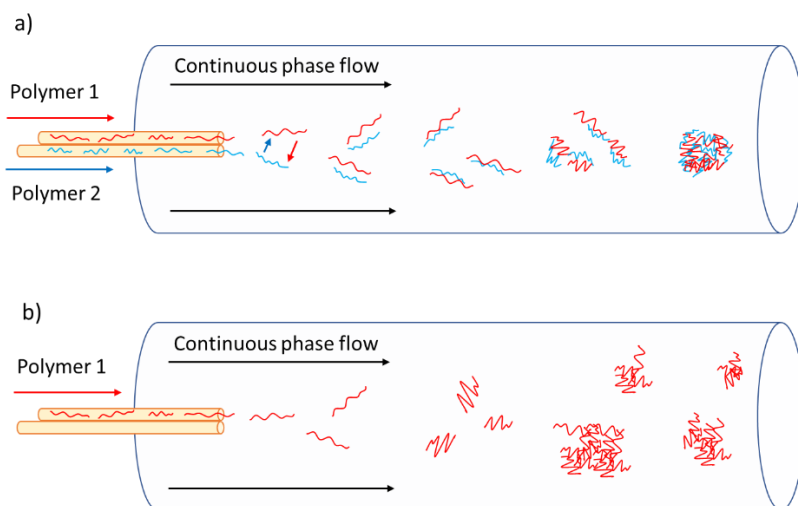


Figure 5.8. Schematic representation of the mechanism of a) PEC NP formation with two oppositely charged polymers *via* electrostatic attraction and nanoprecipitation, and b) PE NPs formation with single polymer only *via* nanoprecipitation. The illustration shows two side-by-side capillary tubes injecting polymer solutions into the collecting tubing. Polymer solutions mix with the continuous phase flow, and polymers start to self-assemble.

When both formation mechanisms appeared, PEC NPs formed uniformly, and the final PNP size became very narrowly distributed (Figure 5.7). This was due to two different mechanisms acting together to form monomodal PNPs (Figure 5.8.a). However, when a single polymer was injected, the electrostatic attraction could not take place, and the PNPs were formed due to the nanoprecipitation (Figure 5.8.b). Only nanoprecipitation was also able to force the polymer molecules to self-assemble (Figure 5.9).

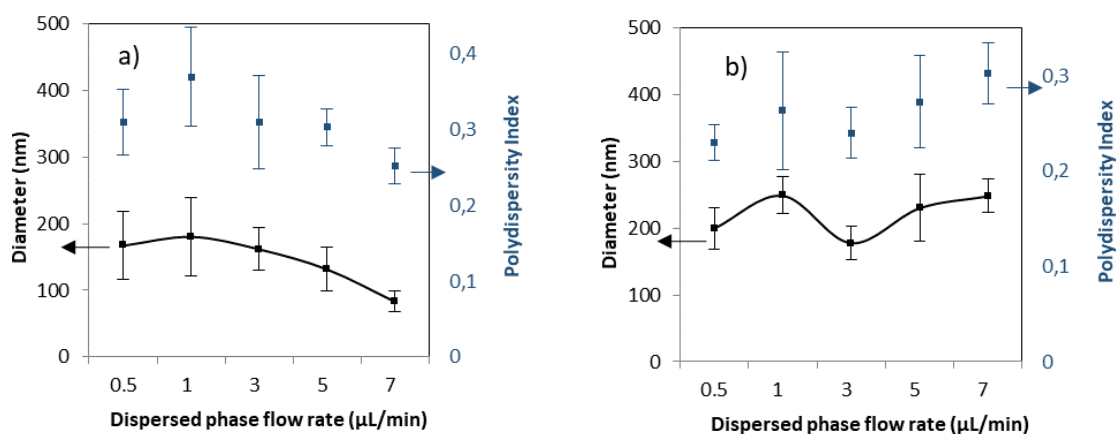


Figure 5.9. DLS average size and size distribution results of a) PAA and b) PDADMAC NPs produced with the side-by-side capillary device at 6/200 $\mu\text{L}/\text{min}$ dispersed/continuous flow rates (40 μm capillary ID, and 1.6 mm collecting tubing diameter).

Figure 5.9 shows the average size became larger, thus randomly distributed in size. In this context, the electrostatic interaction was avoided by injecting only one polymer solution, and the formed PNPs were characterized with DLS. By eliminating the electrostatic interaction, the size and size distribution of PNPs increased up to 150 nm for PAA NPs (Figure 5.9.a), and 200 nm for PDADMAC NPs (Figure 5.9.b). The PNPs were widely distributed, however, at a higher dispersed phase flow rate of 7 $\mu\text{L}/\text{min}$, it was possible to reach below 100 nm PAA NP size (PDI = 0.25). These results verified that, with the side-by-side capillary device, it was possible to form PE NPs also with a single mechanism (nanoprecipitation). Comparing the NPs' size obtained with one single polymer (Figure 5.8) and two oppositely charges polymer solutions (Figure 5.7), it can be concluded that electrostatic attraction not only induced a significant reduction in NPS size (70 nm vs 180 nm) but also allowed the production of more monomodal particles.

Smaller chains can be found to be less probable to self-assemble inside the large collecting tubing volume, whereas, larger molecules and their complex structures were more probable to form bigger statistical coils and in consequence bigger PNPs. In the following part, other PEC NPs were produced to demonstrate this mechanism was not limited to only PAA and PDADMAC PEs.

5.3.3 Other polyelectrolytes capable of forming PEC NPs

In this part, other polymers, namely dextran (negatively charged) and chitosan (positively charged), were studied to fabricate Dextran/PDADMAC, and PAA/Chitosan PEC NPs (Figure 5.10). In this context, dextran, PDADMAC, PAA and chitosan solutions were prepared at 1 % w/v, then injected by using syringe pumps to form PEC NPs.

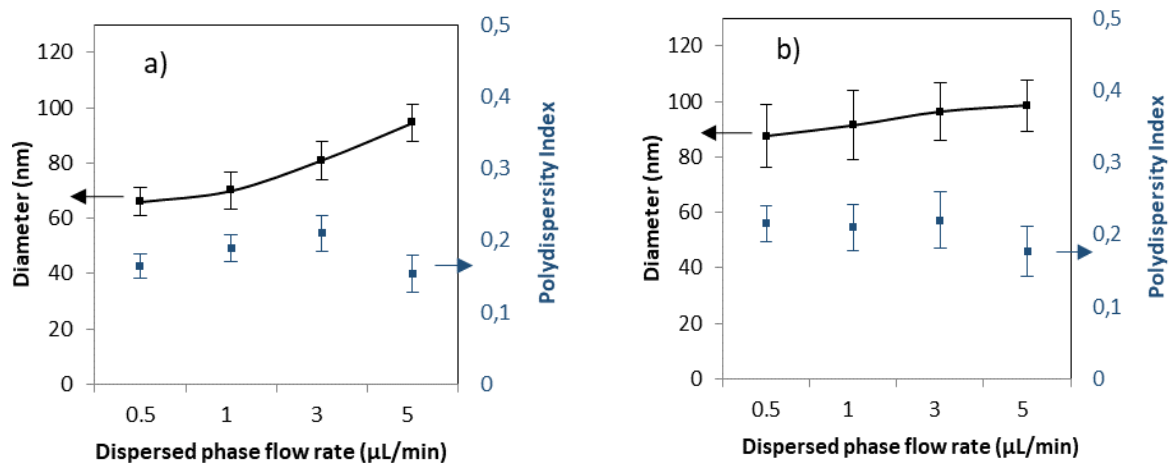


Figure 5.10. DLS results of PEC NPs produced with a side-by-side capillary device consisting of two capillaries of 40 μm ID, collecting tubing of 1.6 mm diameter at 200 $\mu\text{L}/\text{min}$ continuous phase flow rate, and made of a) Dextran/PDADMAC, and b) PAA/Chitosan.

The number average size of dextran/PDADMAC PEC NPs increased from 66 nm (PDI = 0.17) to 95 nm (PDI = 0.15) when the flow rate increased from 0.5 to 5 $\mu\text{L}/\text{min}$ (Figure 5.10.a). Surprisingly, the average size of PAA/chitosan NPs followed pretty much the same trend as previously discussed but with globally higher diameters (Figure 5.10.b). This can be explained by the effect of polymer type and their Mw. Polymers with higher water-loving indexes could act differently from polymers with lower values. For example, the Log P value for chitosan is 3.2, whereas, this value for dextran is – 2.9 (see 2.1.2). Similarly, the Mw of polymer could affect the polymer-polymer interactions and also the nanoprecipitation.

Overall, all the produced PEC NPs were found below 100 nm and narrowly distributed. However, these trends were not following what was achieved with PAA/PDADMAC NPs, where a smaller size was recorded at 5 $\mu\text{L}/\text{min}$ flow rate (Figure 5.7.b). In this case, this could be related to both molecular weights, and charge density of the polymers employed (see 2.1.2). Indeed, the chitosan molecule had less charge density compared to the PDADMAC molecule. This could lead to stronger electrostatic attraction yielding smaller PEC NPs. However, the mechanism at play was still not completely elucidated and will require further studies.

5.3.4 Side-by-side capillary collecting tubing

In this part, the collecting tubing composing the side-by-side capillary device was found to be effective to control the average size of PEC NPs (Figure 5.11). For this purpose, two dispersed phases at 1 % w/v concentration (PAA and PDADMAC) were injected through the capillaries at a flow rate ranging from 1 $\mu\text{L}/\text{min}$ to 10 $\mu\text{L}/\text{min}$, and at a constant continuous phase flow rate of 200 $\mu\text{L}/\text{min}$ for three different collecting tube diameters. It can be observed a non-monotonic variation of the particles' size concerning the dispersed flow rates; started to decrease from 83 nm to reach the smallest value of 62 nm at 4 $\mu\text{L}/\text{min}$, and then increased again at higher dispersed phase flow rates (Figure 5.11.a). It reached a narrowly distributed 72 nm monomodal size at 8 $\mu\text{L}/\text{min}$. Following the reduced value of size in the range of 4 $\mu\text{L}/\text{min}$ to 8 $\mu\text{L}/\text{min}$, and the larger size at 10 $\mu\text{L}/\text{min}$, it was suggested that the size increase could be due to a larger number of molecules connecting electrostatically. Thus, at 10 $\mu\text{L}/\text{min}$ of the dispersed phase flow rate, PEC NPs started growing larger due to a higher number of polymer molecules involved in the PEC NP synthesis. Considering this, the collecting tubing diameter was reduced to expect the PEC NPs to further grow in size (Figure 5.11.b).

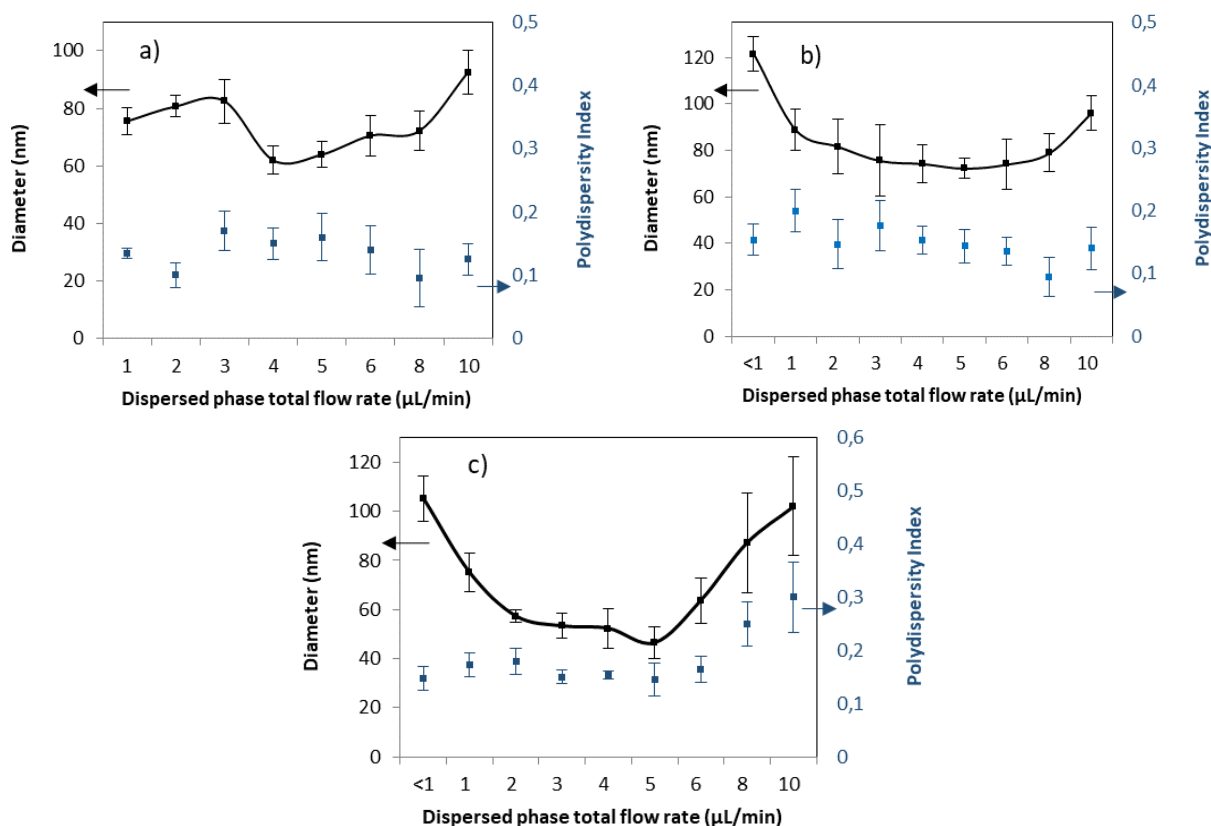


Figure 5.11. DLS average size and size distribution results of PAA/PDADMAC NPs produced with the side-by-side capillary device at 6/200 $\mu\text{L}/\text{min}$ dispersed/continuous flow rates (40 μm capillary ID) and varying the collecting tubing diameter a) 1.6 mm, b) 1 mm, c) 0.5 mm.

It was possible to observe 10 ± 2 nm larger PEC NPs with smaller collecting tubing (1 mm) diameter at the same operating parameters of 200 $\mu\text{L}/\text{min}$ continuous phase flow rate, and disperse phase flow rates between <1 to 10 $\mu\text{L}/\text{min}$ (Figure 5.11.b). Here, the NP size was stable at a larger flow rate range, and the size reached 80 nm at 8 $\mu\text{L}/\text{min}$. After further reducing the collecting tubing diameter to 0.5 mm (Figure 5.11.c), NP size further increased at the flow rate of 8 $\mu\text{L}/\text{min}$ to 87 nm, and the size was widely distributed ($\text{PDI} \geq 0.25$).

Interestingly, with 0.5 mm collecting tubing diameter, at flow rates between 2 $\mu\text{L}/\text{min}$ and 6 $\mu\text{L}/\text{min}$ the PEC NPs size were found more than 20 nm smaller compared to the previous results. Especially, at 5 $\mu\text{L}/\text{min}$ disperse phase flow rate the NP size reached the minimum value of 46 nm, which was 28% lower than the results (64 nm) achieved with a 1.6 mm collecting tubing diameter, and 36% lower than the size of NP produced with 1 mm collecting tubing diameter.

Overall, the collecting tubing diameter was highly effective while producing PEC NPs, and this can be an important tool while changing the dispersed phase flow rates to achieve desired PNPs properties.

5.3.5 Polymer molecular weight effect on final product properties

In the previous parts, we fabricated PAA/PDADMAC and other PEC NPs at constant polymer molecular weights (Mw). In this part, we compared polyelectrolyte NPs based on low (100 kg/mol) and high (500 kg/mol) PDADMAC molecular weights. The polymer with highest Mw will be called PDADMAC* thereafter. In order to compare the produced PEC NPs properties, two 40 μm glass capillaries and 1 mm collecting tubing were used. 1 % w/v PAA in water was injected with the first capillary, 1 % w/v PDADMAC solution was injected with the second capillary, and propan-2-ol was injected at 200 $\mu\text{L}/\text{min}$ in the continuous phase by using 0.5 mm collecting tubing. All the produced samples were then collected in glass vials containing propan-2-ol.

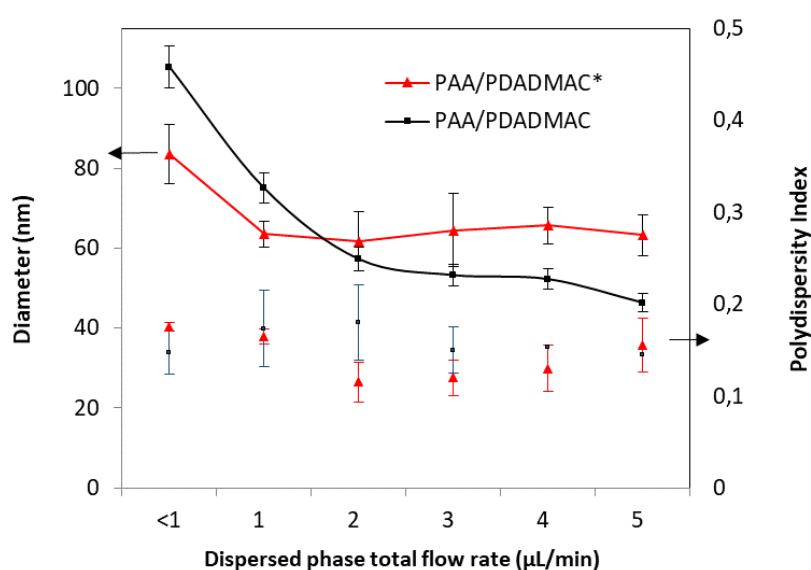


Figure 5.12. Average size (solid lines) and size distribution (points) results of PAA/PDADMAC, and PAA/PDADMAC* NPs produced with the side-by-side capillary device at 200 $\mu\text{L}/\text{min}$ continuous flow rate (40 μm capillary ID, 0.5 mm collecting tubing ID). PDADMAC* refers to higher Mw of the polymer (see 2.1.2).

In Figure 5.12, it was observed that higher Mw (PAA/PDADMAC*) leads to an increased average size at a dispersed phase flow rate above 2 $\mu\text{L}/\text{min}$, when compared to PAA/PDADMAC NPs. This can be explained by a longer polymer chain resulting in larger polymer complexes, which form PEC NPs through nanoprecipitation following the electrostatic interactions. At a very low dispersed phase, the number of polymer molecules was less in water, however, solvent diffusion was faster. This could lead to the nanoprecipitation mechanism dominating over the electrostatic attraction leading to larger, and less controlled PNP formation. It can be also observed that at a higher dispersed phase flow rate (5 $\mu\text{L}/\text{min}$) the difference between the two PEC NPs' size was more than 35% (46 nm to 63 nm). This was achieved by simply increasing the Mw (from 100,000 g/mol to 500,000 g/mol) of PDADMAC.

5.3.6 Morphological characterizations

In this part, following the PEC NPs production, the TEM technique (see 2.3.2.1) was used to observe the morphology of the produced PAA/PDADMAC NPs. First, these PEC NPs were achieved by injecting 1 % w/v PAA solution through 75 μm capillary glass tube, 1 % w/v PDADMAC solution through the second 75 μm capillary glass tube, and propan-2-ol alcohol phase through the collecting tubing. The flow rates were maintained at 3 $\mu\text{L}/\text{min}$ with the first capillary, 3 $\mu\text{L}/\text{min}$ with the second capillary, and 200 $\mu\text{L}/\text{min}$ for the continuous phase. The produced PEC NPs were directly collected in alcohol and analyzed with the TEM (Figure 5.13).

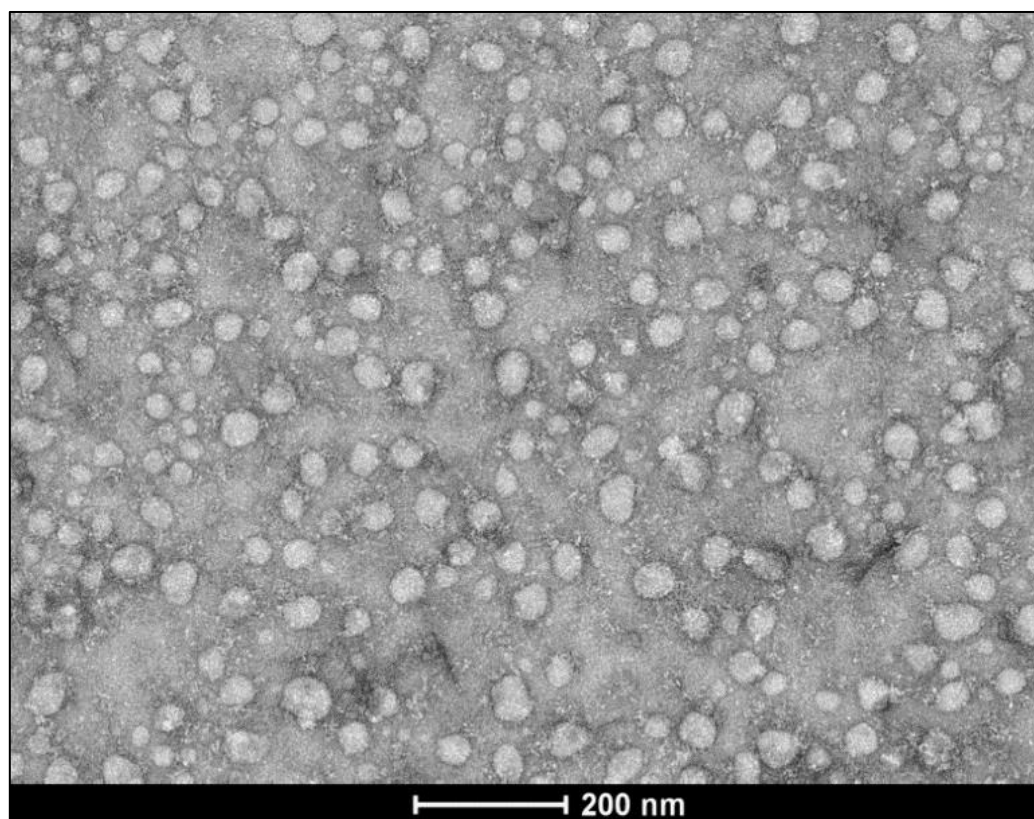


Figure 5.13. TEM image of PAA/PDADMAC complex NPs produced with the side-by-side capillary device.

Following the TEM imaging, it was verified that the produced PEC NPs were in the nano range, 60 nm on average of 500 PEC NPs, and narrowly distributed (PDI = 0.15). These NPs can be found in different shapes; however, they represent a single-density material (Figure 5.13). A single color observed by TEM was a sign of PEC material. Two different polymers agglomerated to form a single matrix complex NP. This was different from the previous images (Figure 5.4), where two populations of NPs (PAA and PDADMAC NPs) co-existed. More precisely, two polymers electrostatically interacted to form a single-body PEC matrix. Noteworthy, DLS results (Figure 5.14) were coherent with size and size distribution observed from TEM images.

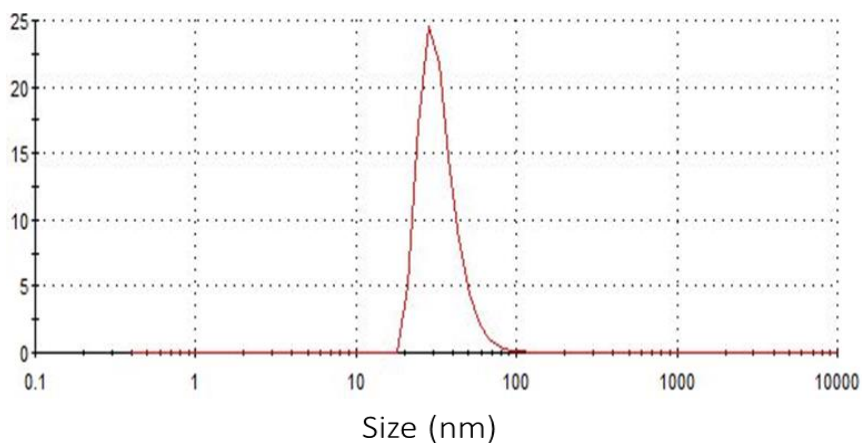


Figure 5.14. DLS size result of 1/1 w/w PAA/PDADMAC complex NPs (PDI = 0.1).

In a second experiment, the polymer concentration was increased from 1 % w/v to 10 % w/v, and the PEC NPs were achieved with similar properties. These NPs were characterized by the TEM technique (Figure 5.14).

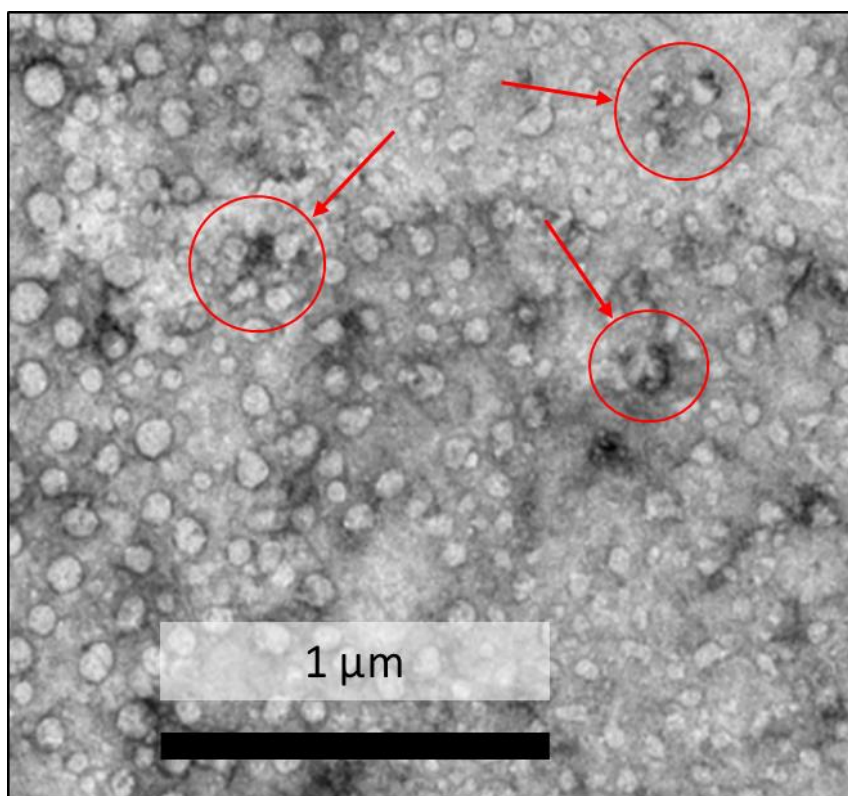


Figure 5.15. TEM image of PAA/PDADMAC NPs produced at 200 $\mu\text{L}/\text{min}$ continuous, and 6 $\mu\text{L}/\text{min}$ disperse phase flow rates containing 10 % w/v of each PE.

The produced PEC NPs have an average monomodal size below 100 nm (65 nm, PDI = 0.2), however, small populations composed of agglomerated NPs can be observed compared to the PEC NPs produced at lower concentrations (Figure 5.15, red circles). This probably happened due to a high

polymer concentration leading to increased nanoprecipitation, at the same time agglomeration of individual NPs was observed with single PE NPs where electrostatic interactions were avoided. This was expected to be further studied with additional experiments to better understand this newly developed non-emulsion-based NP production method.

5.4 CONCLUSION

This chapter covered both emulsion and non-emulsion methods to fabricate PNPs made of oppositely charged PEs. Here, the side-by-side capillary setup was introduced as a novel non-emulsion-based PEC NP fabrication method. In this context, first, PEC formation with PAA and PDADMAC solutions was described, then w/o emulsions were prepared with the sonicator technique at 1-3 % w/v SPAN80 emulsifier concentration in hexadecane. Then two emulsions were processed with the μ RMX technique, and at lower surfactant concentrations an intensified electrostatic interaction was observed between two emulsion droplets later with TEM imaging, however, PEC NPs were not formed. This phenomenon was then applied in the side-by-side capillary device to further *in-situ* reduce the surfactant concentration to intensify PEC NP formation. This was highly successful, yielding monomodal PNPs of below 100 nm.

In the second part, it was possible to achieve PEC NPs as small as 46 nm by directly using PE solutions. This allowed the production of NPs with a one-step surfactant-free process. Following the process optimization to achieve PAA/PDADMAC NPs, it was demonstrated that other polymers can also be used to produce PEC NPs by using the side-by-side capillary device. In this context, dextran/PDADMAC, and PAA/chitosan NPs were produced, and size below 100 nm was achieved, however, the experiments revealed that the polymer type and molecular weight can affect the final product properties. Then, production at different collecting tubing diameters was studied and it was demonstrated that smaller collecting tubing diameters can lead to a higher number of polymer molecules to electrostatically interact. Reducing the tubing diameter down to 1 mm generates PEC NPs with an increase in diameter of 10 ± 2 nm. The smallest collecting tubing diameter of 0.5 mm, further increased the size at each disperse phase flow rate, however, the smallest PEC NP size (46 nm) was detected with 0.5 mm collecting tubing at 5 μ L/min.

This work proposes to implement side-by-side capillary device to fabricate PEC NPs in one-step surfactant-free continuous process. It allows to fabricate PEC NPs of different materials faster than the conventional emulsion methods. It's also believed that the produced PNPs can encapsulate a molecule of interest and thus could be applied in a variety of industrial fields.

5.5 BIBLIOGRAPHY

- [1] I. U. Khan, C. A. Serra, N. Anton, and T. F. Vandamme, "Production of nanoparticle drug delivery systems with microfluidics tools," *Expert Opin. Drug Deliv.*, vol. 12, no. 4, pp. 547–562, 2015, doi: 10.1517/17425247.2015.974547.
- [2] H. Lu, S. Zhang, J. Wang, and Q. Chen, "A Review on Polymer and Lipid-Based Nanocarriers and Its Application to Nano-Pharmaceutical and Food-Based Systems," *Front. Nutr.*, vol. 8, no. December, pp. 1–13, 2021, doi: 10.3389/fnut.2021.783831.
- [3] D. Bahamonde-Norambuena, A. Molina-Pereira, M. Cantin, M. Muñoz, K. Zepeda, and C. Vilos, "Polymeric Nanoparticles in Dermocosmetic," *Int. J. Morphol.*, vol. 33, no. 4, pp. 1563–1568, 2015, doi: 10.4067/s0717-95022015000400061.
- [4] A. A. Barba *et al.*, "Engineering approaches for drug delivery systems production and characterization," *Int. J. Pharm.*, vol. 581, no. March, p. 119267, 2020, doi: 10.1016/j.ijpharm.2020.119267.
- [5] F. Noël, C. A. Serra, and S. Le Calvé, "Design of a novel axial gas pulses micromixer and simulations of its mixing abilities via computational fluid dynamics," *Micromachines*, vol. 10, no. 3, pp. 1–16, 2019, doi: 10.3390/mi10030205.
- [6] J. Allan *et al.*, "Regulatory landscape of nanotechnology and nanoplastics from a global perspective," *Regul. Toxicol. Pharmacol.*, vol. 122, no. October 2020, p. 104885, 2021, doi: 10.1016/j.yrtph.2021.104885.
- [7] M. J. Derry, T. Smith, P. S. O'Hora, and S. P. Armes, "Block Copolymer Nanoparticles Prepared via Polymerization-Induced Self-Assembly Provide Excellent Boundary Lubrication Performance for Next-Generation Ultralow-Viscosity Automotive Engine Oils," *ACS Appl. Mater. Interfaces*, vol. 11, no. 36, pp. 33364–33369, 2019, doi: 10.1021/acsami.9b12472.
- [8] M. Vauthier, M. Schmutz, and C. A. Serra, "One-step elaboration of Janus polymeric nanoparticles: A comparative study of different emulsification processes," *Colloids Surfaces A Physicochem. Eng. Asp.*, vol. 626, no. June, p. 127059, 2021, doi: 10.1016/j.colsurfa.2021.127059.
- [9] J. Wallyn *et al.*, "A new formulation of poly(MAOTIB) nanoparticles as an efficient contrast agent for in vivo X-ray imaging," *Acta Biomater.*, vol. 66, pp. 200–212, 2018, doi: 10.1016/j.actbio.2017.11.011.
- [10] F. Goudon, Y. Clément, and L. Ripoll, "Controlled release of retinol in cationic co-polymeric nanoparticles for topical application," *Cosmetics*, vol. 7, no. 2, pp. 1–9, 2020, doi: 10.3390/COSMETICS7020029.

- [11] A. Nasir, A. Kausar, and A. Younus, "A Review on Preparation, Properties, and Applications of Polymeric Nanoparticle-Based Materials," *Polym. - Plast. Technol. Eng.*, vol. 54, no. 4, pp. 325–341, 2015, doi: 10.1080/03602559.2014.958780.
- [12] T. Pulingam, P. Foroozandeh, J. A. Chuah, and K. Sudesh, "Exploring Various Techniques for the Chemical and Biological Synthesis of Polymeric Nanoparticles," *Nanomaterials*, vol. 12, no. 3, 2022, doi: 10.3390/nano12030576.
- [13] M. Rahman, S. Laurent, N. Tawil, L. Yahia, and M. Mahmoudi, "Nanoparticle and Protein Corona," pp. 21–44, 2013, doi: 10.1007/978-3-642-37555-2_2.
- [14] N. Kolishetti *et al.*, "Engineering of self-assembled nanoparticle platform for precisely controlled combination drug therapy," *Proc. Natl. Acad. Sci. U. S. A.*, vol. 107, no. 42, pp. 17939–17944, 2010, doi: 10.1073/pnas.1011368107.
- [15] A. Mahboubian, S. K. Hasheminein, S. Moghadam, F. Atyabia, and R. Dinarvand, "Preparation and in-vitro evaluation of controlled release PLGA microparticles containing triptoreline," *Iran. J. Pharm. Res.*, vol. 9, no. 4, pp. 369–378, 2010, doi: 10.22037/ijpr.2010.902.
- [16] S. Ding *et al.*, "Microfluidic-Assisted Production of Size-Controlled Superparamagnetic Iron Oxide Nanoparticles-Loaded Poly(methyl methacrylate) Nanohybrids," *Langmuir*, vol. 34, no. 5, pp. 1981–1991, 2018, doi: 10.1021/acs.langmuir.7b01928.
- [17] N. Visaveliya, A. Knauer, W. Yu, C. A. Serra, and J. M. Köhler, "Microflow-assisted assembling of multi-scale polymer particles by controlling surface properties and interactions," *Eur. Polym. J.*, vol. 80, pp. 256–267, 2016, doi: 10.1016/j.eurpolymj.2016.03.015.
- [18] M. Vauthier and C. A. Serra, "One-step production of polyelectrolyte nanoparticles," *Polym. Int.*, vol. 70, no. 6, pp. 860–865, 2021, doi: 10.1002/pi.6178.
- [19] S. Ding *et al.*, "A new method for the formulation of double nanoemulsions," *Soft Matter*, vol. 13, no. 8, pp. 1660–1669, 2017, doi: 10.1039/c6sm02603f.
- [20] S. Ding, C. A. Serra, N. Anton, W. Yu, and T. F. Vandamme, "Production of dry-state ketoprofen-encapsulated PMMA NPs by coupling micromixer-assisted nanoprecipitation and spray drying," *Int. J. Pharm.*, vol. 558, no. December 2018, pp. 1–8, 2019, doi: 10.1016/j.ijpharm.2018.12.031.
- [21] Q. Mei *et al.*, "Formulation and in vitro characterization of rifampicin-loaded porous poly (ϵ -caprolactone) microspheres for sustained skeletal delivery," *Drug Des. Devel. Ther.*, vol. 12, pp. 1533–1544, 2018, doi: 10.2147/DDDT.S163005.
- [22] P. Zhu, H. Zhang, and H. Lu, "Preparation of polyetherimide nanoparticles by a droplet evaporation-assisted thermally induced phase-separation method," *Polymers (Basel)*, vol. 13, no. 10, 2021, doi: 10.3390/polym13101548.

- [23] V. Lohmann, M. Rolland, N. P. Truong, and A. Anastasaki, "Controlling size, shape, and charge of nanoparticles via low-energy miniemulsion and heterogeneous RAFT polymerization," *Eur. Polym. J.*, vol. 176, no. June, p. 111417, 2022, doi: 10.1016/j.eurpolymj.2022.111417.
- [24] S. Ding, C. A. Serra, T. F. Vandamme, W. Yu, and N. Anton, "Double emulsions prepared by two-step emulsification: History, state-of-the-art, and perspective," *J. Control. Release*, vol. 295, no. December 2018, pp. 31–49, 2019, doi: 10.1016/j.jconrel.2018.12.037.
- [25] O. D. H. Jasmina, "Preparation of Nanoemulsions by High-energy and Low-energy emulsification methods," *Springer Nat. Singapore*, vol. 62, pp. 317–322, 2017, doi: 10.1007/978-981-10-4166-2.
- [26] C. A. Serra *et al.*, "Coupling microreaction technologies, polymer chemistry, and processing to produce polymeric micro and nanoparticles with controlled size, morphology, and composition," *Macromol. React. Eng.*, vol. 7, no. 9, pp. 414–439, 2013, doi: 10.1002/mren.201300101.
- [27] J. P. Martins, G. Torrieri, and H. A. Santos, "The importance of microfluidics for the preparation of nanoparticles as advanced drug delivery systems," *Expert Opin. Drug Deliv.*, vol. 15, no. 5, pp. 469–479, 2018, doi: 10.1080/17425247.2018.1446936.
- [28] B. K. Johnson and R. K. Prud'homme, "Mechanism for rapid self-assembly of block copolymer nanoparticles," *Phys. Rev. Lett.*, vol. 91, no. 11, pp. 1–4, 2003, doi: 10.1103/PhysRevLett.91.118302.
- [29] I. U. Khan *et al.*, "Microfluidic conceived Trojan microcarriers for oral delivery of nanoparticles," *Int. J. Pharm.*, vol. 493, no. 1–2, pp. 7–15, 2015, doi: 10.1016/j.ijpharm.2015.06.028.
- [30] R. Karnik *et al.*, "Microfluidic Platform for Controlled Synthesis of Polymeric Nanoparticles Rohit," *Nano Lett.*, vol. 8, No. 9, no. 2906–2912, 2008.
- [31] K. Ouzineb, C. Graillat, and T. F. McKenna, "Study of compartmentalization in the polymerization of miniemulsions of styrene and butyl methacrylate," *J. Appl. Polym. Sci.*, vol. 91, no. 1, pp. 115–124, 2004, doi: 10.1002/app.13181.
- [32] K. H. Roh, D. C. Martin, and J. Lahann, "Biphasic Janus particles with nanoscale anisotropy," *Nat. Mater.*, vol. 4, no. 10, pp. 759–763, 2005, doi: 10.1038/nmat1486.
- [33] C. Hacettepe, R. K. Farman, T. Program, and S. Tez, "Serbest Radikal Temizleyici Madde İçeren Nanopartiküler Tasiyici Sistemlerin Tasari Mi Ve Değerlendirilmesi," 2010.
- [34] Y. Wang, S. Chen, H. Sun, W. Li, C. Hu, and K. Ren, "Recent progresses in microfabricating perfluorinated polymers (Teflons) and the associated new applications in microfluidics," *Microphysiological Syst.*, vol. 1, no. September, pp. 1–1, 2018, doi: 10.21037/mps.2018.08.02.

- [35] O. Campana and D. Wlodkowic, "Ecotoxicology Goes on a Chip: Embracing Miniaturized Bioanalysis in Aquatic Risk Assessment," *Environ. Sci. Technol.*, vol. 52, no. 3, pp. 932–946, 2018, doi: 10.1021/acs.est.7b03370.

General conclusion and perspectives

Context

In this thesis, **four objectives** were successfully achieved:

- The fabrication of biodegradable polymeric nanoparticles, usable in drug delivery, with a controlled diameter below 200 nm, in a biocompatible and eco-friendly approach;
- The one-step production of Janus polymeric nanoparticles in an elongational-flow emulsification device;
- The design of (anisotropic) polyelectrolyte nanoparticles in an elongational-flow emulsification device;
- The use of a traditional microfluidic side-by-side capillary device to develop a novel method of nanoparticle production.

Chapter 3: One-step production of highly monodisperse size-controlled poly(lactic-co-glycolic acid) nanoparticles for the release of a hydrophobic model drug

Emulsification-evaporation method was a reliable way to produce biodegradable, biocompatible poly(lactic-co-glycolic acid) nanoparticles (PLGA NPs). After a successful elaboration of unloaded NPs with the pre-saturation method, rifampicin was encapsulated into NPs at different drug loads. Interestingly, the unloaded PLGA NPs and drug-loaded PLGA NPs had different diameters, respectively 94 nm and 63 nm. Considering the particles' diameter and size dispersity, the optimum encapsulation efficiency of 40% was achieved at 5% w/w initial drug concentration. Morphology analyses showed the difference between size, monomodality of unloaded and drug-loaded NPs and a non-degradable characteristic of the PLGA matrix within 8 days. In vitro release from drug-loaded PLGA NPs under sink conditions showed that the drug quantity can be controlled by varying the initial drug weight content. Overall, this work opened innovative perspectives for the design of controlled drug release systems.

Chapter 4: One-step elongational-flow synthesis of anisotropic polymeric nanoparticles used as drug carriers

In this chapter, several strategies to implement the emulsification-evaporation method for the one-step production of different PNPs' structures were demonstrated. The results showed that the sizes of PNPs varied dramatically, with more than 40% of size difference between the different material conditions, such as the use of various continuous/dispersed phase volume ratio or the pre-saturation

method. The parameter that influence the most the particles' size was pre-saturation and drug-loaded conditions. Indeed, PNPs' diameters of 64 nm, 76 nm, and 78 nm were achieved for single PLGA, PMMA, and binary-blend PMMA-PLGA NPs respectively by using these conditions. Then, two single, and two binary-blend PNPs were used to encapsulate rifampicin in order to study and compare their cargo capacities. The highest release percentage value (xx%) was achieved with the polymeric Janus nanoparticles (PMMA/PSS) due to the gradual dissolution of the second matrix (PSS), leading to more drug molecules to escape the nanoparticle.

Overall, it was possible to fabricate various anisotropic polymeric nanoparticles, with a single-step process.

Chapter 5: Process design and optimization of polyelectrolyte complex nanoparticles' production

Both emulsion and non-emulsion methods to fabricate polymeric nanoparticles were studied and a new strategy was developed in this chapter. Here, a side-by-side capillary setup was introduced as a novel non-emulsion-based fabrication method. In a first part, polyelectrolyte nanoparticles of PAA and PDADMAC were prepared with the μ RMX and the side-by-side capillary device. The latter allowing to reduce the surfactant concentration to intensify a polyelectrolyte complex formation. As a result, monomodal polyelectrolyte nanoparticles with a diameter below 100 nm were produced.

In a second part, with the side-by-side capillary setup, it was possible to achieve PEC NPs' size as small as 46 nm by directly using polyelectrolyte solutions instead of polyelectrolyte emulsions. This allowed the production of polyelectrolyte complex (PEC) NPs with a one-step, surfactant-free process. Following the process optimization to achieve PEC NPs with oppositely charged polymers, it was demonstrated that other polymers can also be used to produce small (<100 nm) PEC NPs in the side-by-side capillary device such as dextran, poly(acrylic acid or chitosan. Without any surprise, the experiments revealed that the polymer type and molecular weight can affect the final product properties, such as the size, size distribution, and their cargo properties. Moreover, it was observed that reducing the collecting tubing diameter predominantly increased the PEC NPs' diameter.

Overall, this work proposed to implement a side-by-side capillary device to fabricate PEC NPs in one-step surfactant-free continuous process. It also allowed to fabricate PEC NPs of different polymers faster than the conventional emulsion methods.

Perspectives

Both elongational-flow based emulsification device and side-by-side capillary device have significant advantages that could be used on laboratory as well as industrial scales. The improved diameter control can be achieved at precisely controlled fluid flow, also by consuming less energy as compared to conventional devices. The materials to be mixed can vary depending on the application, which could be either cosmetics, drugs or food industry. After this thesis, there are many perspectives in polymeric nanoparticles fabrication field to design and develop new strategies for wide-range of applications and to fulfill the rapidly growing PNPs' market. The next steps could consist of studying the PNPs' porosity and the influence of the process parameters on the PNPs' permeability. This study can open new opportunities to achieve highly controlled and sustainable drug delivery properties since higher permeability could lead to faster drug release. It would be also interesting to investigate the evaporation kinetics of polymer solvents in emulsion-based design, which can directly affect the PNP self-assembly, and eventually its' permeability. It would be also attractive to study the solvent exchange, and its effect on PNPs' size and morphology. In side-by-side capillary device, the production can be intensified by increasing the polymer concentration while reducing the polymer molecular weight, controlling the solvent diffusivity, changing the capillaries' inner diameter and/or by multiplying the number of capillaries used.

Production scientifique

Articles dans des journaux à comité de lecture

Articles publiés

1. Javid Abdurahim, Christophe A. Serra*, Christian Blanck, Madeline Vauthier*, One-step production of highly monodisperse size-controlled poly(lactic-co-glycolic acid) nanoparticles for the release of a hydrophobic model drug, *Journal of Drug Delivery Science and Technology*, **2022**, *71*, 103358.

Articles en preparation

2. Javid Abdurahim, Christophe A. Serra, Madeline Vauthier, Novelties concerning the production of polymeric nanoparticles for selective applications

3. Javid Abdurahim, Christophe A. Serra, Madeline Vauthier, One-step synthesis of complex and anisotropic polymeric nanoparticles: application to the encapsulation of a model drug

4. Javid Abdurahim, Christophe A. Serra, Madeline Vauthier, Continuous production of polyelectrolyte complex nanoparticles with a side-by-side capillary device.

Communications lors de conférences

Communications orales

1. Javid Abdurahim, Christophe A. Serra, Madeline Vauthier, Elaboration of the size-controlled polymeric nanomaterials; a model drug encapsulation and in-vitro release studies, Curiosity : Conférence des Jeunes Chimistes Franco-Allemands, 30 juin – 1 juillet 2022, Mulhouse, France

2. Javid Abdurahim, La Société Chimique de France et les jeunes en Alsace, congrès annuel de l'école doctorale 182, 22 mars 2022, Strasbourg, France

3. Javid Abdurahim, Christophe A. Serra, Madeline Vauthier, One-step elongational-flow focusing production of the size-controlled polymeric nanomaterials; Rifampicin encapsulation and in-vitro release studies, 1er congrès de l'UFAZ-Unistra-ASOIU, 29 novembre – 2 décembre 2021, Bakou, Azerbaïdjan

4. Javid Abdurahim, Ane Larrea, Victor Sebastian, Christophe A. Serra, Madeline Vauthier, One-step production of nanoemulsions for biomedical applications: drug-loaded size-controlled biodegradable polymeric nanoparticles, SETCOR Nanotech France Conférence internationale, 21-23 juin 2021, Paris, France

5. Javid Abdurahim, Christophe A. Serra, Madeline Vauthier, One-step production of the size-controlled polymeric nanomaterials; Rifampicin encapsulation and in-vitro release studies, ED182 Congress, 7 juin 2021, Strasbourg, France

Communications par affiche

1. Ahmad Abdul Ghani, Raphaël Galois, Julie Thiercelin, Christophe A. Serra, Madeline Vauthier, Javid Abdurahim, One-step elongational-flow focusing production of PLGA-PMMA nanoparticles, Session Poster des étudiants ECPM, 10 Mars 2022, Strasbourg, France

2. Javid Abdurahim, Marc Schmutz, Christophe A. Serra, Madeline Vauthier, Dégradation des nanoparticules PLGA, Prix de l'exposition d'art scientifique pour les meilleures images, 4ème Edition de l'Exposition d'Art Scientifique de l'Association des Chercheurs Internationaux de Strasbourg, 29 novembre 2021, Strasbourg, France

3. Javid Abdurahim, Ane Larrea, Victor Sebastien, Christophe A. Serra, Madeline Vauthier, Nanoemulsions for biomedical applications; drug-loaded size-controlled monomodal biodegradable polymeric nanoparticles, Cnano Conférence internationale, 22-26 novembre, 2021, Toulouse, France.

Development of an intensified process for the one-step production of isotropic and anisotropic polymeric nanoparticles

Résumé

Les nanoparticules polymères (PNPs) peuvent être conçues pour une large gamme d'applications dans des domaines tels que la nanomédecine, les cosmétiques ou l'agriculture. Ces domaines se développent rapidement et nécessitent de nouvelles approches telles que des procédés rapides, continus, biocompatibles et respectueux de l'environnement pour améliorer la production de PNP. Cependant, certains processus en une étape sont entravés par le mauvais contrôle des propriétés des PNPs induites par le mécanisme de formation via des dispositifs conventionnels. La majorité de ces dispositifs utilisent des opérations par lots ou incluent des matériaux chimiquement réactifs et agressifs, qui doivent être fortement évités dans la plupart des applications. Au cours de ces travaux de recherche, des PNPs ont été fabriquées selon trois méthodes différentes à base d'émulsion et une nouvelle méthode sans émulsion. Dans toutes les méthodes, des polymères préformés et des matériaux hautement biocompatibles ont été utilisés. Ainsi, des nanoparticules uniques de poly(acide lactique-co-glycolique) dans une plage de diamètre allant de 60 nm à 100 nm ont été obtenues, puis des PNPs anisotropes composés de poly(méthyl-méthacrylate) et de poly(styrène-sulfonate) ont été développés et comparés pour l'administration de médicaments. De plus, un système microfluidique à capillaires côte-à-côte a été développé en tant que nouveau dispositif à flux continu en une seule étape qui a permis la production de différentes nanoparticules complexées de polyélectrolytes dans une gamme de diamètres allant de 40 nm à 120 nm. Ce procédé a été optimisé pour permettre de contrôler la taille et la distribution de tailles des PNPs.

Mots-clés : production en une étape, nanoparticule de polymère, émulsification, microfluidique, flux élongationnel, micromélangeur, anisotropie, polyélectrolyte, complexe, capillaire côte-à-côte

Abstract

Polymeric nanoparticles (PNPs) can be designed for a wide range of applications in fields such as nanomedicine, cosmetics, or agriculture. These fields are rapidly growing, requesting novel approaches such as rapid, continuous, biocompatible and eco-friendly processes to improve PNPs' production. However, some one-step processes are impeded by the poor control on PNPs' properties induced by the mechanism of formation via conventional devices. Majority of these devices use batch operations, or include chemically reactive and aggressive materials, that are highly avoided in most PNP's applications. In this research, PNPs were fabricated in three different emulsion-based methods, and one novel non-emulsion-based method. In all the methods, pre-formed polymers and highly biocompatible materials were used. Firstly, single poly(lactic-co-glycolic-acid) nanoparticles which diameters ranged from 60 nm to 100 nm were achieved, then blend and anisotropic PNPs with poly(methyl-methacrylate) and poly(styrene-sulfonate) were developed and assessed in drug delivery. Additionally, a side-by-side capillary setup was developed as a novel one-step continuous flow device that allowed the production of different polyelectrolyte complex nanoparticles with monomodal diameters ranging from 40 nm to 120 nm. This process was optimized to allow controlling PNP's size and size distribution.

Keywords: one-step production, polymeric nanoparticle, emulsification, microfluidics, elongational-flow, micromixer, anisotropy, polyelectrolyte, complex, side-by-side capillary